A study of the surface modification of polyethylene by corona and plasma discharge and of some stable free radicals, using esca and other techniques

Herbert Frederick Beer

University of Durham

A thesis entitled

A STUDY OF THE SURFACE MODIFICATION OF POLYETHYLENE BY CORONA AND PLASMA DISCHARGES AND OF SOME STABLE FREE RADICALS, USING ESCA AND OTHER TECHNIQUES

Submitted by

HERBERT FREDERICK BEER, M.A., (CANTAB.),
M.Sc., (Dunelm), C. Chem., F.R.I.C.
(College of St. Hild and St. Bede)

A candidate for the Degree of Doctor of Philosophy

1980

To Katherine

Acknowledgements

The work described in this thesis was carried out under the supervision of Professor D. Clark and I wish to record my appreciation of his help and encouragement throughout. I would like to thank the Department of Engineering Science at Durham University for their assistance in carrying out lap-shear tests, and R. Hart for the fabrication of various pieces of apparatus. Thanks are also due to J.A. Sidwell, of the Rubber and Plastics Research Association at Shawbury, for determining antioxidant levels in the polyethylene samples used.

The polyethylene samples used were kindly supplied by the Metal Box Company and the free radical samples by Professor Ballester of Barcelona University.

Finally I would like to thank the Governors of St. Hild and St. Bede for the granting of study leave in connection with this work and Mrs. R. Hart for typing this thesis.

Memorandum

The work described in this thesis was carried out at the University of Durham between October 1975 and June 1979. Except where acknowledged by reference, it is the original work of the author and has not been submitted in whole or part for any other degree.

The substance of some of this material has already been presented in a paper entitled "Some aspects of Structure and Bonding in the Perchlorodiphenylaminyl Radical revealed by ESCA", by D.T. Clark and H.F. Beer, Tetrahedron 34 491 1978

A b s t r a c t

The surface modification of polyethylene by Corona and Plasma discharges is studied by X-Ray photoelectron spectroscopy and multiple internal reflection spectroscopy. Wettabilities are used to observe changes in surface energy and the strengths of bonds formed using adhesives are measured. A short account is given of the importance to manufacturers of being able to increase the surface energies of polymers.

The conditions needed to establish the corona discharge and the nature of the corona discharge are discussed. The reactions occurring within the plasma formed by the discharge and the various reactive species formed are considered and the effects of these species are discussed. Plasma discharges at low pressures and their effects on polymer surfaces are also considered.

The surface modification of polyethylene by both corona and plasma discharges is shown to be associated with an increase in the oxygen functionality of the surface. The relationships between the increase in oxygen and carbon functionalities are discussed and the possible groups formed are suggested. Many of these are polar in character and include hydroxyl, carbonyl, carboxylic, carbonate and hydroperoxide groups together with ether and possibly peroxide (non polar) groups. These groups are found to be produced even when only traces of oxygen are present. The use of nitrogen gas is shown to produce high levels

of amine and amide functions.

The polar groups are believed to be largely responsible for the increased wettabilities of the surfaces and partly responsible for the increased adhesive strength. In this latter case cross linking at the surface is also believed to be important. Some evidence is put forward, from the heat treatment of plasma treated polyethylene, for free radicals being involved in some of the reactions at the surface. The fact that free radicals are not detected after the surface modification in many instances is thought to be due to the fact that they often react completely with oxygen as fast as they are formed. The surface charging of polyethylene during corona discharge is examined and shown to be largely due to deeply trapped electrons rather than merely superficial charges. A comparison is made between corona and plasma discharges and the suitability of each method in different situations is considered.

The structure and bonding in the perchlorodiphenyl aminyl radical is investigated to see if this could help in the investigation of the effects of corona and plasma treatment of polyethylene. The results, though interesting in themselves, reveal that the multiplet splitting effect is too small for this effect to be used in investigating surface changes in polyethylene.

Table of Contents

Page

Appendices

Chapter 1

The Importance and Relevance of Polymer Surfaces

.1 Introduction

.2 Surface Treatment

a) Reason

b) Method

c) Result

d) Comparison of Surface and Bulk Properties

.3 Related work on Etching

a) Sodium in liquid Ammonia

b) Ion Etching

c) Electron Etching

.4 Future Developments

.5 Free radicals

Polymer Surfaces

.1 Introduction

Before the introduction on a large scale of synthetic polymers for making fabrics, sheet materials and more solid objects, the only available materials were, of course, natural ones, or slightly modified natural ones. Thus materials such wool, silk, and cotton, which need little or no pre-treatment and a material such as flax, which only needs a comparatively simple process to separate the fibres, were used for fabrics. Wood, apart from seasoning, needs no treatment and was used for making solid objects. A material like leather, however, needs rather more complicated treatment to preserve it and to make it waterproof. Paper may be made from some fibres by a relatively simple process, but the chemistry of making paper from wood pulp is quite complex.

These natural materials have been selected, no doubt by a process of trial followed by either retention or rejection, because they had certain desirable properties. These properties would include mechanical, chemical, thermal, and electrical properties though these latter have only become important during the last hundred years. It may be coincidence that the natural materials that were selected because of properties of strength, rigidity and overall stability also possessed a number of desirable surface properties. However, the aesthetic appearance and "feel" of a material is important and the ability of a surface to

accept dyes, paint and printing inks and also to form reasonably strong glued joints is desirable for many materials. Another surface property that is often required is the ability to disperse static charges, though for some purposes such as capacitor dielectrics and electrets the converse may be what is needed. Most natural materials fit the first requirement in that they have comparatively high surface conductances, or bulk conductances so do not carry persistent charges. This will, of course, make them unsuitable in many cases for use in capacitors and other electronic devices. Synthetic polymers often have very low surface and bulk electrical conductances and this can produce problems in fabrics and sheet materials, due to the build up of persistent static charges. This can in fact produce sparks when used in clothing, or more seriously when used for conveyor belt materials where sparks may be hazardous and may cause explosions, for example in dusty atmospheres. On the other hand this property, of very low surface conductance, is what is required for capacitor dielectrics and electret materials.

The last forty years has seen the introduction, on a large scale, of many different synthetic polymers with unique combinations of properties that are not found in natural materials. There is also the very interesting fact that many of these polymers have no inherent characteristic appearance or texture but rather their appearance and texture depend on some process during their manufacture and fabrication. In the case of extruded fibers, for example,

the texture or "feel" of the fabric made from them is actually dependent to some degree upon the cross section shape of the fibres[1]. Whereas most extruded fibres have a circular cross section, probably because it is easier to drill round holes than other shapes, the use of a rectangular cross section for the fibres, for example, produces a fabric with a very unpleasant slimy and greasy sensation to touch.

The actual surface properties and appearance are now in fact quite an important factor when selecting a polymer for a particular use. Whereas natural materials often have suitable surface properties it is necessary with many synthetic polymers to produce the required surface properties during some stage in the manufacturing process[2]. This is particularly necessary when the surface of the synthetic polymer is going to be printed, painted or when adhesives are going to be used on the surface. To some extent the difficulty with regard to painting can be overcome by the inclusion of pigments in the mixing stage of production. Where the polymer is to be used for making film for packaging, or for fibres for fabrics inclusion of pigment particles may not be feasible and so it may be necessary to modify the surface so that it will accept printing inks or dyes.

Surface Treatment

a) Reason for Surface Treatment

The polymers which present the chief problems with regard to printing, dyeing, painting and adhesion are those with low surface energies such as the polyolefins. The natural materials in use such as cotton which is principally

cellulose consists of glucose units linked together and it is believed that the ability of the cellulose to accept dyes

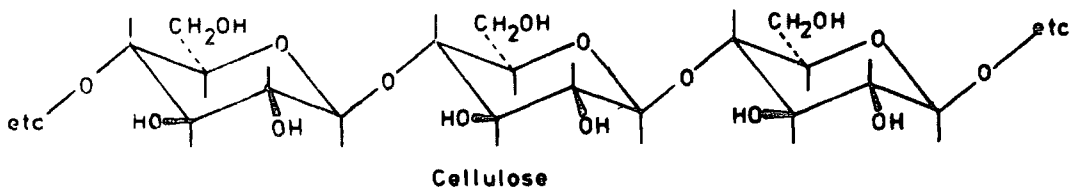

Cellulose

Figure 1 2 1

and printing inks arises from the presence of the hydroxyl groups. These, it is thought, make hydrogen bonds with the dye molecules. Wood is another material containing cellulose and also lignin, and again the presence of hydroxyl groups in these substances is thought to produce bonds with paint and adhesive molecules. Another factor believed to be important in adhesion is surface roughness and wood with its rather porous structure satisfies this requirement. Wool and silk consist of peptide chains, with in the case of wool disulphide cross links between cystein residues. The polar character of the amide structure of the peptide is thought, like the hydroxyl groups, to form bonds of similar nature to hydrogen bonds with other molecules. Due to the amphoteric character of the amide groups, wool and silk may be dyed with either acidic or basic dyestuffs[3]. The presence of absorbed moisture and other impurities on the surfaces of natural materials also leads to surface conductances sufficiently high to allow static charges

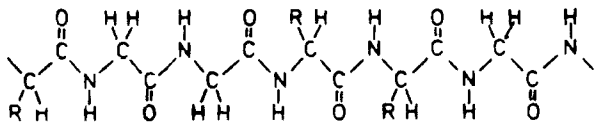

Silk (R is various alkyl groups)

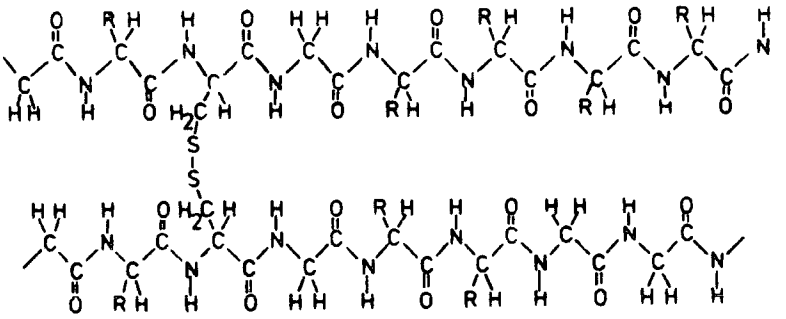

Wool (R is various alkyl groups)

Figure 1 2 2

to leak away except under abnormal conditions of very low humidity. Synthetic polymers, however, tend to have fewer active polar groups in their molecules, for example the nylons

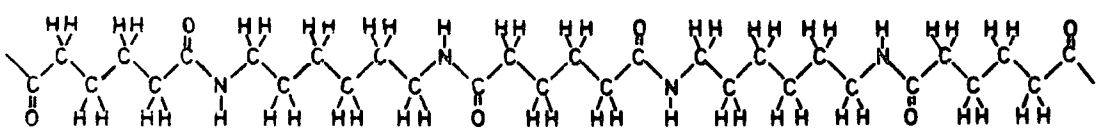

Nylon 6,6

Figure 1 2 3

or much less polar groups, for example polyesters and polyvinyl chloride

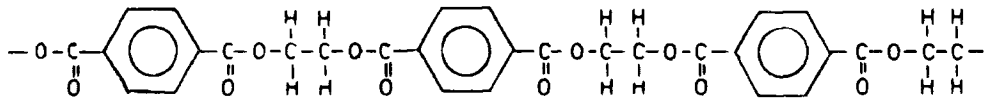

Poly(ethylene terephthalate)

Figure 1 2 4

or in the case of polyolefins and their fully halogenated derivative, virtually no polar groups in the polymer at all.

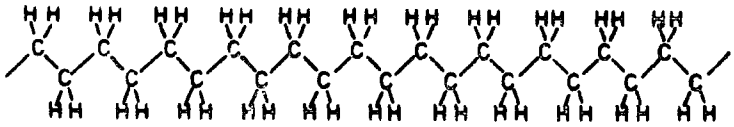

Polyethylene

Figure 1 2.5

As a result of this synthetic polymers, unless treated specifically, become increasingly more difficult to print, dye or glue in the order nylon, polyester and polyolefin.

Even natural materials need some limited treatment which is often just washing with detergent to remove grease and dirt from fibres or surface roughening before glueing wood. In the case of synthetic polymers it is often found that the surface is unreceptive to inks and adhesives and that some specific treatment is required. As a rough guide it has been found that a material needs a critical surface tension for wetting of the order of at least 40 mN m^{-1} before it can be used satisfactorily with commercial inks and adhesives[2].

From table 1.2.1 it is seen that Teflon and Polyethylene will need treatment, whereas polyvinyl chloride, and those with larger critical surface tensions for wetting, should require little or no treatment:

Critical surface tension for wetting / mN m^{-1}	
Polymer	
Polytetrafluoroethylene, Teflon	18
Polyethylene	31
Polypropylene	31
Polyvinyl Chloride	39
Polyethylene Terephthalate, Terylene	43
Polyhexamethyleneadipamide, Nylon	46
Critical surface tension for wetting	ref.2

Table 1.2.1

In fact, it is found that for polyvinyl chloride, terylene, nylon and polymers with similar critical surface tensions for wetting that simple washing with detergent, followed by rinsing, is sufficient surface treatment.

However, large quantities of polyethylene, polypropylene and ethylene co-polymers are now used, especially in the packaging industry and it is especially desirable here to be able to print on the surface. The problem of lack of adhesion can fortunately be overcome by the fact that these polymers have comparatively low melting points and packages can be sealed by simple heating combined with pressure. Thicker sections of these polymers can, of course, as already stated, be coloured by incorporating pigments in the polymer mix. Teflon is perhaps rather a special case with comparatively limited use and often its uses do not necessitate printing though ability to accept adhesives might be useful. In fact, Teflon is often used in situations where its low critical surface tension for wetting, low surface friction, general inertness and low surface conductance are a positive advantage.

b) Methods of Treatment

As stated above, the problem with polyethylene and other polyoelyfines arises from the absence of any polar groups in their molecules. The problem could, therefore, be overcome by some form of surface treatment that would form polar groups either by addition to or modification of the surface. The most obvious idea is to add either oxygen or nitrogen containing groups which by their polar character will cause the surface to wet more easily.

At first chlorine was tried but due to economic and technical reasons the process was soon abandoned in favour of more efficient processes. Exposure to ozone and ultra

violet radiation has been tried but the process is rather slow. Oxidation using sulphuric acid-dichromate solutions is very effective but suffers from the drawback of the hazardous nature of the chemicals and the need for washing and drying the treated polymer. It is, therefore, not suitable for large scale use but it does have the advantage that the whole surface is treated and, especially important, cavities and the interior of an object can be treated effectively.

A simple surface roughening is sometimes used, such as sand blasting or immersion in a hot solvent, which apparently produces a similar effect. It is not known, however, if the treatment causes any other surface modifications or inclusions at or near the surface.

The more commonly used method, at the present, for large scale production are either heat treatment or electrical methods.

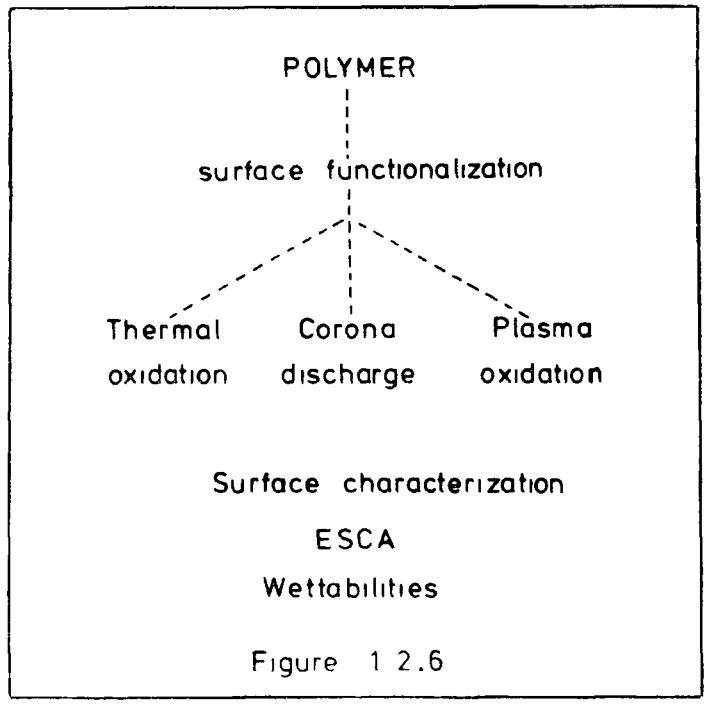

Figure 1 2.6

In the various heat treatments the basic idea is to heat the surface by hot air, infra red radiation or by direct application of a flame, while keeping the interior of the polymer cold. It is not easy to use the heat treatment for thin film, such as is used in packaging, since the thinness of the film makes it difficult to prevent the bulk of the material from becoming hot. Heat treatment by the use of flames is, however, the preferred method for treating blow mouldings, such as bottles, where by using gas flames correctly positioned the outside of the moulding is easily treated. It is true that the inside of mouldings is not treated but in many cases, such as bottles, this is unimportant. Another method rather similar to the use of flames and hot air jets is to use a plasma jet at atmospheric pressure. In this process an inert gas such as argon is blown through an electric arc and the resulting gas stream is allowed to impinge on the polymer surface. Using this method Kiyozumi and co-workers found that the adhesive strength for polyethylene was increased from 0.5 to 10 MPa and that this increase was accompanied by a decrease in the contact angle for a surface water drop from 80^{o} to 20^{o}. This latter angle corresponds to a critical surface tension of wetting of 56 dynes (see Table 1.2.1 for the value for untreated polyethylene).

Low pressure plasma systems are used on a small scale for treating polymers but have the disadvantage of being batch processes. A typical system uses a gas pressure of the order of 25 Pa (0.2 Torr) and an r.f. induced plasma.

Various gases have been tried, such as argon, oxygen and nitrogen, but there seems no advantage, if simple treatment is needed, in not using air (see Chapter 6). The actual treatment time is short but a much greater time is spent in merely loading, pumping out and unloading the vacuum chamber. It does have the advantage though that all of the surface is treated, both the inside and the outside of a container and is suitable for treating small objects that would be difficult to handle on a production line. The process is also a dry one and produces sterile containers which is useful for the drugs industry.

The large scale method which is now commonly used for plastic film is that of corona discharge. The actual mechanics of the method are simple; it may be used for batch processing but is in fact ideally suited for continuous production. The actual nature of the discharge is in some doubt and it is possible that the discharge is not a true corona as understood by physicists and electrical engineers. This being understood, the process may still be called the Corona Discharge Treatment even though, in fact, it is more like a spark breakdown (see Chapter 3).

c) Results

One of the problems associated with any form of surface effect is finding out exactly what the surface consists of. Various methods have been tried, some more successfully than others. It is relatively simple to establish critical surface tensions for wetting and to draw conclusions as to the causes when the bulk of the material has the same composition as the surface. But when the surface layer is only of the order of a nanometre thick then bulk analysis is not very helpful. Scraping the surface is one method[5], but it is difficult to ensure that only the surface layer is removed. Solvent extraction[6] has been used but it assumes that the surface modification will be dissolved and nothing else will. Methods that do not affect the surface and which in fact are non-destructive with regards to the surface layer are in fact more satisfactory. Of these various methods (see Chapter 2, section 7) ESCA and M.I.R. IR are the ones that have been used for the work in this thesis. For the treatments considered in this thesis probably ESCA is the more sensitive[7] since the technique only samples to the depth of the order of a few nanometres while MIR IR samples several hundred nanometres.

The main effect as far as polymer surfaces are concerned is that treatments that are effective in increasing surface energy also increase the level of oxidation of the surface. The results of ESCA and MIR IR

(see Chapter 4) show an increase in carbonyl and hydroxyl groups and possibly also carboxyl groups. Removal of the surface layer by either scraping[5], or solvent extraction[6] also reveals an increase in functional groups containing oxygen.

The static charge that builds up on a polymer surface due to friction, may also be altered by surface modification. It has been reported[8] that the oxidation of nylon 6-6 monofilament by chlorine sensitized photo-oxidation reduces the static build up.

d) Comparison of Surface and Bulk Properties

The main reason for wishing to modify only the surface of a polymer is that it enables the use of a comparatively cheap polymer to be extended[9]. The desired surface properties could often be obtained using other materials but the alternatives may be less economic or may be rather intractable with regard to fabrication. Another factor to be considered is the porosity of the material and the rate at which liquids or gases can penetrate. Thus in the packaging industry a material such as polyethylene has the desirable properties of being relatively impermeable to gases and liquids, but it cannot be easily printed. So a simple and relatively inexpensive treatment, such as corona treatment, which does not affect the bulk properties but increases the printability is desirable. Fortunately it has been found that the bulk property of strength is not seriously altered by surface treatments

though it is true that a slight reduction has been observed[8] in some cases.

Another situation where the ability to modify only the surface is an advantage is in the production of flame resistance fabrics. Although heat resistant polymers are available these obviously have high melting points. By suitable reactions aromatic polyamides and polyacrylonitriles can be made to react with the polymer to form heterocyclic rings that raise the melting point of the polymer. This effect can be restricted to the surface of fibres by using short reaction times[8] and so a fibre can be obtained with a high melting point surface that protects a lower melting point interior. So initial ease of fabrication (the lower melting point polymer) followed by surface treatment (formation of a higher melting point surface) gives a material with increased flame resistance compared to the original material.

.3 Related Work on Etching

a) Sodium in Liquid Ammonia

Teflon and related fluoropolymers have very low surface energies, the critical surface tension for wetting of teflon being 18 mN m^{-1}. It is therefore not surprising that ordinary adhesives will not form joints with teflon, nor will the surface accept conventional inks. These difficulties may be overcome by treating the surface with a solution of sodium in naphthalene-tetrahydrofuran, or sodium in liquid ammonia[10]. These treatments cause the surface of the polymer to darken and also increase the

surface energy. Riggs and Dwight[10] have shown, using ESCA, that the effect of increasing the surface energy may be correlated with the amount

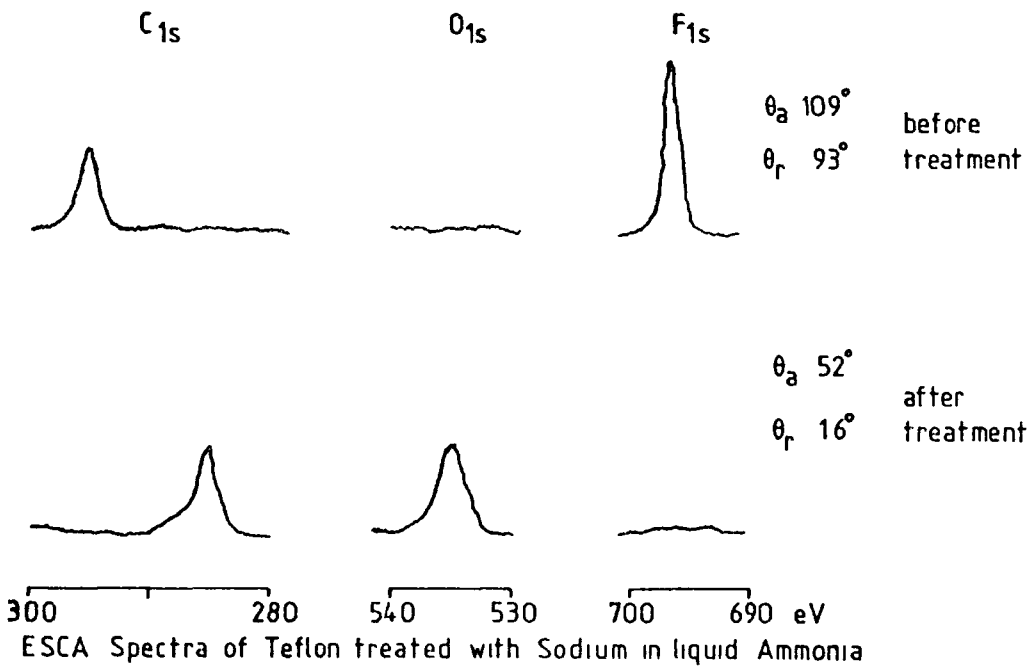

ESCA Spectra of Teflon treated with Sodium in liquid Ammonia

Figure 131

of fluorine and oxygen and the nature of the carbon bonding in the surface layer.

Miller and co-workers[11], using potassium in liquid ammonia, discovered an increase of approximately four orders

of magnitude in the surface area of teflon and also the presence of double bonds after the treatment. This latter observation is supported by the work of Riggs and Dwight[10] who found that the surface of teflon would take up bromine after treatment.

b) Ion Etching

Teflon and other polymers may also be etched and their surface energies increased by bombardment with ions of various species, such as the noble gases and oxygen. By means of ESCA Clark et al[7] have shown that extensive cross linking takes place and that the fluorine level in the surface layers goes down after etching. By coupling their ion etching equipment with a quadropole mass spectrometer Smolinsky and Vasile[12] were able to show that fluorine was removed from the surface and also carbon and hydrogen.

c) Electron Etching

Effects similar to those resulting from ion bombardment have also been reported by Mayoux[13] using electrons. Changes in surface energy are not given but by using MIR IR hydroxyl, carbonyl and double bonds were detected. Absorption spectra in the UV region also revealed evidence of unsaturation. Another effect resulting from electron bombardment is the formation of free radicals, some of which appear to be quite stable. It has been suggested that the brown appearance of polyethylene after irradiation is partly due to trapped free radicals.

.4 Future Developments

By forming active sites on the surface of a polymer it is possible not only to produce simple polar groups but also to graft on more complex entities. The purpose of these may be to modify the surface for reasons such as forming adhesive joints or for printing. In some instances it may be possible to use the activity of the surface to induce graft polymerisation, as for example in the work by Sakata and Goring[14] on the grafting of ethyl acrylate onto cellophane, after corona treatment. It is also possible that the surface treatment, followed perhaps by grafting, might be used to produce catalyst materials[15]. In view of the long chain nature of the original polymers it has been suggested that these synthetic polymer catalysts would have enzyme-like activity and would proceed by "template" mechanism.

A technique, for inducing graft polymerisation, that may become increasingly important is the use of nuclear radiation to produce the active sites on the polymer chain. Using this technique Memetea and Stannett[16] have been able to graft styrene onto poly(ethylene terephthalate) fibres. Another development is the use of Lewis acids to etch the surface of nylon fibres so that after treatment the fibres will bond together[8]. By this means a web of fibres may be treated with an active gas, such as a hydrogen halide, and then after removing the activating gas the fibres bond together to form a non-woven fabric. This process produces a fabric similar to that produced by the process of felting but with a more open texture.

.5 Free Radicals

It is thought that free radicals might play some part in corona and plasma treatment of polymer surfaces (see Chapters 4, 5 and 6). Some work was therefore carried out on some stable free radicals, provided by Professor M. Ballester of Barcelona University. This work is presented in Chapter 7 where the case of the perchlorodiphenyl aminyl radical is discussed in some detail.

Chapter 2

X-Ray Spectroscopy for Chemical Application

ESCA

.1 General Introduction

.2 Development

.3 Theory of Electron Spectroscopy

a) Photo ionisation

b) Relaxation

c) Shake Up and Shake Off

d) Auger and X-Ray Fluorescence Spectroscopies

.4 Instrumental Details

a) X-Ray source

b) Sample chamber

c) Sample handling

Solid, liquid, gas

d) Electron Energy Analysis

e) Electron Detector and Data acquisition

.5 Calculation of Binding Energies

a) Binding Energy

b) Sample Charging

c) Absolute Binding Energies

d) Use of reference peaks C_{1s} Au_{4f}

.6 Various Features of ESCA

a) Binding Energies

b) Chemical Shifts

c) Fine Structure

i) Spin orbit splitting

ii) Multiplet splitting

iii) Electrostatic splitting

d) Satellite Peaks

e) Line Widths

f) Sampling Depth

g) Peak Intensities

i) X-Ray flux

ii) Cross section

iii) Spectrometer Factor

iv) Electron Mean Free Path

v) Number Density

h) Analytical Depth Profiling

i) Deconvolution

.7 General Aspects of ESCA

a) Sensitivity of ESCA and other techniques

b) Advantages of ESCA

c) Disadvantages of ESCA

d) Hierarchy of ESCA Information

e) Developments in ESCA

.1 Introduction

The first person to observe though not to investigate the phenomenon of photo emission was Heinrich Hertz, working on radio waves at Karlsruche[17] in 1877. He did not investigate the matter, which was in fact a nuisance[18] as far as his experiments were concerned. Hallwachs[19] might really be said to have begun the study of photo emission by his observations in 1888 of the effect of ultra-violet light on electrically charged sheets of zinc.

The emission of electrons by X-Ray radiation was studied by de Broglie[20,21] and Robinson[22,23,24] who analysed the electron energies of the photo electrons with a magnetic analyser. When a material was irradiated they found that, starting with the ultra-violet radiations, only a few electrons were released. However, when the frequency was increased and the energy of the quantum became larger ($E = h\nu$), at a certain point a large increase in the number of the electrons was observed. After this point, referred to as an absorption edge, the number of electrons decreased until a higher frequency when again the number of electrons greatly increased.

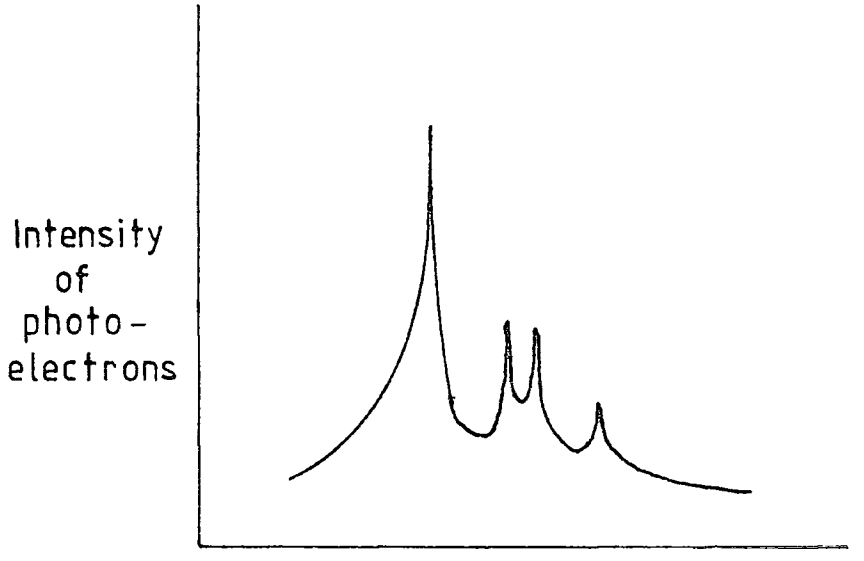

Electron spectra of MgO with $Cu_{K\alpha}$ X-Rays

Figure 2.11

The absorption edges could be correlated with the energy levels of the electron orbitals in the atom but at that time the resolution of the electron energies was not sufficient to reveal any fine structure details in their spectra. It was not in fact until the 1950's that the development of high resolution energy analysers for β-ray analysis[25] provided the necessary resolution for X-Ray photo electron spectroscopy.

.2 Development

In the early 1950's Siegbahn and co-workers at Uppsala University, Sweden, developed an iron free double focussing electron spectrometer for high resolution studies

of β-ray energies[25]. This was used in 1954 to study the electron energies of photo electrons ejected by X-Rays and they observed that a sharp line could be resolved from each absorption edge. This line represents the kinetic energy of photo electrons that have not suffered energy losses and therefore corresponds to the binding energy of the atomic level from which they come. The kinetic energy could be measured with a precision of a few tenths of an electron volt and using this new technique K. Siegbahn and co-workers[26] were able to study in detail the photo electron spectra of copper and its oxides. It was not however until the observation of two distinct ls peaks, from the different oxidation states of sulphur in sodium thiosulphate, in 1964, that the possibilities of photo electron spectroscopy were fully appreciated.

.3 Photo Electrons and Related Spectroscopics

a) Photo ionisation

When a molecule is irradiated with X-Rays, then electrons with binding energies less than that of the existing radiation may be ejected. Typical X-Ray sources in current use are Mg $K_{\alpha_{1,2}}$ and Al $K_{\alpha_{1,2}}$ with photon energies of 1253.7 eV and 1486.6 eV respectively. The electrons ejected may be either core or valence electrons though these latter are usually studied using ultra-violet photo electron spectroscopy[27] with He(I) radiation, 21.22 eV or He(II) radiation, 40.8 eV.

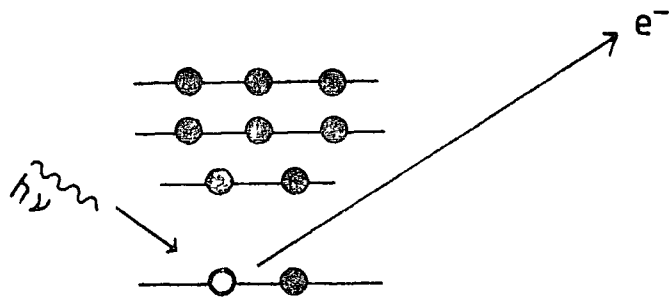

The Photoionisation Process

Figure 2.3.1

For an isolated molecule, that is one in the gas phase the kinetic energy KE of the photo electron is given by:-

$$KE = h\nu - \beta E - E_r \qquad 2.3.1$$

where h is Plank's constant, ν is the frequency, βE is the binding energy of the photo electron and E_r is the recoil energy of the atom or molecule. The recoil energy E_r is usually negligible for light atoms when using typical X-Ray sources for example Mg $K_{\alpha 1,2}$ and Al $K_{\alpha 1,2}$. Siebahn and co-workers[28] have calculated the recoil energies, using AlK_α (1486.6 eV), for H = 0.9 eV, Li = 0.1 eV, Na = 0.04 eV, K = 0.02 eV and Rb = 0.01 eV. However using high energy X-Rays, for example Ag K_α (22000 eV) the recoil energy of Li is 2 eV and recoil energies for light elements must be taken into account.

Recent studies by Cederbaum and Domcke[29], have shown that modification of the vibrational band envelopes of light elements may also occur. Nevertheless using current routine instruments the recoil energy is usually regarded as negligible and is normally discounted. The kinetic energy for photo electrons from molecules in the gaseous state is therefore taken to be the difference between the energy of the X-Rays ($h\nu$) and the binding energy of the electrons. Equation 2.3.1 therefore becomes:-

2.3.2 $KE = h\nu - BE$

And the binding energy of the electrons is obtained from measuring the kinetic energy of the electrons and subtracting this from the kinetic energy of the X-Rays.

2.3.3 $BE = h\nu - KE$

The situation when dealing with solids is slightly more complex and binding energies are referred to the Fermi level[30]. The relationship between the binding energies for solid and gaseous samples will be dealt with more fully in section 5 of this Chapter.

The cross section for photoionisation for a particular electron varies with photon energy[27,28,31] and valence electron spectra studied by ultra-violet electron spectroscopy and ESCA show considerably different intensity ratios.

Several processes may accompany photo ionisation and these may be divided into two main categories depending upon whether they are slow compared to the original photo ionisation or occur within a similar time span. Electron

relaxation, shake up and shake off occur within a similar time span and result in modification of the kinetic energy of the photo electrons. Auger emission and X-Ray fluorescence are comparatively slow processes and cause little effect on the kinetic energy of the photo electrons.

b) Electronic Relaxation

The photo emission process is complete within a time span of approximately 10^{-18} seconds[32] and accompanying this there is a substantial electronic relaxation of the valence electrons[33,34,35]. Theoretical and experimental studies have shown that the relaxation energy is a sensitive function of the electronic environment of a molecule[36-40]. Using the Hartree-Foch formalism calculations have been carried out using Koopmans' Theorem[41] and by LCAO MO theory[42,43,44] on the neutral and core ionisation states. The disadvantage of Koopmans' theorem is that it implicitly ignores relaxation energies and in many cases gives incorrect binding energies which, if the relaxation energies are sufficiently different, may produce an incorrect ordering of energy levels. The problem of the LCAO MO self consistent field (SCF) methods is that the Hartree-Fock operator itself depends on the one electron eigenfunction. It does though provide, in principle, a formalism for approximate solutions to any desired degree of accuracy.

Relaxation energies associated with core ionisations of first row atoms are considerable[40,45] and are caused by the reorganisation of the valence electrons in response

to the decreased shielding of the nuclear charge. This reorganisation changes the spatial distribution of the remaining electrons, a factor which is not taken into account by Koopmans' Theorem. The change in potential is much larger when a core electron is ionised than when a valence electron is ionised since core electrons have a larger screening coefficient. This is shown by the fact that relaxation energies for core electrons are approximately an order of magnitude greater than for valence electrons. Thus calculated values for the relaxation energies for the C_{1s} and $C_{1\pi}$ orbitals in CO, using LCAO MO SCF, are 11.4 eV and 1.8 eV respectively[40,45].

The differences between relaxation energies for closely related molecules are small and therefore they only cause small changes in binding energies. Thus Koopmans' Theorem and ΔSCF calculations give similar estimates for shifts even though Koopmans' Theorem does neglect electronic relaxations[40].

c) Shake Up and Shake Off

The ejection of a core electron, with its large shielding effect is accompanied by substantial electronic relaxation. There is also the probability that the photo ionisation will be followed by the simultaneous excitation of a valence electron so that either it moves to an unoccupied orbital (shake up) or it is ejected (shake off).

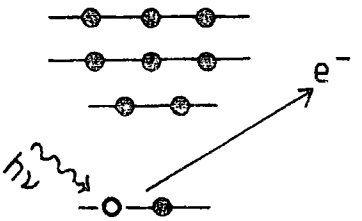

Photoionisation

$M + h\nu \rightarrow {}^{*}M^{+} + e^{-}$

$KE = h\nu - BE$ 2.3.2

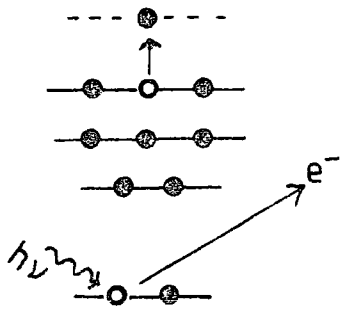

Shake-up

${}^{*}M^{+} \longrightarrow {}'M^{+}$

$KE = h\nu - BE - \bar{E}'$ 2.3.4

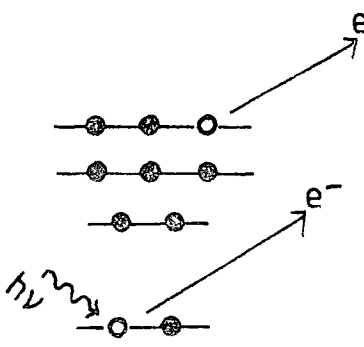

Shake-off

${}^{*}M^{+} \longrightarrow M^{++} + e^{-}$

$KE = h\nu - BE - \bar{E}$ 2.3.5

Figure 2.3.2

The energy for both these processes comes from the original photo ionisation and so there is a need to take the energy($\bar{E}$ and $\bar{E}'$) into account in considering the kinetic energy of the photo electron.

It may be shown that the shake up process obeys monopole selection rules,
as indicated on equations 2.3.6 - 2.3.8

$$\psi_i = \sum_{u=1} C_{ui} \phi_u \qquad \ldots 2.3.6$$

$$\psi'_f = \sum_{v=1}^{n} K_{vf} \phi'_v \qquad \ldots 2.3.7$$

$$P_{f \leftarrow i} = N \left| \sum_{u=1}^{n} K_{uf} C_{ui} \langle \phi'_u | \phi_u \rangle \right|^2 \qquad \ldots 2.3.8$$

where ψ_i is the initial state wave function

and ψ'_f is the final state wave function.

In some ways shake up may be regarded as an analogue of ultra-violet spectroscopy but this analogy should not be taken too far.

The relationship between shake up, shake off and electronic relaxation energies was first established theoretically by Manne and Åberg[46]. They showed that the weighted mean of the direct photoionisation, shake up and shake off peaks corresponds to the binding energy of the unrelaxed system.

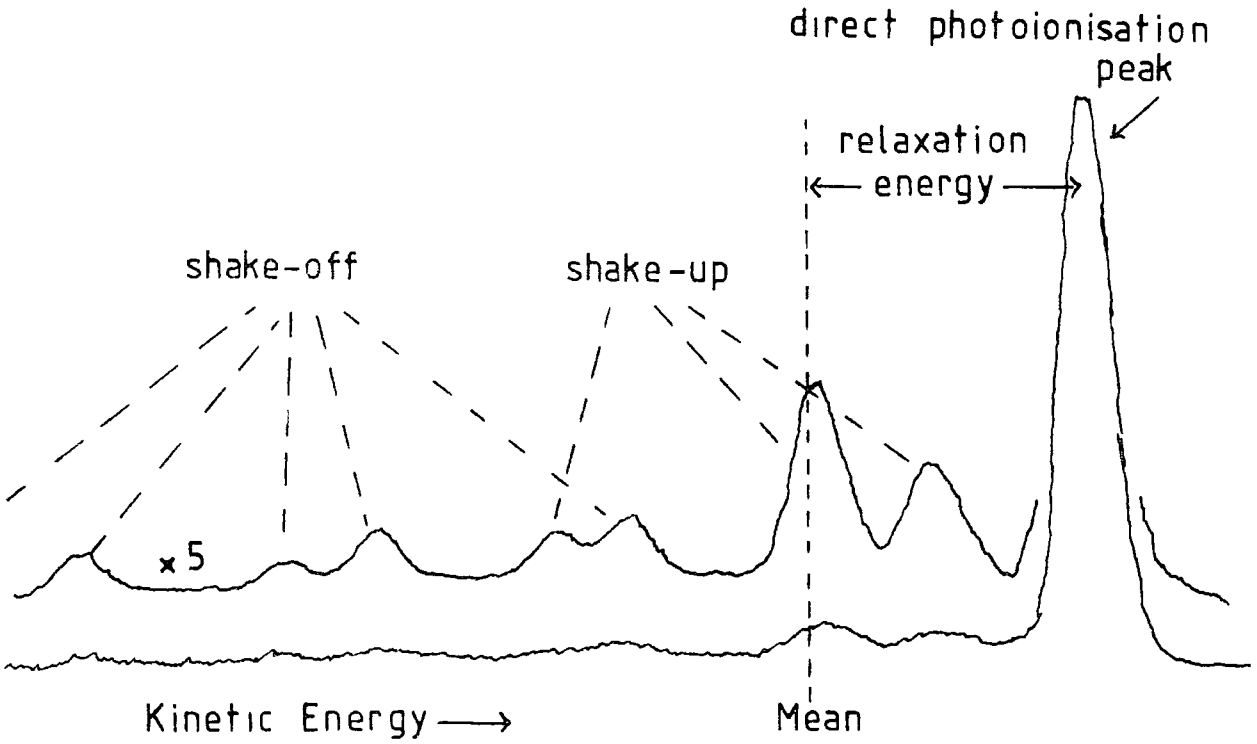

Relationship between relaxation energy, Koopmans' Theorem (mean) and the relative intensities of direct photoionisation, shake-up and shake-off

Figure 2.3.3

The transition probabilities for high energy shake off processes are relatively small compared to the shake up processes, which are usually of lower energy and these transitions of higher probability fall reasonably close to the weighted mean. In principle the relaxation energy should be available from experimental data of direct photo-ionisation, shake up and shake off but in practice this is not so. The problem arises from the presence of the "inelastic tail" which is caused by the direct photo electrons losing energy by a variety of inelastic processes. This produces a broad energy band which peaks at

approximately 20 eV below the direct ionisation peak. This inelastic tail effectually obscures many of the much smaller shake off peaks and so calculations of relaxation energies from experimental data are not possible. In general all systems should show shake up and shake off peaks but due to the inelastic tail only those systems that give relatively high intensity low energy shake up will produce these peaks in their spectra.

Shake up and shake off structure has been studied in organic[47,48] and inorganic[49,50] materials with particular attention being paid to 'd' block elements. The subject of shake up effects has been the subject of a recent review[51].

d) Auger and X-Ray Fluorescence Spectroscopies

The ejection of a core electron by an X-Ray photon leaves a hole in that atom and the de-excitation of the hole state can occur by X-Ray fluorescence and Auger electron emission. Both these processes are comparatively slow compared to the photo ionisation and so they do not have much effect on the kinetic energy of the original photo electron.

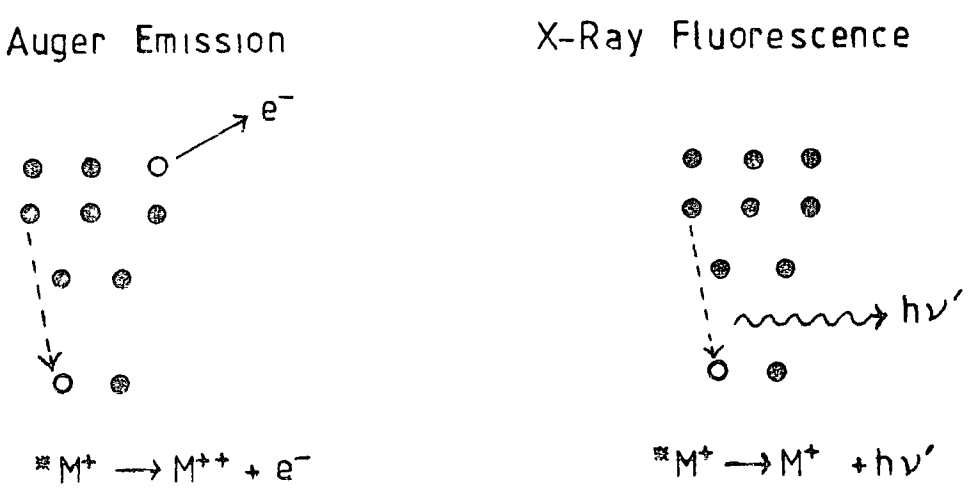

Figure 2 3 4

In Auger electron emmission an electron drops from a higher level (energetically) to fill the core hole and at the same time an electron is ejected from the atom. When the electron drops from a valence orbital the Auger spectrum is related to the energies of both the valence and core orbitals. When the electron drops from an inner orbital, a Coster-Kronig transition[52], the Auger spectrum is related to the inner orbital transition. Such spectra are often very well resolved[52,53], but unfortunately cause a broadening of the ESCA spectrum due to the very short lifetime of the process. For a Coster-Kronig process to occur the energy difference between the orbitals must be sufficient to be able to eject an electron from a higher orbital. Because of this limitation Coster-Kronig processes are only observed in elements with atomic numbers less than 40.

The other process of de-excitation, X-Ray fluorescence, is not very efficient for lighter elements but is a higher probability process for atoms with atomic numbers greater than $\sim$ 35 (see figure 2.3.5 below).

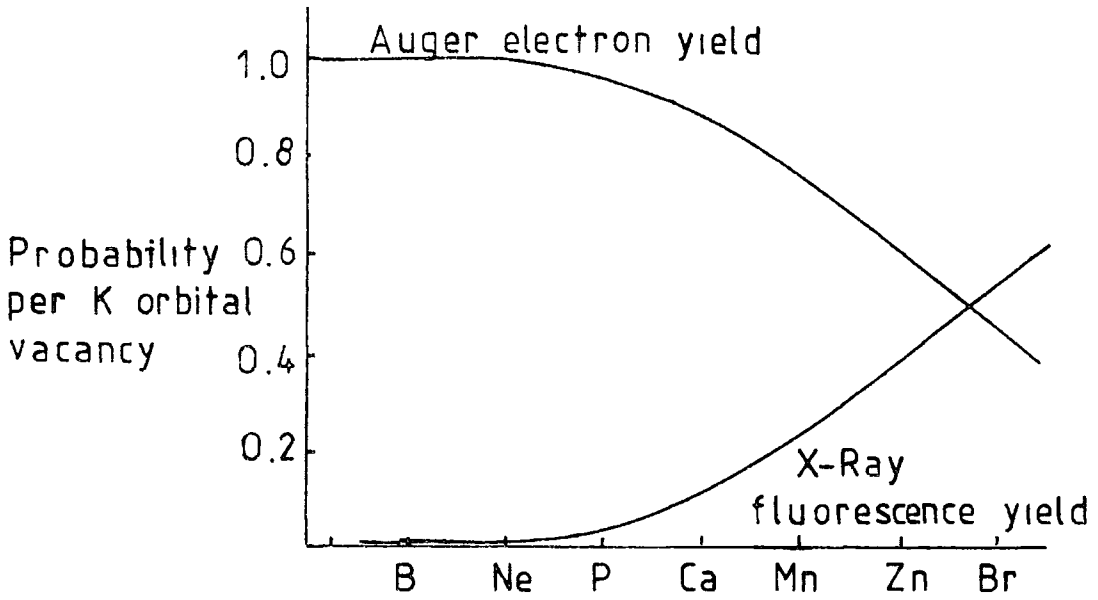

X-Ray Fluorescence and Auger electron probabilities as functions of atomic number

Figure 2.3.5

The probability of Auger emmission and X-Ray fluorescence is a function of atomic number[28] and is illustrated in figure 2.3.5 above. It can be seen that Auger emmission is important for lighter elements while X-Ray fluorescence is more important for heavier atoms[54].

Auger electron spectroscopy as such uses an electron beam of typically 2 k eV rather than X-Ray photons. The technique is very much one of surface analysis since the penetration depth of the exciting electrons is only about 5 atomic layers or approximately one nanometre[55]. It is very sensitive and it is possible under ideal conditions

to detect concentrations of atoms down to the level of approximately 10^{15} atoms m^{-2} (the surface packing of many solids is of the order of 10^{19} atoms m^{-2}). However, the incident beam of electrons in Auger spectroscopy is approximately three orders of magnitude greater in flux than a normal ESCA photon beam. Therefore although Auger spectroscopy is very useful for studying the surfaces of metals and semiconductors the radiation damage[56] caused to organic materials presents a severe problem when studying polymers.

X-Ray fluorescence spectroscopy is a good method of qualitative analysis[54] for elements with atomic numbers greater than ten. Concentration down to 0.1% may be routinely determined and under favourable conditions concentrations down to 0.01% may be determined for heavier atoms. As a surface technique X-Ray fluorescence suffers from the disadvantage that it samples a relatively thick layer, for example using 100 kV X-Rays the sampling depth may be of the order of 100 micrometres, or 1 million atomic layers. Where the element being measured is known to lie in the surface layers ($\leqslant$ 10 atomic layers) it is quite a useful technique and from a sample area of 1 cm^2 concentrations of between 0.1 to 10 micrograms may be detected. This corresponds approximately to a monolayer at the surface[57].

.4 ESCA Instrumentation

The work in this thesis was carried out on an AEI ES 200 AA/B spectrometer, a schematic diagram of which is given below.

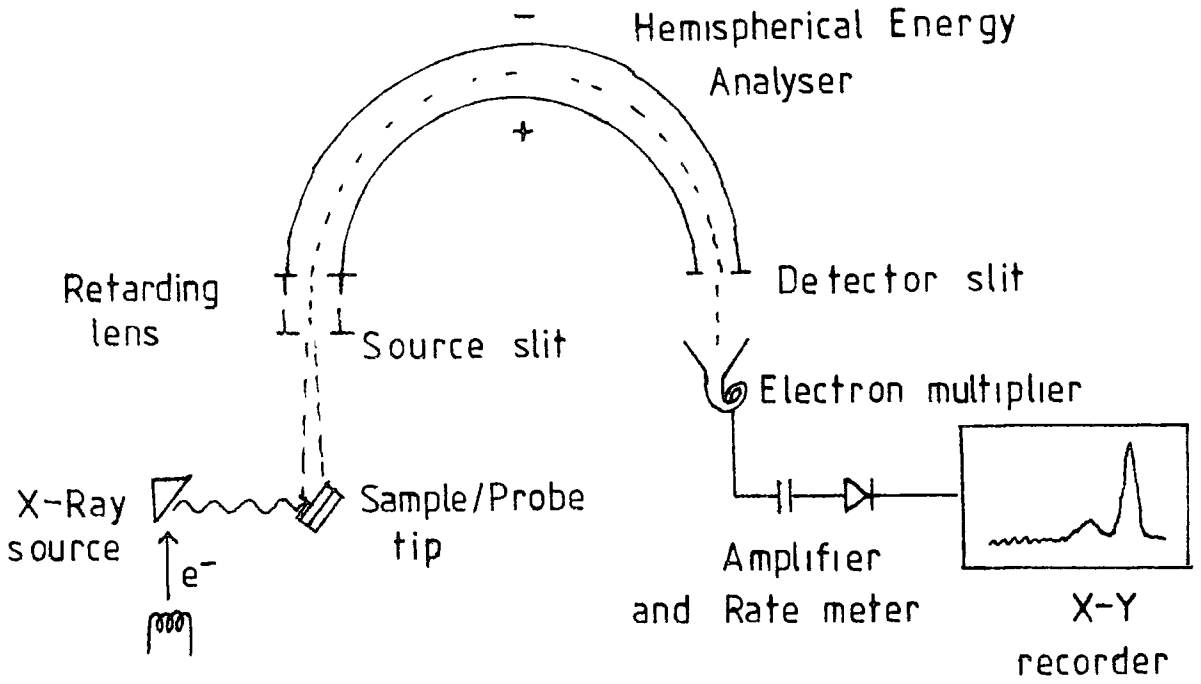

AEI ES 200 AA/B Spectrometer

Figure 2.4 1

a) X-Ray Source

The high voltage supply is from a Marconi Elliott GX 14 unit with integrally variable voltage, 0-60 kV and current, 0-80 mA. The spectrometer itself is equipped with two X-Ray sources of hidden filament of Henke design[58]; a a non-monochromatised Mg $K_{\alpha 1,2}$ and a monochromatised $AlK_{\alpha 1,2}$. The monochromator for the $AlK_{\alpha 1,2}$ uses slit filtering[36] and diffraction from the $10\bar{1}0$ plane of quartz at the Bragg angle of 78.3°. Monochromators used on other

machines may use this system or dispersion compensation or "fine focussing"[59].

The operating conditions and characteristics of the two X-Ray sources are given below.

	Anode Voltage	Anode Current	X-Ray Energy	FWHM	Wavelength
Mg Anode	12 kV	15 mA	1253.7 eV	0.7eV	
Al Anode	15 kV	35 mA	1486.6 eV	0.9eV	834 pm

Using the monochromator the line width of the AlK_{α} is reduced to approximately 0.3 eV but at the same time the intensity is also greatly reduced.

For the work in this thesis only the Magnesium anode was used. The X-Ray spectrum for a tungsten anode is shown below[60].

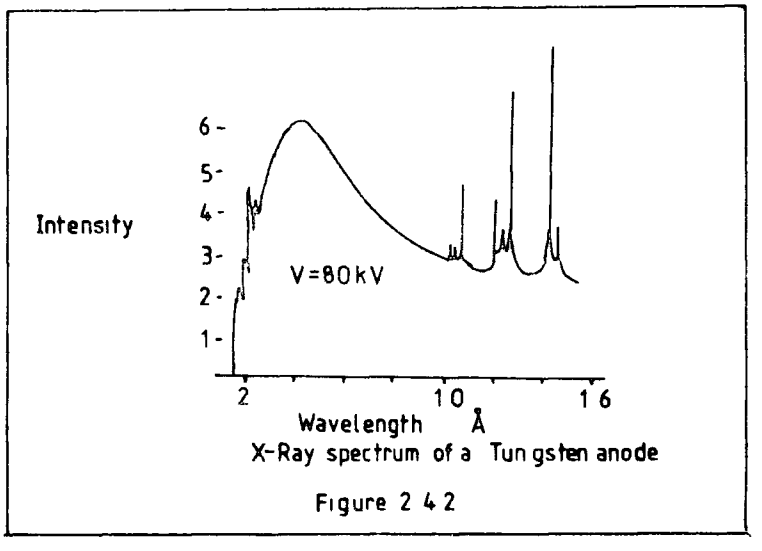

Figure 2 4 2

The spectrum consists of the characteristic line spectrum superimposed on a continuum (bremstrahlung), the shape of which depends only on the energy of the electrons

and not on the anode material. The cut off frequency ν_o is obtained from the expression:-

$$h\nu_o = E \qquad 2.4.1$$

where h is Plank's constant and E is the electron kinetic energy. The total X-Ray energy per electron, E_T, is found by integration over all of the continuum and is given by

$$E_T = k\ ZE^2 \qquad 2.4.2$$

where $k = 0.7 \times 10^{-4}$ when E_T and E are expressed in MeV and Z is the atomic number of the anode material. The fraction of the electron kinetic energy that is converted is therefore given by:-

$$E_{T/E} = k\ Z\ E$$

For a magnesium anode and voltage of 12 kV E_T/E is only about 10^{-3}%.

The magnesium anode is isolated from the sample chamber by a thin aluminium window to prevent interference due to electrons from the filament. In order to reduce the risk of scattered electrons exciting X-Ray radiation from the aluminium window the filament is operated at near ground potential (+ 10V) and the anode at high positive potential.

b) The Sample Chamber

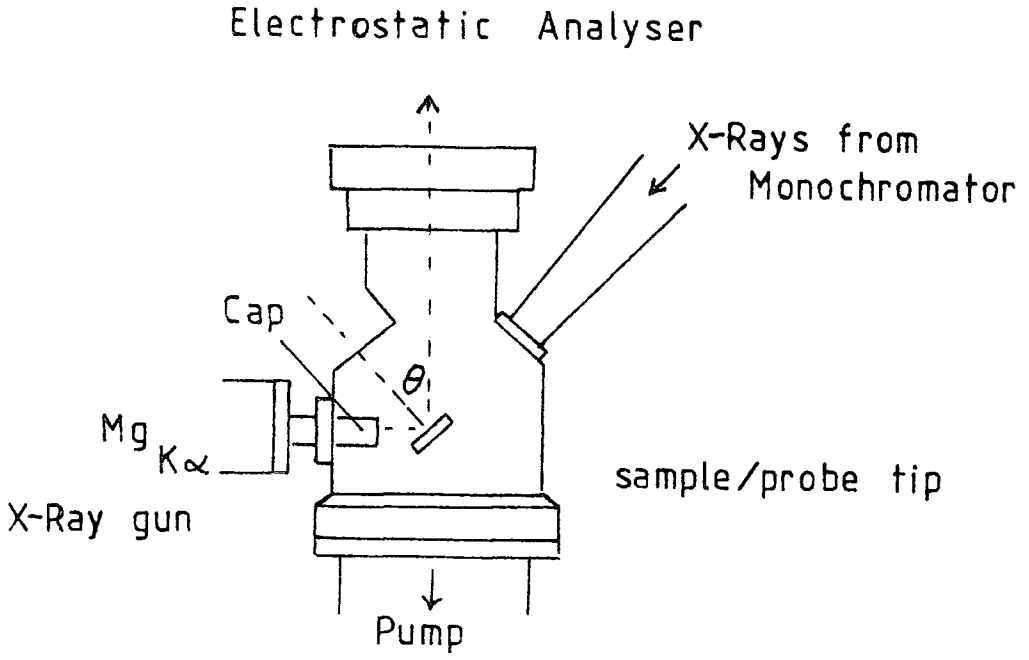

Relative positions of X-Ray sources, sample and electron energy analyser

Figure 2.4 3

The sample chamber has several access ports for sample introduction and treatment facilities. Two of the ports are equipped with insertion lock systems with high vacuum gate valves which enable probes to be inserted without having to let the whole system up to atmospheric pressure. It does however limit the normal operating pressure in the sample chamber to approximately 10^{-8} torr though under favourable conditions a pressure of the order of 10^{-9} torr is obtainable. By using the probes samples may be entered easily into the sample chamber and also angular

studies (see section.6) may be carried out.

c) Sample Handling

Solid samples are usually mounted on the tip of a sample probe by means of double sided "scotch" insulating tape, in the case of powders by pressing the powder onto the tape and then tapping off the excess that has not adhered.

Solids that dissolve readily in a solvent may be solution cast onto a piece of gold foil. Since ESCA is a surface sensitive technique it is important to use clean apparatus and pure solvents containing no involatile residues which would be included on the surface on evaporation of the solvent. It is also important to ensure that no solvent remains bonded to the solid after evaporation. Solids that will sublime without decomposition may be sublimed onto a piece of gold foil. The piece of gold with either the solution cast or sublimed film may then be fixed to the probe tip by small metal screws or double sided "scotch" tape. One problem that the use of "scotch" tape causes is that of sample charging, a matter that is dealt with in section .5 of this chapter. By using a probe tip that can be cooled volatile solids may be studied, without this facility the heating effect of the X-Rays would soon cause them to sublime under the vacuum conditions. A cooled probe also allows liquids to be handled as they may be inserted via the second insertion lock using a reservoir shaft or direct inlet shaft and then

condensed on the probe tip, which may be cooled with liquid nitrogen. The probe available on this instrument has a variable temperature control and may be operated at temperatures from liquid nitrogen to + 400°C.

Siegbahn has developed two techniques where liquids and solutions may be studied as submillimeter beams[61] or as a film on a wire loop[60] passing through the X-Ray beam and continually being wetted by the liquid.

Gases may be studied by condensing onto the cooled probe in much the same way as liquids. Some electron spectrometers have however the facility to study molecules in the gas phase in which case liquids may also be studied by the same method. ESCA studies carried out using molecules in the gas phase have the following advantages[36] compared to studies using solids.

i) There is no inherent broadening of the levels due to solid state effects.

ii) Problems of sample charging are removed.

iii) Increased signal to noise ratio.

iv) Radiation damage is of less importance unless the sample is recirculated.

v) By mixing with standard gases peaks may be readily calibrated.

vi) There is the possibility of distinguishing between inelastic losses and shake up and shake off by varying the sample pressure.

vii) Direct comparison with theoretical calculations is made easier.

When a sample has been in the ESCA instrument for an appreciable time (of the order of an hour) it is often observed that there is an appreciable build up of hydrocarbon contamination. It has been found that most of this contamination comes from hydrocarbons "boiling off" the X-Ray cap and contaminating the sample[62]. By cooling the X-Ray cap much of this contamination can be eliminated and on the instrument used this is normally done by water. Notwithstanding this, a small amount of such contamination may be of advantage as a reference peak (see section .5).

d) Electron Energy Analyser

The electron energy analyser used on the ES 200 is based on the principle proposed by Purcell[63] in 1938 and is a hemispherical double focussing electrostatic analyser which is totally enclosed by a mu-metal field to eliminate any magnetic interference. The electron energy analyser needs to have a resolution of 1 in 10^4 in order to carry out ESCA studies. The resolution of the analyser $\Delta E/E$ depends on the mean radius of the hemispheres, R, and on the combined width of the source and collector slits W.

$$\Delta E/E = \frac{R}{W}$$

To improve the resolution three things may be done:-

i) Reduce the slit widths W, which reduces the signal intensity,

ii) Increase the mean radius R of the hemispheres which increases the engineering costs and the overall pumping requirements,

iii) Reduce the kinetic energy E of the electrons before they enter the electron analyser.

A compromise has therefore to be made on these three and so the slit widths are adjusted to give sufficient signal intensity while the ES 200 AA/B uses a retarding lens to slow the electrons down before they enter the analyser. This enables the size of the two hemispheres to be kept to a reasonable size so as to reduce mechanical distortions and to keep engineering costs down. The retarding lens used in fact serves two purposes:

i) By reducing the kinetic energy of the electrons the resolution requirements on the analyser are reduced[64].

ii) By increasing the distance between the sample chamber and the analyser there is more flexibility for sample handling. The analyser is physically large and would seriously impede sample handling if this separation did not exist.

Electrons entering the analyser with the required kinetic energy may be focussed at the detector slit by one of two methods:

i) by scanning the retarding potential to the lens and keeping the potential difference between the two hemispheres constant. This means that the detector slit receives electrons with constant kinetic energy and this method gives greater sensitivity at kinetic energies of less than

500 eV. This method of operation normally operates with the electron emerging from the analyser with kinetic energies of either 65 or 130 eV.

ii) By simultaneous scanning the retarding potential applied to the lens and the potential difference between the two hemispheres. This method gives a greater sensitivity at higher electron kinetic energies and is the method used on this ES 200 AA/B.

The overall resolution $\Delta E_M/E$ of the system depends on a number of other contributions as well as the resolution of the analyser. For a solid sample and assuming Gaussian line shapes ΔE_M can be calculated from

$$(\Delta E_M)^2 = (\Delta E_x)^2 + (\Delta E_{Cl})^2 + (\Delta E_s)^2 + (\Delta E_{ss})^2 \quad \ldots 2.4.3$$

where ΔE_x is the line width of the X-Ray radiation line.

ΔE_{Cl} is the natural width of the electron energy in the level being studied.

ΔE_s is the line broadening due to spectrometer irregularities, which may vary with electron emission energy E, and slit widths. The ΔE_{ss} is the line broadening due to solid state effects in the sample.

Of these contributions the only ones which can be varied to any degree are ΔE_x by using a monochromator and ΔE_s by varying the source and collector slits.

e) Electron Detection and Data Acquisition

The electrons focussed by the analyser pass through the collector slit and then enter an electron multiplier. The output from the multiplier is then amplified and fed into a data handling system. In view of the focal plane properties of the double focussing analyser it would be feasible to use a multichannel detector system to observe simultaneously many different spectral peaks. Such a system would bring about substantial increases in the speed of data acquisition and would enable real-time investigation of changes in materials.

The signals from the electron detection and amplifying system may be handled in one of two ways.

i) The kinetic energy of the photo electron is scanned continuously from a fixed kinetic energy until another predetermined higher kinetic energy is reached. The signal from the amplifier may be fed into a ratemeter or recorded on an X-Y recorder directly against the kinetic energy of the electrons. In this case a graph of electron counts per second versus kinetic energy of the electrons is obtained.

ii) The kinetic energy of the electrons passing through the analyser is scanned stepwise from a fixed kinetic energy to another higher predetermined kinetic energy. The increments are typically 0.1 eV and at each increment

the counts may be measured for a fixed time or a fixed number of counts may be timed. The data obtained is then stored in a multi-channel analyser and usually the process is set to repeat automatically for a fixed number of scans. This enables signal to noise ratios to be enhanced since the signal increases in proportion to the number of scans while the noise, which is a random fluctuation, only increases in proportion to the square root of the number of scans.

In both of these methods where the time of data acquisition is long (of the order of an hour) long term sample changes may have to be considered. For example, hydrocarbon contamination may alter peak ratios and time dependent sample charging may produce erroneous spectra.

.5 Calculation of Binding Energies

a) Binding Energy

The reference level in ESCA is taken to be the vacuum level for gases, and the binding energy of an electron is defined as the energy required to remove the electron from the orbital it is in to infinity (vacuum level). The binding energy of the electron in an ESCA experiment is then given by equation 2.3.3. In the case of solids however the outer electronic levels are broadened into bands, and a potential barrier exists at the surface. It is therefore more convenient to refer the binding energies to the Fermi level[28]. The Fermi level E_f is defined by

$$\int_0^{E_f} N(E)\,dE = N \qquad \ldots 2.5.1$$

where $N(E) = Z(E) \cdot F(E)$. $Z(E)$ is the density of states for electrons, that is the number of energy levels between E and $E + \Delta E$, $F(E)$ is the Fermi probability distribution, that is the probability that a Fermi particle in a system in thermal equilibrium at temperature T will be in a state with energy E.

$$F(E) = (e^{(E-E_f)/kT} + 1)^{-1}, \quad kT \ll E_f \qquad 2.5.2$$

N is the total number of electrons in the system and the electrons fill the available states up to the Fermi level.

The work function ϕ_s of a solid is defined as the energy gap between the free electron (vacuum level) and the Fermi level in the solid. The vacuum levels for the solid and the spectrometer may be different and the photo electrons will therefore experience a retarding or accelerating potential equal to $\phi_s - \phi_{spec}$, where ϕ_{spec} is the work function of the spectrometer.

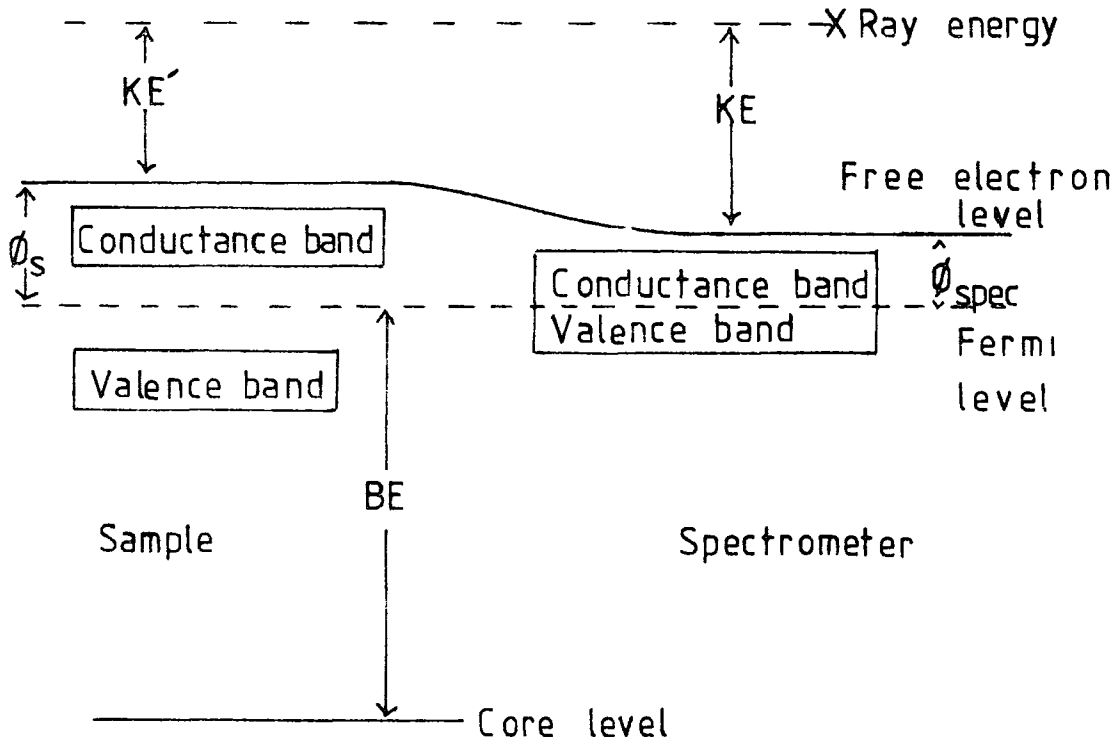

Relationship between the kinetic energy of photo-electrons, binding energy and the work function of sample and spectrometer

Figure 2 5.1

The kinetic energy KE, of the electrons when they enter the analyser will therefore be slightly different from the kinetic energy KE′ with which they are ejected from the sample. However provided the sample and the electrometer are in electrical contact their Fermi levels can adjust to the same level and the binding energy of the electrons can be calculated from

$$BE = h\nu - KE - \phi_{spec} \qquad 2.5.3$$

The binding energy of the electrons can therefore be found without knowing the work function of the sample since it depends on that of the spectrometer which will be a constant correction to all binding energies and for different samples. Metal samples may easily be made to have electrical contact with the spectrometer but in the case of insulating materials it is often assumed that the X-Ray radiation will produce sufficient charge carriers so that the Fermi levels can adjust to thermodynamic equilibrium. However in many instances, for example, with polymer samples, this is not so and the sample may become electrically charged. For the polymers studied in this thesis sample charging, for instance, was often found to produce shifts of the order of 3 or 4 e-volts (see Chapter 4).

b) Sample Charging

The presence or absence of sufficient charge carriers may be shown by applying a D.C. bias to the sample holder. If the sample holder is in electrical contact with the sample the shift in energy scale will follow the applied D.C. bias voltage[65]. This technique is equally suitable for use with conducting materials and Ascerelli and Missoni[65] have used the technique to determine the position of the vacuum level.

Several investigations have shown that the primary photo electrons are rapidly slowed down by the interaction with matter and can generate intense currents of slow

secondary electron clouds at the surface of the sample[66,67,68]. These secondary electrons play an important role in establishing the electrical equilibrium at the surface of the sample. They have been found to make up approximately 20% of the photo electron flux in a conducting sample and 99% of the flux in an insulating sample. Where these secondary electrons are insufficient to remove sample charging and electrical equilibrium is not achieved it is possible to use electron 'flood guns'[69] to make up the deficiency. The removal of bremsstrahlung by monochromators very considerably reduces the supply of secondary electrons and sample charging with thick insulating samples may prpduce a shift in kinetic energy of several hundred electron volts. The use of an electron flood gun will alleviate this but it is of course possible to negatively charge an insulating sample and it is not easy to control the amount of electrons with sufficient accuracy compared to other methods. An alternative way of producing low energy electrons is to illuminate the interior of the sample chamber with U.V. radiation from a low pressure, low power mercury lamp via a quartz viewing port[70]. Sufficient secondary electrons are produced by photo-emission from the metal surfaces to reduce sample charging to a low level. It has been shown by Clark, Dilks, et al[71,72] that sample charging far from being merely a nuisance, can be used to give other important information. They distinguished between time dependent and equilibrium

surface charging and were able to show that for samples insulated from the spectrometer the equilibrium charge was a function of the photoionisation cross section. As an example of the use of this it is possible to compute, for different organic polymer structures, relative photo ionisation cross sections per unit area for the different structures. Measurements of equilibrium surface charging enable information to be obtained then concerning the structure of different polymer specimens. Their studies of time dependent surface charging showed that the charging at first increased and then decreased to an equilibrium value and from this they deduced that hydrocarbon contamination steadily increased with time of exposure to the X-Ray flux. The fact that sample charging slowly changes with time is a factor that must be taken into account when the time taken to record spectra is appreciable and in some instances, polytetrafluoroethylene for example, it is better to wait until equilibrium is reached. The sample charging, SC, of a specimen is defined according to equation 2.5.21 below,

$$h\nu = BE + KE + SC \qquad 2.5.21$$

c) Absolute Binding Energies

Theoretical calculations are usually for isolated molecules in the gas phase and the reference level is taken as the vacuum level. Measurements, however, are often made on solids where the Fermi level is the reference level and so it is of some value to know what the connection is between the two reference levels. For core

ionisations from an atom A in a molecule AB the binding energies in the solid and the vapour may be compared using a Born-Haber cycle. The various stages in the Born-Haber cycle are shown in figure 2.5.2 below.

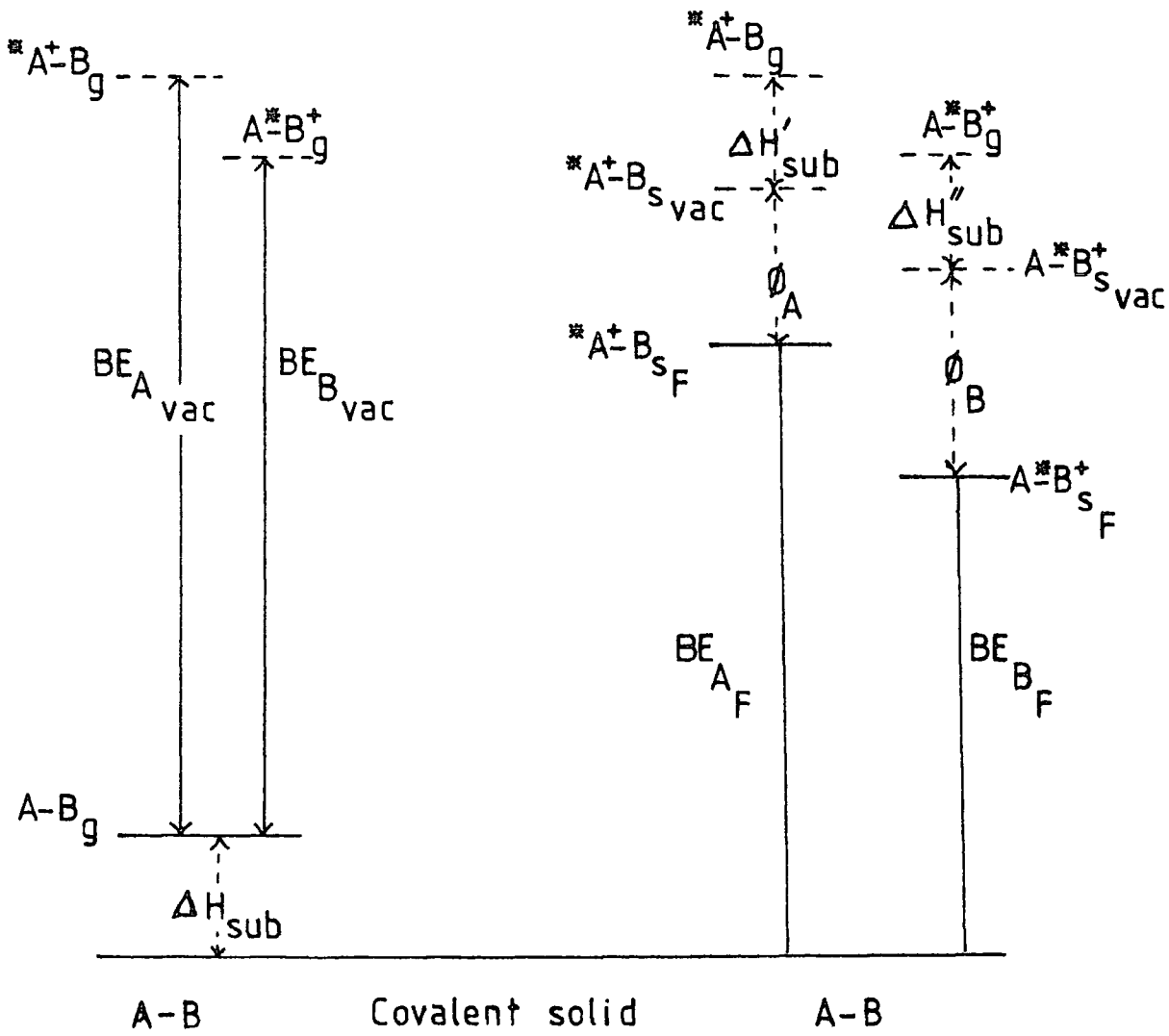

Relationship between binding energies measured in solid and gas phases for a covalent substance A-B

Figure 2.5.2

$$A\text{-}B_s \rightarrow A\text{-}B_g + \Delta H_{sub} \qquad 2.5.3$$

$$A\text{-}B_g \rightarrow {}^*A^+\text{-}B_g + e^-_{vac} + BE_{A\ vac} \qquad 2.5.4$$

$${}^*A^+\text{-}B_g \rightarrow {}^*A^+\text{-}B_s - \Delta H'_{sub} \quad \text{(in solid A-B)} \qquad 2.5.5$$

$$e^-vac \rightarrow e^-_{Fermi} - \phi_A \qquad 2.5.6$$

from which

$$A\text{-}B_s \rightarrow {}^*A^+\text{-}B_s + \Delta H_{sub} - \Delta H'_{sub} - \phi + BE_{A\ vac} \qquad 2.5.7$$

(in solid A-B)

$$\text{But } A\text{-}B_s \rightarrow {}^*A^+\text{-}B_s + BE_{A_F} \text{ (in solid A-B)} \qquad 2.5.8$$

$$\text{and therefore } BE_{A_{Vac}} + \Delta H_{subs} = BE_{A_F} + \phi_A + \Delta H'_{sub} \qquad 2.5.9$$

The binding energy difference between solid and vapour therefore depends not only on the work function ϕ of the solid but also on the energy required to remove a molecule from the solid, ΔH_{sub}, and on the energy of placing the core ionised species back into the solid, $\Delta H'_{sub}$. Although actual binding energies are higher for gaseous molecules than for those measured on solid samples the shifts in binding energies for different atoms in the molecule in both gaseous and solid phases are similar.

Thus from equation 2.5.9

$$\Delta BE = \left(BE_{A_{vac}} - BE_{B_{vac}} \right)$$

$$= \left(BE_{A_F} - BE_{B_F} \right) + \left(\Delta H'_{sub} - \Delta H''_{sub} \right) + \left(\phi_A - \phi_B \right) \quad \ldots 2.5.10$$

For organic molecules typical values are $BE_{C_{1S_F}} \sim 290$ eV, $\Delta H_{sub} \sim 0.5$ eV and $\phi \sim 5$ eV, chemical shifts, ΔBE, as measured are often of the order 0-10eV.

But $$\left(\Delta H'_{sub} - \Delta H''_{sub} \right) \simeq 0 \quad \text{and} \quad \left(\phi_A - \phi_B \right) \simeq 0$$

and so $$\Delta BE_{vac} \simeq \Delta BE_F \quad \ldots 2.5.11$$

For different samples, X and Y, the shift in binding energies will be

$$\Delta BE = \left(BE_{X_{vac}} - BE_{Y_{vac}} \right) + \left(\Delta H_{X_{sub}} - \Delta H_{Y_{sub}} \right)$$

$$= \left(BE_{X_F} - BE_{Y_F} \right) + \left(\Delta H'_{X_{sub}} - \Delta H'_{Y_{sub}} \right)$$

$$+ \left(\phi_X - \phi_Y \right) + \left(\delta_X - \delta_Y \right) \quad \ldots 2.5.12$$

However for closely related substances

$$(\phi_X - \phi_Y) \simeq 0 \quad \text{and} \quad (\delta_X - \delta_Y) \simeq 0$$

also $$(\Delta H_{X_{sub}} - \Delta H_{Y_{sub}}) - (\Delta H'_{X_{sub}} - \Delta H'_{Y_{sub}}) \simeq 0$$

and therefore $\Delta BE_{XY_{vac}} \simeq \Delta BE_{XY_F}$ 2.5.13

Equations 2.5.11 and 2.5.13 hold to a fair degree of approximation provided that there are no strong intermolecular interactions, for example hydrogen bonding. They do not necessarily hold for ionic lattices which of course contain strong interactions between ions. For ionic solids an analogous series of processes similar to those illustrated in figure 2.5.2 are obtained and considering an ion M with Charge Z in an ionic lattice[62] we have:-

$$M^{Z}_{L} \longrightarrow M^{Z}_{g} + \Delta H_{M_{sub}} \qquad 2.5.14$$

$$M^{Z}_{g} \longrightarrow {}^{*}M^{Z+1}_{g} + e^{-}_{vac} + BE_{M_{vac}} \qquad 2.5.15$$

$${}^{*}M^{Z+1}_{g} \longrightarrow {}^{*}M^{Z+1}_{L} - \Delta H'_{M_{sub}} \text{ (in lattice)} \qquad 2.5.16$$

$$e^{-}_{vac} \longrightarrow e^{-}_{F} - \phi_{M} \qquad 2.5.17$$

From which

$$M^{Z}_{L} \longrightarrow {}^{*}M^{Z+1}_{L} + \Delta H_{M_{sub}} + BE_{M_{vac}} - \Delta H'_{M_{sub}} - \phi_{M} + e^{-}_{F} \qquad 2.5.18$$

But $$M^{Z}_{L} \longrightarrow {}^{*}M^{Z+1}_{L} + BE_{M_F} + e^{-}_{F} \qquad 2.5.19$$

and therefore $$BE_{M_{Vac}} + \Delta H_{M_{sub}} = BE_{M_F} + \Delta H'_{M_{sub}} - \phi_{M} \qquad 2.5.20$$

Processes 2.5.14 and 2.5.16 are similar to lattice energies and in fact 2.5.15 is the lattice energy for a lattice in which interchange of the cations and anions yields an indistinguishable lattice, this is a characteristic of most MX lattices[73]. These "lattice" energies are not simply related to Z and it is unlikely that the heat of sublimation ΔH_{Msub} and the energy of placing the ion back into the lattice $\Delta H'_{Msub}$ will be the same for a common ion in different lattices. Thus while core electron binding energies in gaseous ions have a smooth correlation with Z[71] there is no reason to expect more than a rough correlation between the binding energies in the lattice and the charge Z.

d) Use of Reference Peaks

Given the problems outlined above in .5c, the most convenient technique for finding binding energies is to employ a suitable reference peak. From the observed kinetic energy of the photo-electrons corresponding to the reference peak a correction factor can be simply calculated and the true binding energies of the other peaks can be found. The two most commonly used reference peaks at the present are the C_{1s} peak from carbon in which is taken as 285eV and the $Au_{4f\ 7/2}$ peak, which is taken as 84.0 eV.

The C_{1s} reference material may be deliberately leaked in or added to the original sample, or more commonly arises from hydrocarbon contamination. This is in fact the simplest way for referencing polymers and

such material usually is deposited as a monolayer which acquires the same surface potential as the sample[68].

If the sample has been deposited on gold, either by solution casting or sublimation it may be possible to use the $Au_{4f_{7/2}}$ peak as a reference. This assumes that the layer is thin enough for the gold to show through the spectrum and also that the sample is in electrical contact with the gold. This being the case it provides a very convenient method of energy referencing[75]. An alternative possibility is to deposit the gold on the surface by vapour deposition. There is, when this is carried out, a tendency for the gold to be deposited by a nucleation process which results in "islands" of isolated gold on the surface[76] rather than a smooth monolayer. These gold "islands" on a polymer are electrically isolated from each other and though in general they follow the surface charge and do not react with the polymer exceptions to both these are known. Betteridge and co-workers[77] have shown that in some instances the width and position of the gold signals can change with time, temperature and sample material. In the case of polyethylene and polytetrafluoroethylene decorated with gold Ginnard and Riggs[78] have shown that the absolute shift from the gold signal increases as the gold layer increases in thickness. This is probably due to the higher photo electron flux from the gold which produces a phenomenon known as differential sample charging. Another possible drawback

to the use of gold decoration is that since the gold is normally evaporated from a filament the possibility of surface damage must be considered. This damage may cause surface reactions to occur between absorbed molecules or cross linking and also evaporation of the sample or degradation and loss of small molecules. Therefore, for organic materials and polymers the use of gold decoration is not recommended[79].

Since the factors which determine the absolute and relative binding energies of core electrons, may be shown to be very short range in nature[72] it is sometimes possible to study smaller molecules, containing the appropriate structural features, as thin films in electrical contact with the spectrometer. Such films can then be referenced in a straightforward manner and then using them as models comparisons may be made with thicker insulating materials, containing the same structural features, and thus allowance made for the sample charging.

.6 Features of ESCA Spectra

a) Binding Energies

The core electrons of an atom are essentially localised and do not take part in bonding. Therefore their binding energies are characteristic of the particular element and not of compounds made from them. A knowledge of core binding energies will therefore permit the detection and identification of an element

in a sample[28]. Typical examples of approximate core electron energies for some elements are shown in table 2.6.1.

	Li	Be	B	C	N	O	F	Ne
1s	55	111	188	284	399	532	686	867

	Na	Mg	Al	Si	P	S	Cl	Ar
1s	1072	1305	1560	1839	2149	2472	2823	3203
2s	63	89	118	149	189	229	270	320
$2_{p1/2}$	31	52	74	100	136	165	202	247
$2_{p3/2}$	31	52	73	99	135	164	200	245

Electron Energies/eV

Table 2.6.1

As the atomic number of the element increases there comes a point where not all the core electrons can be ejected using Mg $K_{\alpha 1,2}$ (1253.7 eV) or Al $K_{\alpha 1,2}$ (1486.6eV) X-Ray radiation but there are always core levels that may be studied.

When choosing a core level for study the following factors should be considered:

i) The electrons in the core level should have a high cross section for photo-ionisation in order to maximise the intensity of the spectrum.

ii) The escape depth of the electrons should be taken into account (see part h of this section).

iii) There should be no interference from other peaks in the same region of kinetic energy.

iv) The line width should be narrow. For example, for chlorine it is usual to study the 2p levels rather than the 2s, since the line width of the latter is broadened by the short lifetime of the hole states due to the highly efficient Coster-Kronig relaxation process[53].

v) The peak should stand out well from the background noise, that is, have a high signal to noise ratio. High backgrounds are often produced from the inelastic tail of strong peaks of higher kinetic energy.

vi) In the study of multiplet peaks it is often convenient to study the photo-ionisation from s levels since the interpretation of the data is relatively straightforward. Thus for first row 'd' block elements the 3s level is often studied even though the signal to noise ratio is less favourable compared to the ratio for other levels.

b) Chemical Shifts

Although core electrons are localised on atoms, their energies are sensitive to the electronic environment of the atom[75]. Thus while the binding energy for a core level is characteristic of that element, differences in the electronic environment of an atom in a molecule will produce small shifts in the binding energy. These small shifts are referred to as 'chemical' shifts and are often representative of a particular structural feature.

The classic illustration of this is the C_{1s} spectrum of ethyl trifluoroacetate, the high resolution spectrum of which was produced by Siegbahn's group in 1973 at Uppsala (see figure 2.6.1). Some typical values of chemical shifts are also given on page 61.

The theoretical interpretation of chemical shifts has been carried out by six distinct but inter-related methods:-

i) Koopmans' Theorem

ii) Core Hole Calculations (LCAO MO SCF)

iii) Equivalent Cores Model

iv) Charge Potential Model

v) Quantum Mechanical Potential Model

vi) Many Body Formalism.

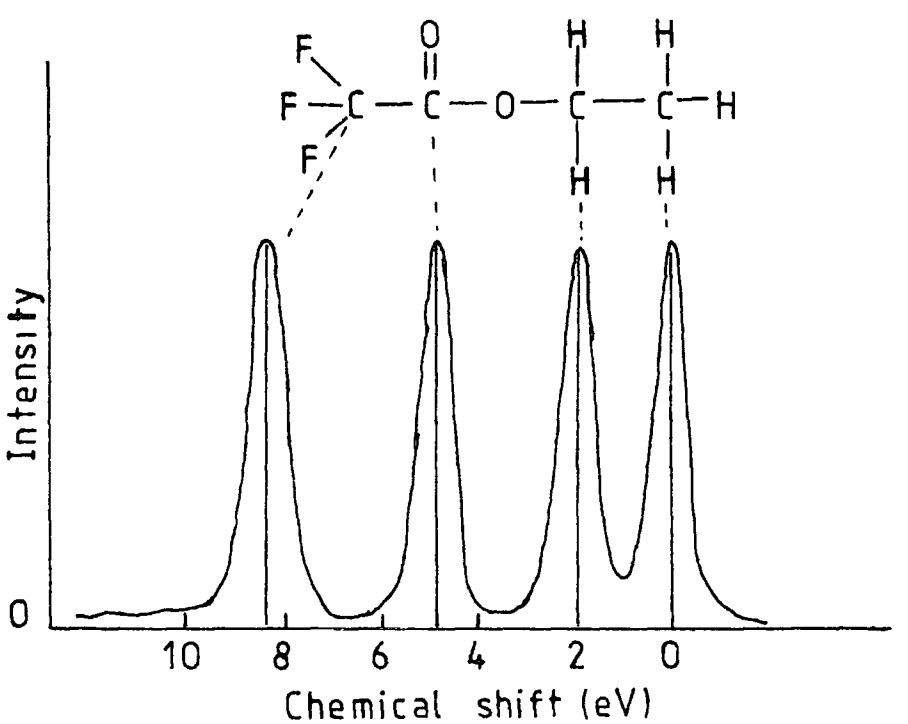

C_{1s} spectrum of ethyl trifluoroacetate

Figure 2.6.1

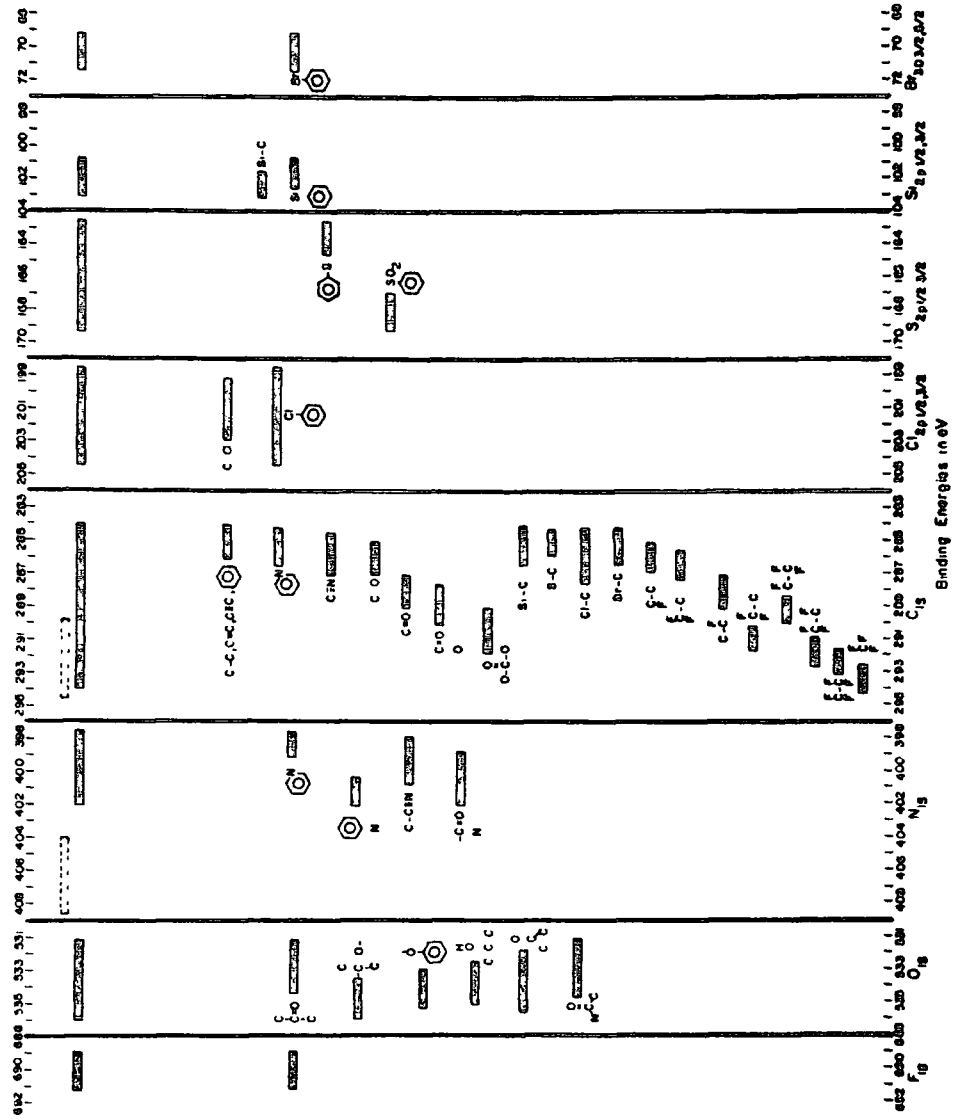
Binding Energy Ranges
Functional Group
Binding Energy Ranges
Binding Energies in eV

i) Koopmans' Theorem[41].

Koopmans' theorem ignores relaxation energies and also relatavistic and correlation energies and calculates binding energies from the ground state properties of the wave functions. The contribution from relatavistic[80] and correlation[81] effects are small for light elements but the neglect of relaxation energy means that absolute binding energies calculated by this method are too large. For a closely related series of molecules, where the relaxation energies are similar, Koopmans' method may give a reasonable correlation for chemical shifts compared with experimental results. However, where relaxation energies differ Koopmans' method can give incorrect values.

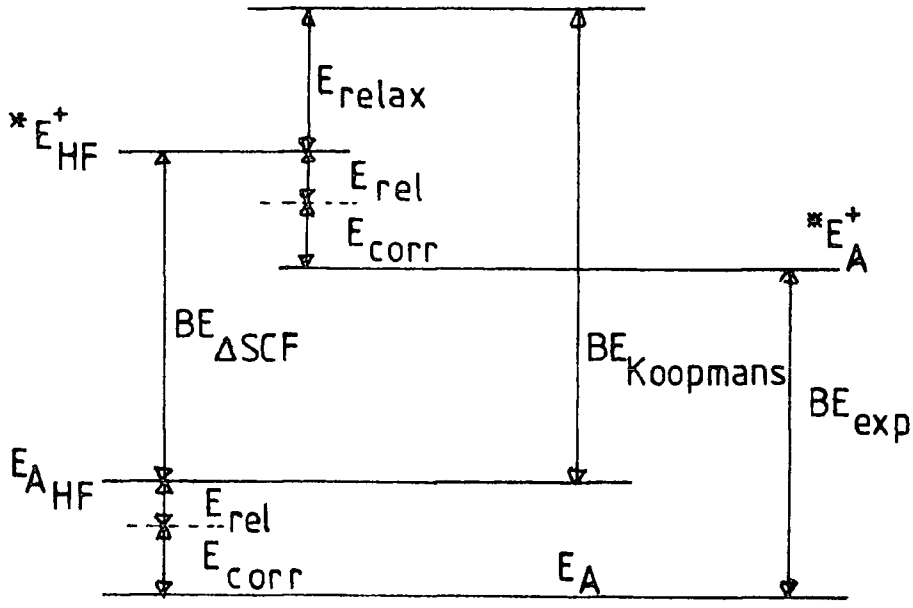

Relationship between Experimental and Calculated Binding Energies for Atom A

Figure 2.62

ii) Core Hole State Calculations

This method, ΔSCF, like Koopmans' ignores relativistic and correlation energies but does take into account relaxation energy. The energy of the ground state molecule and the core hole state of the ion are found by Hartree Fock calculations and from these the binding energy for the reaction is found

$$A \longrightarrow {}^{*}A^{+} + e^{-} \qquad \Delta E = BE$$

The relationship between the experimental, Koopmans' and the core hole state binding energies is shown in figure 2.6.2 from which it is seen that

$$RE = BE_{Koopman} - BE_{Exp.}$$

and $$BE_{\Delta SCF} = BE_{Exp}$$

The core hole state calculations do assume that the computed hole states are orthogonal to all lower energy states of the same symmetry. There seem to be no a priori reasons why this should be so and if it is not then both systematic and random errors may be introduced. However, calculations have been made, in which configurations were "locked" to those of the ground state[82] which suggest that this difficulty does not arise[83]. The calculations of Bagus[34]

on the hole states of neon and argon show that using ΔSCF the inner shell ionisation potentials agreed quite well with the experimental results. Schwartz[84] has carried out a series of calculations using ΔSCF on the first row hydrides and these results are compared to the experimental values obtained by Siegbahn and co-workers[31] in table 2.6.2. The core hole state calculations are in very good agreement with the experimental results and therefore would seem to confirm Bagus' view[34] that simple configuration SCF wave functions can give practical, if not rigorous, values for the upper bounds of the energies of inner orbital hole states.

Molecule	Orbital Energy (Koopmans' Theorem)	Core Hole State (ΔSCF)	Experimental[31]
BH_3	207.3	197.5	-
CH_4	304.9	291.0	290.7
NH_3	422.8	405.7	405.6
H_2O	559.4	539.4	539.7
HF	715.2	693.3	-
Ne	891.4	868.8	870.2

1s Electron Binding Energies/eV

Table 2.6.2

The question arises, when there are several equivalent sites for the core hole in the molecules, as to whether

the core hole is localised or delocalised over the equivalent sites as, for example, the nitrogens in N_2 and the carbon atoms in benzene. Snyder's model[37], based on Slater's shielding constants, predicts that delocalising the hole over t centres would produce a charge of 1/t, and a relaxation energy of $1/t^2$, of the localised hole. This model also predicts a relaxation energy for ionisation from a 1s hole in a nitrogen atom to be 13.7 eV which would be reduced to 6.8 eV for N_2 if the hole were delocalised. These values may be compared with the value, predicted from the experimental results of Siegbahn and co-workers[31], and the results of Cade and co-workers[85], using Koopmans' theorem, of 16.7 eV for the relaxation energy. Further evidence for the localisation of core states is provided by the observation of satellites from the O_{1s} peak of CO_2[86] and from the O_{1s} and outer C_{1s} peaks of C_3O_2[87]. These satellites would not be expected from a delocalised hole since no change in symmetry of the molecule would have occurred and the transitions are only monopole allowed[86].

iii) Equivalent Cores Model

The equivalent cores model was developed by Jolly and Hendrickson[73] to calculate shifts in core binding energies from ground state thermodynamic data. The model assumes that "when a core electron is removed from an atom in a molecule or ion, the valence electrons relax as if the nuclear charge on the atom had increased by one unit". Atomic cores that have the same charge are

considered to be chemically equivalent and interchangeable. The following example shows how the principle may be used to estimate the gas phase shift in the C_{1s} binding energy between carbon atoms in methane and fluoromethane.

The carbon 1s binding energy in methane, BE_{CH_4} is given by the energy of the process

$$CH_4 \longrightarrow {}^*CH_4^+ + e^- \quad \Delta E = BE_{CH_4} \qquad 2.6.1$$

where * indicates a vacancy in the C_{1s} core orbital.

$${}^*CH_4^+ + N^{5+} \longrightarrow NH_4^+ + {}^*C^{5+} \quad E = \delta_0 \qquad 2.6.2$$

This reaction is the exchange of the ${}^*C^{5+}$ core and the equivalent N^{5+} core. Summing reactions 2.6.1 and 2.6.2 gives

$$CH_4 + N^{5+} \rightarrow NH_4^+ + {}^*C^{5+} + e^- \quad \Delta E = BE_{CH_4} + \delta_0 \qquad 2.6.3$$

A similar reaction may be written for CH_3F, (or any other compound containing a carbon atom).

$$CH_3F + N^{5+} \rightarrow NH_3F^+ + {}^*C^{5+} + e^- \quad \Delta E = BE_{CH_3F} + \delta_1 \qquad 2.6.4$$

The difference between the reactions 2.6.3 and 2.6.4 then gives

$$CH_3F + NH_4^+ \rightarrow NH_3F^+ + CH_4 \quad \Delta E = BE_{CH_3F} - BE_{CH_4} + (\delta_1 - \delta_0) \qquad 2.6.5$$

The strong form of the equivalent cores approximation states that $\delta_1 = \delta_0 = 0$ and thus the gas phase shift in the C_{1s} binding energy between methane and

fluoromethane is given by the energy, ΔE, of reaction 2.6.5. However, provided that $\delta_1 = \delta_0$ that is the energy of core exchange is the same and independent of molecular environment, equation 2.6.5 still gives the shift in binding energy. This assumption is known as the weak form of the equivalent cores approximation.

Some typical gas phase data are given in table 2.6.3 and it is seen that in general there is quite good agreement between experimentally observed shifts and those calculated from thermodynamic data[89].

Atomic Core Level	Compound	Experimental Shift /eV	Thermodynamic Data Shift/eV
N_{1s}	NH_3	0	0
N_{1s}	$(CH_3)_2NH$	- 0.7	- 0.7
N_{1s}	CH_3NH_2	- 0.3	- 0.4
N_{1s}	N_2	4.35	3.5
N_{1s}	NO	5.5	4.4
C_{1s}	CH_4	0	0
C_{1s}	CO	5.4	4.1
C_{1s}	CO_2	6.8	6.9
C_{1s}	CF_4	11.0	12.3

Experimental and Thermodynamic
Binding Energy Shifts

Table 2.6.3

The main restriction to the use of the equivalent cores method is the absence and/or unreliability of thermodynamic data especially with regard to the positive ions involved in the reaction. However the heats of reaction may be obtained from SCF calculations on the molecules and ions in their ground states and the theoretical validity of the equivalent cores method has been demonstrated by Clark and Adams[90,91] in their work on small molecules. Pople and co-workers[92,93] have shown that for reactions involving closed shell species even minimal basis set (STO 3G) calculations, which are relatively inexpensive with regard to computer time, can reliably reproduce heats of reaction. The results are particularly accurate in cases where the number and type of bonds, that is single, double, etc., are the same in both reactants and products since the correlation energies are very small. Such processes have been designated as "isodesmic reactions". It is also possible to use semi-empirical calculations, which are comparatively inexpensive with regard to computer time, to calculate heats of reaction and then predict in a qualitative manner the chemical shifts. Thermodynamic data refer to isoelectronic cations with their nuclei in the equilibrium positions, but since photo-ionisation is a rapid process compared to nuclear motion it is more realistic to consider cations with the same geometry as the parent molecule. This condition may be used in molecular orbital calculations

and also by using the same geometry many of the two electron integrals may be retained in ab initio calculations on molecules and iso-electronic cations thus reducing the amount of computing time. When more than one core level of the element is being studied the equivalent cores method will predict the same shifts in binding energy for all the core levels.

iv) Charge Potential Model

The charge potential model relates the core electron binding energies with the charge on the atom on which core ionisation takes place and the potential from the charges on the remainder of the molecule[31]. If a charge is removed or added to the valence level of a molecule the electrostatic potential within the valence shell is changed. When an electron is removed from a valence orbital, radius r to infinity the potential energy within the radius of the orbital is lowered by 1/r and the core ionisation energy is therefore reduced by 1/r. When the electron is not removed to infinity but to another atom, distance R, the lowering of potential energy, and core ionisation energy, is reduced by 1/R. The resulting chemical shift for the core electrons thus becomes

$$\Delta E_{core} = \frac{1}{r} - \frac{1}{R} \qquad 2.6.6$$

In the case of covalent bond formation when the amount of charge transferred is q the chemical shift is given by

$$\Delta E_{core} = (\frac{1}{r} - \frac{1}{R})\ q \qquad 2.6.7$$

In the case of solids lattice effects have to be considered but as far as core electrons are concerned, since orbital overlap is negligible, then to a first approximation neighbouring atoms can be regarded as point charges. Therefore a summation of the point charges in the crystal will give the potential, V_i, at the centre of atom i, and thus the binding energies of the core electron.

$$V_i = \sum_{j \neq i} \frac{q_j}{r_{ij}} \qquad 2.6.8$$

where r_{ij} are the centre to centre inter ionic distances and q_j is the charge on ion j

This model has been extended to covalent compounds by Siegbahn and co-workers[31] who considered the change in potential as arising from a one centre component associated with the change in the number of valence electrons on the atom and a two centre component originating from the electron distribution in the remainder of the molecule.

The chemical shift thus becomes

$$\Delta E_{core} = kq_i + \sum_{j \neq i} \frac{q_i}{r_{ij}} \qquad 2.6.9$$

and the core binding energy

$$E_{core} = E_o + kq_i + \sum_{j \neq i} \frac{q_i}{r_{ij}} \qquad 2.6.10$$

where E_o is a reference binding energy, k is the average interaction between a core and valence electron on the atom, q_i is the charge on atom i and r_{ij} are the inter-atomic distances.

The use of a point charge model assumes that there is no overlap between the core orbitals of the atom considered and the electron orbitals of the other atoms in the molecule. Using this assumption all valence electron CNDO/2 SCF MO[94] calculations have been carried out on quite complex molecules. Good descriptions have been obtained but since the charge potential model may be related to Koopmans' theorem, which neglects electronic relaxation, it suffers from the same defects.

The use of the charge potential model in studies of structure and bonding in molecules is illustrated in figure 2.6.3.

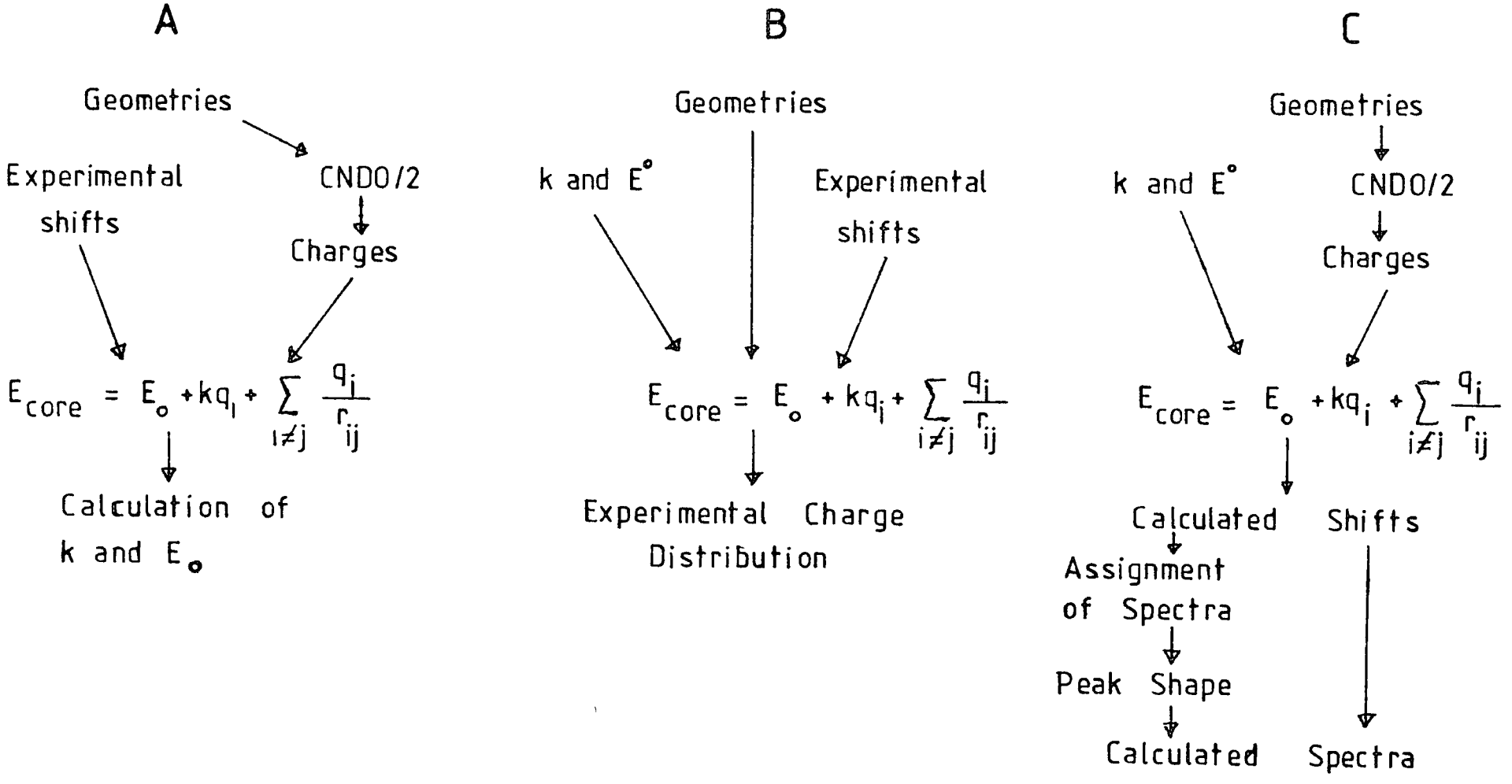

Uses of the Charge Potential Model

Figure 2.6.3

Provided that the geometry of the molecule is known it is possible as in A to calculate the values of k and E_o for a given core level in a particular element. Then using these values of k and E_o and the geometry of other molecules containing the element it is possible to calculate charge distributions as in B. It is also possible as shown in C to use the charge potential model to assign peaks within a spectrum. This is particularly useful when assigning binding energies, which differ only slightly, to various atoms within a molecule. A knowledge of E_o is not important in this case since it is only the ordering of the peaks that is important. Clark and co-workers[95,96,97] have made extensive use of this method of assigning binding energies.

It is worth considering briefly the relationship between shifts in core binding energies and organic chemists' intuitive ideas concerning charge distributions in molecules. Since valence electron distributions in molecules are continuous functions, the assignment of "charges" to atoms within a molecule is somewhat arbitrary and depends on how the overlap density is partitioned between atoms. Theoretically calculated charge densities are therefore only an approximate estimate as to the electron density round an atom. Nevertheless provided its limitations are understood, the idea of charge distributions in a molecule is a useful concept.

v) Quantum Mechanical Potential Model

Since the electron distribution within a molecule is continuous it is somewhat arbitrary to assign electron densities to individual atoms. Schwartz[98] and Basch[99] have developed the potential at the nucleus model as an alternative to the charge potential model. It does however lack the conceptual simplicity of the charge potential model, and another drawback is that it does not include relaxation energies. Davis and Shirley[100] have extended the model to include relaxation energy. The binding energy of a 1s core electron is given by [100].

$$-E_{core\ 1s} \approx \epsilon_{1s} + \tfrac{1}{2} \langle 1s | V_R | 1s \rangle \qquad 2.6.11$$

Where ϵ_{1s} is the orbital energy and V_R is a relaxation potential energy arising from the difference between the Hartree Foch potential V_K of the passive orbital in the final 1s hole state, and the initial state.

From this may be derived

$$-E_{core\ 1s} = \tfrac{1}{2} \left[\epsilon_{1s} + {}^{*}\epsilon_{1s} \right] \qquad 2.6.12$$

where ${}^{*}\epsilon_{1s}$ is the orbital energy of a 1s electron in the hole state.

Writing the orbital energy ϵ, as the sum of the interaction energy of the 1s electron with its own

nucleus, plus a potential energy term for interaction of the 1s electron with other electrons and nuclei gives

$$E_{core\ 1s} = \langle 1s|h|1s\rangle + \langle 1s|V|1s\rangle \qquad 2.6.13$$

The first term in this equation is negligibly small[95], and combining equations 2.6.12 and 2.6.13 gives

$$-E_{core\ 1s} \simeq \tfrac{1}{2}\langle 1s|V + V^{*}|1s\rangle \qquad 2.6.14$$

and the chemical shift between two compounds $\Delta E_{core\ 1s}$ is given by

$$\Delta E_{core\ 1s} \approx -\tfrac{1}{2}\Delta\langle 1s|V + V^{*}|1s\rangle \qquad 2.6.15$$

To a good approximation, the right hand side of this equation can be replaced by the difference in the potential energy at the atomic nucleus $\emptyset$, between one molecule and another. Therefore, for example, for carbon 1s orbitals

$$\Delta E_{core\ C_{1s}} = \frac{e}{2}\Delta\left[\emptyset_{C} + \emptyset_{C^{*}}\right] \qquad 2.6.16$$

Using CNDO calculation it is not possible to calculate ϕ_{C^*} directly, but using the equivalent cores approximation $\phi_{C^*} = \phi_N$ and therefore

$$\Delta E_{\text{core } C_{1s}} = \frac{e}{2} \Delta \left[\phi_C + \phi_N\right] \qquad 2.6.17$$

For carbon atoms good agreement is obtained, both with and without allowance for relaxation effects, but in the case of nitrogen, inclusion of relaxation effects gives much greater agreement between experimental and calculated shifts.

vi) Many body formalism

The calculation of ionisation potentials within the many body formalism using Green's function[101,102], is an alternative to the methods given above. The method takes into account electronic relaxation and correlation effects, but is expensive with respect to computing time, and again, like the quantum mechanical potential model, lacks the conceptual simplicity of the charge potential model.

The method is of most use for valence electron transitions, that is ultra violet photo electron spectroscopy, shake up, shake off and Auger transitions. The calculations give good agreement with experimental results[103].

c) Fine Structure

i) Spin-orbit splitting

When an electron orbital has an orbital quantum number greater than 1, that is a p, d, or f orbital, then coupling can occur between the spin S, and orbital L angular momenta. This coupling causes splitting to occur in the energy level of the orbital, and when photoionisation takes place, a doublet is observed instead of a simple peak. For the lighter elements, up to about the lanthanides, it can be shown that the total angular momentum, J, may be obtained by summing first the individual spin momenta and the individual orbital angular momenta separately. The resulting total spin momentum S_T and orbital angular momentum L_T are then coupled to give a total momentum

$$J_T = L_T + S_T$$

This type of coupling, known as Russell-Saunders Coupling[104], occurs in the lighter elements where the spin-orbit coupling is weak, compared to electrostatic interaction. Where the spin-orbit coupling is strong compared to electrostatic interaction then the individual spin and orbital momenta couple to give a resultant j_i. These individual momenta, j_i, then couple with the electrostatic interactions to give a final momentum J_T. This situation where spin and orbital momenta couple individually and then the resultants couple is known as jj coupling[104].

The relative intensities of the two peaks of the doublets, that are observed, are proportional to the ratio of the degeneracies of the states which is quantum mechanically defined as 2J + 1. The relative intensities of the J states for s, p, d and f orbitals is shown in table 2.6.4.

Orbital	Orbital Quantum Number	Total Quantum Number	Intensity Ratio $(2J' + 1/2J'' + 1)$
s	0	1/2	no splitting
p	1	1/2, 3/2	1:2
d	2	3/2, 5/2	2:3
f	3	5/2, 7/2	3:4

J states for s, p, d and f orbitals

Table 2.6.4

Examples of experimentally observed peaks from C_{1s}, Cl_{2p}, Ag_{3d} and Au_{4f} are shown in figure 2.6.4.

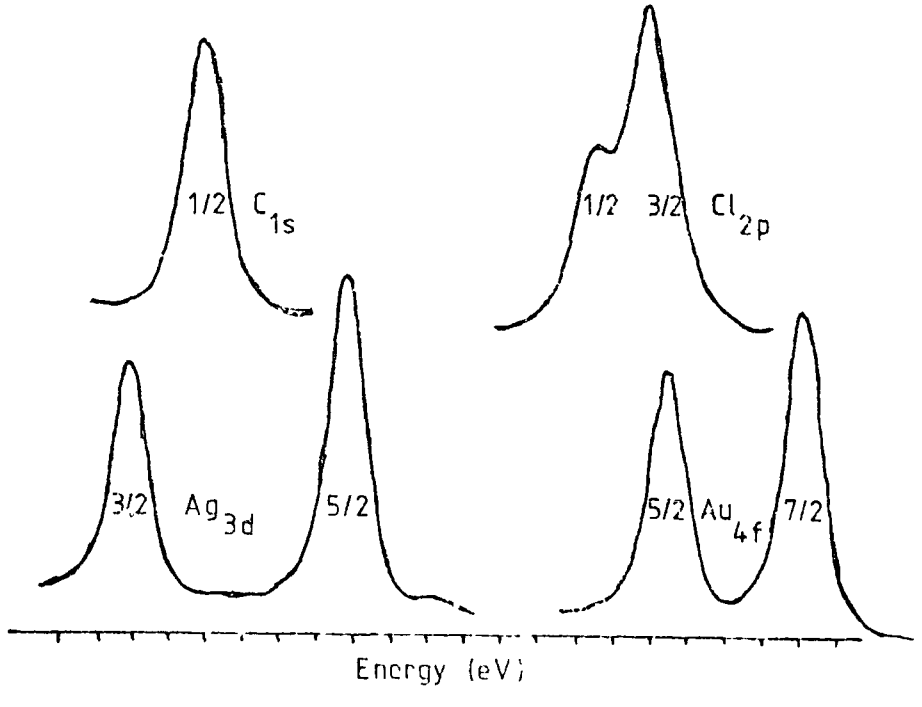

Spin orbit splittings in C_{1s}, Cl_{2p}, Ag_{3d} and Au_{4f} core levels

Figure 2.6.4

ii) Multiplet Splitting

Multiplet splitting occurs in paramagnetic systems and is caused by interactions of the unpaired electrons with the unpaired core orbital electrons remaining after photo-ionisation. The phenomenum was predicted by Watson and Freeman[105] before being observed by Fadley and co-workers[106] for the 3s levels in some fluorides and oxides of manganese and iron, which contain unpaired 3d electrons. The interpretation of the 'S' splitting is not easy except for cases involving 'J' hole states. In these cases the van Vleck coupling model[107] may be used though this was originally developed for atoms.

After photo-ionisation the two possible final states have a total spin of $S \pm 1/2$ where S is the total spin of the l^n configurations of the ground state. The splitting, ΔE, between the two states $S + 1/2$ and $S - 1/2$ is proportional to the multiplicity of the ground state and is given by

$$\Delta E = (2\ S + 1)\ K \qquad 2.6.18$$

where K is the exchange integral between the core, c, and the valence, v, electrons under consideration and is defined by

$$K = \left\langle \phi_v(1)\ \phi_c(2) \left| \frac{1}{r_{12}} \right| \phi_v(2)\ \phi_c(1) \right\rangle \qquad 2.6.19$$

The intensities of the peaks are proportional to the

degeneracies of the final states and is given by

$$\left[2(S + \tfrac{1}{2}) + 1\right] : \left[2(S - \tfrac{1}{2}) + 1\right] = (S+1) : S \qquad 2.6.20$$

The magnitude of the splitting of the peak for a given atom provides information concerning the localisation or delocalisation of unpaired electrons in a compound[28,108,109] since the greater the localisation and spin density on an atom the greater will be the observed splitting. If the fraction of spin density on the i th atom is f_i then the multiplet splitting is given, approximately by[108]

$$\Delta E = f_i \ (2 S + 1) \ K_i \qquad 2.6.21$$

Siegbahn and co-workers[31] have studied the simple molecules N_2, NO and O_2 in the gas phase and have found that the N_2 peaks show no sign of splitting while the NO and O_2 peaks are clearly split (see figure 2.6.5). This is caused by the presence of unpaired electrons in the case of NO and O_2 whereas N_2 contains no unpaired electrons (see figure 2.6.6).

The nitrogen molecule has a closed shell and the 1s core level after photo emission of one of its electrons is degenerate with respect to spin and should therefore show no splitting. The NO molecule however has one unpaired electron in the 2π orbital and therefore after emission of either an oxygen 1s or nitrogen 1s electron the NO^+

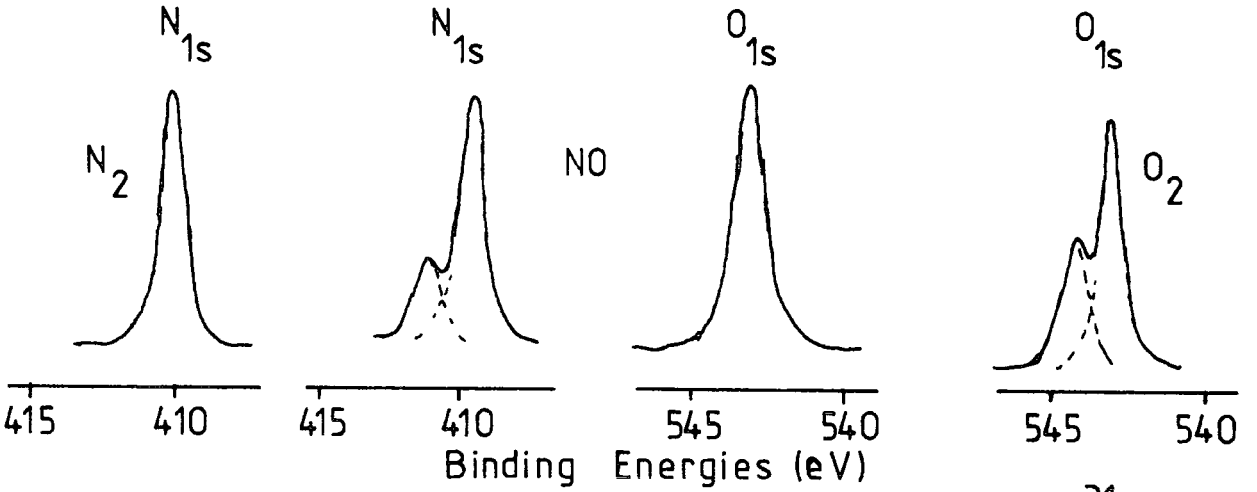

ESCA peaks for N_2, NO and O_2, gas phase [31]

Figure 2.6.5

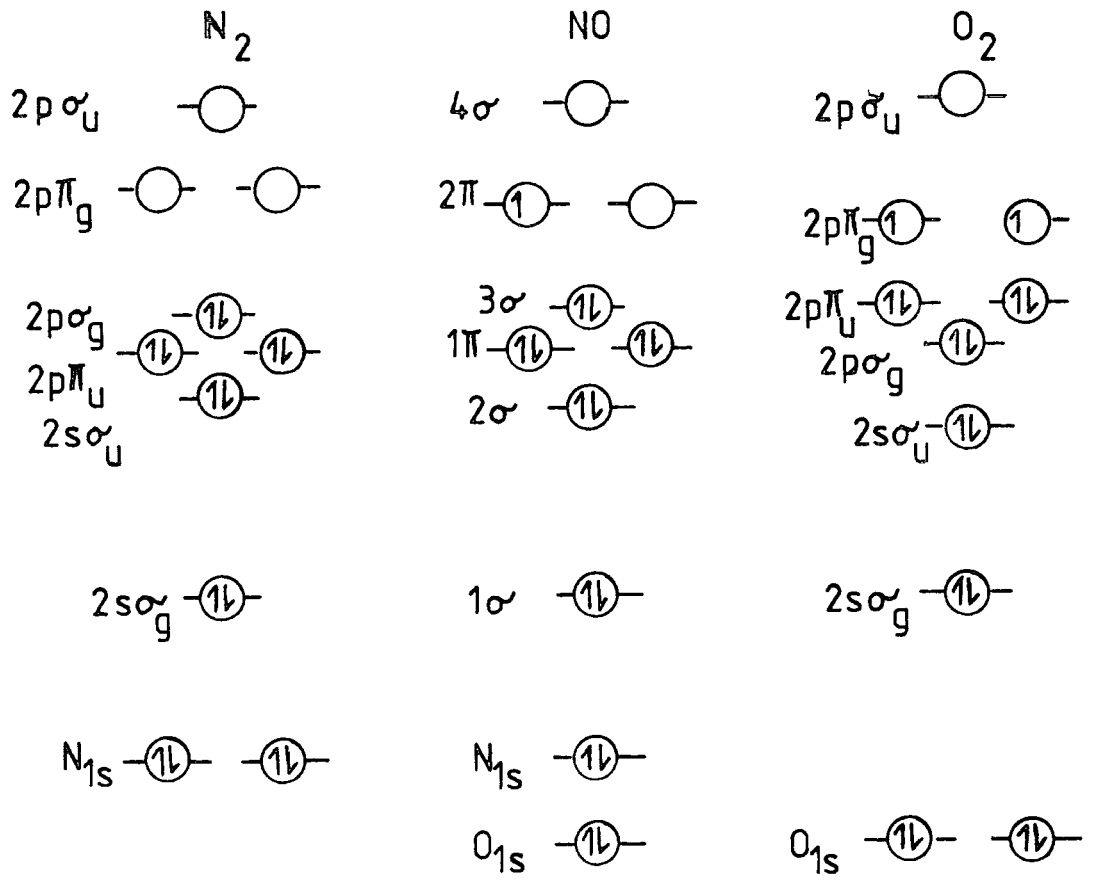

Electronic configurations of N_2, NO and O_2

Figure 2 6 6

molecule is left with a total spin of either 1 or 0, that is either in a triplet or singlet state. Thus multiplet splitting is expected and is observed in the nitrogen peak for NO. The oxygen peak, in NO, though not split is broadened and so it is assumed[31] that this broadening is due to splitting. The O_2 molecule has a similar electronic configuration to NO but with two unpaired electrons in its outer π_g type orbital and once again splitting of the oxygen peak is observed.

The magnitude of multiplet splittings are independent of sample charging effects and the reference level. Multiplet splittings in photo electron spectroscopy have been reviewed in some detail by Fadley[117].

ii) Electrostatic Splitting

This is caused by the differential interaction between the external electrostatic field and the spin states of the core level being investigated. It has been observed for a number of systems, for example, the $5p_{3/2}$ levels of uranium and thorium and in some compounds of gold[111,112]. Correlation has been observed between electrostatic splitting and the quadropole splittings obtained from Mossbauer spectroscopy[113], which arise from the interaction of the nuclear quadrupole moment with an inhomogenous electric field.

Due to the inherently amorphous structure of organic polymers it is unlikely that quadrupole fields will be induced within the bulk structure and it is therefore unlikely that electrostatic splitting will

be observed in these systems.

d) Satellite Peaks

Satellite peaks arising from shake up, shake off and Auger effects have been discussed in section.3 of this chapter. The X-Ray source itself is also a cause of satellite peaks though these may be eliminated by using monochromatised X-Rays, for example, the $Al_{K\alpha}$ X-Rays. The peaks have a higher kinetic energy than the main photo electron peak and are caused by the small percentage of $K_{\alpha 3,4}$ and $K_{\alpha 5,6}$ radiation[31] which arises from KL double hole and KLL triple hole states of the emitting atom[114].

The aluminium window on the cap which isolates the X-Ray anode from the sample chamber (see section .4a) may also give rise to some $Al_{K\alpha 1,2}$ radiation which will give rise to a satellite displaced by 232.9 eV to higher kinetic energy when using an Mg anode.

e) Line Widths

The various effects contributing to the total line width have been mentioned in section .4d on the electron analyser. The natural line width at half maximum peak height of the core level under investigation, ΔE_{Cl} and of the incident radiation ΔE_X are obtained from the uncertainty principle and are given by[112]

$$\Delta E . \Delta t \simeq h/2\pi \qquad 2.6.22$$

Where Δt is the lifetime of the state and h is Plank's constant.

The line widths of some X-Ray atomic energy levels are given in table 2.6.5 (a line width of 1 eV corresponds to a lifetime of approximately 6.6×10^{-16} sec.[115]).

Level	Atom						
	S	Ar	Ti	Mn	Cr	Mo	Ag
1s	0.35	0.5	0.8	1.05	1.5	5.0	7.5
$2p_{3/2}$	0.1	-	0.25	0.35	0.5	1.7	2.2

Full Widths at Half Maximum of
X-Ray Atomic levels / eV

Table 2.6.5

The photo electron emission process is thought to take place within a time interval of the order of 10^{-18} sec,[115] while nuclear relaxation times are of the order of 10^{-13} sec,[71] and the core hole created has a lifetime of the order of 10^{-16} sec.[113] The process is thus sudden with respect to nuclear relaxation but not with respect to electronic relaxation. The line widths also reveal that in general there is no advantage in studying more tightly bound core electrons since the greater line width may obscure chemical shifts that are revealed by studying less tightly bound electrons. Small changes in line widths,

of the order of 0.1 eV, have been observed to be caused by chemical effects which have a small effect on the lifetime of the core hole state[116,117]. This emphasises that peak intensities should be measured by area and not by height.

f) Sampling Depth

The relative positions of the X-Ray source, sample and electron analyser are shown in figure 2.6.7. If the photo electrons are emitted from a depth, d, of the sample their true path length will be d´where

$$d' = d \operatorname{cosec} \theta \qquad 2.6.23$$

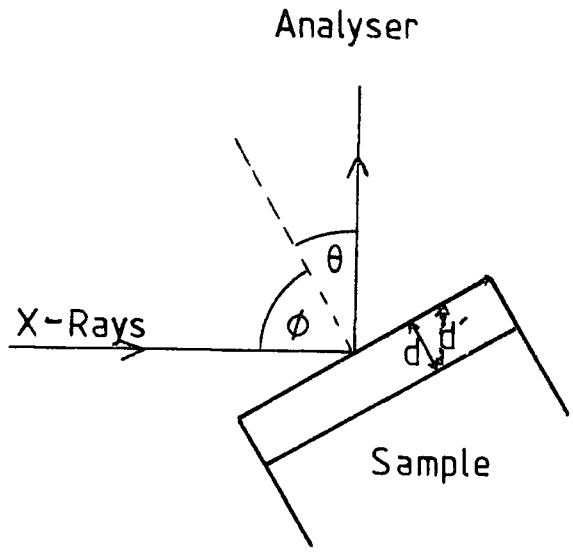

Geometry of ESCA Sample Region

Figure 2.6.7

Due to the short mean free paths of electrons in solids (see below) it is possible to study surface

features and compare them with bulk and subsurface compositions by carrying out experiments at different values of θ[118]. For the work in this thesis the X-Ray beam ($Mg_{K\alpha 1,2}$) was at right angles to the analyser ($\phi + \theta = 90^{o}$) and the two values of θ used were 30^{o} and 70^{o}. This gives the ratio of the sampling depths as

$$\frac{d_{30}}{d_{70}} \simeq \frac{2.5}{1} \qquad 2.6.24$$

The variation of the angle ϕ, the angle of incidence of the X-Rays, is of much less importance when considering sampling depths since the mean free paths of X-Ray photons in solids is of the order of 10^{-6} m[119]. This is two or three orders of magnitude greater than electron mean free paths[120-123] and so the X-Ray flux will remain essentially unattenuated.

The sampling depth is defined as the depth from which 95% of the signal peak comes from and is related to the electron mean free path, λ, by

$$\text{Sampling depth} = -\lambda \ln 0.05 \simeq 3\lambda \qquad 2.6.25$$

As an example for carbon 1s levels, studied using $Mg_{K\alpha 1,2}$ the kinetic energy of the photo emitted electrons is $\sim$ 960 eV and the mean free path of the electron is $\sim$15 Å [122]. The sampling depth at $\theta = 30^{o}$ is therefore $\sim$39 Å and at $\theta = 70^{o}$ the sampling depth is $\sim$15 Å.

g) Peak Intensities

For an infinitely thick homogeneous sample the fraction of the elastic (no energy loss) photo-ionisation

peak, dI_1, corresponding to photo-ionisation from a core level 1, in a layer of thickness dx, at a depth x is given by[124,125]

$$dI_1 = F \alpha_1 N_1 k_1 e^{-x/\lambda_i} dx \qquad 2.6.26$$

where I_1 is the intensity arising from core level 1,

F is the exciting photon flux,

α_1 is a function of the cross section for photo-ionisation from core level 1,

N_1 is the number of atoms per unit volume on which core level 1 is located,

k_1 is a spectrometer dependent factor,

λ_1 is the inelastic mean free path for the photo emitted electron,

x is the depth from which the photo electrons come.

Integration of 2.6.26 gives

$$I_1 = \int_0^\infty F \alpha_1 N_1 k_1 e^{-x/\lambda_1} dx \qquad 2.6.27$$

and $$I_1 = F \alpha_1 N_1 k_1 \lambda_1 \qquad 2.6.28$$

These various factors and the parameters on which they depend are discussed below.

1) X-Ray Flux, F

The X-Ray flux from the source is primarily dependent on the power applied to and the efficiency of the X-Ray gun (see section .4a above). As stated in

section .6f the X-Ray flux is virtually unattenuated with respect to the sampling depth from which the photo electrons come. However, the angle of incidence ϕ of the X-Rays and the analyser angle θ do have an effect on the intensity of the photo-ionisation peak. It has been shown both theoretically and experimentally by Henke[57,126] that at large values of ϕ refraction of collimated X-Rays in the outermost surface layers of the sample causes an effective increase in the X-Ray flux in these layers. This causes an enhancement of the photo electron emission as determined by ESCA. However, with current spectrometers this phenomenon is rarely observed since samples are seldom optically flat and X-Ray beams are not collimated (but see section .7d below). Also a large value for ϕ together with other factors involved in conventional spectrometers produces a very poor signal to noise ratio.

At lower values of ϕ a further effect on the X-Ray flux is observed which is important when the beam width is wider than the sample.

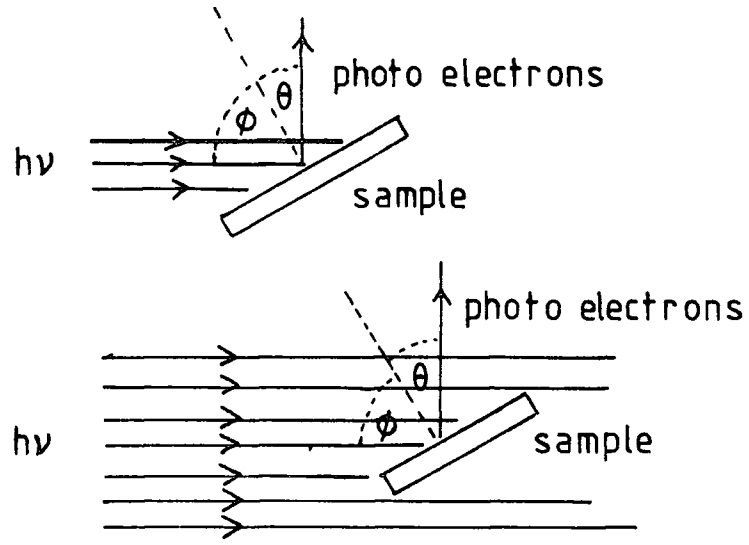

Narrow and wide X-Ray beams

Figure 2.6.8

It is seen from figure 2.6.8 that when the beam is narrower than the sample that the total X-Ray flux hitting the sample is not affected by varying ϕ. However, with a beam that is wider than the sample the X-Ray flux hitting the sample varies as cos ϕ and as ϕ is increased this causes the signal intensity to decrease.

For the particular spectrometer, an AEI ES 200 AA/B, on which the work for this thesis was carried out Clark and Shuttleworth[127] have investigated the spatial distribution of the derived signal intensity with regard to sample area. Using a composite probe tip (see figure 2.6.9) containing gold plated pins set in epoxy resin they were able to show that the largest contribution to the signal came from a small area, approximately 0.25 cm^2 out of a total area of 1.4 cm^2. The largest contribution, as

determined using the composite probe shown in figure 2.6.9, was observed to

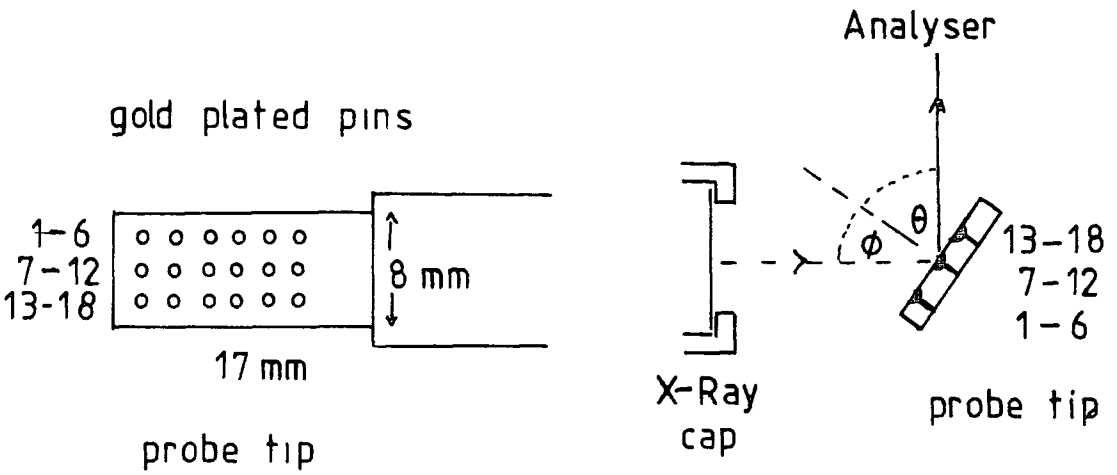

Composite probe tip and relative position in the sample chamber

Figure 2.6.9

come from pins 9 - 12 at all angles (Θ) and no signal was observed to come from pin number 1 at any angle. At a take-off angle of 30° no contribution was observed from pins 13 - 18 and pins 9 - 12 contributed approximately 63% of the total signal. At 75° the total absolute intensity was much smaller and contributions were observed from all pins, except number 1. Thus at a higher take-off angle, Θ, a much greater area of the probe was sampled and though pins 9 - 12 still contribute over 30% of the total signal intensity there is a more uniform

contribution from all parts of the probe.

Variations in the angle Θ can also cause variations in the signal intensity and though not strictly speaking being variations in X-Ray flux, since spectrometers commonly use fixed geometries for X-Ray source and analyser, variations in signal intensity from combinations of ϕ and Θ variations may occur. For a given value of Θ the entrance slit of the analyser "sees" a sample area proportional to cos Θ and as Θ is increased this effect tends to decrease signal intensity.

Since as ϕ increases Θ decreases these two effects discussed above act in opposition and produce an overall function, which may be expressed in terms of Θ, $f_i(\Theta)$, for a core level i. It has been observed experimentally[128] that f_i exhibits a maximum value around a value of Θ of 35^{o} when the X-Ray source and the analyser are situated at right angles.

Equation 2.6.28 may be modified to include this function of Θ and the photo electron intensity I_i becomes

$$I_i = f_i(\Theta)\, F \alpha_i N_i k_i \lambda_i \qquad 2.6.29$$

where $f_i(\Theta)$ is determined experimentally.

ii) Photo Ionisation Cross Section

The cross section for photo-ionisation of a core level i is a parameter which describes the probability of the core level electron being ionised when irradiated by a photon of known energy[129]. The parameter α_i only includes the fraction of photo-ionised electrons accepted

by the analyser and is a function both of the core level to which it relates and the energy of the incident photon. It, α_i, may be calculated from the fundamental properties of the atom[130], or it may be determined experimentally from gas phase ESCA data[31].

The radial distribution of photo-ionised electrons from a core level i is not uniform and α_i is a function of Φ, the angle of detection with respect to the incident photons[125]. The photo-ionisation cross section parameter α_i is given by[131,132]

$$\alpha_i = \alpha_i^{Tot} / 4\pi \left[1 - \tfrac{1}{4} \beta_i \left(3\cos^2 \Phi - 1\right)\right] \qquad 2.6.30$$

where α_i^{Tot} is the total cross section of the core level and β_i is the asymmetry parameter[133].

For a particular spectrometer and using the same X-Ray source and with a fixed value of Φ then α_i is normally a constant. Using either $Mg_K\alpha_{1,2}$ or $Al_K\alpha_{1,2}$ the photo-ionisation cross section parameter α_i for the core levels of most elements is within two orders of magnitude of that of the C_{1s} level[130] and thus ESCA has a convenient sensitivity range for most elements. The cross section for core levels are normally considerably higher than those for valence levels[130] though it should be remembered that less tightly bound electrons will have a smaller natural line width (see section .6e above).

iii) Spectrometer Factor

The spectrometer factor k_i includes contributions due to geometric factors such as the solid angle of acceptance of the analyser slit and analyser transmission characteristics and detector efficiency, these latter two being energy dependent.

iv) Electron Mean Free Path

The mean free path of an electron, λ_i , in a solid is defined as the distance in a solid through which electrons must travel before the number, which have not suffered inelastic collisions, is reduced to 1/e of the original number. Electron mean free paths may be calculated theoretically[121] or determined experimentally[122,123]. The mean free path, λ_i , is a function of the kinetic energy of the photo-ionised electrons and ranges from ~ 4 Å for electrons of about 80 eV kinetic energy to ~ 30 Å for electrons of about 1500 eV.

v) Number Density

The number of atoms per unit volume, N_i, on which the core level is localised is not directly related to the density of the sample. However, it has been observed that for similar materials of different densities, the higher density material produces a larger ESCA signal for a given core level[70]. A more important consequence of N_i is that the relative signal intensities for core levels in a homogeneous sample are directly related to the overall stoichiometries of the atoms in the sample. Thus

for two core levels ı and ȷ we get from equation 2.6.29

$$\frac{I_1}{I_J} = \frac{\alpha_1 N_1 k_1 \lambda_1}{\alpha_J N_J k_J \lambda_J} \qquad 2.6.31$$

it being assumed that $f_1(\theta) = f_J(\theta)$.

If ı and ȷ are the same core levels for the same element but in different chemical environments then

$$\alpha_i k_i \lambda_i \approx \alpha_j k_j \lambda_j$$

and so

$$\frac{I_1}{I_j} = \frac{N_1}{N_j} \qquad 2.6.32$$

If however ı and ȷ are different core levels for different elements then

$$\alpha_i k_i \lambda_i \neq \alpha_j k_j \lambda_j$$

but the ratio of these may be determined experimentally using samples of known stoichionetry for a particular spectrometer.

h) Analytical Depth Profiling

It is often important to determine if the surface composition of a sample is the same as that of the bulk material (see also section .6f above). The simplest case is that of a single homogeneous component of thickness d on a homogeneous base as illustrated in figure 2.6.10.

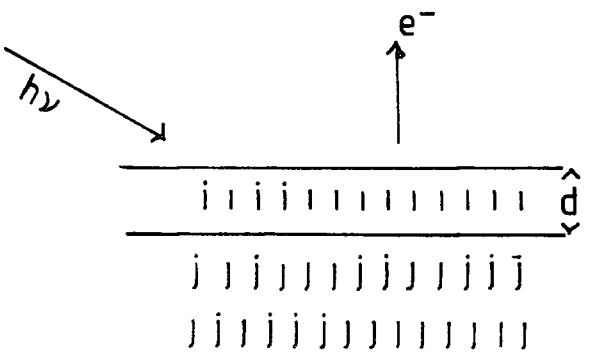

Substrate/Overlayer Model

Figure 2.6 10

The intensity of the signal arising from the overlayer is obtained by integrating equation 2.6.26 between x = o and x = d which gives

$$I_1 = F\alpha_1 N_1 k_1 \lambda_1 (1 - e^{-d/\lambda_1}) \qquad 2.6.33$$

which including angle effects from equations 2.6.23 and 2.6.29 becomes

$$I_1 = f_1(\Theta)\, F\alpha_1 N_1 k_1 \lambda_1 (1 - e^{-d/\lambda_1}) \cos\Theta \qquad 2.6.34$$

The intensity of the signal arising from the substrate is obtained by integrating equation 2.6.26 between x = d and x = ∞ which gives

$$I_J = F\alpha_J N_J k_J \lambda_J e^{-d/\lambda_J} \qquad 2.6.35$$

which including angle effects from equations 2.6.23 and 2.6.29 becomes

$$I_j = f_j(\theta) F \alpha_j N_j k_j \lambda_j e^{-d/\lambda_j} \cos\theta \qquad 2.6.36$$

Electron mean free paths are a function of energy[129] and in the range normally encountered in ESCA, which is normally $>$ 300 eV, the electron mean free path increases in energy. As a consequence of this, and the effect of λ_j on the intensity of I_j from the substrate as given by equation 2.6.36, the attenuation of a signal arising from a core level in the substrate by an overlayer, will depend strongly on the kinetic energy of the photo emitted electrons. Thus a non-fluorine containing overlayer on a fluorine containing substrate will result in a decrease in the F_{1s}/F_{2s} ratio since the kinetic energy and mean free path of the F_{1s} photo electrons are greater than those of the F_{2s} photo electrons.

Therefore in order to use depth and angular studies for analytical purposes it is necessary to determine accurately the electron mean free paths, for the kinetic energies of interest, in the materials being studied.

1) Deconvolution and Measurement of Peak Areas

The overall resolution of a peak $\Delta E_M/E$ has been discussed in section .4d where ΔE_M is obtained from equation 2.4.3.

$$(\Delta E_M)^2 = (\Delta E_x)^2 + (\Delta E_{CI})^2 + (\Delta E_s)^2 + (\Delta E_{ss})^2 \qquad 2.4.3$$

ΔE_x has been discussed in section .4a and in the case of common X-Ray sources possesses a Lorenzian line

shape. ΔE_{Cl} has been discussed in section .6e and is usually taken to be of Lorenzian line shape as also is ΔE_{ss}, while ΔE_s is usually taken to be Gaussian in shape. The combination of the various contributions to ΔE_M produces a hybrid shape with a Gaussian distribution dominating the line shape and with a Lorenzian character to the tails. It has been shown that the assumption of a pure Gaussian shape for the observed peaks introduces only a small error in line shape analysis[31].

The need for deconvolution and line shape analysis arises from the fact that the line width ΔE_M measured with current instruments, without monochromatisation, often compares unfavourably with the chemical shifts. This causes overlapping of peaks and in some instances only a very broad peak is observed instead of the separate components.

The methods of deconvolution fall into two main categories:- i) the enhancement of resolution by mathematical manipulation of the raw data, and ii) curve fitting by simulation using analogue or digital systems.

i) Deconvolution by mathematical methods has been reviewed by Carley and Joyner [134]. The methods discussed are the Fourier Transform and various iterative processes, these latter often being based on Van Cittert's method. The authors conclude that deconvolution by mathematical enhancement may bring about an improvement in resolution comparable to that obtained by the use of a monochromator.

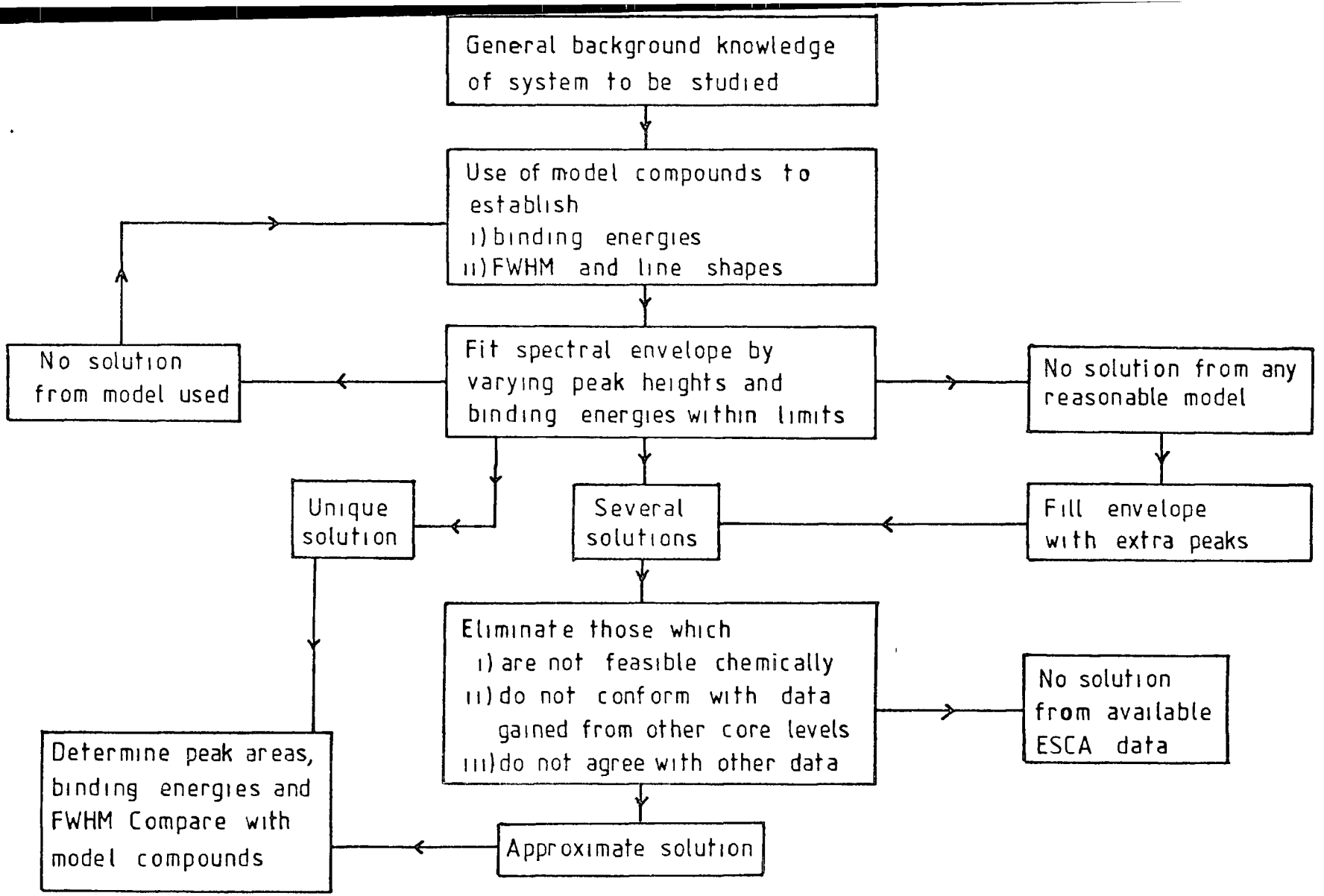

Curve fitting by simulation

Figure 2 6 11

ii) Curve fitting by simulation requires the close control of a number of variables, for example, binding energy, line width and peak height. Because of this the use of an analogue system is more convenient than digital analysis with a large computer. For the work in this thesis deconvolution was performed by analogue simulation using a Dupont 360 curve resolver. On this binding energy, line width and peak height are controlled by the operator as is also line shape though this is usually set for a Gaussian form. The basic approach to curve simulation is shown in figure 2.6.11.

In deconvolution by methods (i) and (ii) a certain amount of caution is required as it is often possible to obtain more than one solution from which the correct one must be chosen.

.7 General Aspects of ESCA

a) ESCA is an extremely powerful tool especially with respect to surface composition. For bulk analysis it must be used with caution since in many cases it only samples to a depth of the order of 10^{-8} m and what is obtained may be a composition heavily weighted by components at the surface (but see section .6h above). The relative sensitivities of ESCA and some other common analytical techniques are shown in table 2.7.1

b) Advantages of ESCA

The principle advantages of ESCA, some of which may be shared by other techniques are:-

Bulk Techniques	Minimum Detectable Quantity / g
Infra Red	10^{-6}
Atomic Absorption	10^{-9} - 10^{-12}
Vapour Phase Chromatography	10^{-3} - 10^{-7}
High Pressure Liquid Chromatography	10^{-6} - 10^{-9}
Mass Spectrometry	10^{-10} - 10^{-15}
Surface Techniques	
ESCA	10^{-10}
Neutron Activation	10^{-12}
Ion Scattering Spectrometry	10^{-15}
X-Ray Fluorescence	10^{-7}
Auger Spectroscopy	10^{-14}
Secondary Ion Mass Spectrometry	10^{-13}
Multiple Internal Reflection Infra Red Spectroscopy MIR IR	10^{-10}

Sensitivities of Various Analytical Techniques

Table 2.7.1

i) The sample may be solid, liquid or gas and the amount required is small being approximately 10^{-3} g of solid, 10^{-7} dm^3 of liquid and 5 x 10^{-4} dm^3 of gas (at STP).

ii) The process is virtually non-destructive, since the X-Ray flux is small (0.1 milli rad. sec^{-1})[135], and few changes occur in the sample while spectra are being run.

iii) The technique is independent of the spin properties of the nucleus and can be used to study any element of the periodic table, with the exception of hydrogen.

iv) Materials may be studied "in situ" with a minimum of preparation.

v) The technique provides a large number of information levels from a single experiment.

vi) The data is often complementary to that obtained by other techniques.

vii) For solids ESCA has the unique capability of differentiating surface from subsurface and bulk phenomena (see section .6h) though some information on this can also be obtained from MIR IR.

viii) The information relates directly to bonding and molecular structure and applies to both inner and valence orbitals of the molecule enabling a thorough analysis of electronic structure to be made.

ix) The information levels are such that "ab initio" investigations are possible and the theoretical

basis is well understood.

c) Disadvantages of ESCA

There are however some disadvantages associated with ESCA.

i) The overall costs of the instrumentation is high.

ii) While the technique has excellent depth resolution the spatial resolution is poor and an area of approximately 0.3 cm^2 is normally sampled.

iii) If the surface layer is comparatively thick, that is greater than 100 Å, it is not possible to determine the bulk composition by ESCA without sectioning the sample.

iv) Hydrogen is not detectable using ESCA.

d) Hierarchy of ESCA Information

The hierarchy of information levels available in ESCA experiments is as follows.

i) The technique gives absolute binding energies, relative peak intensities and binding energy shifts. It also provides element analysis, analytical depth profiling and identification of structural features.

ii) Shake up and shake off satellites may be observed and monopole excited states and their energy separation, with respect to direct photo-ionisation peaks, measured. Relative intensities of components with respect to the direct photo-ionisation peak are also obtained.

iii) The technique gives information for paramagnetic

molecules on spin states and distribution of unpaired electrons from observations of multiplet effects.

iv) For valence energy levels long range effects may be found directly.

v) For solids, by using a fixed angle between the analyser and X-Ray source and by varying the angle between the sample and X-Ray analyser (Θ) surface, subsurface and bulk effects can be differentiated. By varying the angle between the X-Ray source and the analyser, information can be obtained concerning the angular dependence of cross section, the asymmetry parameter β and the symmetries in all levels.

e) Current Developments

The problem of sample contamination, especially by hydrocarbons deposited within the sample chamber, has already been mentioned in section .4c. Since these hydrocarbons may originate from oil in pumping systems, (diffusion and rotary pumps), turbomolecular pumps[31] which operate without oil are coming into use. Absence of hydrocarbon contamination for use in energy referencing might then occur but could of course be readily overcome (see section .5e).

When gases are being studied and when monochromatizers are being used lack of brightness of the original X-Ray source leads to long exposure times when recording spectra. This may be overcome by using rotating water cooled anodes[31] which enable the power input to the

anode to be increased. The anode current in these systems may be increased to approximately 500 mA instead of the more usual operating value of approximately 20 mA the voltage being the same, that is approximately 10 kV. As an alternative to conventional X-Ray sources synchrotron radiation[136] may be used though due to the need for access to a synchrotron source this will not replace X-Ray sources on conventional instruments. A synchrotron does however provide X-Rays with an almost continuously variable wavelength and which are almost completely collimated in the plane of the synchrotron ring. The X-Rays are also completely plane polarised in the plane of the ring. The collimation means that the synchrotron radiation may be easily monochromatised in a crystal monochromator.

Another development is the use of "split" anodes, where half the anode surface is say magnesium and the other half say titanium. By comparatively simple electrostatic deflection the electron beam that impinges on the anode may be switched from one anode material to the other thus simplifying the change from one X-Ray source to another, of different energy.

The use of mathematical techniques for deconvolution[134] is an area where there is considerable scope for development (section .61) as also is the use of multi-channel analysers[31], which would greatly speed up the rate of data acquisition. This can be important with

sensitive materials even though the total X-Ray flux is not large, since when the signals are weak, or when angular studies are being carried out it may take more than an hour to record all the peaks in the spectrum from one sample.

Chapter 3

Corona and Plasma Discharges

.1 Introduction

.2 Basic processes in gaseous electronics

a) Ionisation and Activation by Impact

i) Electron

ii) Ion/molecule and Molecule/molecule

iii) Photon

b) Recombination and Deactivation

c) Particle Velocity, Energy, Collision Frequency

.3 Corona

a) General aspects

b) Direct Current Corona Discharges

i) Positive wire, negative plane

ii) Negative wire, positive plane

iii) Plane parallel electrodes

c) Alternating Current Corona Discharges

d) Ions and Molecules formed in Corona

i) Discharges in air

ii) Discharges in Oxygen

iii) Discharges in Nitrogen

iv) Discharges in Argon

.4 Surface Treatment by Corona Discharge

a) General aspects

b) Electrical characteristics

c) Corona Discharge Equipment

i) Electrode design

ii) Power supplies

.5 Plasma Discharges

a) General aspects

b) Reactive Species in Plasmas

i) Plasma Discharge in Air at 0.2 Torr

ii) Plasma Discharge in Oxygen at 0.2 Torr

c) Photon Emission of Plasmas

.1 Introduction

The initiation of chemical reactions, by electrical discharges, has been known and observed for over a hundred years[137]. Early workers were hampered by lack of equipment to produce a continuous high voltage electrical supply, having to rely on electrostatic generators which only gave an intermittent supply. It was not in fact until the induction coil was invented by Ruhmkorf[138] in 1851, that a continuous high voltage source could be obtained. Low voltage arcs had been discovered by Humphry Davy in 1808, using a voltaic pile, but had not been regarded by him as important scientifically. The other important technique, developed shortly after the introduction of the induction coil, was that of Geissler, who discovered how to fuse platinum electrodes into glass. By fusing two such electrodes into a glass vessel and then reducing the air pressure electrical discharges could be observed when an induction coil was connected to the two electrodes. Using Geissler's technique and induction coils Plucker (1859), Hittorf (1869), Goldstein (1876), and Crookes (1879), were able to investigate the properties of the, then mysterious, rays emitted from the cathode in a discharge tube. The actual nature of these mysterious rays, although the subject of much research, was not in fact discovered until 1897 by Thompson. He showed that the cathode rays were sub-atomic particles approximately a thousand times (1837) lighter than a hydrogen atom. These sub-atomic particles

were given the name 'electron' by Lorentz. While Crookes Hittorf and others were trying to understand the nature of cathode rays other work was being carried out using Geissler tubes as spectroscopic light sources. It was this work that led Rayleigh to propose the "water melon" model for the atom, where negative charges were imbedded in a positive jelly. It was possible to explain the hydrogen spectrum using this model but it failed for all other spectra and the Rutherford nuclear model, 1911, was shown to be more successful.

The way in which the glowing discharge in a Geissler tube varied with the pressure, electrode geometry and type of gas was studied very intensively but was not fully understood until the nature of the electron had been discovered. A typical appearance of a gas discharge tube is shown in figure 3.1.1.

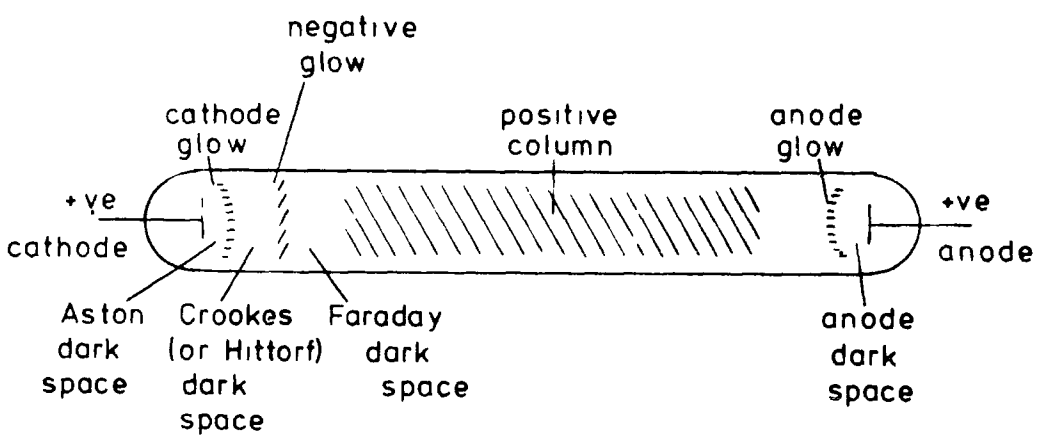

Appearance of gas discharge at low pressure

Figure 3 1 1

The Aston dark space is normally only visible at low pressures since as the pressure rises the cathode glow becomes brighter and appears to cover the cathode surface completely. The Faraday dark space is very variable in length and is not always observed and the positive column may be broken up with striations.

In the eighteenth century many workers had observed that the charge on electrically charged bodies slowly leaked away. This was investigated by Coulomb who showed in 1785 that there was an actual passage of electrical charge through the air. This he concluded was due to the molecules of the air becoming charged by contact with his charged object and then being repelled and thus carrying away the charge. However Wilson (1900) showed that when the charged object was inside a closed container, the maximum leakage was proportional to the volume of the container. This fact was incompatible with Coulomb's theory of molecules becoming charged on contact with the object. This observation of Wilson's led to the acceptance of the idea that some kind of 'atom of electricity' was involved in the discharge process. The discovery of X-Rays by Rontgen (1895) and radioactivity by Becquerel (1896) led to the observation that gases could be made conductors by these mysterious X-Rays. Rontgen found that electrically charged bodies could be readily discharged by means of his X-Rays and Thompson and Rutherford (1896) showed that the X-Rays produced both positive and negative

charged particles. As is now known the natural background of cosmic radiation produces a small number of ions in the air and it is these ions which, by making the atmosphere slightly conducting, cause electrical charges to slowly leak away.

Once the nature of the elementary charged particles, the electrons, the positive ions and the negative ions, were recognised the way was opened for considerable advances in gaseous discharges. Much of this work was carried out by Townsend and co-workers, who based their explanation on the idea of the "average" electron and the "average" ion. These ideas, though fruitful at first, had severe limitations and coupled with other experimental problems caused development of understanding of gas discharges to slow down in the late 1920s and early 1930s. Then in 1935 Allis and co-workers introduced the concept of electron energy distribution functions in place of the "average" electron concept. The experimental problems were caused by mercury contamination from the mercury diffusion pumps used and the mercury filled vacuum gauges. This problem was overcome in the 1940s by Druyvesten and Penning and coupled with the work of Allis enabled a real match between theoretical concepts and experimental data to be made.

Originally the field was designated as "Electrical Discharges in Gases" or the "Passage of Electricity through Gases". This was later shortened to "Gas

Discharge Physics" and then with the advent of the field of electronics in the 1940s the name was changed to its current one of "Gaseous Electronics". The term "Plasma Physics" is sometimes used as well, though strictly speaking this term, as defined by Langmuir, only applies to the main section of the discharge, the positive column. In this region there is complete space charge neutralisation, that is, the number of electrons is the same as the number of ions.

Some of the main events in gaseous electronics which helped in formulating the ideas concerning the processes taking place are given in table 3.1.1.

Date	Concept	Originator
1600	Electricity	Gilbert
1742	Sparks	Desagulier
1785	Conduction in Gases	Coulomb
1808	Diffusion	Dalton
1808	Arc (discharge)	Davy
1817	Mobility	Faraday
1821	Arc (name)	Davy
1834	Cathode and Anode	Faraday
1834	Ions	Faraday
1848	Striations	Abria
1859	Cathode rays (Kathodenstrahlen)	Plücker
1860	Mean Free Path	Maxwell
1879	Fourth State of Matter	Crookes
1880	Paschen Curve	La Rue and Müller
1889	Maxwell-Boltzmann distribution	Nernst
1891	Electron (charge)	Storey
1895	X-Rays	Röntgen
1897	(Cyclotron) frequency	Lodge
1898	Ionisation	Crookes
1899	Transport Equations	Townsend
1899	Energy gain equations	Lorentz
1901	Townsend coefficients	Townsend
1905	Diffusion of charged particles	Einstein
1906	Electron (particle)	Lorentz
1906	Plasma frequency	Rayleigh
1914	Ambipolar diffusion	Seeliger
1921	Ramsauer effect	Ramsauer
1928	Plasma	Langmuir
1935	Velocity Distribution Functions	Allis

Discoveries in Gaseous Electronics[134]

Table 3.1.1

.2 Basic Processes in Gaseous Electronics

a) Ionisation and Activation[139,140,141]

i) By Electron Impact

Free electrons, positive and negative ions, photons and excited molecules may all be produced by collisions between electrons and gas molecules in a gaseous electrical discharge. Consider the situation where a gas is in a container with two electrodes which are connected to a high voltage supply. If a free electron is introduced, perhaps caused by a cosmic ray or by cold cathode emission, if the voltage is high, then it will be accelerated by the electric field according to:-

$$\frac{dV}{dt} = \frac{q}{m} \cdot E \qquad 3.2.1$$

where $\frac{dV}{dt}$ is the acceleration, q is the charge and m is the mass of the electron and E is the electric field strength. This acceleration will continue until the electron has a collision with a gas molecule. If the energy of the electron, at the time of the collision, is low then only elastic scattering will occur. At higher energies inelastic collisions will occur and molecules will become excited to higher energy states and eventually may become ionised[139]. From a consideration of the elastic collisions it may be shown that the electrons have an effective "Maxwellian" temperature approximately two orders of magnitude greater than the molecule or ion temperature[139]. Typical values for discharges are T_e approximately 30000 K

(about 2 eV) and T_m about 300 K (0.02 eV), where T_e is the electron "temperature" and T_m is the molecule "temperature".

When the electric field strength is increased then inelastic collisions of electrons and molecules will occur and these inelastic collisions may cause excitation and also ionisation of molecules.

$$e^- + A \longrightarrow 2e^- + A^+$$

$$e^- + A \longrightarrow e^- + A^*$$

There is also the possibility of secondary electron emission by ion impact on the cathode, which will increase the overall electron density. The threshhold energies for excitation are lower than those for ionisation and also the cross sections for excitation tend to be larger than those for ionisation at higher energies. It has been shown[141] that the cross sections for excitation and ionisation are both functions of velocity and increase rapidly from zero at the threshhold energy for the process and then pass through a maximum. This maximum is of the order of ten to a hundred eV, compared to the average energy of the electrons of about 2eV.

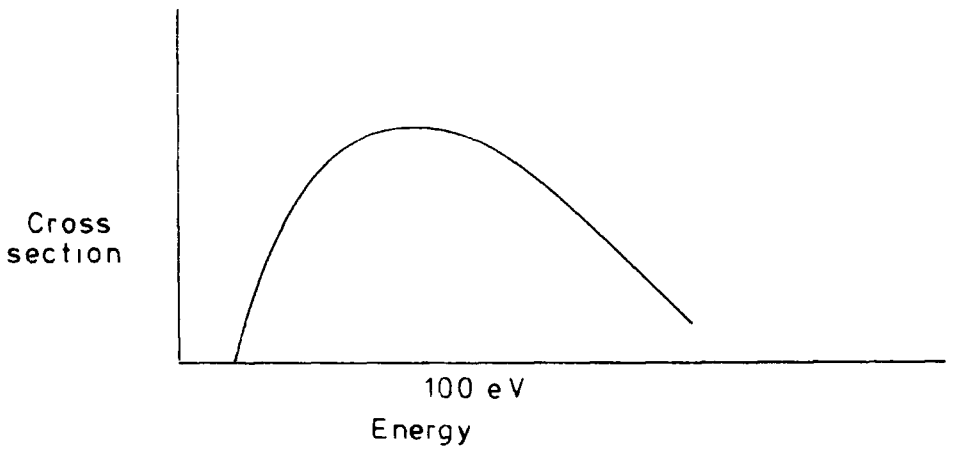

Schematic representation of the variation of cross section for ionisation or excitation by electron impact

Figure 3 2 1

The high energy tail of the electron energy distribution will therefore be more effective in producing excitation than ionisation. The excitation caused by the electron impact is largely responsible for the light emitted by a discharge (see also section .5 below).

$$A^* \longrightarrow A + h\nu$$

For radiating states the lifetime of A^* is of the order of 10^{-8} seconds and there is not much chance of a reaction occurring before the photon is emitted and the radiation simply escapes from the discharge. However, if the radiation takes place to the ground state then

the photon can be reabsorbed by other atoms and molecules. This process is termed "resonance radiation absorption" and under these circumstances the photon diffuses out through the discharge. This in effect gives an excited atom whose lifetime is several times the lifetime of the activated atom. It is also possible for excitation to a true metastable state to occur where the activated state has a comparatively long lifetime which may be of the order of microseconds or even seconds. For example helium in its ground state $1s^2\ ^1S_o$ may be excited to $1s\ 2s\ ^3S_1$ by electron impact. It cannot however return to its ground state by simple emission of radiation since this transition is forbidden and it can only return to the ground state as a result of a collision.

When the particle that is excited is a molecule then there is a possibility of dissociation taking place provided that the energy of the electron is greater than the dissociation energy of the molecule. For example:-

$$e^- + H_2(^1\Sigma^+_g) \longrightarrow e^- + H_2(^3\Sigma^+_g) \rightarrow e^- + H^\cdot + H^\cdot$$

$$e^- + O_2 \rightarrow O^\cdot + O^-$$

$$e^- + O_2 \rightarrow O^* + O^-$$

Although electron impact excitation and ionisation is the major process in gaseous electronics various other processes may also have important effects.

ii) Ion/molecule and molecule/molecule impact

The cross section for excitation and ionisation by impact with a fast atom or ion are, like those for electron

impact, functions of the velocity of the atom or ion. The variations of the cross section with velocity resemble that for electron impact (see figure 3.2.1), being zero at the threshold energy and rising rapidly to a maximum. Due to the much larger masses of atoms and ions their energies at a given velocity are much greater than those of electrons and the kinetic energies at the maximum for excitation or ionisation cross sections are of the order of thousands of electron volts instead of tens of electron volts as in electron impact.

For a given kinetic energy, due to their much greater mass atoms and ions will have a much lower velocity than electrons and therefore will tend to have lower cross sections for excitation. Since however the cross section for excitation increases with velocity then at high velocities and energies it is to be expected that excitation by ion and atom impact will become important. For example the Helium singlet

5016 Å, $1s\ 3p\ ^1P_1 - 1s\ 2s\ ^1S_o$

and the triplet 5876 Å $1s\ 3d\ ^3D - 1s\ 2p\ ^3P$

may be produced by either electron or helium atom bombardment. In the case of electrons the maximum occurs when the electron energies are 100 eV and 30 eV respectively and in the case of helium atoms at greater than 6000 eV and 2500 eV respectively[141]. With such large energy differences the corresponding velocities of the electrons and helium atoms are of a similar order of magnitude. Thus for the singlet line $V_e = 5.9 \times 10^{10}$ m sec^{-1} and

$V_{He} > 0.5 \times 10^{10}$ m sec^{-1}, and for the triplet line $V_e = 3.2 \times 10^{10}$ m sec^{-1} and $V_{He} = 0.4 \times 10^{10}$ m sec^{-1}.

The magnitude of the energy required to make ion or molecular impact efficient is not usually met with in gaseous discharges though it is found in radiation chemistry using high energy sources. Nevertheless even at the energies more commonly met with in gas discharges some of the effects can be important. Examples of these are given below.

The OH^- ion is not produced directly[140,141] from impact of electrons and water molecules but is produced by charge exchange

$$O^- + H_2O \rightarrow OH^- + OH^\cdot$$

and

$$H^- + H_2O \rightarrow OH^- + H_2$$

In fact for electron impact on water molecules the process that is observed is

$$e^- + H_2O \rightarrow HO^\cdot + H^-$$

Depending on the pressure the OH^- may be formed as such or as a cluster with water molecules

$$OH^-.\ (H_2O)_n$$

Charge transfer may occur between ions and molecules:-

$$H^+ + H_2O \rightarrow H^\cdot + H_2O^+$$

$$O^+ + N_2 \rightarrow O^\cdot + N_2^+$$

$$O^- + O_2 \rightarrow O_2^- + O^\cdot$$

The O_3^- ion has been identified, perhaps a precursor to ozone

$$O^- + 2O_2 \longrightarrow O_3^- + O_2$$

Also produced are various molecular species of the noble gases.

$$Ar^* + Ar \longrightarrow Ar_2^+ + e^-$$

$$He^* + H_2 \longrightarrow HeH^+ + H^\cdot + e^-$$

Although these combinations Ar_2^+ and HeH^+ would not normally be regarded as being stable, within the region of the plasma and compared to the stability of other excited and ionised groups they may be regarded as being stable compounds.

It is possible to infer the formation of other interesting species formed in discharges. Thus Herbst, Patterson and Lineberger[142] were able to show that the peroxy isomer of NO_2^-

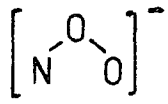 instead of 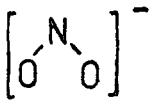

was formed in a plasma of oxygen containing traces of nitrogen.

As stated earlier in this section the kinetic energies of ionised and neutral molecules in gas discharges are not usually large enough to bring about ionisation by impact. Where however the energy of a metastable state of one constituent is higher than the ionisation of another constituent then Penning ionisation can occur[136]. The process is very efficient when the difference in energy levels is small, giving effectively quite large cross

sections for ionisation. The common molecular gases have ionisation energies below those of the metastable states of helium and neon and thus small traces of the former may have a considerable effect on the behaviour of helium and neon in gas discharge experiments.

For example,

$$He\ (1s\ 2s\ {}^1S) + Ar \longrightarrow He + Ar^+({}^2P_{3/2}) + e^-$$

It should be noted that ionisation may also be produced by Associative Ionisation

$$He\ ({}^1S) + Ar \longrightarrow He\ Ar^+ + e^-$$

But the two may be distinguished since the relative probabilities of Penning and Associative Ionisation depend on the energy conditions. Associative Ionisation occurs when the energy difference between the metastable state and the ionisation energy is greater than the collision energy and Penning ionisation occurs if it is not.

iii) Photon Impact

In a gas discharge, after the initial excitation and ionisation by electron impact, photons may be produced by the following processes (see also section .5 below).

$$A^* \longrightarrow A + h\nu$$

and

$$A^+ + e^- \longrightarrow A + h\nu$$

These photons thus produced may cause further excitation and ionisation of similar or different species. Thus in air oxygen molecules may be ionised by photons from either nitrogen or oxygen.

$$O_2 + h\nu \longrightarrow O_2^+ + e^-$$

In addition to this ionising effect photons may liberate electrons from ions by the process of photo detachment

$$NOO^- + h\nu \longrightarrow NO + O^\cdot + e^-$$

$$O^- + h\nu \longrightarrow O^\cdot + e^-$$

$$O_2^- + h\nu \longrightarrow O_2 + e^-$$

One of the important results that can be obtained from the measurement of photo detachment energies is the electron affinity of the neutral species formed since the electron affinity should be equal to the minimum value of the photon energy for photo detachment[140].

Although not strictly an electrical discharge process ionisation may be induced by multiphoton absorption by gas molecules using a focussed laser beam. Using a focussed laser beam it is possible to ionise a gas when its ionisation energy, U_1, is higher than the photon energy, $h\nu$, h being Plank's constant and ν being the frequency. This implies that a gas molecule simultaneously absorbs $U_1/h\nu$ quanta, which would normally be impossible. Since atoms and molecules only exist in discrete energy states photon absorption should only take place when there is resonance between two allowed states and the quantum $h\nu$. However it is possible for a virtual state of the atom to exist, after absorbing a photon, for a time, t, not exceeding $1/\nu$ according to the Uncertainty Principle. A second photon can be absorbed during this time to give a second higher virtual state with energy $2\ h\nu$, this state existing for a time $1/2\ \nu$. Provided photons can be

absorbed with sufficient frequency, that is from the intense focussed laser beam, then when $nh\nu \geq U_1$ the gas will ionise (n is an integer)[140].

b) Recombination and Deactivation

The various activated and ionised species in a gas discharge system may lose their energy and charge by a number of different processes. One of the simplest is by diffusion to the sides of the container where on impact charge may be neutralised and activation energy exchanged. The electrons in the plasma tend to diffuse more slowly owing to Coulomb forces than they would in the absence of positive ions. The current density of the electrons, S_e, and of the positive ions, S_+, as they diffuse will be given by

$$S_e = - D_e \nabla n_e \quad \text{and} \quad S_+ = - D_+ \nabla n_+ \qquad 3.2.2a,b$$

where n is the number of electrons or ions and D is the diffusion coefficient. Under the influence of an electric field, E, in the x direction a mobility term must be introduced and the equations become

$$S_e = - D_e \frac{dn_e}{dx} - n_e \mu_e . E \qquad 3.2.3$$

and

$$S_+ = - D_+ \frac{dn_+}{dx} + n_+ \mu_+ . E \qquad 3.2.4$$

where μ is the mobility of the electron or ion. If the plasma is electrically neutral then

$$S_e = S_+ \qquad \text{and} \qquad n_e = n_+ = n$$

and equations 3.2.3 and 3.2.4 may be combined, eliminating

the electric field E

$$S = -\left(\frac{D_e \mu_+ + D_+ \mu_e}{\mu_+ + \mu_e}\right)\frac{dn}{dx} \qquad 3.2.5$$

The ambipolar diffusion coefficient, D_a, is defined by

$$S = -D_a \cdot \frac{dn}{dx} \qquad 3.2.6$$

and hence $$D_a = \frac{D_e \mu_+ + D_+ \mu_e}{\mu_+ + \mu_e} \qquad 3.2.7$$

But since $$\frac{D_+}{\mu_+} = \frac{kT_+}{e} \quad \text{and} \quad \frac{D_e}{\mu_e} = \frac{kT_e}{e}$$

and $\frac{1}{\mu_+} \ggg \frac{1}{\mu_e}$ equation 3.2.7 becomes

$$D_a \simeq \frac{k\mu_+}{e}\left(T_+ + T_e\right) \qquad 3.2.8$$

and $$D_a = \frac{k\mu_+ T_+}{e}\left(1 + \frac{T_e}{T_+}\right) = D_+\left(1 + \frac{T_e}{T_+}\right) \qquad 3.2.9$$

If the electron temperature is the same as the ion temperature, as in the case of an after-glow then the ambipolar diffusion coefficient is just twice the value of D_+. In a plasma however the electron temperature is approximately a hundred times that of the positive ions and ambipolar diffusion will proceed more rapidly than would the diffusion of free ions. Likewise ambipolar diffusion will be slower than would be the diffusion of free electrons. The effect is that the electron diffusion is slowed down by the drag of the ions and this keeps the electrons from diffusing out rapidly from the plasma. It has been shown[140] that ambipolar diffusion is important when the concentrations of positive ions and electrons are large and approximately equal. When the concentrations are low then "free" diffusion occurs and electrons are lost more rapidly from the plasma.

Ions and electrons could be removed by the simple process of radiative recombination.

$$H^+ + e^- \longrightarrow H + h\nu$$

and

$$H^+ + e^- \longrightarrow H^* + h\nu$$

The probability of this process of radiative recombination occurring is however low and it is thought that either a ternary collision takes place

$$X^+ + e^- + e^- \longrightarrow X^* + e^-$$

or

$$X^+ + e^- + M \longrightarrow X + M$$

or a dissociative recombination occurs, for example in helium

$$e^- + He_2^+ \longrightarrow He + He$$

A process rather like that of radiative recombination is dielectronic recombination. This involves an electron recombining with a positive ion and the electron going into an energy level higher than the ionisation potential but not being released. The electron then falls into a level below the ionisation potential and so ionisation cannot take place

$$He^+ (1s) + e^- \longrightarrow He (2 p n l) \rightarrow He (1snl) + h\nu$$

The probability of the process occurring depends on the relative magnitudes of the lifetimes of the two states and is usually quite small. However it has been suggested that at high electron temperatures, of the order of 10^6K, it could well be important.

c) Particle Velocity, Energy and Collision Frequency

Before the application of an electric field, the velocity distribution of gas molecules is Maxwellian. However, with the application of an electric field, the velocity distribution of the electrons becomes Druyvesteynian[139,140], and is given by

$$f(v) = A \exp - \left(\frac{v}{\alpha}\right)^4 \qquad 3.2.10$$

where v is the velocity, A is a normalisation factor such that

$$4\pi \int_0^\infty f(v)\, v^2\, dv = 1 \qquad 3.2.11$$

$$\alpha = \left[\frac{4}{3a^2} \cdot \frac{M}{m} \left(\frac{e}{m} \right)^2 \left(\frac{E}{n} \right)^2 \right]^{1/4} \qquad 3.2.12$$

where $a = q_m(v)$, $q_m(v)$ being the momentum transfer cross section for elastic collision at the speed v.

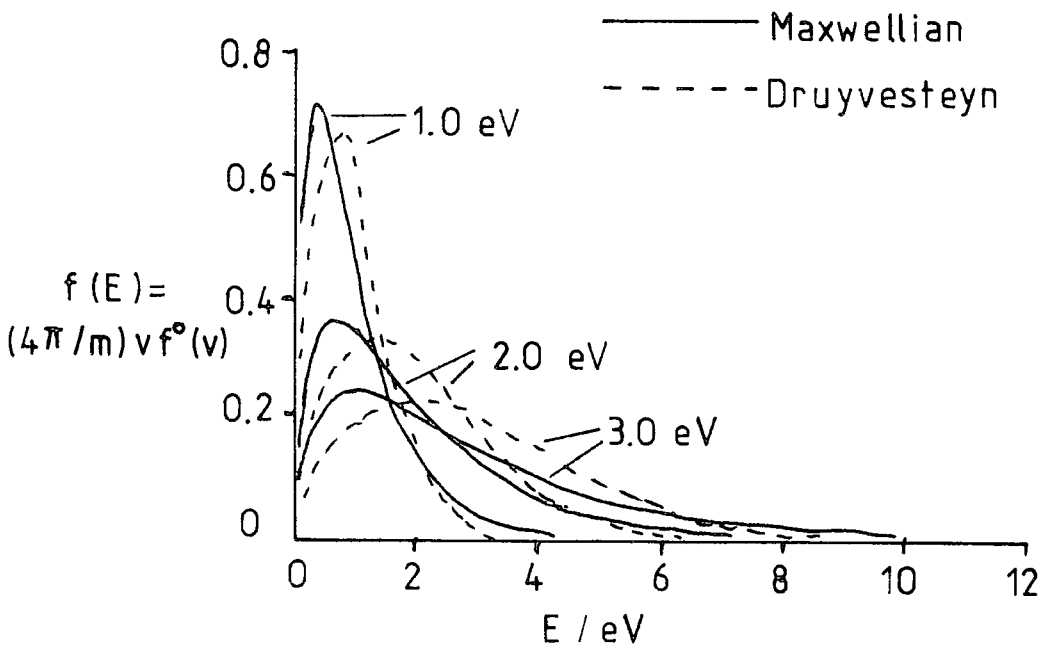

Maxwellian and Druyvesteyn Distributions [144]

Figure 3.2.2

The Druyvesteyn distribution holds for constant momentum transfer cross section and for cases where the electron velocities are much greater than those of the ions and molecules. It does not hold when inelastic processes are taking place but is more useful as a first approximation in these cases than is the Maxwell distribution. The distribution function is similar in shape to the Maxwell distribution for a given mean speed but has a slightly higher more probable speed and the high energy tail is diminished.

It can then be shown[140] that the average velocity, $\bar{c}$, of an electron between collisions is given by

$$\bar{c} \simeq \left[\frac{M.e^2 E^2 \lambda^2}{m^3} \right]^{1/4} \qquad 3.2.13$$

where M is the mass of the heavier particle, e is the electron charge, E is the electric field, λ is the electron mean free path and m is the electronic mass.

From this the mean kinetic energy of the electron may be obtained

$$1/2 \cdot m (\bar{c})^2 \propto 1/2 \cdot m (\bar{c^2}) \simeq \frac{1}{2} \cdot \sqrt{\frac{M}{m}} \cdot eE\lambda \qquad 3.2.14$$

and since $kT_e = \frac{1}{2} \cdot m \bar{c^2}$ where k is Boltzmann's constant the electronic "temperature", T_e, may be found. In electric discharges electron velocities are generally

much higher than ion and molecular velocities and the electron "temperature" is often of the order of 30000 K compared to the gas temperature of about 300 K, as has previously been noted.

Since the electrons and ions frequently make collisions they move through the plasma at a lower velocity than their average velocity. This drift velocity v_D may be related to the average velocity $\bar{c}$ by

$$v_D^2 = \frac{K}{2} \cdot \bar{c}^2 \qquad 3.2.15$$

where $$K = \frac{8}{3} \cdot \frac{m\,M}{(m + M)^2} \cdot \left(1 - \frac{T_g}{T_e}\right)$$

assuming (Townsend) that a constant fraction of the energy is lost on each collision. The collision frequency, ν, for electrons and ions may be obtained from

$$\nu_e = \frac{e}{m\,v_{De}} \cdot E \qquad 3.2.16$$

and $$\nu_i = \frac{e}{M\,v_{Di}} \cdot E \qquad 3.2.17$$

Typical values of drift velocities for electrons and reduced collision frequencies, in some common gases, are shown in figure 3.2.2[143]. Typical values of drift velocities for ions and reduced collision frequencies are shown in figure 3.2.3[143]. The parameter $E/_p$, the reduced field, where E is the electric field and p is the pressure, is important since it is connected with

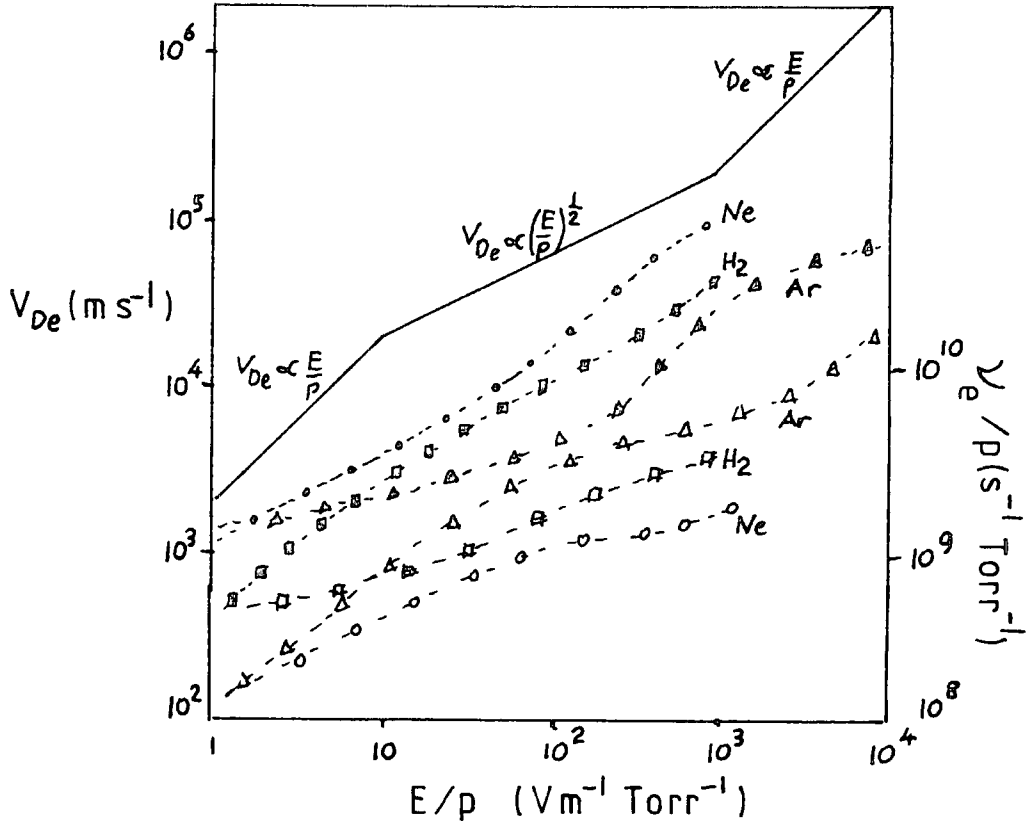

Drift velocities and reduced collision frequencies for electrons in some gases

Figure 3.2.2

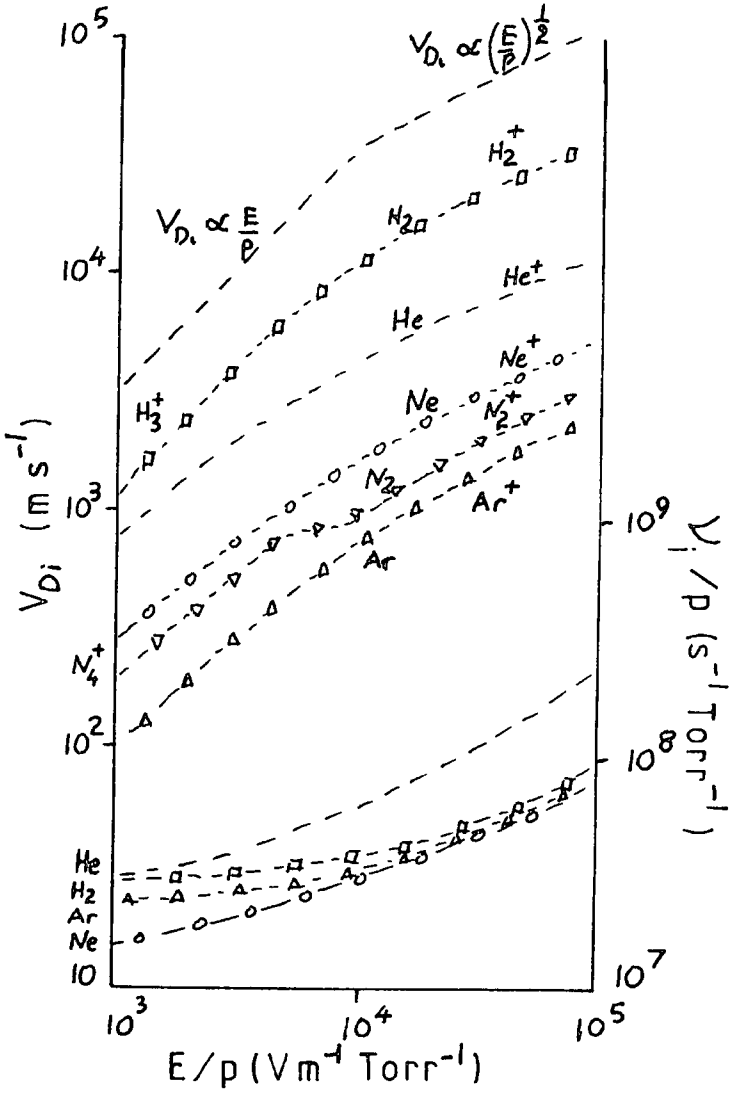

Drift velocities and reduced collision frequencies for ions in some gases

Figure 3.2.3

the energy an electron acquires between collisions. The electron mean free path is proportional to the reciprocal of the gas pressure, p, and the acceleration of the electron is proportional to the voltage E. The energy that an electron gains between collisions will be proportional to the time it is accelerating and the acceleration. The former is proportional to the mean free path and the latter to the voltage as stated above and so $E/_p$ will be a measure of the energy gained per collision.

Even though electrons, molecules and ions are frequently colliding in a gas plasma not many of the collisions will result in activation or transfer of other than elastic energy. This is because many excitation processes require minimum threshold energies to be exceeded[141] which are often of the order of several electron volts. The average energy of the electrons, and ions, in a gas discharge is usually only of the order of 2 or 3 eV and it is only those electrons, or ions, in the rapidly diminishing high energy tail which have sufficient energy to cause activation and ionisation.

.3 Corona

a) General Aspects

The type of discharge obtained in a gas, between two electrodes, is determined by the potential difference, the gas pressure and the current density that is obtained. This latter is determined partly by the electrode design and separation which are other important

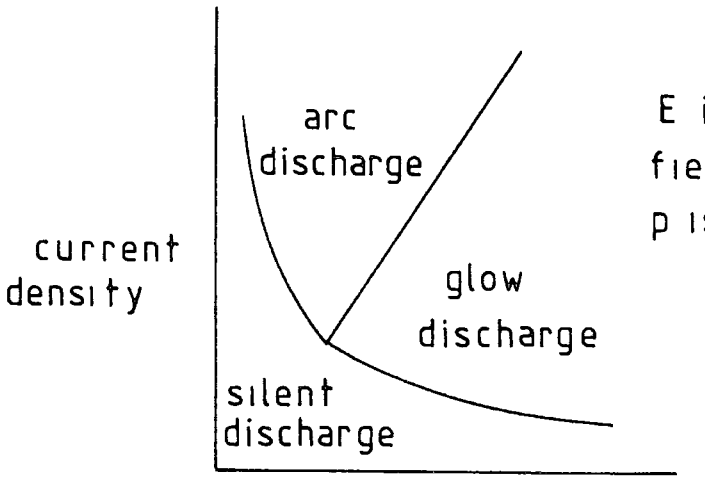

E is the electric field strength and p is the gas pressure

Basic Types of Electric Discharge

Figure 3.3.1

factors. Three basic types of electric discharge may be distinguished; silent, glow and arc discharge. The conditions under which a particular type of discharge may be obtained is shown schematically in figure 3.3.1.

By varying the gas pressure and electric field one type of discharge may be turned into another, the current density depending upon the type of discharge. At atmospheric pressure as the voltage between two electrodes is increased there is initially observed a silent discharge due to the conductivity of the gas arising from ionisation caused by the background cosmic radiation. The current density in the silent discharge is quite low. As the electric field is increased then a particular type of silent discharge, called a corona discharge, is observed, usually when a non-homogeneous electric field is used. This is often obtained using one electrode with a small radius of curvature and the other electrode with a much larger radius of curvature. Near to the electrode with the smaller radius, and therefore with the most inhomogeneous electric field, a glowing layer is observed, called the corona.

The glow is caused by impact ionisation in the corona and estimations of the energy of the positive ions in the corona give a value of approximately 100 eV. When the current intensity is sufficiently high the corona discharge changes into a spark discharge[145].

b) Direct Current Corona Discharge

As previously stated the electrode design is important in determining the type of discharge and this is illustrated in figure 3.3.2a and b for certain basic electrodes. Figure 3.3.2a illustrates the voltage-current characteristics when the electric field at the anode is highly stressed by using a wire or sharp point as the anode and a plane or sphere of much greater radius as the cathode. Figure 3.3.2b shows the characteristics when the converse geometry is employed and when the electric field round the cathode is highly stressed.

i) Positive Wire, Negative Plane

Considering first the case where the positive electrode has the highly stressed field, that is a positive corona, figure 3.3.2a. As the voltage is increased from zero there is a small increase in current in region A, due to the presence of a few electrons and ions caused by cosmic radiation. There will be statistical fluctuations in the current in this region due to the random characteristic of the background cosmic radiation and eventually the current will saturate in the region B.

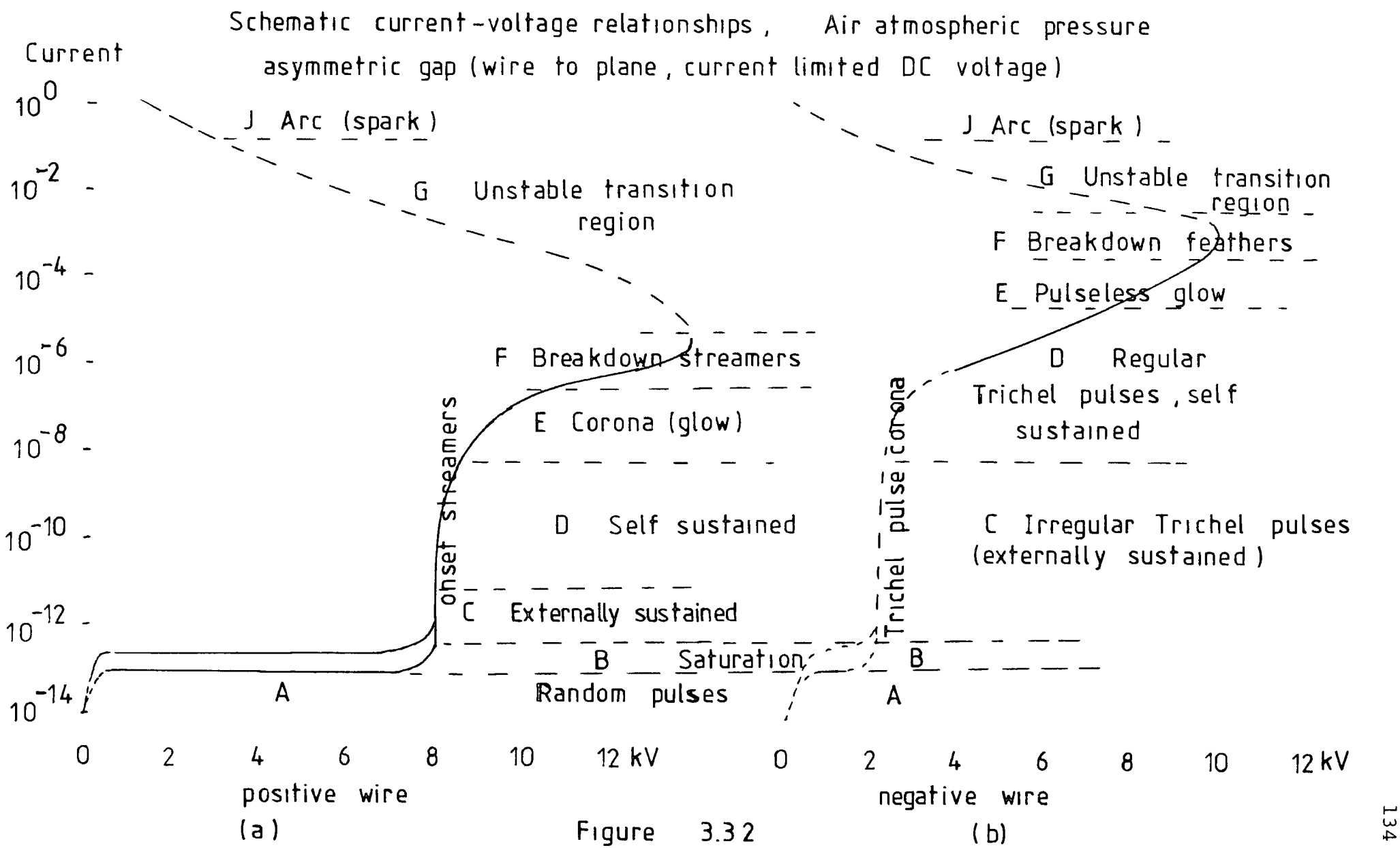
Schematic current-voltage relationships, Air atmospheric pressure
asymmetric gap (wire to plane, current limited DC voltage)
Current
10^{0}
10^{-2}
10^{-4}
10^{-6}
10^{-8}
10^{-10}
10^{-12}
10^{-14}
J Arc (spark)
G Unstable transition region
F Breakdown streamers
E Corona (glow)
D Self sustained
C Externally sustained
B Saturation
A
Random pulses
onset streamers
0 2 4 6 8 10 12 kV
positive wire
(a)
J Arc (spark)
G Unstable transition region
F Breakdown feathers
E Pulseless glow
D Regular Trichel pulses, self sustained
Trichel pulse corona
C Irregular Trichel pulses (externally sustained)
B
A
0 2 4 6 8 10 12 kV
negative wire
(b)

Figure 3.32

As the voltage is increased the primary electrons from cosmic radiation acquire sufficient energy to cause activation of molecules which may then emit radiation. This is the region C and it is characterised by larger current impulses than in A and B, and by the observation of "onset" streamers of visible radiation which branch out from the anode towards the cathode. In the region D a similar process to C is observed but the primary electron energies are now sufficient for electron impact ionisation to begin, see section .2a.1. The discharge does not become continuous in the regions C and D because of the space charge effect of ion accumulation round the positive, stressed, electrode. As the electrons in the space around the positive electrode fall onto the electrode they leave an accumulation of positive ions. These positive ions set up a space charge and effectively reduce the electrical field stress round the anode and until these positive ions have moved away, towards the cathode, the electric field is insufficient for another streamer to form.

A further increase in voltage causes the onset of the true corona, region E, and a disappearance of the onset streamers. Sufficient electrons are produced by avalanches to maintain the glow, which appears as a sheath round the anode. The presence of a large number of positive ions reduces the field strength round the anode and streamers are no longer formed. Detailed studies have shown though that even in this discharge there are

still high frequency ripples on the current[145]. Further increases in voltage, and of field strength, however, overcome the space charge effect and streamers are once more observed, together with the corona glow in region F. After this the discharge enters an unstable region, G, where current and voltage are inversely related and this leads to eventual spark or arc breakdown, J.

In an arc vaporisation of electrode material occurs and the ions resulting from this vaporisation carry very large currents. Also a comparatively large volume of gas plasma is raised to a high temperature. What may then happen is that the low resistance of the arc leads to a drop in the voltage between the electrodes due to the resistance of the external circuit. The discharge then cuts itself off until the gap voltage is sufficient to cause breakdown and the process is repeated. This in fact provides a definition of an arc compared to a spark in that an arc is a continuous discharge and a spark is a discontinuous discharge.

ii) Negative Wire, Positive Plane

When a highly stressed field round the cathode is used, that is a negative corona, the first effect on increasing the voltage is much the same as for a positive corona. That is, there are small random current bursts due to electrons formed by cosmic radiation, up to point B. In the region C, electron avalanches are formed by electron impact and these, together with the ions formed,

produce irregular current pulses, called Tricel pulses. At the same time the positive ions falling onto the cathode cause emission of light both from the cathode and ion/molecule collisions. As the field is increased the Tricel pulses increase in size and become more regular, region D. The parameter that has most effect on the pulses is the radius of the cathode which affects both the amplitude and frequency of the current pulses[146]. It has been shown by Fieux and Botteau[146] that when the cathode radius r is greater than 0.125 mm and for gaps greater than 10 mm that

$$\frac{dF}{dI} = 2.27\ r^{-1}$$

where F is the Tricel pulse frequency in kilohertz and I is the current in micro amps.

Increasing the voltage changes the pulsed discharge into a continuous one, region E. However, unlike the positive corona, where the onset streamers disappear in the true corona, in the negative corona the Tricel pulses persist in the pulseless glow. What in fact occurs is that the Tricel pulses are incorporated into a continuous current. Like the positive corona, further increases in voltage cause the appearance of "feathers", Region F, to the negative corona and eventually at higher voltages the discharge enters an unstable region G and finally breaks down to an arc or spark, in region J.

iii) Plane Parallel Electrodes

It has been found that using plane parallel electrodes that it is not possible to obtain a stable corona discharge[147]. This is illustrated schematically in figure 3.3.3. The first two regions A and B are, like those for positive and negative corona, the result of primary electrons caused by cosmic radiation. In regions C and D electron avalanching begins; in C this is observed as intermittent current pulses and in region D as more regular and frequent current pulses. The progression from B to C and D is marked by only a small increase in voltage and in C and D no streamers of visible radiation are observed. From D the discharge, on increasing the voltage, enters an unstable region where current and voltage are inversely related and the discharge then breaks down to an arc or spark. It has been shown by Corbine[146] that in fact a corona will not be formed on parallel wires, with radius r and gap distance d, in air if the ratio d/r is less than 5.85. When d/r is less than 5.85 a spark is obtained and thus it would be expected that plane parallel electrodes would also break down with a spark and not a corona. In the case of negative coronas it has also been shown[146] that when the gap separation is less than 2.5 mm spark breakdown is obtained without corona discharge.

c) Alternating Current Corona Discharges

The behaviour of the discharge under alternating

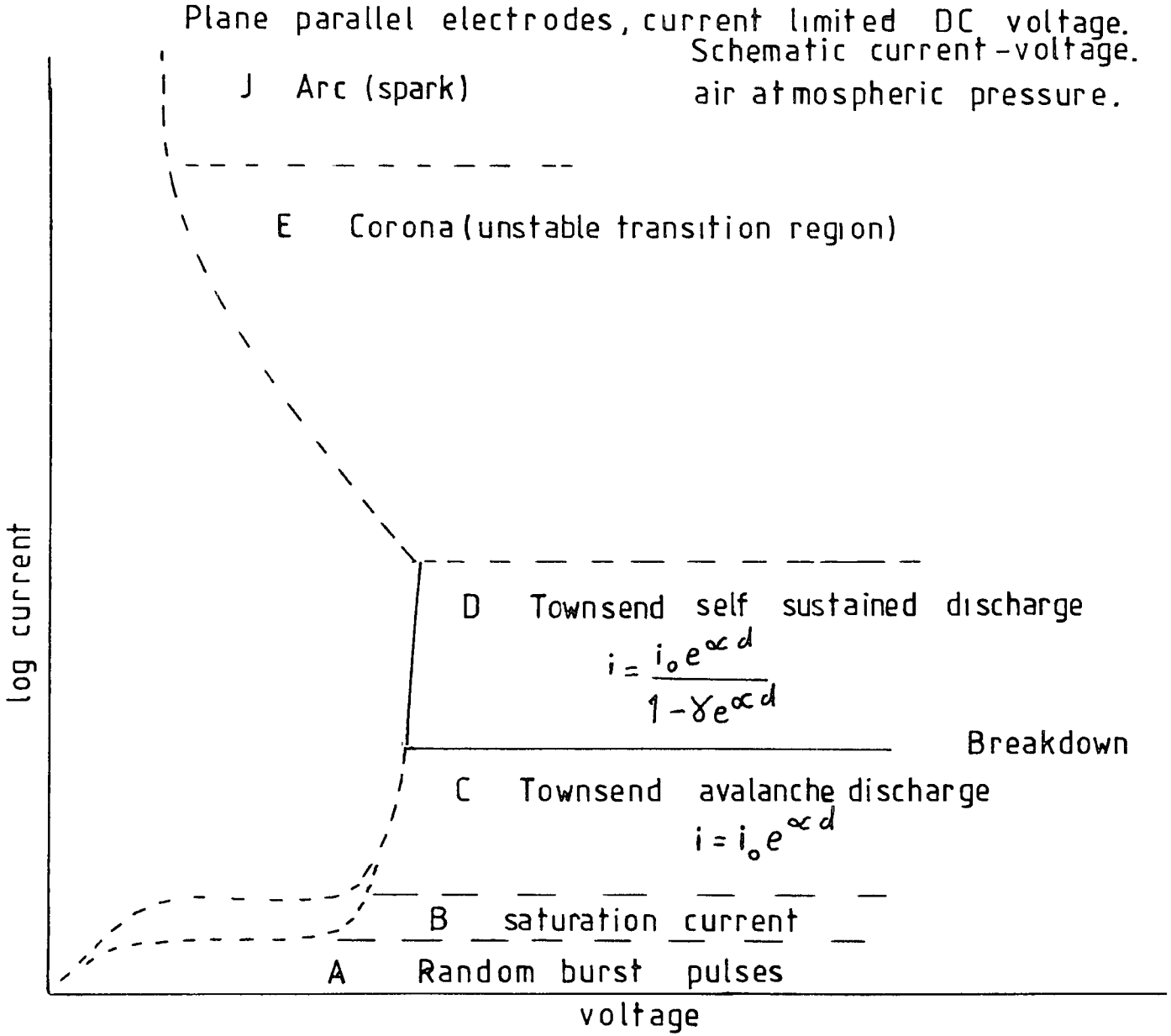
Plane parallel electrodes, current limited DC voltage.
Schematic current-voltage.
air atmospheric pressure.
J Arc (spark)
E Corona (unstable transition region)
D Townsend self sustained discharge
$i = \frac{i_o e^{\alpha d}}{1 - \gamma e^{\alpha d}}$
Breakdown
C Townsend avalanche discharge
$i = i_o e^{\alpha d}$
B saturation current
A Random burst pulses
log current
voltage

Figure 3.3.3

voltage conditions will resemble that of direct voltage conditions provided that the frequency is such that the ions produced under one half cycle are removed before the start of the next half cycle. When however the electrode gap and frequency are both sufficiently large so that there are still ions left in the gap at the end of one half cycle, the behaviour of the discharge will be quite different. Berger et al[146] have shown that the effect of ions can last for up to 5 milliseconds and that as the frequency is increased the effect of the residual ions is more pronounced. The influence of residual ions may also cause a lowering of the breakdown voltage. When carrying out the work described in Chapter 4 of this thesis, it was observed that the discharge, using alternating current of approximately 3 k Hz, and its effects were quite different compared to using a direct current supply.

d) Ions and Molecules formed in a Corona

The commercial treatment of polymer surfaces by corona discharge uses gases, normally air, at atmospheric pressure and containing variable amounts of water vapour. Under these circumstances a complex series of reactions may occur in the gas phase leading to the formation of various ions including hydrated species. Even where water vapour is excluded there may be sufficient water vapour absorbed on the polymer surface for hydrated ions to be formed. The gases used in the work presented in this thesis are air, oxygen, nitrogen and argon, all

containing variable amounts of water vapour, and these are the ones that will be discussed. The ions and other species that may be present are deduced from the work of Shahin[148] and since his results are only for pressures up to 40 torr a certain amount of extrapolation is required. In view of this the nature and compositions of the gas plasmas suggested below must be regarded with caution and further work in this area is indicated.

i) Discharges in Air

The principal species to be expected are O_2^+, O_4^+, $O^+.(H_2O)_n$, NO^+ and NO[148]. At the same time, and in some instances as possible precursors to these species, various other activated molecules and ions may be formed. Examples of these are singlet oxygen, O_2^* $a^1\Delta g$, O_2^- from electron attachment, atomic oxygen[144] and atomic nitrogen. The work by Mayoux and co-workers[149] on the emission spectra of corona discharges suggests that N_2^* and N_2^+ may also be formed.

ii) Discharges in Oxygen

When the water content was low the only ions detected by Shahin[148] were O_2^+ and O_4^+. Singlet oxygen, O_2^- and atomic oxygen may also be formed[144]. The presence of water vapour allows the formation of various hydrated ions such as $(H_2O)_2^+$, H_3O^+ and OH^+ might be found, possibly formed in the following reactions

$$O_2^+ + 2\ H_2O \longrightarrow O_2^+ . (H_2O)_2$$

$$(H_2O)_2^+ + O_2 \longrightarrow H_3O^+ + OH + O_2$$

$$OH + O^+ \longrightarrow OH^+ + O$$

iii) Discharges in Nitrogen

In nitrogen the ions and activated molecules present are very dependent upon the presence or absence of water vapour and oxygen. Even small concentrations of these two gases have large effects on the results. In the absence of both, the principal species to be expected at atmospheric pressure are N_2^+ , N_2^+, N and N^+. When small amounts of oxygen are present then the principal positive ion appears to be O_2^+. Shahin also notes that small amounts of oxides of nitrogen are formed from traces of oxygen. The presence of water vapour allows the formation of a number of hydrated species such as hydrated protons and also the formation of NO_2^+.

iv) Discharges in Argon

In the absence of water vapour and oxygen the only species present will be Ar^*, Ar^+ and possibly Ar_2^+. The presence of water vapour and traces of oxygen are likely to produce a similar effect as in nitrogen and would allow the formation of O_2^+ and hydrated protons.

.4 Surface Treatment by Corona Discharge

a) General Aspects

The commercial treatment of polymeric material, both synthetic and natural, by corona discharge, is

normally carried out at atmospheric pressure using air containing variable amounts of water vapour. The gap separation of the electrodes, 1 to 2 mm, is such that even where rod or bar electrodes are used the gap geometry may be regarded as approximating to that of plane parallel electrodes (see section .3.b.iii above). In view of this a simple corona is unlikely to be formed but the discharge is more like a plasma formed by rapidly repeating spark discharges along the electrode gap[149,150]. Although an alternating supply is normally used, of frequency 50 - 10^4 Hz, this is unlikely to alter the situation since the ions and electrons formed during a half cycle will have sufficient time to cross the gap. This may be shown from the fact that the operating voltages are of the order of 10 kV, giving a field strength in the gap of the order of 10^4 kV m^{-1} and a reduced field E/p of the order of 10^4V m^{-1} $torr^{-1}$. Consideration of figures 3.2.1 and 3.2.2. then gives the drift velocities of electrons and ions under these conditions as being of the order of 10^5 and 10^3 m $sec.^{-1}$ respectively. This is sufficiently fast for them to be able to cross a gap of 1 - 2 mm at frequencies of 10^4 Hz and so from this point of view therefore the discharge may be regarded as a D.C.discharge.

Although as indicated above the commercial process does not involve a simple corona discharge the terminology is now well established and the various phenomena may be considered as arising from a corona

discharge even though the plasma is the result of spark discharges. The characteristics and variables of the corona discharge are shown schematically in figure 3.4.1 and the various electrical characteristics will be considered below while the chemical effects on polymers will be dealt with in Chapters 4 and 5.

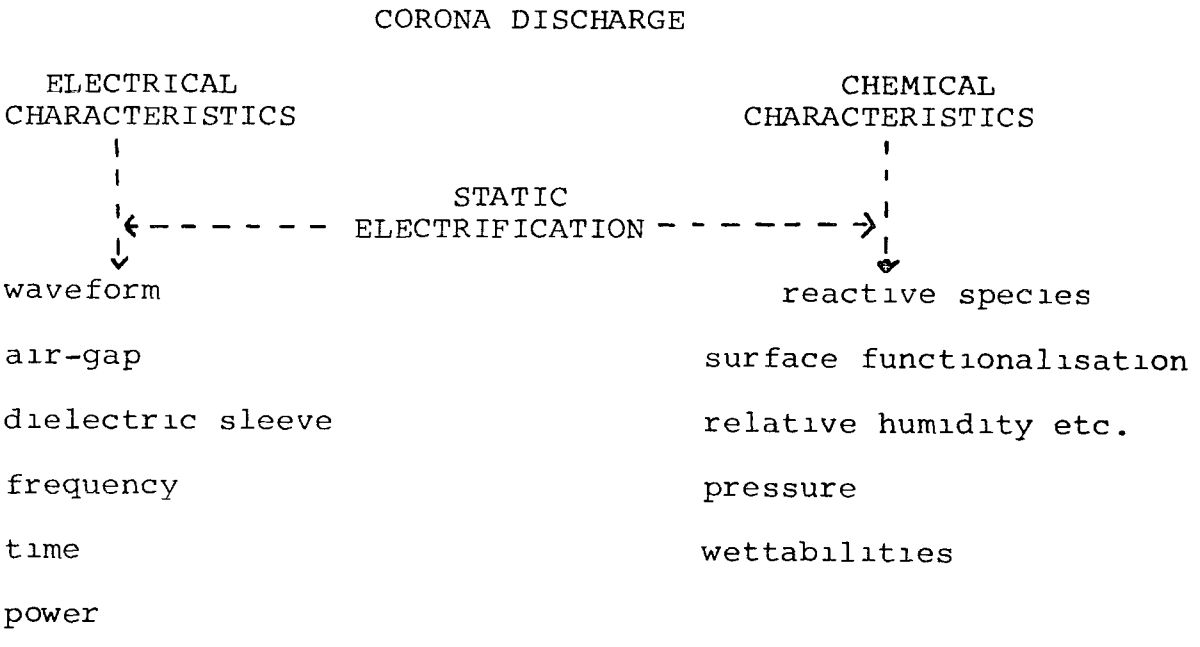

Figure 3.4.1

The effect of the discharge on polyethylene and other polymers is known to increase the ability of the surface to accept normal commercial printing inks. This is known to be due to an increase in the critical surface tension for wetting, see Chapter 5, though the reasons why the treatment produced this effect were not originally known. The increase in critical surface tension for wetting is often measured commercially by the ASTM wipe test. This involves the use of "Visking" solutions of known surface tension. These solutions are usually mixtures of dimethyl formamide and ethyl cellusolve, with a simple dye to facilitate observations. The solutions are available in a number of standard solutions of different surface tensions ranging from approximately 30 to 60mN m^{-2}. The procedure is to wipe a smear of different visking solutions across the polymer surface and observe their behaviour within 1 or 2 seconds. Then taking solutions in increasing order of surface tension that solution, which just does not break into droplets on the surface, is noted. This solution is taken as just managing to wet the surface and its surface tension is recorded as the critical surface tension for wetting of that surface. Although the method is somewhat dependent on the way it is carried out, with practice it does give consistent and reasonably accurate results in a very short time.

b) Electrical Characteristics

The electrical discharge, occurring in a corona discharge for the surface treatment of plastics, differs from other discharges in that the path of the discharge through the gas terminates at one end at an insulating layer. Also alternating current must be used and in fact as previously mentioned (.3c above) the use of direct current gives quite a different result. This will be discussed in more detail in Chapter 4.

The electrical characterisation of the discharge and the energy input may be found from a consideration of the work of Manley[152]. This work was on the ozonator discharge but the same principles may be applied to the corona discharge process.

Essentially the gap and its shunt capacitance Cg are in series with the polymer dielectric which serves as a buffer capacitance C_b. Before the gap breaks down the capacitance of the system, figure 3.4.2, is given by

$$\frac{1}{C} = \frac{1}{C_g} + \frac{1}{C_b}$$

When the gap breaks down the gap conducts and its effective capacitance is zero and the capacitance of the system is then C_b. When the gap breaks down charge is placed on the dielectic surface which builds up a back voltage that limits the total charge that is accepted. Considering figure 3.4.3 and going clockwise the gap

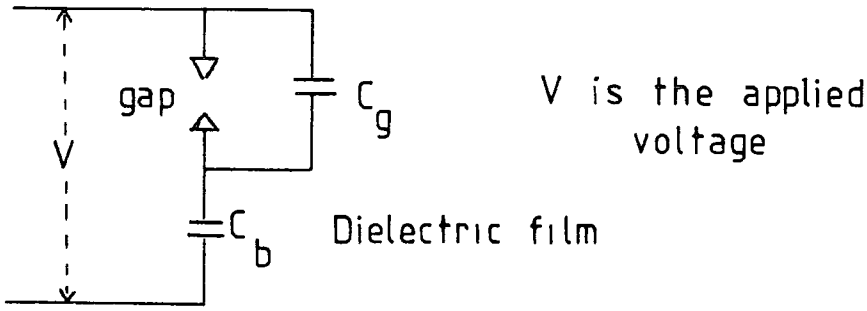

Equivalent electrical circuit of gap and polymer film

Figure 3.4.2

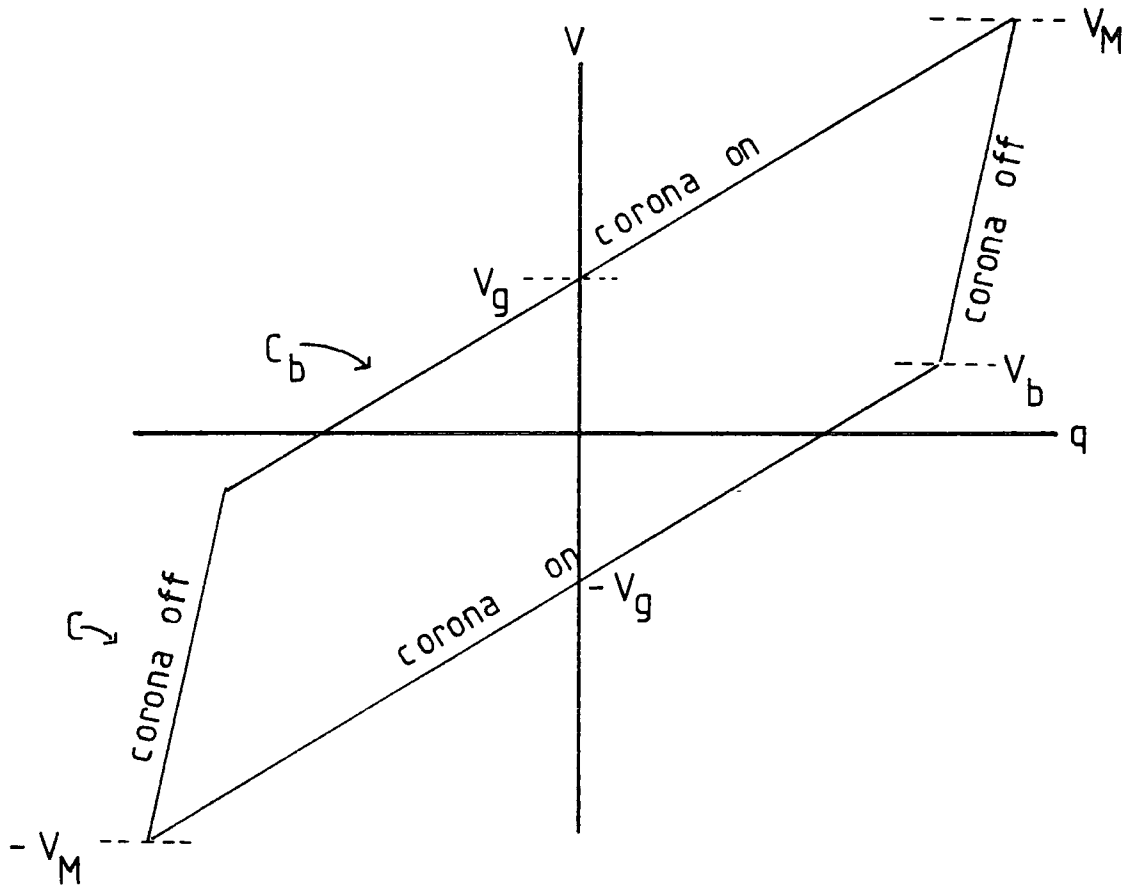

Voltage/charge phase diagram for corona discharge[153]

Figure 3.4.3

first breaks down at V_g and the corona discharge begins until V_M is reached. At this point the voltage supply is reversing and the corona discharge ceases[152] due to the back voltage resulting from charge build up[153]. At this point the current flow also ceases as charge is removed from the capacitance, now $(C_g + C_b)/C_gC_b$, until the effective voltage across the gap is sufficient to fire the gap. This effective voltage is given by the instantaneous applied voltage minus the voltage caused by the charge remaining on the buffer electric. The instantaneous applied voltage V_b when this occurs is given by[153]

$$V_b = V_M - 2\,V_g\left(\frac{C_g + C_b}{C_b}\right) \qquad 3.4.1$$

The corona discharge continues until the voltage reaches $-V_M$ and once again the discharge is quenched. The cycle then repeats with two luminous corona bursts per cycle interspersed with two dark periods[152] The energy, E, for each corona cycle is given by

$$E = 4\,V_g\,C_b\left[V_M - V_g\left(\frac{C_g + C_b}{C_b}\right)\right] \qquad 3.4.2$$

and the power imput, P, per second is given by

$$P = 4f\,V_gC_b\left[V_M - V_g\left(\frac{C_g + C_b}{C_b}\right)\right] \text{ watts} \qquad 3.4.3$$

where f is the frequency

From this equation it is seen that a low break down voltage for the gap does not result in an increase in corona power input but rather the reverse. Furthermore, all other factors being unchanged, V_M controls the energy and it would appear from the work of Rosenthal and Davis[153] that the shape of the voltage waveform is relatively unimportant. They also found that the corona power input did in fact vary directly with frequency as suggested by equation 3.4.3. In practice they observed that the voltage / charge phase diagram did tend to diverge from the ideal parallelogram in figure 3.4.3, and also that V_g varied with V_M. These factors tend to limit the usefulness of the parallelogram based power equation but it does provide some useful information. Although Rosenthal and Davis[153] found that the voltage waveforms shape was not important in calculating corona input energy they did find that asymetrical waveforms could lead to undesirable static charge remaining on the film. This static charge build up is always present in corona treatment but they found it was reduced using symetrical waveforms. This residual static charge may also be further reduced by a second treatment using frequencies of the order of a megahertz[154] though it is likely that this is a plasma discharge rather than the corona "spark" discharge.

Equation 3.4.3 suggests that simply increasing the frequency will increase the power input and therefore presumably the effectiveness of the treatment. There are however practical difficulties to the use of very high

frequencies, not the least being electrical noise interference of communication systems. This is more difficult to suppress at high frequencies and in practice the frequencies adopted are of the order of a few kilo-hertz with some equipment operating at 50-60 hertz (normal electrical supply frequency).

c) Corona Discharge Equipment

i) Electrode Design

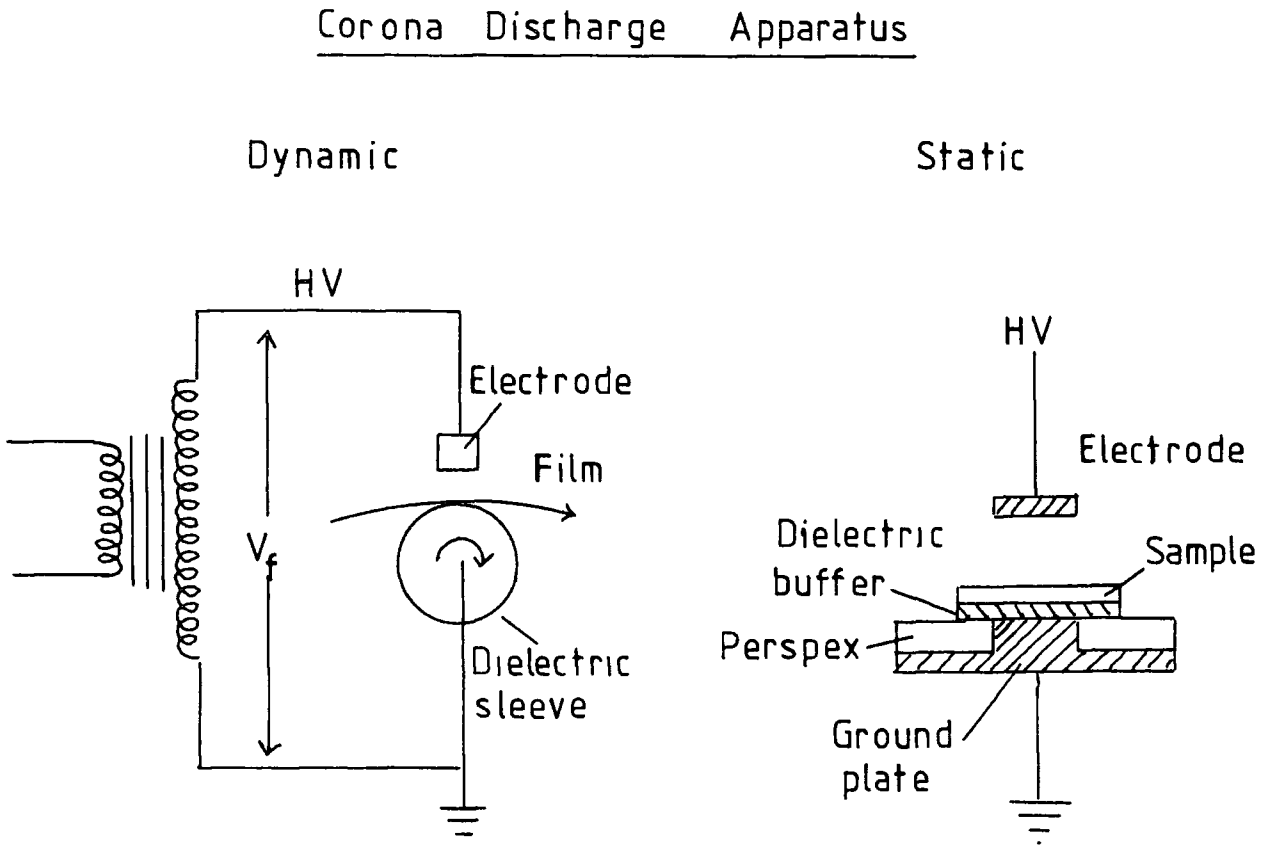

Figure 3.4 4

Corona discharge treatment may be carried out by either a dynamic process or a static process and these are illustrated schematically in figure 3.4.4. The static process is not normally used on industrial processes but is often more convenient for small scale investigations and is the method used for the work described in Chapters 4 and 5 of this thesis. The industrial process is usually concerned with the large scale treatment of polymer film and for this purpose the dynamic process is more convenient and economical. The basic principles are the same in both cases with the film to be treated being in contact with a buffer dielectric which is fixed to one electrode. Then there is a small gap, typically between 1 and 3 millimetres between the film surface and the second electrode which is normally of bare metal. The purpose of the buffer dielectric is principally to prevent burn-through[155] in the case of pin holes or weak patches in the film, and it is usually made as thin as possible. There is a certain amount of heating as a result of the corona discharge and this affects the useful life of the dielectric coating.

In the static process the upper electrode is usually a flat plate which has to be maintained parallel to the lower electrode to avoid the discharge taking place at the nearest point between the two electrodes. In the dynamic process the upper electrode is usually a bar or

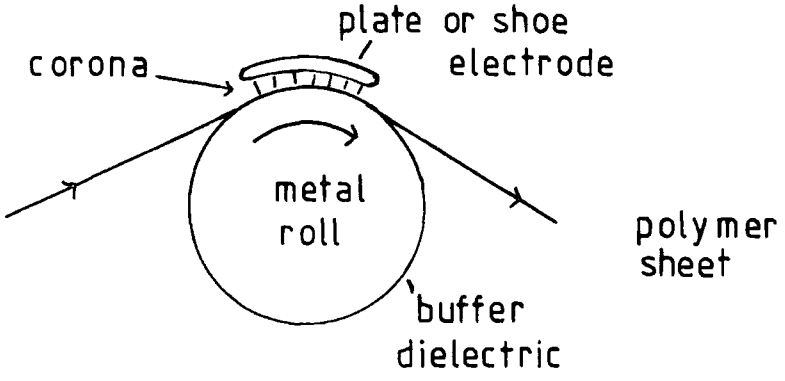

Figure 3.4.5

knife edge arranged parallel to the lower roll, though in some cases a curved metal shoe electrode[155] is used as shown in figure 3.4.5. One of the advantages of the shoe over the bar or knife edge electrode is that the film is subject to a longer corona treatment due to the larger area covered by the corona. This can be overcome when using bar or knife edge electrodes by using more than one electrode spaced round the roll. Also it has been observed that there is a "fan out" of the corona from the bars[153] and that a 1 cm bar projects as a 2.5 cm width at the film surface. A disadvantage of the shoe electrode is the problem of ensuring the gap distance is maintained accurately over the whole surface to avoid localising the discharge. This problem is not as severe using bar or knife edges but is still present. Also bar and knife edges tend to vibrate at the frequency of the alternating supply voltage. What has been found in practice is that a threaded rod[155] or bar with fine grooves gets round some

of these problems. The edges of the thread, or grooves, enable the discharge to be established uniformly along the rod and also the threaded rod does not vibrate as much.

ii) Alternating Power Supply[156]

The alternating power supply may be provided by rotating generators, inverters or vacuum tube amplifiers. The rotating generators may in fact be the normal alternating supply voltage merely stepped up by a high voltage transformer but more often is a motor alternator producing a supply at between 1 to 10 kHz. Following the motor alternator there is a high voltage transformer and a tuning circuit to match the load to the supply.

The inverter may be thought of as a rectifier operating in reverse, changing DC to AC and normally operates as an untuned circuit with the corona reactor. The advantage of the inverter over the motor alternator is the absence of moving parts and ease of installation.

The disadvantage of both the motor alternator and the inverter is that they both produce sine wave outputs and it has been suggested[155] that the ideal voltage waveform is a symetrical sawtooth. This waveform can be most easily produced by a vacuum tube power amplifier which may be fed in fact with any desirable waveform. There is probably scope here for the development of solid state power amplifiers.

.5 Plasma Discharges

a) General Aspects[157]

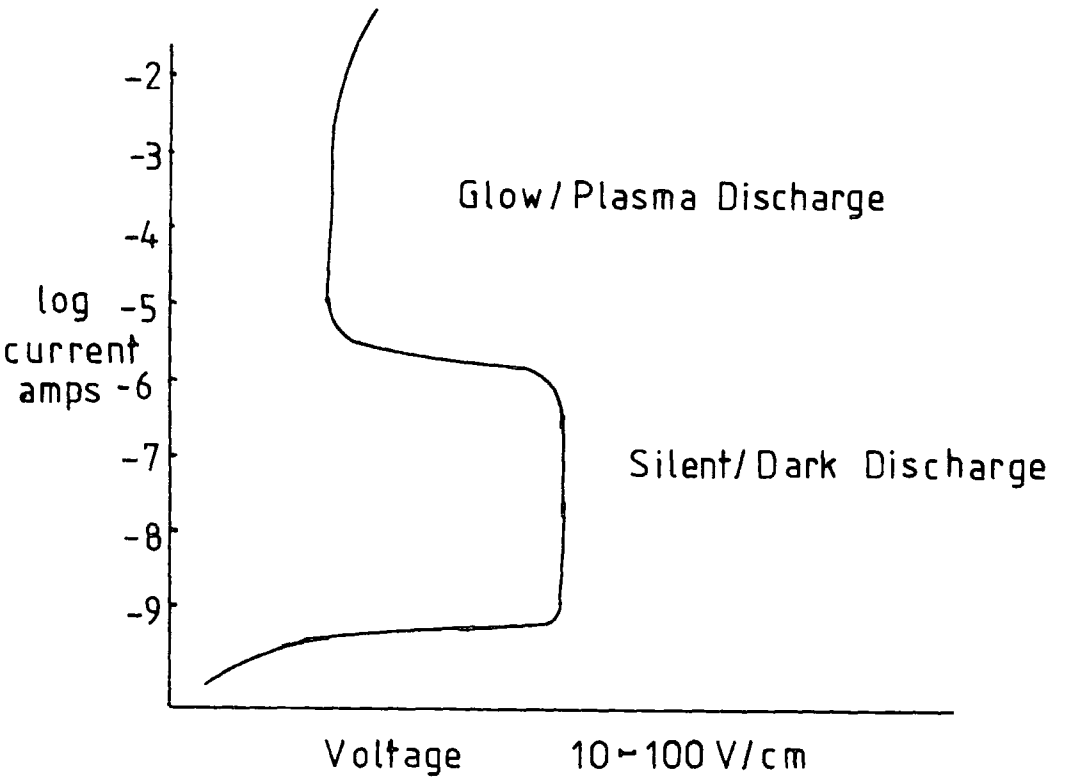

Schematic current-voltage relationship of a low pressure gas discharge

Figure 3.5 1

The current-voltage relationship for a low pressure gas discharge is shown schematically in figure 3.5.1.

At low gas pressures, of the order of 1 torr, the first type of electrical discharge that is obtained is the silent discharge due to ionisation of the gas by cosmic radiation. As the voltage is increased a glow appears close to the cathode and then with a small increase in voltage the discharge becomes established as a luminous glow throughout the gas. Either AC or DC may be used and the aspects of interest in glow discharge experiments are outlined below.

Electrical Power	Coupling Mechamism	Plasma Environment
DC	Resistive	Current
AC: low frequency	Capacitive	Pressure
AC: RF	Inductive	Gas Flow and Temperature
AC: Microwave		Reactant Phases
		Electric and Magnetic Field
		Photon Emission

One of the problems of using resistive coupling is that electrodes must be placed in the gas. These electrodes may then become contaminated and side effects caused by this contamination. At frequencies above 1 MHz this can be readily overcome by capacitive or inductive coupling[158].

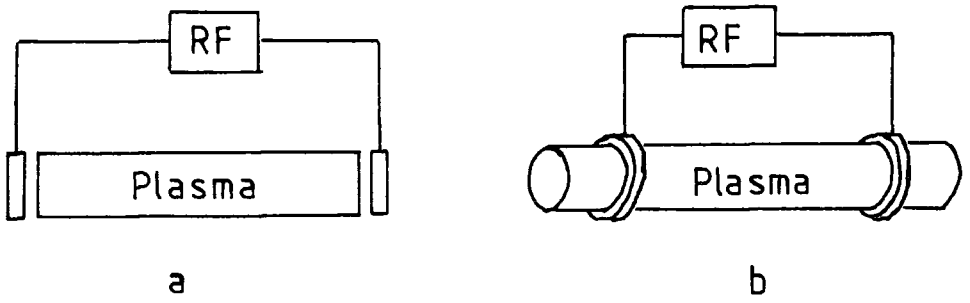

Capacitive coupling

Figure 3.5.2 a & b

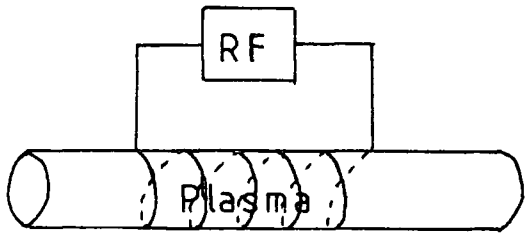

c

Inductive coupling

Figure 3.5.2 c

b) Reactive Species in Plasmas

Plasmas excited by electrical discharges contain a variety of species arising from collisions involving electrons accelerated by the electrical field. Many of the species are energetic enough to cause chemical reactions and a typical plasma may contain electrons, ions, metastables, neutral molecules and free radicals in ground, and excited states and photons of various energies. Possible energy values for these species are given in table 3.5.1 together with some typical bond energies for organic systems[159].

		Energies / eV
Plasma	Electron	0 - 20
	Ions	0 - 2
	Metastables	0 - 20
	UV/Visible	3 - 40

Bond Energies

C - H	4.3	C - C	3.4
C - N	2.9	C = C	6.1
C = O	8.0	C ≡ C	8.4

Energies available in a glow discharge and some typical bond energies

Table 3.5.1

The plasma discharge experiments, for the work in this thesis (see Chapter 6) were carried out using a pressure of 0.2 torr and a frequency of 13.56 MHz. Air and oxygen were both used and possible species present in each case are given in (i) and (ii) below.

i) Plasma Discharge in Air at 0.2 Torr[148]

The principal positive ion will be O_2^+ formed by the following reactions

$$N_2^+ + O_2 \longrightarrow N_2 + O_2^+$$

$$O_2 + e^- \longrightarrow O_2^+ + 2\ e^-$$

At the pressure used NO and NO^+ will also be present

$$O_2 + N_2^+ \longrightarrow NO^+ + NO$$

Another possible ion is the peroxy isomer of NO_2^-, $[N{-}O{-}O]^-$ which has been observed in oxygen plasmas containing nitrogen[142]. Other species present will be atomic oxygen, atomic nitrogen, singlet oxygen and N_2^*. At the low pressure, 0.2 torr, the presence of N_4^+ is unlikely, neither are hydrated protons likely to be formed.

ii) Plasma Discharges in Oxygen at 0.2 Torr[148]

At the pressure and temperature used the only ion likely to be present is O_2^+. Other species present will be atomic oxygen, singlet oxygen and O_3. Hydrated protons and OH^+ are unlikely to be formed.

c) Photon Emission of Plasmas

The term glow discharge has arisen due to the emission of light from the plasma. Yet the photon emission in the ultra violet and especially the vacuum ultra violet may in fact be two orders of magnitude greater than that of visible light[160]. This has been shown to be the case for argon at 0.1 torr by Clark and co-workers[160]. Their results show that for an argon plasma at 0.1 torr most of the photon emission is associated with the Ar I resonance lines at 1048.2 and 1066.7 Å resulting from transitions of the neutral atom, $3p^5 4s \rightarrow 3p^6$. The rest of the photo emission was almost entirely from Ar II

resonance lines at 932.1 and 919.8 Å resulting from transitions of the singley ionised system, $3s3p^6 \longrightarrow 3s^2 3p^5$. They also found that the electro-magnetic radiation output increased with power input into the plasma and that output was affected by pressure changes. The other important factor was that the relative intensities of the Ar I and Ar II lines changed as these two parameters, power and pressure were altered. For diatomic gases such as nitrogen and oxygen transitions between molecular orbitals may be involved[161], in the case of oxygen that between $B^3\Sigma_u$ and $X^3\Sigma_g$ has been observed, giving a line in the spectrum at 2000 Å. In low temperature and low pressure nitrogen plasmas the following transitions have been observed[161], with some lines in fact in the near infra red.

N_2	$B^3\pi_g$	- $A^3\Sigma^+_u$	10500	IR
N_2	$C^3\pi_u$	- $B^3\pi_g$	3400	UV
N_2^+	$B^2\Sigma^+_u$	- $X^2\Sigma^+_g$	3900	UV/Visible
N_2^+	$A^2\pi_u$	- $X^2\Sigma_g$	11000	IR

The emission spectra, for "corona" discharges at atmospheric pressure in air, has been studied by Rodura, Mayoux and Loubière[149] who observed lines due to the transitions

N_2	$C^3\pi_u$	- $B^3\pi_g$	
N_2^+	$B^3\Sigma^+_u$	- $X^2\Sigma^+_g$	

Their spectra also revealed that using an alternating electrical discharge and polyethylene as a dielectric that NH radicals, or groups may be formed.

Chapter 4

Surface Oxidation by Corona

.1 Introduction

.2 Experimental Details

a) Samples

b) Reactor with Disc Electrodes

c) Glass Tube Reactor for Controlled Atmospheres

d) Corona Power Supply

.3 ESCA Results using

a) Air

b) Oxygen

c) Nitrogen

d) Argon

e) Humidity Effects, Heating

f) Air saturated with Perfluorobenzene Vapour

.4 Infra Red Spectra, MIR

.5 Iodine Liberation

.6 Discussion and Consideration of Results

.1 Introduction

The treatment of polymer surfaces is a method of considerable technological importance (see Chapter 1). Although the process has been used for over two decades[155], to improve the surface energy of polymers, the reasons why the process works have only been poorly understood. This has been partly due, originally, to the thinness of the layer treated, of the order of 10^{-8} m, and the lack of any suitable analytical technique for analysing such a thin layer.

The corona treatment process has many advantages over chemical and physical processes of treatment, especially when treating thin film material such as is used in the packaging industry. The advantages include the fact that the reaction is inherently "clean" and involves no hazardous chemicals apart from ozone which results from the discharge. It is not thought that this ozone is directly involved in the surface treatment process since exposure of polymer films to ozone does not produce a comparable effect to corona treatment for the same length of time. While the corona treatment produces considerable changes in the surface energy, as measured by wetting tension, peel strength and shear strength on glueing, the bulk properties of the material are unchanged.

There are no reliable means of estimating either the thickness of the modified layer produced, unless a

step profile is assumed[162], or the concentration profile for the polymer surface. However, the thickness of the layer is assumed to be of the order of 10^{-8}m and the concentration profile is thought to be like that shown in figure 4.1.1.

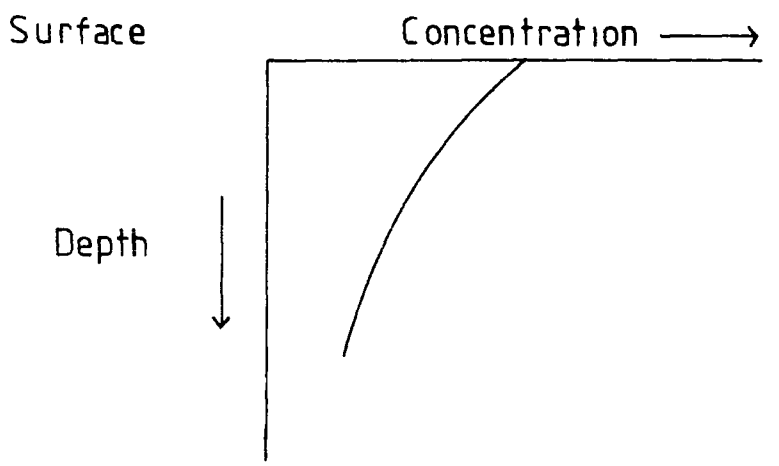

Assumed Concentration/Depth Profile for Corona Treatment of Polyethylene

Figure 4.1.1

In view of the thinness of the modified layer it is not possible to use conventional analytical techniques to determine the concentration of the surface layer. Thus conventional infra red and ultra violet spectra show virtually no change in polyethylene after corona treatment though it was possible to detect a slight difference after 30 minutes' exposure to corona treatment and using four thicknesses of treated film (see section .4 below). Techniques have been developed for removing the surface layer

by abrasion and then employing conventional analytical techniques on the scrappings. It has been shown however that this method leads to deep scoring of the surface in some places while other parts are left virtually untouched[163]. It cannot be certain therefore that all of the surface layer has been removed and that no unmodified substrate has been removed. Furthermore the surface layer is destroyed and further work on it is not possible. The use of solvents to remove the surface layer has been suggested but it cannot be certain that all the modified layer is removed and that no unchanged substrate has been dissolved. In fact in section .5 of this chapter it will be seen that while immersion in a solvent may remove some of the surface modification not all the effects are removed (see also Chapter 5.2).

The principal method used in this work to analyse the surface modification, caused by corona treatment, is that of ESCA. This method as was discussed in Chapter 2 is ideally suited to the problem since the penetration depth for analysis by ESCA is of the order of 3×10^{-9}m, when using magnesium or aluminium targets in the X-Ray source. This small penetration and therefore analysis only of the surface material can in other instances be a disadvantage since the surface of many materials may well be slightly different in composition to the interior. In fact in the case of corona treatment ESCA does not penetrate sufficiently far to sample all the treated layer.

Thus though it has been possible in this study (see section .3 below) to carry out ESCA studies at different angles of take-off and hence different depths in the sample (see Chapter 2.6f) it has not been possible to carry out a complete depth profile.

The other method used in this work for analysing the surface layer is that of Multiple Internal Reflection Infra Red spectroscopy (MIR IR). This method like ESCA is non-destructive and only samples the surface layer (see section .4 below). Unfortunately, the sampling depth[163], of the order of 10^{-6}m, is much greater than the depth of the corona modified layer, approximately 10^{-8}. This means that the spectrum has a very strong component from the unmodified substrate and the surface modifications produced only show up as weak components of the spectrum.

The plasma produced by a corona discharge is complex and it is not possible, at this stage, to resolve the total corona energy into its many components, such as radiation, ions, electrons, activated molecules and other species. In view of this complexity it is not possible to state, with certainty, which of the various components are responsible for the surface modification of polyethylene in a corona discharge. A certain amount of work has, however, been done by Mayoux[164] using UV radiation, electron and ion beams. The results of these he compares to the effect on polyethylene of a corona

discharge. This will be dealt with again in section .7 of this chapter.

Figure 4.1.2 summarises the various plasma systems, either occurring naturally or produced in laboratories, defined in terms of their electron density n (cm^{-3}) and average electron energy kT_e(eV). λ_D is the Debye length, a function of the square root of the electron energy to density ratio[144].

.2 Experimental Details

a) Samples

The polymers dealt with were either high density or low density polyethylene, supplied by the Metal Box Company. Both polymers were in the form of thin film, approximately 0.1 mm thick and were normally used straight from the roll without any pre-treatment. Handling of the actual samples was avoided to prevent contamination and the effect of rinsing with acetone before treatment was tried to see if there was any residual surface grease. This rinsing did not, however, cause any observable change in the overall effect of corona treatment compared to unrinsed samples and so the washing with acetone was discontinued. Samples of both films were sent to the Rubber and Plastics Research Association of Great Britain's research laboratories at Shawbury to ascertain the levels of antioxidants present. The results, as obtained by J.A. Sidwell at RAPRA are:-

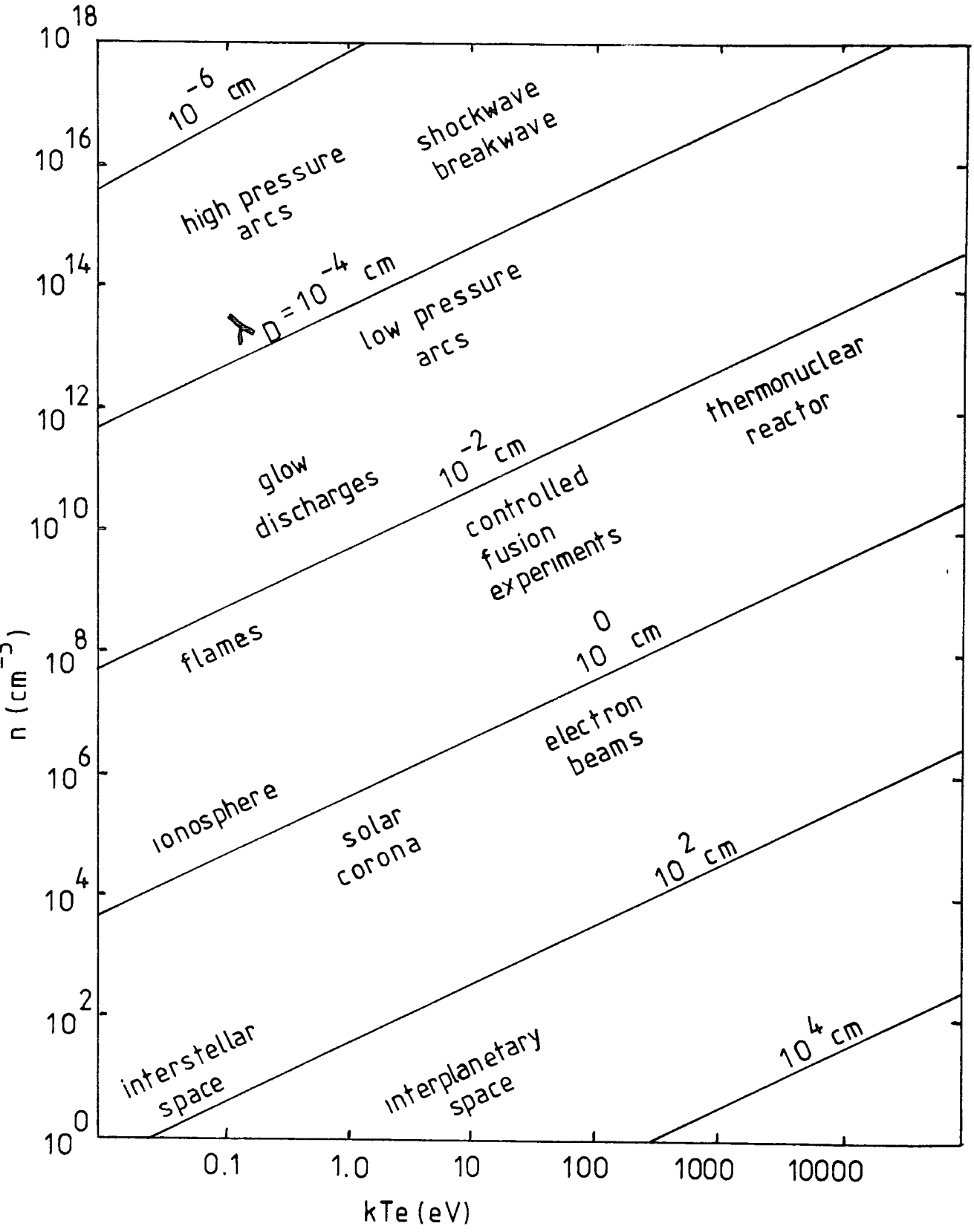

Plasmas found in Nature and in the Laboratory

Figure 4 1.2

High Density Polyethylene	TFE 554
Irganox 1076	0.014%, 0.017%
[Octadecyl 3-(3,5- ditertbutyl - 4 - hydroxy phenyl) propionate]	
Low Density Polyethylene	C37 T F E 628
Topanol OC	0.034%, 0.030%
(2,6 - ditertbutyl - p - cresol)	
Irganox 1010	0.022%, 0.021%
[Pentaerythritol tetra - 3 -(3,5 - ditertbutyl - 4 - hydroxyphenyl) propionate]	

It is not thought that these levels of antioxidant will have much effect on the corona treatment and there seems to be no evidence (see sections .3 and .4 below) of either concentration or depletion of the immediate surface with respect to these antioxidants. The effect of slip agents and additives on corona treatment has been examined by Spell and Christenson[165]. They found that corona treatment could cause migration of additives to the surface and also that some additives diffused to the surface before treatment. Furthermore if additives were present at the surface in sufficient concentration they could then affect wettabilities and adhesion.

b) Reactor using Disc Electrodes

The apparatus consists essentially of two plane parallel aluminium discs, one attached to an insulated moveable rod and the other to a grounded aluminium plate. To prevent arcing taking place the grounded aluminium plate is covered by a thick sheet of perspex and the movable disc is provided with a guard disc, also made of perspex. To prevent arcing through pinholes or weak points in the polymer film a buffer dielectric was fitted across the lower grounded electrode. This is illustrated schematically in figure 4.2.1 and shown in more detail in the photograph on page 171 and in the drawing in appendix 3. The electrodes are contained in a stoutly constructed perspex box fitted with suitable safety switches. For convenience the apparatus is mounted on top of the power supply. By means of a hole in the perspex box the discharge can be carried out in atmospheres enriched with various gases. It is not possible with this reactor to eliminate completely all traces of air and to overcome this problem another reactor was constructed inside a glass container (see c below).

The separation of the upper electrode from the polymer film can be varied by a rack and pinion drive on the rod and a reduction gear system. The gap separation can be set at any distance between 0 and 3 cm, though usually it was left at 2 mm. This particular distance was chosen mainly for convenience, though commercial corona treatment equipment often uses smaller gap distances.

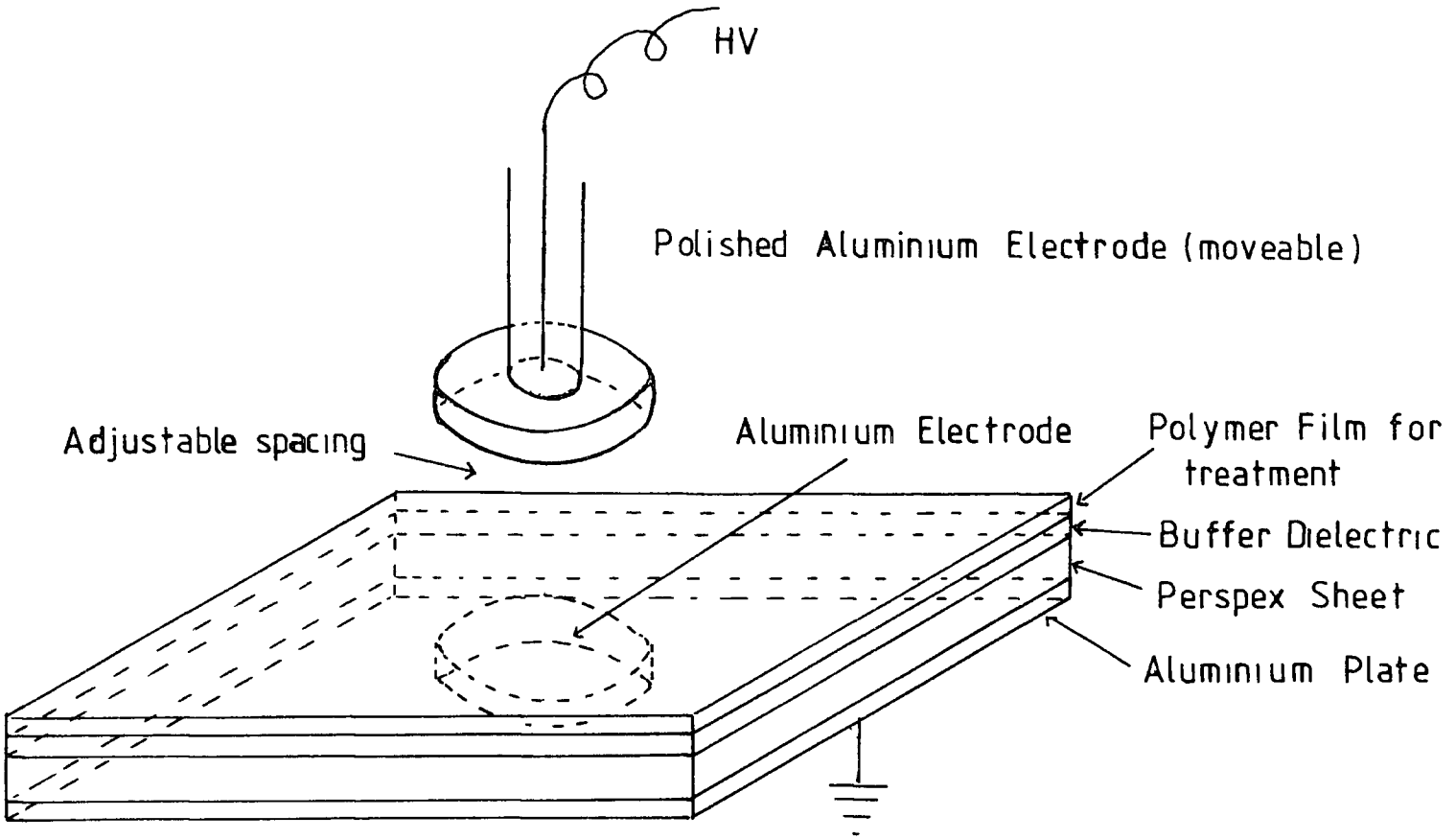

Variables

Electrode-Film spacing

Power input

Power duration

Schematic Illustration of Corona Reactor using Disc Electrodes

Figure 4 2.1

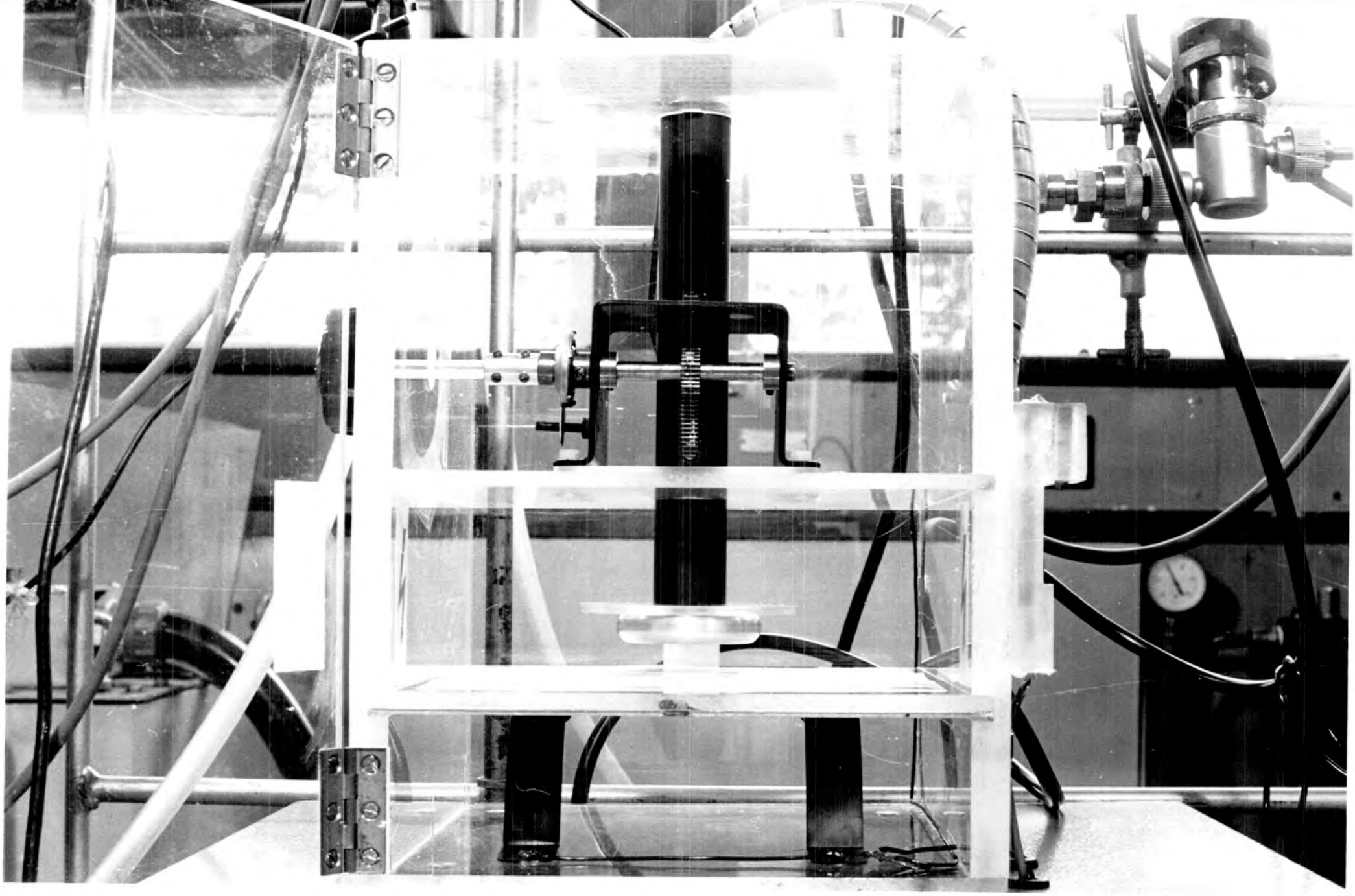

However, on this particular electrode assembly it was found difficult to maintain the gap separation across the gap using a 1 mm separation. This was due to the slight buckling of the film as it came off the roll. Using a 2 mm gap this effect was less obvious and also as soon as the corona discharge commenced it was observed that the charge deposited on the polymer film (see Chapter 5) caused the film to lie flat on the buffer dielectric. When a 1 mm gap was used, in some cases the charge deposited was observed to cause the polymer film to adhere to the upper electrode and in other cases partially to both electrodes. The gap separation, 2 mm, was obtained approximately using a simple scale and then checked using a piece of 2 mm aluminium sheet.

c) Glass Tube Reactor for Controlled Atmospheres

This reactor was mounted directly on the spectrometer and enabled samples to be exposed to a corona discharge in different gases. Then by means of a specially long probe the samples could be inserted directly into the spectrometer without exposure to the atmosphere. Figure 4.2.2 is a drawing of the reactor, which is also shown in the photograph on page 175. Other details of electrodes and probe assemblies are shown in appendix **3**. The reactor consists of a pyrex tube 16 cm long and 5 cm in diameter sandwiched between two stainless steel flanges using viton 'O' rings. Halfway along the glass tube was fused a standard

greaseless vacuum tap. The tap insert was removed and a special insert unit (see appendix 3) was made from teflon to put in its place. This enabled an electrode, connected to the high tension supply, to be positioned near the end of the probe tip which was used as the grounded electrode. The tap mechanism enabled the electrode spacing to be altered easily, the gap separation being measured by a cathometer. Samples were mounted at the end of a half inch stainless steel probe by means of double sided scotch tape and then the probe assembly inserted into the reactor. After positioning the probe tip and sample under the other electrode, the electrode spacing was adjusted to the required distance, 2 mm. By evacuating the reactor and filling with the required gas and repeating this several times, the reactor was filled with the desired atmosphere. The earthing connections were then checked and the high tension supply connected. Before switching on, other workers nearby were warned and then the corona discharge operated. Since this only took a few seconds no great inconvenience was caused. However, in view of the voltages involved, of the order of 10 to 20 kV this was felt to be a necessary precaution. The HT supply was then disconnected and the special insert operated to move the electrode out of the way of the probe. The reactor vessel could then be evacuated by means of an Edwards ED50, two stages 50 l. min^{-1} rotary pump. Since this pumping arrangement corresponds to the normal system employed in introducing samples into the spectrometer

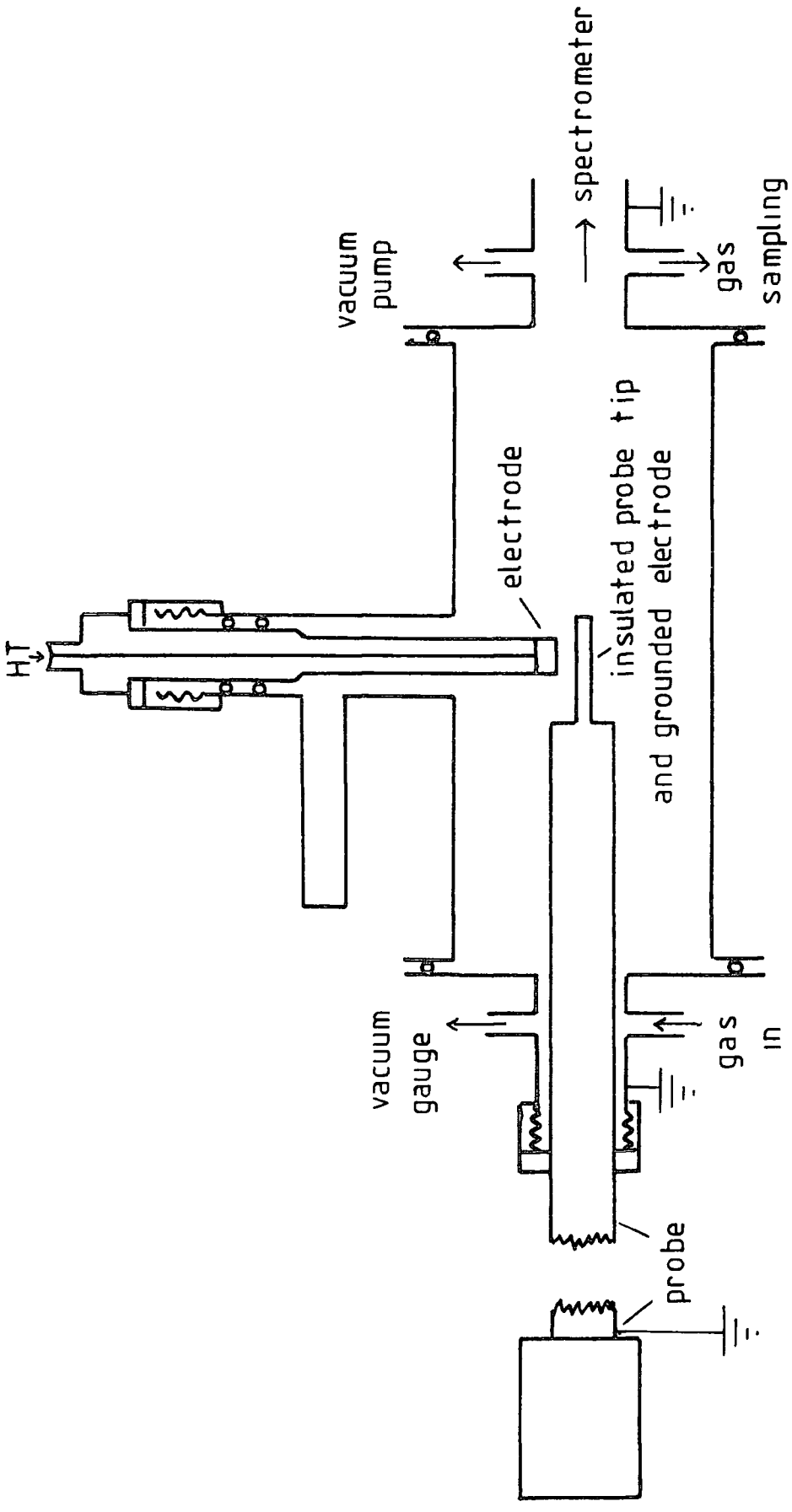

Reactor and Electrode Assembly

Figure 4.2.2

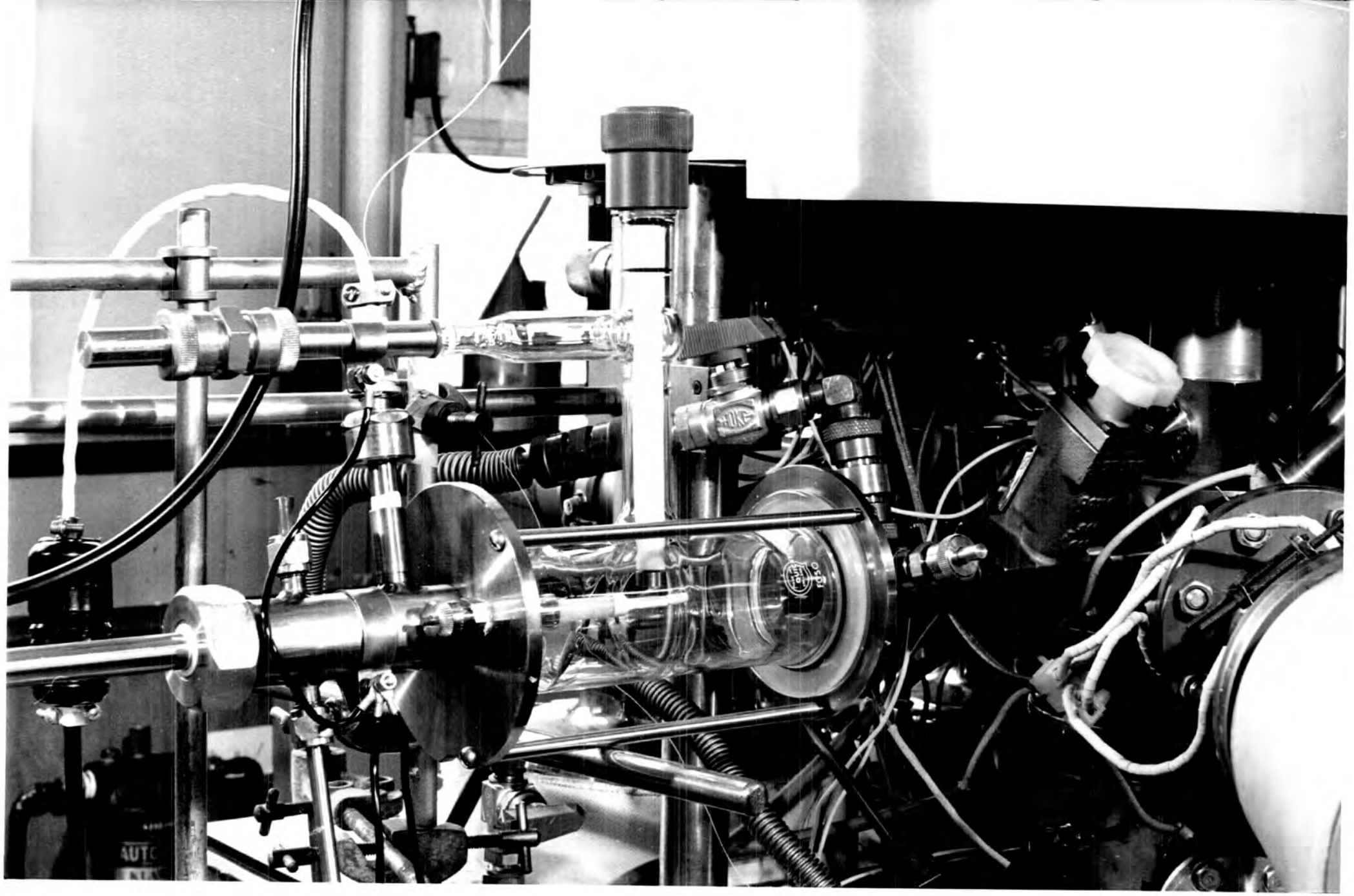

it was then relatively easy to insert the probe directly into the spectrometer.

An interesting phenomenon was seen, when using damp gases in the reactor, in that when the vacuum pump was connected the reactor acted as a miniature cloud chamber. This effect was noted to persist for upwards of 5 minutes after the corona discharge ceased. Thus using 100% humidity in air and opening the tap to the vacuum pump immediately the whole reactor was observed to fill with mist. If 5 minutes were allowed to elapse before opening the tap to the vacuum pump the effect was scarcely discernable and was no different from the effect observed when the corona discharge had not been used. Although not a quantitative measure, this does give some estimate as to how long the ions etc., formed in the corona discharge can persist.

d) Corona Power Supply

The high voltage supply unit is shown briefly in Figure 4.2.3 below and in more detail in appendix 2. The method of operation is briefly as follows. The condenser, C_D, is charged up to some pre-selected voltage, from the rectified mains supply. The thyristor, THY 1, is then switched on and the condenser discharges through the primary of an induction coil (a 12 volt car ignition coil). This produces a damped oscillation in the secondary, with a frequency of approximately 3 kHz. The voltage output is controlled by altering the

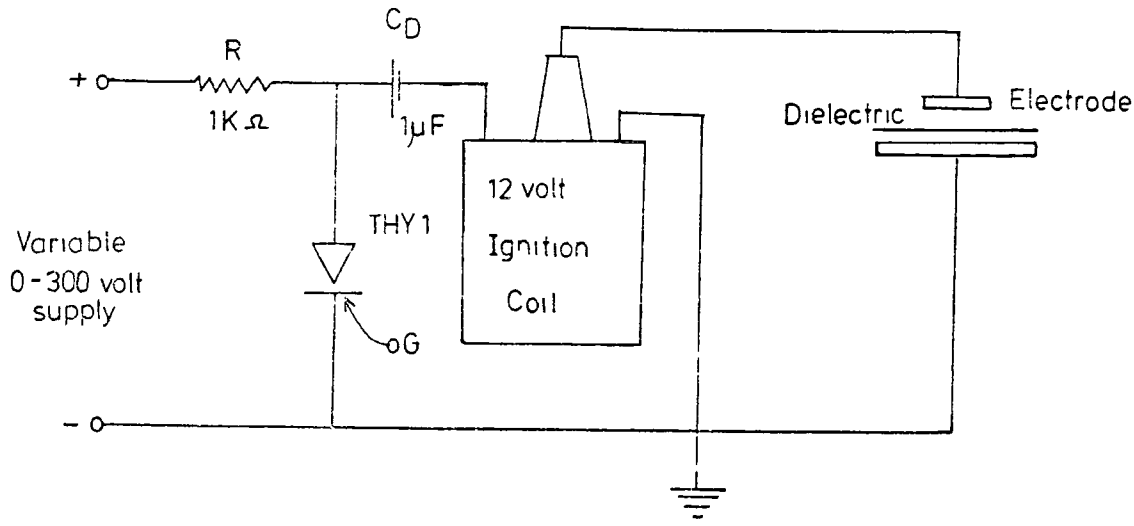

High voltage supply unit

Figure 4 2.3

charging voltage supplied to C_D. The frequency with which the thyristor becomes conducting is controlled by another circuit which produces pulses at approximately 250 Hz. The actual time for which the power supply is producing pulses is fixed by a simple timing device. The details of these subsidiary circuits are given in appendix 2.

The voltage and current output waveforms, when the apparatus is connected to the disc electrodes, are shown in figures 4.2.4 below. Not readily visible in the figures, but just discernable on the oscilloscope are very short duration ($\sim$ 1 microsecond) current pulses of comparatively large magnitude. These short duration current pulses were also observed when a D.C. discharge was employed. (see below).

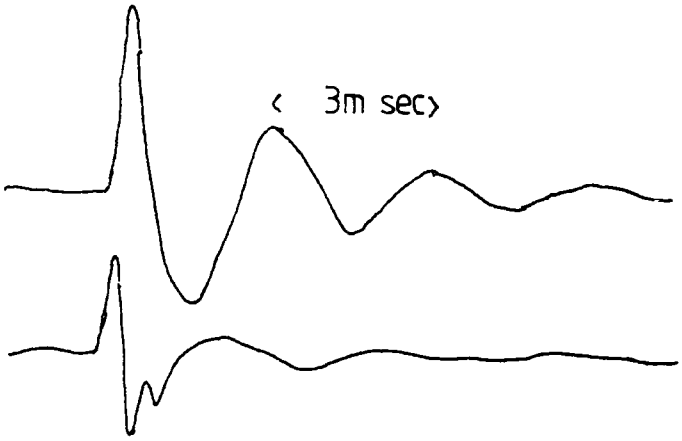

Voltage (top) and current (bottom) output wave forms.

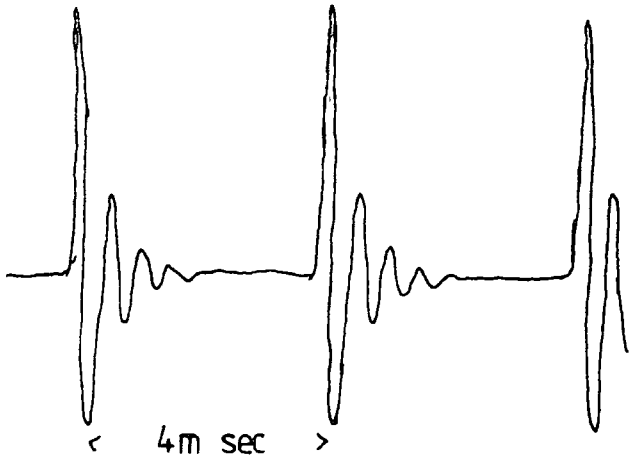

Voltage output showing pulse frequency

Figure 4 2 4

It was found that the maximum voltage, with the discharge running was approximately 11 kV and with no discharge the maximum recorded voltage was approximately 24 kV. For safety reasons neither the high voltage divider unit (capacitive) nor the resistor used to measure the discharge

current were left in the circuit during normal use (see appendix 2 for details).

It would be of some use to know the power imput to the actual corona discharge, that is the power dissipated across the gap. Unfortunately the electrical characteristics, capacitance, inductance and resistance, of the equipment used are unknown and not readily calculable. It is therefore not possible to allow for the interaction of the impedence of the equipment and that of the measuring circuits and oscilloscope. Thus the phase angle between the voltage and the current cannot be found. However, using the method proposed by Manley[152] it is possible to obtain an estimate for the power input. Thus from equation 3.4.2 it can be calculated that the power per pulse is of the order of 2.4 mJ and that the power input per second is of the order of 0.6 J. A rather similar value is obtained if the circuit is treated as a simple AC circuit with a phase angle of zero. Even when the power imput to the discharge is known it is still not possible to resolve the total energy into its many components such as light, heat, ion formation etc. Furthermore which of the many components is chiefly responsible for the surface treatment is still not known[164].

As stated earlier, some work was done using a DC discharge. The voltages used were from 12 to 25 kV, and also disc electrodes with a 2 mm gap. A buffer dielectric and piece of high density polyethylene were placed in

the apparatus as normal. The results observed were that no corona discharge was observed but that the apparatus behaved like a "leaky" condenser charging up. Thus there was an initially large current of the order of a few milliamps which rapidly fell to a much lower value. Little continuous current was observed below 19 kV but between 20 and 25 kV currents of the order of 0.05 to 0.15 milliamps were noted. At the same time a persistent "ticking" sound was heard and transient current pulses of up to 10 milliamps were recorded. It is possible that these two are connected, and these transient phenomena were observed for all voltages above 12 kV. The form of these transient current pulses was shown on an oscilloscope and is illustrated below.

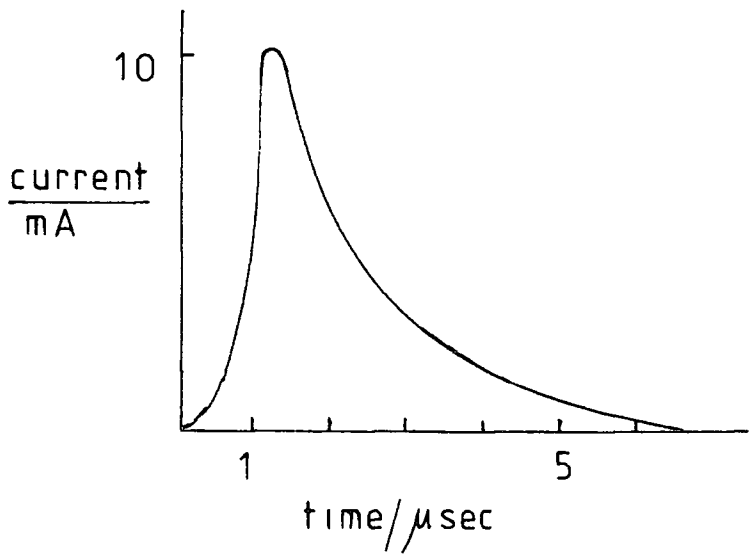

Transient Current Pulse, D.C. Discharge

Figure 4.2 5

.3 ESCA Results

As previously stated (Chapter 2.4) the spectra were recorded on an AEI ES 200 AA/B spectrometer using $Mg_{K\alpha 1,2}$ radiation of energy 1253.7 eV. The $Au_{4f7/2}$ level at 84.0 eV binding energy was used for calibration purposes and under the conditions employed had a full width at half maximum, FWHM, of 1.15 eV. Deconvolution of the spectra was carried out on a Dupont 310 Curve Resolver and the measured energies are given with a possible error of $\pm$ 0.2 eV and the area ratios to $\pm$ 5%.

The background information presented thus far strongly suggests that corona discharge treatment in air increased the surface free energy of polymers. It seems likely that this increase is associated with an increase in oxidative functionalisation. Extensive studies[166] have previously been made of the typical range of functionalities which are likely to occur and some theoretical binding energies for model compounds are shown in Figure 4.3.1.

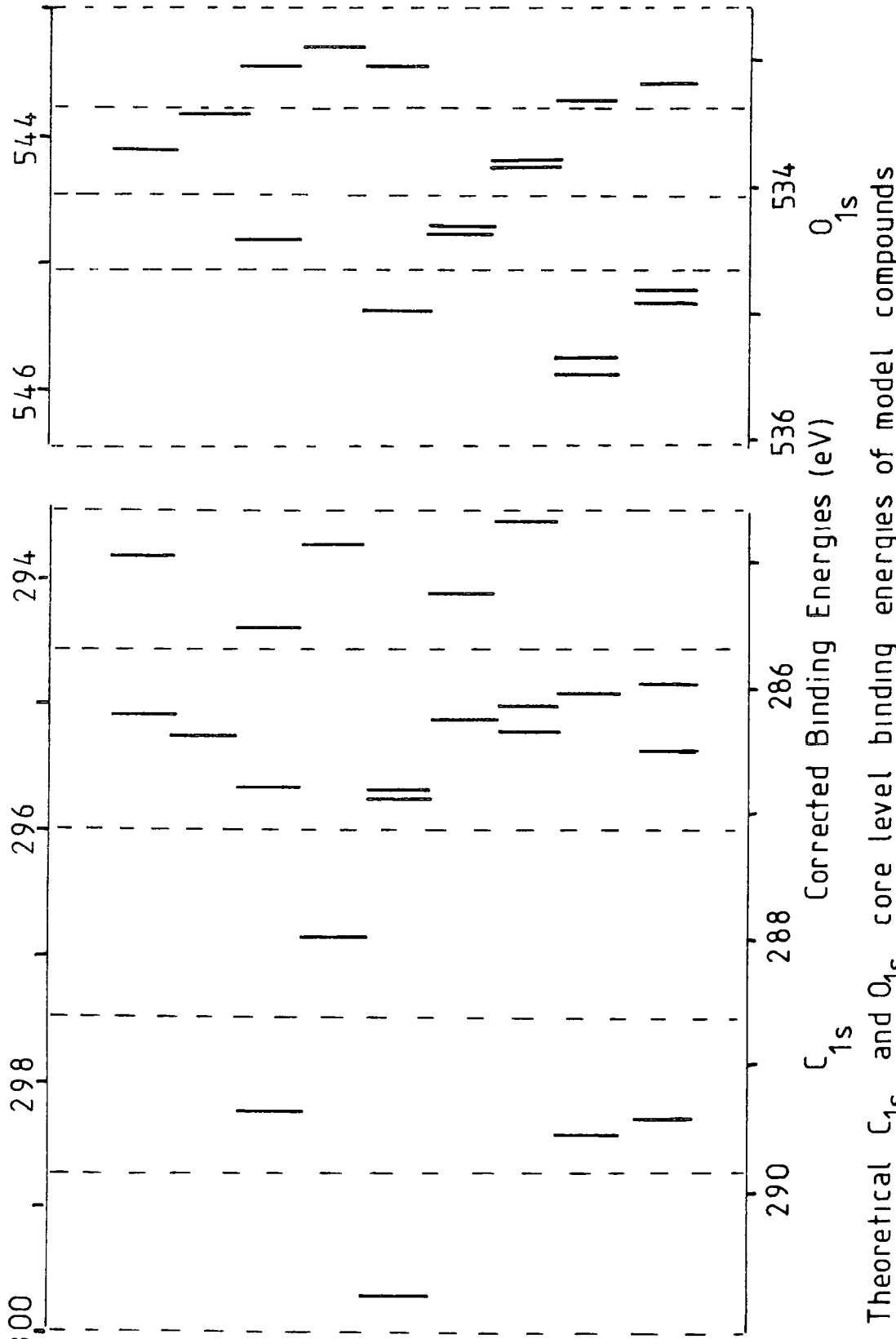

Theoretical C_{1s} and O_{1s} core level binding energies of model compounds

Figure 4.3.1

As far as this work is concerned the important structural features of carbon are

Structure	Binding Energy/eV
C - H	285
C - O	286.6
C = O	287.8
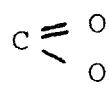	289.2
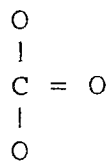	290.3

Binding Energies for Different Carbon Structural Features

Table 4.3.1

When carrying out deconvolution of the C_{1s} spectra no allowance was made for $\underline{C}$ - ONO_2 which would appear at 287.1 eV even though -O-$\underline{N}O_2$ at 408.1 eV was observed in some spectra. Neither was allowance made for $\underline{C}$-NH_2 though again N_{1s} peaks were observed that could be due to amine and amide features. However, the nitrogen spectra were often of low intensity and in some cases believed to be lost in the background noise. Ignoring the nitrogen effects on the C_{1s} binding energies is not therefore likely to produce serious errors. The oxygen spectra consisted of a number of closely overlapping peaks that could not in general be resolved uniquely

by the method adopted for the C_{1s} spectra (see below). Nevertheless some deconvolution was attempted but not too much reliance should be placed on the detailed results.

At first sight it would appear that the unresolved spectra for carbon 1s are too complex to allow unique deconvolutions to be obtained. However by using an analogue curve fitting procedure with Gaussian curves positioned at 285, 286.6, 278.8, 289.2 and 290.3 eV and treating the height as a variable a unique deconvolution can be achieved with a full width at half maximum of 1.7 eV. This curve fitting procedure produces unique deconvolutions for the C_{1s} spectra of the oxidised polyethylene samples. The typical FWHM of 1.7 $\pm$ 0.1 eV compared with a FWHM of approximately 1.4 eV for a simple homopolymer under the same conditions is suggestive of several environments contained in each of the component signals, although the secondary, or β shift induced by oxygen is small.

As previously stated unique deconvolutions of the oxygen spectra were not easily attained. However for some spectra reasonable deconvolutions could be made. This was done by positioning peaks at 532.7, 533.5, 534.3 and 535.5 eV for doubly bonded oxygen in carboxyl functions, singly bonded oxygen in alcohols, ethers and peroxides and carbonyl oxygen, singly bonded oxygen in acids, esters and hydroperoxides, and singly bonded oxygen in carbonates, oxy acids and peroxyesters respectively[167]. For some oxygen spectra a further peak at 531.8 eV corresponding to amide

oxygen was also used. The possibility of producing peroxy structural features[168], during the discharge process, which then subsequently undergo transformations to other functionalities cannot be discounted and some discussion of this is presented in a later section.

While the corona discharge was running the apparatus using disc electrodes was continually purged with the gas being used. When the glass tube reactor was used purging did not take place and neither did exposure to the atmosphere unless this was done intentionally. The pressure and temperature were ambient, that is approximately 760 mm of mercury and 20^{o}C. The relative humidity was not controlled except in the glass tube reactor.

The general appearance of the spectra, as recorded, is as shown in Figure 4.3.2. The spectra consists of broad envelopes of overlapping peaks and the deconvoluted peaks are shown for the C_{1s} spectra. When the various results are considered the most obvious effect of corona treatment is a very rapid increase in the oxygen functionality, even for very short treatment times. This is apparent even when gases other than air or oxygen are used. Thus when nitrogen and argon were used the oxygen content was increased. However, due to the experimental arrangements it is possible that some oxygen from the air remained. It has in fact been reported[169] that quite small traces of oxygen, 0.8%, in nitrogen are sufficient to bring about significant oxidation.

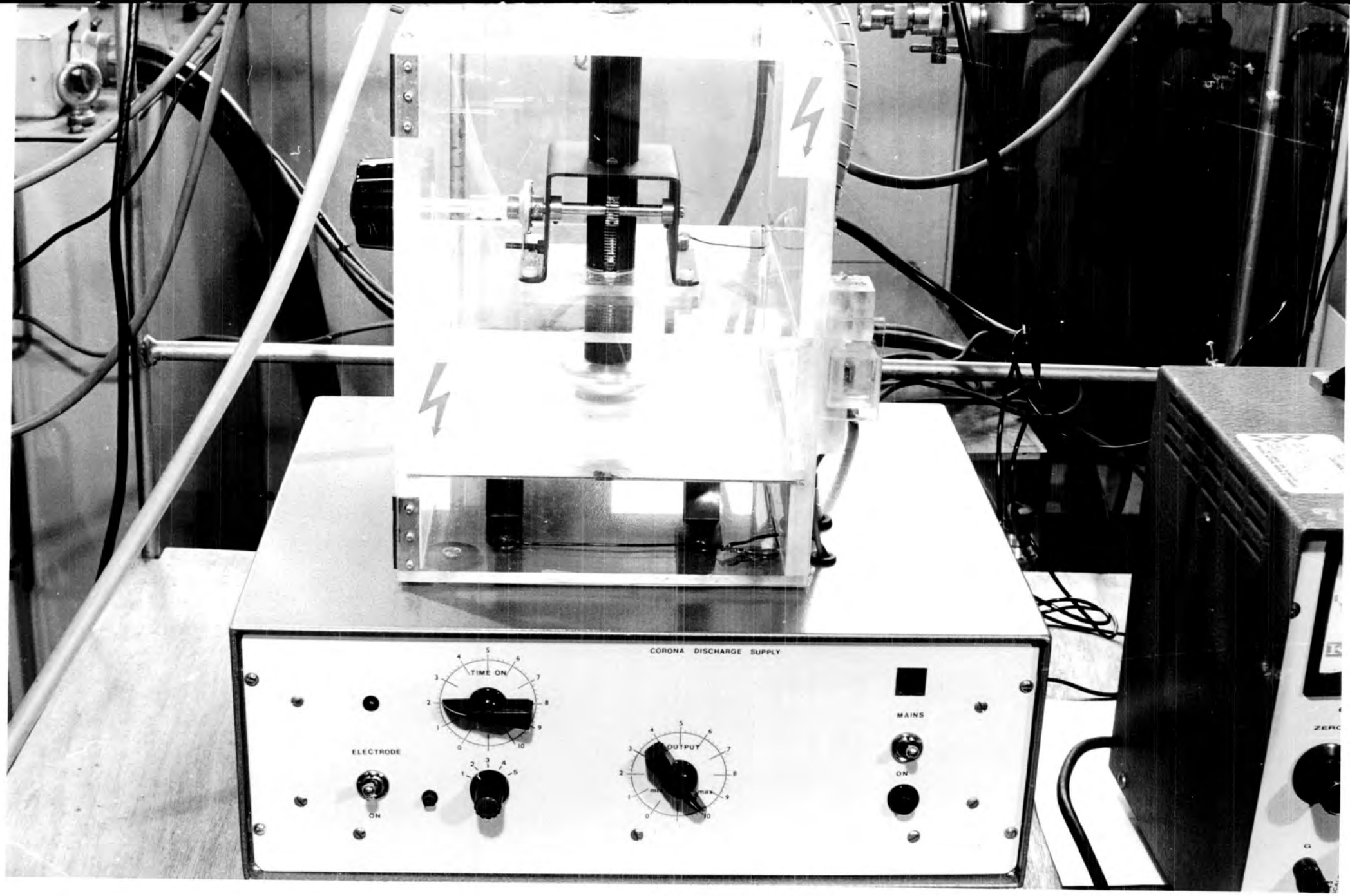
CORONA DISCHARGE SUPPLY
TIME ON
ELECTRODE
ON
OUTPUT
MAINS
ON

Corona Time \ Binding Energy / eV	286.6	287.8	289.2	290.3	402	535.5
As received	8.4	1.7	1.2			6.4
1 sec	13.4	6.6	3.0	1.2	0.5	30.5
2 sec	17.4	7.4	6.6	0.7	0.7	47.4

Area Ratios for the Spectra shown in Figure 4.3.1 below

Table 4.3.2

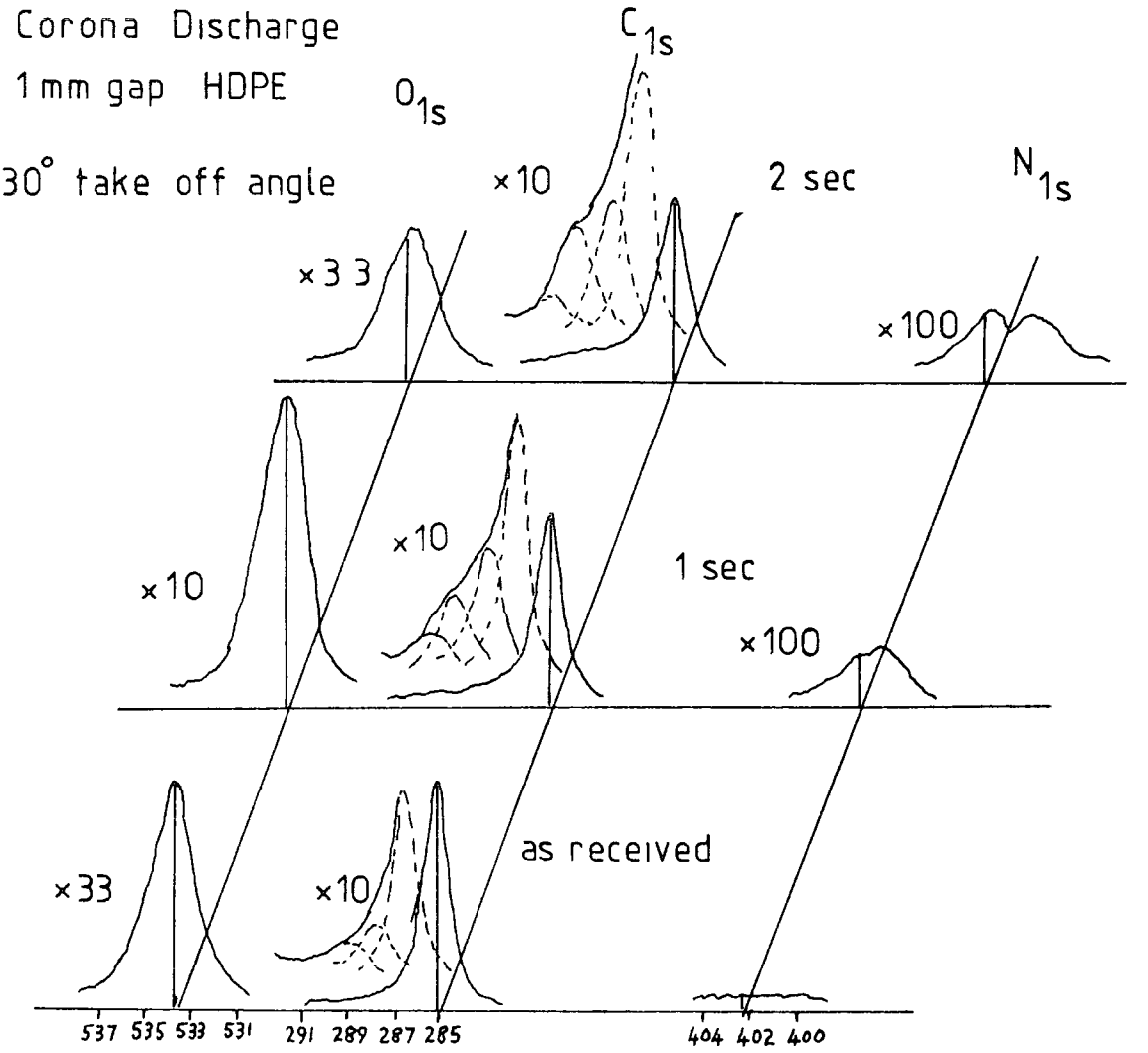

Spectra as recorded and deconvoluted for HDPE

Figure 4 3.2

The presence of absorbed oxygen and water vapour are also believed to be important[170].

The results for the untreated samples show that even before corona treatment there is a readily detectable oxygen level. This seems to be associated primarily with a singly bonded C-O group, C_{1s} binding energy 286.6 eV and a doubly bonded C=O carbonyl group, C_{1s} binding energy 278.8 eV. The presence of a carboxyl group, C_{1s} binding energy 289.2 eV is doubtful since it only appears at very low intensity for the untreated samples. In fact it may arise as a systematic operator error caused by the way in which the deconvolutions were carried out. This was done as previously stated for all the C_{1s} spectra by setting up the curve resolver with a number of curves at the required binding energies and fixed full widths at half maxima. Then beginning at the highest binding energy curves were added to obtain the best fit for the C_{1s} spectrum. The area for the C_{1s} peak at 286.6 eV may also be slightly overestimated due to its proximity to the large peak at 285 eV. This peak corresponds to hydrocarbon and in the tables of area ratios is always taken as 100% and is not included in the tables.

If the area ratios for carbon and oxygen bonded in different groups and stoichiometries are known it is possible to get some idea as to how the carbon and oxygen are bonded in different groups on the surface of the polyethylene. For example, the C-O group with C_{1s} binding

energy of 286.6 eV could be a hydroxyl group, either C-O-C, or peroxide C-O-O-C group. The first and last of these it is true would give the same carbon:oxygen ratio but the second would give a different ratio to the others. It should therefore, theoretically, be possible to distinguish the presence of ether links by a lower carbon:oxygen ratio than for the others. In practice due to the difficulty of resolving individual oxygen peaks this is not always possible but some general conclusions can be drawn from the data.

The expected area ratio for carbon to oxygen with stoichimetry 1:1 can be obtained from a consideration of the ESCA spectra of poly (ethylene terephthalate) which are given in Figure 4.3.3 and in Table 4.3.3. The formula for the polymer is $+C_6H_4\overset{\overset{O}{\|}}{C}-O-CH_2\ CH_2\ O-\overset{\overset{O}{\|}}{C}+_n$, which would suggest area ratios for the C_{1s} peaks to be 1:1:3 for peaks at 289.2, 286.6 and 285 eV respectively. This is not quite what is obtained which is 26:32:100 for a 30^{o} take-off angle. However the peak at 289.2 eV, which is due to the carboxyl group is reduced due to shake up while as previously stated the peak at 286.6 eV may be slightly overestimated due to its proximity to the large peak at 285 eV. Furthermore the peak at 285 eV is reduced by shake up, 6.3% and making allowance for all of these would suggest a reasonable estimate for the area ratios is 29:29:100. This is of course not a ratio of 1:1:3 but this is largely due to a "turning in" of oxygen functional groups (see below). Taking the estimated area ratios for

C_{1s} peak at 285 eV taken as 100%

C_{1s}	286.6 eV	289.2 eV	Shake up at ΔE= 6.6 eV
	32	26	6.3
	24	10	6.6

O_{1s}	532.7 eV	534.3 eV
	48	48
	28	28

Area Ratios for Poly(ethylene terephthalate) Film

Table 4.3.3

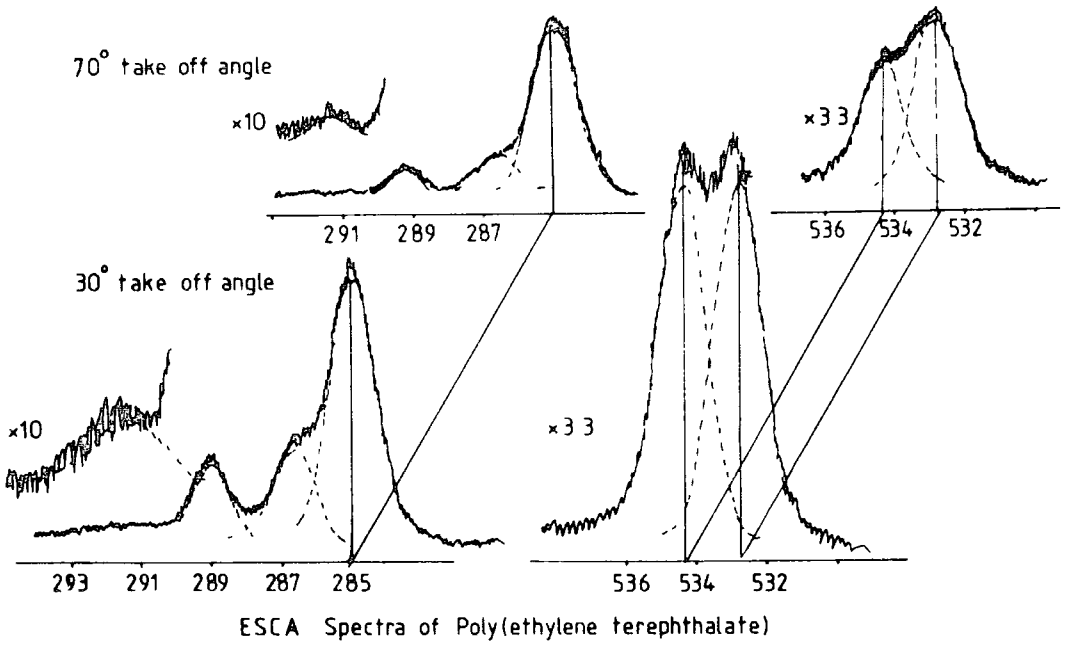

ESCA Spectra of Poly(ethylene terephthalate)

Figure 4 3 3

the carbon 1s peaks at 289.2 and 286.6 eV with the corresponding oxygen area ratios at 532.7 and 534.3 eV gives the carbon:oxygen area ratios for a 1:1 stoichiometry as

C : O :: 1 : 1.7

for both doubly and singly bonded carbon to oxygen.

It will be seen that the area ratios for 70° take-off are somewhat different to those at 30° take-off. This is largely due to the "turning in" of the oxygen functional groups of the polymer. The carboxylic ester groups if present at the surface of the polymer produce a higher energy state, because of their polar character, than if the hydrocarbon groups, less polar, are directed outwards. Therefore during fabrication, which will involve extrusion from a melt the polymer film will be produced with the more polar groups turned inwards from the surface to lower the final surface energy. The 70° take-off spectra samples only a very thin surface layer and will record a spectrum in which the hydrocarbon, C_{1s} 285 eV peak is overestimated and the carboxyl, ester and oxygen functionalities are underestimated. Using the 30° take-off spectrum will largely avoid this error due to the much greater (2.5 times) sampling depth.

a) Spectra obtained from Corona Treatment in Air (Tables 4.3.4 - .9)

The results show clearly the similarities and

differences between low density polyethylene LDPE and high density polyethylene HDPE. The LDPE and HDPE both oxidise very rapidly with initially the surface and subsurface layers being oxidised to approximately the same extent. For the LDPE however the 70^{o} take-off angle spectra reveal that the surface level of oxidation after passing through a maximum soon falls to a lower limiting value. For HDPE the O_{1s} 70^{o} take-off spectra rise sharply with time, level off and then rise to their final values. For both types of polyethylene the subsurface layer finally acquires a greater degree of oxygen functionality than the outer layer and this is remarkably similar for both types. A possible explanation of these facts is that the surface of the polymer becomes degraded during treatment. The more highly branched LDPE might be expected to degrade more rapidly as branches are cleaved and more highly oxidised fragments would be removed from the surface keeping the oxygen functionality low. For the subsurface layer the level of oxygen would be determined solely by the injection parameters which might be expected to be similar for both types of polymer. This idea of surface degradation is supported by the fact that the upper metal electrode becomes coated, in time, with a greasy deposit persumably arising from deposition of fragments from the surface of the polyethylene. To examine this idea of surface degradation further samples were weighed before and after the corona treatment.

However the mass changes were very small and the results inconsistent for the treatment times used. In fact Kim and Goring[6] report an increase in mass of between 0.1 and 0.3% after a 30 minute corona treatment in oxygen. They conclude that oxygen addition was outweighing any loss of carbon atoms.

As stated earlier the oxygen peaks were difficult to deconvolute but when this was done it is seen that oxygen functionalities are produced at binding energies 532.7, 533.5, 534.3 and 535.5 eV. These could correspond to all the functional groups mentioned above and so it is useful to consider if all the groups are present. Using the area ratio already calculated for the carbon and oxygen stoichiometry of 1:1, that is

C : O : 1 : 1.7

the existence of some particular groups may be inferred. Taking the oxygen peak at 534.3 eV this could be either (or all)carboxylic acid, esters or hydroperoxide. The carbon peak at 289.2 eV corresponds to carboxylic functions and using this and the area ratio mentioned above it is possible to infer the existence or otherwise of hydroperoxides. For LDPE, Table 4.3.4 and HDPE, Table 4.3.5, it is seen that there has to be a high proportion of hydroperoxide present. In fact, apart from the surface of LDPE, 70^{o} take-off, most of the 534.3 eV peak seems to

	C_{1s}				N_{1s}		O_{1s}			
	286.6	287.8	289.2	290.3	402	400.5	532.7	533 5	534.3	535 5
As received	4 6	0.9	0 2				1 24	0 1	0.3	
	3 8	0.8	0 1				1 6	0.1	0.6	
0 5 sec	7 2	2.8	1.8	0.2			4.4	3.7	5.4	1.2
	5.8	2 2	0 9	0.1			2.8	6	4	1.4
1 sec	10	3 8	2.3	0.6			2.6	3.7	10.2	2.3
	6.1	2.3	1.3	0 1			5	7.6	2.8	0.9
2 sec	9 4	4.7	3.4	0.3			4.2	9	9.6	3
	7.6	3.5	2.2	0.6			3.3	7.4	7.6	1.8
3 sec	14	7	5	1.4	0.41		2.4	3.6	20.4	9
	6 4	3	1.7	0 2			2.8	3.9	5.2	1
50 sec	15.3	8.1	10.8	2.7	0.84	0.36	3.6	6	34.8	9
	8.4	2.2	3.1	0.6		0.16	1.8	3.2	7.8	2

LDPE Air Corona 2mm gap Area ratio

Table 4 3.4

	C_{1s}				N_{1s}			O_{1s}			
	286 6	287 8	289.2	290.3	402	400.5	399	532.7	533.5	534.3	535.5
as received	6	1 2							2.10	1 62	0.6
	4	0.8						3.6	0.12	0.72	
sec	6	3 8	1.8	0.5		0.08		12.8	3.6	10.8	0 8
	6.6	3	1.4	0.4				18.2	1.2	7	0 6
3 sec	8 6	4	2.4	0 6		0.4		5.4	4.8	12	2.4
	8	3	2	0.4	0.2	0.27		16	3	3.3	0
7 sec	11.7	7.7	4.7	1		0 4	0.4	11	3	25	4.7
	12	7.3	4.7	1		0.7		18	5	18	3
15 sec	15	11 7	7	2.3	0.6	0 6	0.6	12	6	37	10
	13	8.5	5.3	1		0.42	0.63	26	4	32	3

HDPE Air Corona Area ratio

Table 4 3.5

	C_{1s}			O_{1s}	
	286.6	287.8	289.2	533.5	
A	3.48	1.1	0.2	1.40	
	4.4	1.1	0.4		1.7
B	4.5	1.8	0.6	6.1	
	5	2.1	0.8		7.5
C	4.5	1.7	0.6	4.1	
	3.2	1.4	0.5		4.1

Area ratios

HDPE DC Discharge 2mm gap 5 mins

A - 12 kV, upper electrode positive

B - 25 kV, upper electrode positive

C - 25 kV, upper electrode negative

Table 4.3.6

Heating time	C_{1s}				N_{1s}			O_{1s}				
	286.6	287.8	289 2	290.3	408	402.2	400.5	532.7	533.5	534.3	535.5	Total O
No treatment	18	13	13	3	1.6	1.2	0.7	19	15	27,6	6	67.6
	20	13	12	3	1.4	0.3	1	21	16	23	4	64
2 minutes	14	8	7 7	4	0.67	0.3		12.4	11.3	18,7	4.2	46.6
	14	8	8	5				13.3	11.3	16	3.3	43.9
5 Minutes	17	10	7	1.3	1.2	0.3	2.3	14.7	10	18 7	4.7	48.1
	16	10	6.7	1.3	0.67	0.3	1.9	15.3	10	16	4	45.3
10 minutes	18	10	7.3	2	0.5	0.5	1.1	15	10.3	18	4.3	47.6
	17	10	6.7	1	0.3	0.5	1.1	14.7	9.7	14	4	42.4

Area ratios. HDPE 15 secs Air Corona Both sides, followed by heating at 75°C

Table 4.3.7

	C_{1s}				N_{1s}	O_{1s}
	286.6	287.8	289.2	290.3	400.5	533.5
A	12.7	9.3	5.3	2		39.3
	9	4.2	2.8	0.4		20
A´	14	4.4	2.0	0.3		19.4
	8.6	3.8	1.8	0.1		18.4
B	17	10.7	6.0	2.7		44
	8.2	4.7	2.7	0.2		24.8
C	19.3	8.0	5.0	3.0		36.7
	10.4	4.2	2.7	0.7		21
D	13	5.0	1.6		9.5	8.4
	16	5.0	0.7		10.6	12.6
E	14	5.2	1.2		8.8	10
	15	4	0.6		8.0	9.8

Area ratios. LDPE, Corona Discharge in Glass Tube Reactor for 3 secs
A & B in Air, A´ the back of the probe for result A
C in dry air, D in nitrogen, 0.5% O_2 , E in nitrogen exposed to air for 10 minutes before recording the spectra

TABLE 4.3.8

	286.6	287.8	289.2	290.3	408	402.2	400.5	532.7	533.5	534.3	535.5	Total O
29 Mar *	22	8	12	3	2			14	18	36	6	74
Dry Air	22	12.3	14.7	5.0				14 3	20.7	36 7	11.3	83
30 Mar	22	8.7	14.7	4	1.5			12	20	34	10.3	76.3
Dry Air	19.3	8 7	14.7	3.7	0.33			10.7	20	36	10 7	77.4
29 Mar	19.3	15	17 3	7	1.9			31	54	51	10	146
Wet Air	19.3	14.7	17.3	6	1.4			22	42	46	9	119
30 Mar **	19 7	13.3	15	5.3	2			12	22	50	10	94
Wet Air	20	16	16	2.3	0.8	0.6	0.8	16	35	39	3	93
Dry Air Exp at 30°*,	22	8	12	3	2			14	18	36	6	74
after 2 hrs	16 7	5.3	9.3	2.3				15	19	20	2	56
Wet Air ** Exp at 30°,	19.7	13.3	15	5.3	2			12	22	50	10	94
after 2 hrs	16.3	10	13	2.7			1	20	31	18	4	73

HDPE Reaction Chamber 15 secs Air Corona, Dry and Sat. with H_2O
Power max, 2 mm gap

Table 4.3.9

be due to hydroperoxide.

The results of calculations for some of the results in Tables 4.3.7 and 4.3.9 are shown in Table 4.3.10.

	C_{1s} 289.2 eV	Calc O_{1s} 534.3eV	Obs O_{1s} 534.3 eV
A	13	22.1	27.6
	12	20.4	23
Á	7.7	13.1	18.7
	8	13.6	16
B	12	20.4	36
	14.7	25.0	37
B´	9.3	15.8	20

A´ from a sample, heated at 75°C for 2 mins.

B´ from a sample after 2 hours in the ESCA spectrometer

Area ratios, calculated and observed from the data given in Tables 4.3.7 and 4.3.9.

Table 4.3.10

These calculations assume that there is comparatively little peroxy acid or peroxy ester formed.

The ESCA results after a sample has been in the spectrometer for 2 hours also support the idea of hydroperoxides being formed. Hydroperoxides would be expected to be unstable with respect to the effect of X-Ray bombardment and some decomposition would be expected.

This is what is observed in Table 4.3.10 for B and B´where the difference between the calculated and observed O_{1s} peak becomes less after 2 hours in the spectrometer. This loss cannot just be due to volatile fragments being lost since heating corona treated polyethylene to 75°C does not produce the same effect (see results A and A´ in Table 4.3.10). Also when a hydroperoxide decomposes it would be expected that a reduction in the oxygen peak at 534.3 eV would be accompanied by an increase in the oxygen peak at 533.5 eV, which corresponds to singly bonded oxygen in hydroxides, ethers and peroxides. This is in fact what is seen ir the results in Table 4.3.9. It would be unrealistic to expect an exact correspondence since some material may be lost during the X-Ray bombardment, which does also produce some heating of the sample. The results in Table 4.3.7 in fact suggest that some material is lost from the surface of the polymer.

Similar deductions concerning other oxygen functionalities cannot be so readily made from the peak areas. Thus the oxygen peak at 535.5 eV could be due to singly bonded oxygen in carbonate groups or peroxy acid functions. Carbonate carbon would be associated with two singly bonded oxygens giving

C : 2 O :: 1 : 3.4

The peak areas are low compared to those discussed concerning hydroperoxides and the relative errors therefore

larger. Using the carbon:oxygen ratio above suggests that most of the oxygen peak at 535.5 can be accounted for by carbonate oxygen. Therefore there is not a great deal of peroxy acid function present.

No firm conclusions can be made concerning the oxygen peaks at 532.7 and 533.5 eV. It cannot be deduced from the ESCA data how much free hydroxyl there is and how much ether there is present. Therefore no decision can be made as to the proportion of the 533.5 eV peak that arises from the three possibilities, hydroxyl, ether or peroxy links. It can be concluded from the C_{1s} peak at 286.6 eV that although some of it is due to ether linkages that it is not all. Further evidence, from other sources, is needed before the matter can be resolved further. The 532.7 eV peak arises from the doubly bonded oxygen in carboxylic acid functions. For LDPE there often appears too little oxygen for the observed C_{1s} 289.2 eV peak while for HDPE the reverse is usually observed. Part of the reason for this may be the use of set peaks in the deconvolution process which assumes that the doubly bonded oxygen appears at this value.

The nitrogen spectra, always weak, were not consistent. Peaks at 400.5 and 402 eV were observed, these being due to amine functions and also at 408 eV this latter being due to nitrate groups. However, peaks at these three binding energies were

not always observed and the peaks had a low intensity, usually of the order of 2% or less, of the 285 eV C_{1s} peak, after 15 seconds of corona treatment. Due to their low intensity it was not possible to come to any conclusions regarding their effects on either the C_{1s} spectra or the O_{1s} spectra. Any effect from a nitrogen peak of such low intensity would be lost amongst the experimental deviations normally observed. On one occasion, see Table 4.3.9, a nitrate peak was observed to disappear during a period of 2 hours in the spectrometer to be replaced by another at 4.005 eV, corresponding to an amine. The two peaks were similar in magnitude and so it is possible that the nitrate ion had been reduced. A somewhat similar effect was noted when samples of corona treated HDPE were subjected to heat treatment, see Table 4.3.7. In these instances though the nitrate peak at 408 eV did not entirely disappear.

Some experiments were carried out, using the disc electrodes connected to a high voltage D.C. supply. The ESCA results are tabulated in Table 4.3.6 and it can be seen that there is no increase in the oxygen functionality though there seemed to be some increase in the surface energy (see Chapter 5.2).

b) Spectra obtained for Corona Treatment in Oxygen (Tables 4.3.11 - 13)

For both HDPE and LDPE there is an increase in the oxygen functionality but apart from the surface

layer of LDPE the increase is less than that for corona treatment in air. For LDPE the surface layer is much the same as for air treatment and in fact the total level of oxygen functionality is much the same for all the gases used. However, a more detailed study of the oxygen functionalities does reveal some important differences (see section c below). The lower oxygen functionality for HDPE and the subsurface layer of LDPE can be explained by assuming the surface layers degrade faster in the oxygen atmosphere. Thus material is removed before the oxygen content has risen to that of air. The decreased oxygen functionality is matched by a decrease in the carbon 1s functionality, it being noted that for LDPE the 70^{o} take off values for C_{1s} are similar to those for the air treatment. The general level of oxygen functionality seems like the air treatment to be greater for the subsurface layer than that of the surface layer.

In Tables 4.3.11 and 12 the oxygen peaks were deconvoluted using the procedure described previously. While accepting the problems involved and possible errors it is possible to arrive at some conclusions. Considering first the 70^{o} take off angle peaks it is seen that for both LDPE and HDPE the C_{1s} 290.3 eV peaks are very similar for similar treatment times. The O_{1s} 535.5 eV peaks are also similar in size and also, using the C : 20 :: 1 : 3.4 area ratio the O_{1s} peaks seem to be largely arising from carbonate features, shown by the C_{1s} 290.3 eV peak.

There seems to be very little peroxy acid functionality at the surface. The 30^{o} take-off peaks for the same C_{1s} and O_{1s} peaks are not exactly in such good agreement for LDPE and HDPE but allowing for measurement and deconvolution problems, it does not seem there is much difference. The HDPE perhaps reaches a slightly higher level of carbonate functionality but the difference is only small. Once again there seems little evidence for peroxy acid features.

The presence of hydroperoxide may be inferred, as was the case for air corona, from a consideration of the C_{1s} 289.2 eV (carboxyl) peak and the O_{1s} 534.3 eV peak. The area ratio for a one-to-one stoichiometry

$$C : O :: 1 : 1.7$$

enables a theoretical value for the O_{1s} 534.3 eV peak to be calculated from the C_{1s} 289.2 eV peak, carbonate functionality being low. The difference between calculated and observed O_{1s} peak is then an indication of the amount of hydroperoxide present. The results in Tables 4.3.11 and 12 show clearly that hydroperoxides are formed and in the case of HDPE in amounts that are rather similar for both the surface and subsurface layers. Furthermore for HDPE the amount of hydroperoxide changes comparatively little with time reaching quite a high level in a very short time. The case of LDPE is

	C_{1s}				N_{1s}	O_{1s}			
Corona time	286 6	287.8	289.2	290.3	400.5	532.7	533.5	534.3	535 5
As received	3 5	1 9	O 1				1.32	1.92	
	4.5	0.8	0.2			3	1	0.5	
0 5 sec	9	3.4	1.4	0.6		1.1	3.1	5.1	1.1
	7 3	2.4	0 9	0.2		5.7	2.4	3.7	0.1
1 sec	6 6	3	1.8	0.3		4.0	4 O	5.6	1.4
	6 6	1.9	0 8	0.2		5	1.8	2.4	0.5
2 sec	9	3.9	2.8	1.0		1	3.9	8	2.6
	10.2	3.2	1.8	0.4		6.8	5	4.6	1.1
3 sec	9	3.8	3	0.7	0.10	3	6	9.6	1.8
	6	2.6	1.3	0.2	0.1	4.8	2.4	3.6	0.7
30 sec	9.8	3 8	4.0	1 6		2.2	4.8	15	6
	5.4	2 2	2.0	0.4		3.7	4.8	4.4	1.3

LDPE O_2 Corona

Area Ratios

Table 4.3 11

Corona time	C_{1s}				N_{1s}	O_{1s}			
	286.6	287.8	289.2	290.3	402	532.7	533.5	534.3	535 5
1 sec	11 2	4 2	3 6	O 6		6	5.4	14	2.4
	16	3	3.3	0.4		7	11.3	9.3	1 3
3 sec	10.7	5.5	4.4	1 6		3	5	12	3.3
	11.5	3 2	4	0.4		12	4	10	1.3
7 sec	10.7	5.3	6	1 4		8.7	6	13 3	3 3
	12	4	5	0.4		8.8	5	18	1
15 sec	14	6.4	6.4	3 3	0.4	14	4	15.3	2
	12	4	5	0.4	0.4	10	6.7	13.3	1.3

HDPE O_2 Corona Area Ratios

Table 4.3.12

Binding Energy / eV

	C_{1s}				O_{1s}
	286.6	287.8	289.2	290.3	533.5
1	13.5	8.0	4.7	4.7	40
	10.8	2.6	4.2	0.8	29.2
2	3.4	0.6	0.1		1.6
	3.8	1.0	0.4		1.2
3	6	1.3	0.3		0.5
	4.6	1.2	0.3		1.7
4	3.8	0.8	0.1		0.5
	4.9	0.9	0.4		1.3

15 secs. Corona Treatment, O_2, 2 mm gap

Samples at different distances from the discharge

1 at the centre, 2 just outside the visible discharge

3 at a distance of 3cm, 4 at a distance of 10cm

Area Ratios for HDPE

Table 4.3.13

rather different, the amount of hydroperoxide formed at the surface being only small, as is the amount of carboxyl function. For the subsurface layer of LDPE the situation is more like that for HDPE. A much higher level of hydroperoxide is formed than at the surface but this is not formed as quickly as in the case of HDPE. However, eventually the level of oxygen functionality at 534.3 eV becomes much the same for both types of polymer.

The O_{1s} peaks at 533.5 eV are much the same for both LDPE, HDPE and the 30^{o} and 70^{o} take off angles, for corresponding times. There is no such agreement for the C_{1s} 286.6 eV and 287.8 eV peaks, the LDPE peaks tending to be lower than those of HDPE. As stated previously there is insufficient evidence to draw firm conclusions concerning these peaks and the O_{1s} 532.7 peak. However, it does seem that carbonyl features are more prominent in HDPE (287.8 eV peak). Also the higher levels of hydroperoxide at the surface of HDPE, compared to LDPE, is seen in the larger value of the O_{1s} 534.3 eV peak and the C_{1s} 286.6 eV peak.

There was observed a small nitrogen 1s peak at one point for both LDPE and HDPE. This corresponds to amine functionality and probably arises from nitrogen impurity, either in the oxygen gas, or absorbed on the surface of the polymer.

Some samples of polyethylene were taken from portions of the sheet lying outside the corona area.

The results are shown in Table 4.3.13, the oxygen peak being quoted for the centroid,deconvolution not being attempted. It is seen that outside the corona treatment area the levels of oxygen functionality do not differ appreciably from those of untreated polyethylene.

c) Spectra obtained for Corona Treatment in Nitrogen (Tables 4.3.8,.14 and .15)

As for oxygen the surface layer of LDPE reaches a similar value of total surface oxidation as that reached for air treatment. However deconvolution of the O_{1s} peak reveals that the situation is very different. The effects for the subsurface layer and for HDPE are also seen to be quite different than the effects observed for air and oxygen corona treatment.

The nitrogen 1s spectra as might be expected were very obvious and deconvolution revealed nitrogen functionality at approximately 400.5 and 399 eV binding energy. The former corresponds to amine functions and the latter corresponds to amide features. The presence of these two nitrogen functionalities can be used to explain the general aspects of the oxygen 1s spectra.

When the oxygen spectra were deconvoluted it was seen that compared to oxygen and air corona treatment there was a general shift in the O_{1s} binding energies towards lower values. In the O_{1s} spectra quite large signals were observed at 531.7 eV and these may be assigned to amide oxygen. This agrees well with the

	C_{1s}				N_{1s}		O_{1s}				
Corona time	286.6	287 8	289.2	290.3	400.5	399	531.7	532.7	533.5	534.3	535.5
As received	4.6	0.9	0.2					0.5	0.2	0.2	
	4	1.1	0.2					1.2	0.2	0.3	
0 5 sec	4 9	1.2	0 2			0.4	0.4	0.8	0.4	0.4	
	4.3	1.0	0.1			0.4	0.4	0.9	0.4	0.2	
1 sec	8	4	1.4		2	0.7	1.9	3.4	2.2	2.3	0.3
	6.4	2.4	0.7	0.1	1.5	1.3	1.4	2.9	2	1	0.6
2 sec	8.8	5.3	1.4	0.2	1.8	3.1	2.1	5.3	1.4	1.8	0.3
	6.9	4.0	1.0	0.1	2.7	2.7	3.6	4	1.8	0.9	0.4
3 sec	10	8	2.4		6 2	2.6	2.7	7.3	27	3.7	0.7
	8.1	4.8	1.1	0.1	1.8	6.5	3.1	5.2	1.3	1.5	0.3
30 sec	7.7	5.6	4.4	0.2	7.2	4.2	4	8.7	2.3	2.7	0.4
	7.5	4	2.4	0.2	6.4	3.8	3.5	5.2	0.6	0.8	0.4

LDPE N_2 Corona, 2mm gap, Disc Electrodes

Table 4.3.14

Corona time	C_{1s} 286.6	C_{1s} 287 8	C_{1s} 289.2	C_{1s} 290.3	N_{1s} 400 5	N_{1s} 399	O_{1s} 531.7	O_{1s} 532.7	O_{1s} 533.5	O_{1s} 534.3	O_{1s} 535.5
s received	6 4	1.4	0.2						1.5	1.3	0 2
	3.5	1.0	0.1					2.6	0.8		
1 sec	6 5	1.9	0.3		1	2.1	1.4	3 4	1.4	1.2	0 2
	6.0	2 2	0.5		1.1	2.6	2.4	4.2	0.6	1	
3 sec	11 7	7.0	3.0	0 1	7.6	1.2	3	7.1	5.3	5	1
	8 7	6.0	2.6	0.2	4.6	4.8	6.3	9.1	3	4.3	
7 sec	8	8	4	0.1	8 0	9.3	8	8	3	2	
	8	7.3	4.3	0.4	10	4.7	6.7	9.7	3	4.7	
15 sec	7	5.7	5	0.6	12	2.3	4.1	9.3	4	5.3	
	8	5.6	4.8	0.7	8.7	3.3	5	10	2.7	4	
20 mins	8 7	6.9	4.4	0.8	8.3	13	7.1	8	6	1.6	0.5
	8.7	6.7	4	0.6	7	14.3	5	11.3	2	3.3	

Area ratio. HDPE N_2 Corona

Table 4.3.15

observed N_{1s} signals at 399 eV mentioned previously. The O_{1s} signal at 532.7 eV is generally too large to be accounted for by carboxylic acid functions which have a corresponding C_{1s} signal at 289.2 eV. However, the allocation of fixed values of binding energies in the O_{1s} spectra is a little arbitrary and may not exactly match the true binding energies. Some of the 532.7 eV peak may therefore in reality arise from amide oxygen. The presence of high concentrations of nitrogen functionalities also produces complications in the C_{1s} spectra. These were deconvoluted ignoring C_{1s} signals arising from carbon bonded to nitrogen. This does not produce serious errors when the nitrogen signals are only about 1% of the main carbon 285 eV peak but when the N_{1s} peak is of the order of 10% then the errors may be large. For example, the amide carbon 1s signal will fall between 287.8 and 289.2 eV and for exact deconvolution of the carbon 1s spectra peaks other than $\underline{C}$ - O and $\underline{C}$ = O should be used. It is doubtful though if unique deconvolutions could be achieved, with any degree of certainty, if more peaks were introduced.

The O_{1s} peaks at 535.5 eV indicate that for LDPE there is very little carbonate functionality while for HDPE there is a little but not as much as was seen when air and oxygen corona were used. The corresponding C_{1s} peaks at 290.3 eV agree with these O_{1s} peaks as regards carbonate functionality. As for air and oxygen corona the

C_{1s} 289.2 eV and O_{1s} 534.3 eV peaks enable the existence or otherwise of hydroperoxides to be established. In fact there seems to be very little or no hydroperoxide and the C_{1s} peaks are usually too large to match the O_{1s} 534.3 eV peaks if they, the C_{1s} peaks, are all due to carboxylic acid functions. Since though the N_{1s} peaks indicate the presence of amides the problem of the C_{1s} 289.2 eV peaks being too large can be resolved. Strictly speaking though the C_{1s} spectra should be deconvoluted with extra peaks which would in effect reduce the carboxylic carbon peaks to more realistic values for the O_{1s} 534.3 eV peaks.

For treatment in nitrogen gas the total oxygen functionalities reached seem quite high. Therefore experiments were run in the glass tube reactor, using nitrogen gas and a sample of the gas removed and analysed using a mass spectrometer. This gave the oxygen content as 0.5%, perhaps a little high but the seals of the reactor were known to leak slightly. The nitrogen gas also had not been specially purified and was used as supplied by British Oxygen. There were, as well, various "dead" spaces in the reactor and to try to eliminate oxygen from the air the reactor was evacuated and then filled with nitrogen to slightly above atmospheric pressure. This process being repeated three times. This level of oxygen, 0.5% could explain the level of oxidation observed, though it is interesting to note that Evans[169] did not observe any change (MIR IR) when using nitrogen containing 0.5% oxygen for corona treatment.

d) Spectra obtained for Corona Treatment using Argon (Tables 4.3.16 and .17)

The results obtained for both LDPE and HDPE are very similar to those obtained using an oxygen atmosphere. The main differences are that using argon the levels of oxygen functionality at 534.3 and 535.5 eV are lower than those observed for the oxygen corona. The values, taken in conjunction with the C_{1s} peaks at 289.2 and 290.3 eV suggest that using argon the level of hydroperoxide and peroxy acid concentrations are quite small, though it would seem they are still present. This is in contrast with the results for nitrogen corona (see c above) where peroxy functions are virtually non-existent. Another difference was that for LDPE the O_{1s} peak at 532.7 eV reaches a higher value than that observed for the oxygen corona. This seems to correspond to a higher value of the C_{1s} peak at 287.8 eV. This arises from carbonyl carbon and the corresponding oxygen peak should be at or near 533.5 eV. However, the O_{1s} deconvolutions are somewhat subject to error and not easy to determine uniquely. The HDPE on the other hand reaches values for the O_{1s} 532.7 eV and C_{1s} 287.8 eV peaks more like those observed for the oxygen corona though the argon corona peaks at 532.7 eV are eventually larger. The oxygen functionalities rise more slowly, with increasing treatment times than when using oxygen gas. This is not altogether surprising since the oxygen in

the argon is only present as a small impurity and what is being observed is the slow addition of oxygen functions. There is also less likelihood of surface degradation when using argon. When using oxygen it is likely that the surface is continually degrading and so though the initial rise in surface oxidation levels is high the continuous removal of surface material keeps the total level of surface oxidation comparatively low.

The argon seems to contain nitrogen as an impurity as well as oxygen. Thus for LDPE and HDPE peaks corresponding to amine, 400.5 eV and amide 399 eV are seen after prolonged corona treatment (more than 3 sec). No nitrate functions were observed but in view of the low oxygen level ($<1\%$) in the argon this is not surprising.

The visible corona when using argon was considerably different than that observed using other gases. Whereas in those cases the corona discharge was seen as an intense glow, with a myriad small streamers, all contained within the electrode area the appearance when using argon was quite different. The discharge in argon took the form of very long discharges, >10cm, which "snaked" all over the surface of the polymer, starting from the upper electrode and reaching the edge of the grounded plate . No visible discharge, apart from this, due to gas ionisation from electron avalanches was seen in the electrode gap. In view of this and the results obtained when a DC supply was used (Table 4.3.6) it is surprising that the levels of

Corona time	C_{1s} 286.6	C_{1s} 287.8	C_{1s} 289.2	C_{1s} 290.3	N_{1s} 400.5	N_{1s} 399	O_{1s} 532.7	O_{1s} 533.5	O_{1s} 534.3	O_{1s} 535.5
0 5 sec	10	3.2	1 4	0.3			3.4	3.1	6	0.3
	6.5	3.0	0.7	0.2			7	2.2	2.7	0.6
1 sec	7.6	3.6	0.9	0.2			3.6	2.6	3.3	0.3
	6.1	2.2	0.6	0			4.3	1.8	2.4	0.5
2 sec	10	5.2	1.6	0.6			3.4	3.2	6.8	1.2
	6.9	3.7	0.9	0.1			10.3	2.6	3	0.3
3 sec	9.6	6.0	1.5	0.2	1.3		9.6	4	6.3	0.9
	6.8	4.0	1.0	0.3	0.7	0.6	11	2.8	3.8	0.6

LDPE Ar Corona Area Ratio

Table 4.3.16

	C_{1s}				N_{1s}			O_{1s}			
	286.6	287.8	289.2	290.3	402	400.5	399	532.7	533.5	534.3	535.5
1 sec	5.5	3 1	0.7	0.1				0.4	1.5	4.8	0.8
	10.4	2.6	2.2					7.8	4.4	7	1.5
3 sec	7 8	3.6	1.2	0.1		0.3	0.2	7	4.3	5	0.8
	10	3	1.9			0.2	0.2	6.6	6	6	1
7 sec	8	5	1.8	0.3	0.6	0.5	0.2	2.8	3.5	8.6	2
	10	3.3	1.3	0.1		0.8	0.4	5.7	4.1	4.1	1
15 sec	10	5.8	3.0	0.2		1.74	1.24	15.4	4.2	8.2	2
	11	4	2.3			1.4	1.2	16.7	2	4.1	1

HDPE Ar Corona Area Ratios

Table 4.3.17

of oxygen functionalities reach the values that they do.

e) The Effects of Heating, Humidity and Other Conditions (Tables 4.3.7, .8, .9 and 4.5.1)

When the results for samples A and B in Table 4.5.1 are compared with corresponding results in Tables 4.3.4 and .5 it is seen that there is very little change in carbon and oxygen functionalities with time, after corona treatment.

Some of the results in Table 4.3.7 have already been discussed in section a). The results refer to samples of HDPE that had been subjected to, on both sides, corona treatment in air and then subjected to heat treatment for various times. It is probably this treatment on both sides that is the cause of the oxygen and carbon functionalities differing slightly from those observed in other samples treated on one side only. Considering first the oxygen peak at 534.3 eV and the carbon peak at 289.2 eV, calculations show, Table 4.3.10, that the level of hydroperoxide changes very little with heat treatment but that the level of carboxylic acid function (including possible ester) does. Furthermore, there seems to be a slightly higher level of hydroperoxide concentration in the subsurface layer than in the surface layer. The carbon 1s at 290.3 eV and the oxygen peak at 535.5 eV taken together show that the concentration of carbonate features is small and that there is very little peroxy-acid or peroxy-ester. On heating these two peaks,

C_{1s} and O_{1s}, both become smaller. As explained previously the exact nature of the oxygen functionality at 535.5 eV and the carbon functionality at 286.6 cannot be uniquely determined.

One result of heat treatment is an overall reduction of oxygen functionality though as explained above the hydroperoxide concentration changes very little. This loss is possibly due to loss of volatile fragments but some may be due to "turning in" of polar groups to create a surface with lower surface energy.

Some experiments were carried out using the glass tube reactor and varying the relative humidity of the air. The results are shown in Table 4.3.9 and it would appear that using dry air there is little difference in the spectra obtained when air at ambient humidity is used (Table 4.3.4). When air at 100% humidity is used there is however a more noticeable effect in that the oxygen functionality is increased. In fact for one sample the effect was very large. The carbon functionalities are also increased but not for all carbon features. Thus the peak at 286.6 eV, corresponding to carbon singly bonded to one oxygen hardly changes (allowing for variations often observed). This would not though reveal differences in proportions of hydroperoxide, peroxide, hydroxyl and ether groups, all of which would give C_{1s} signals at approximately 286.6 eV. The other carbon 1s peaks are all increased when using air at 100%

humidity, the value being approximately doubled for the peak at 287.8 eV. The C_{1s} peak at 289.2 eV showed a smaller increase, indicating that the amounts of carboxylic acid and ester had not increased much. The peak corresponding to carbonate functions was higher than that for dry air except for one value at 70° take off.

Using the same method as in section a) it is possible to decide upon the presence or absence of hydroperoxides. For all the C_{1s} peaks at 290.3 eV it seems that the oxygen functionality at 535.5 eV can all be explained in terms of carbonate functions. Or rather it might be said that there is insufficient oxygen at 535.5 eV to suggest carboxylic peroxide functions. Therefore it must be associated with carbonate features, the problem being though that the 535.5 eV peak is a little too small, compared to its calculated value. This could however be partly due to the fact that the oxygen peaks are difficult to deconvolute and there may be a systematic error in the O_{1s} results. If there is little or no carboxylic peroxy functionality then the C_{1s} 289.2 eV peaks enable the corresponding O_{1s} peaks at 534.3 eV to be assigned to carboxylic oxygen and hydroperoxide groups. For dry air the ratio of the oxygen peak area at 534.3 eV calculated from the C_{1s} peak at 289.2 eV is given by

C : O :: 14 : 23.8 (approximately for 30° and 70° take off)

whereas the observed value is approximately 14 : 36. This suggests that approximately one third of the oxygen peak at 534.3 eV arises from hydroperoxide groups. Taken with the total oxygen peak area it reveals that approximately 17% of the total oxygen functionality is due to hydroperoxide. For air at 100% humidity the proportion is higher, it also being noted that the spectra were far less consistent on different occasions. The approximate area ratios for C_{1s} at 289.2 eV and that calculated from this for oxygen at 534.3 eV are

C : O :: 16.4 : 27.9

This gives the amount of the O_{1s} peak being due to hydroperoxide as 18.6. This means that about two-fifths of this O_{1s} peak are caused by hydroperoxide and that something like 20% of the total oxygen functionality is due to hydroperoxide.

The results of leaving the samples of HDPE mentioned above in the ESCA spectrometer for 2 hours and then rerunning the spectra are quite interesting (Table 4.3.9). When this is done it is seen that the total carbon and oxygen functionalities are reduced. This was only done for the 30^{o} take off as it was felt that for the 70^{o} take off surface contamination and "easy" loss of volatile fragments would give misleading results. When the functionalities revealed by deconvolution are examined

the results are seen to be more complex than a quick examination would suggest. The carbon 1s peaks are all reduced in intensity but this is not true of the O_{1s} peaks, as deconvoluted. The O_{1s} peak at 535.5 eV becomes smaller after 2 hours and this can be explained by a loss of volatile fragments containing carbonate functional groups. A corresponding loss is seen in the C_{1s} peak at 290.3 eV. The O_{1s} peak at 534.3 eV becomes considerably smaller and this can be partly accounted for by a loss of carboxylic acid functions which is also seen in the reduction of the C_{1s} peak at 289.2 eV. The other oxygen function that appears at 534.3 eV is the hydroperoxide group and using the carboxylic group peak at 289.2 eV it is seen that, after 2 hours in the spectrometer, most of the 534.3 eV peak that remains can be accounted for by the carboxylic acid function. Therefore it would appear that virtually all the hydroperoxide group has decomposed. Now some of the oxygen associated with it will be lost when the group decomposes and so will be removed from the sample. Some will also be lost as low molecular mass fragments are volatalised. Nevertheless it might be expected that some of the oxygen functionality would remain and might appear as either oxygen doubly bonded to carbon and oxygen singly bonded to carbon at 532.7 and 533.5 eV. This is in fact what is observed in that these two peaks actually increase after being in the spectrometer. The sample that has the highest estimated hydroperoxide concentration initially also

seems to be the one in which these peaks increase the most.

The nitrogen functionality shows some interesting changes after samples have been in the spectrometer. For the samples a peak is observed at the start at 408 eV, corresponding to the nitrate group. This peak disappears after two hours exposure to X-Rays and for one sample is replaced by a peak at 400.5 eV, not originally observed. A peak at this binding energy corresponds to amine functions and has been formed from the nitrate group by photoreduction caused by the exposure to the X-Rays.

f) The Effect of Air Saturated with Perfluorobenzene Vapour

(Table 4.3.18)

The results indicate that a considerable amount of grafting onto the polymer has taken place. Furthermore that this has occurred not only on the surface but in the subsurface layer as well and not only of fluorine, a comparatively small atom but also of benzene fragments, comparatively large. This is shown by the presence of shake up peaks for C_{1s} at 291.8 eV and for fluorine 1s at ΔE of 8.1 eV for both 30^{o} and 70^{o} take off angles. The C_{1s} peak, deconvoluted at 290.3 eV is very large and it is interesting that the subsurface layer, as revealed by the area ratio at 30^{o} take off, has a much higher fluorine content than the surface layer. These facts suggest that there is considerable mixing, possibly by turning in, of the surface and subsurface layers

since the penetration by quite large entities seems to take place with ease.

There is quite a large increase in the nitrogen functionality which seems principally to be amine groups with binding energy of approximately 402 eV. The oxygen functionality is perhaps the most surprising feature, showing total levels of between two or three times greater than that observed for normal air corona treatment of this duration (15 seconds). It is difficult to use the method employed in previous sections of this chapter for analysing the results. The presence of carbon-fluorine bonds makes assignment of deconvoluted C_{1s} peaks less certain and this then makes interpretation of the O_{1s} spectra more problematical. It does seem though that much of the oxygen functionality is associated with higher binding energies which is suggestive, in view of the C_{1s} spectra, of hydroperoxides and peroxy acid features. These latter could arise from the presence of oxygen "scavengers" in the form of free radicals formed by fluorine containing species. These free radicals would then react with molecular oxygen to form hydroperoxides.

C_{1s} signal at 285 eV taken as 100

	286.6	287.8	288.9	290.3	291.8 (shake up) eV
C_{1s}	16 12	19 7	16 21	103 32	3 4
N_{1s}	3.7 3.4	401.6 eV			
F_{1s}	128 56	689.2 eV	shake up at ΔE = 8.1 eV 0.8		0.8
F_{2s}	10 4.6	33.5 eV			
O_{1s}	224 102	534.5 eV			

Area ratios for HDPE 15 secs air corona, saturated with perfluorobenzene vapour

Table 4.3.18

.4 Infra Red Spectra

The infra red spectrum for a substance is usually relatively easy to obtain. However the usual transmission spectrum, though carried out on a thin sample, or material combined into a disc, is usually insensitive when only a very thin surface layer of the material is to be examined. There is a need to concentrate the species to be examined to increase their total absorbance, as compared to the absorbance of the bulk material. This can be done by removing the surface layer by scraping[5,163] or by solvent extraction[6]. These however involve an element of destruction and are rather time consuming. The "simpler" and less time consuming method of total internal reflection spectroscopy[162,163] is to be preferred, especially as it is essentially nondestructive. The method relies on the total internal reflection of the infra red radiation and the fact that when total reflection occurs there is some penetration of the radiation from one medium into the other. If medium 2 absorbs at different wavelengths than medium 1, then this absorbance may be observed. Furthermore, since the penetration into medium 2 is only small the technique may be applied to thin surface layers of material 2.

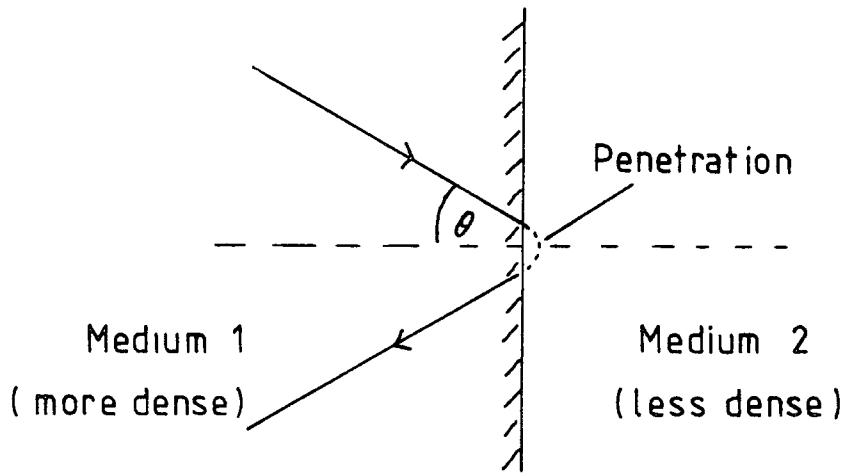

Total Internal Reflection

Figure 4.4.1

The depth of penetration is given by

$$d_p = \frac{\lambda}{n_1 2\pi \left(\sin^2\theta - n_{21}^2\right)^{1/2}} \qquad 4\,4.1$$

where d_p is the distance in medium 2 for the electric field amplitude to fall to e^{-1} of its value at the boundary surface of medium 2

λ is the wavelength of the radiation,

n_1 is the refractive index of medium 1,

θ is the angle of reflection,

and $n_{21} = \frac{n_2}{n_1}$, n_2 being the refractive index of medium 2 (the sample).

The penetration depth d_p is commonly of the order of 10^{-6} m, though it obviously varies with change in wavelength and the refractive indices, n_1 and n_2.

To increase the intensity of absorbance use may be made of a multiple internal reflection, MIR, element giving a number of reflections, each reflection enhancing the absorbance spectrum.

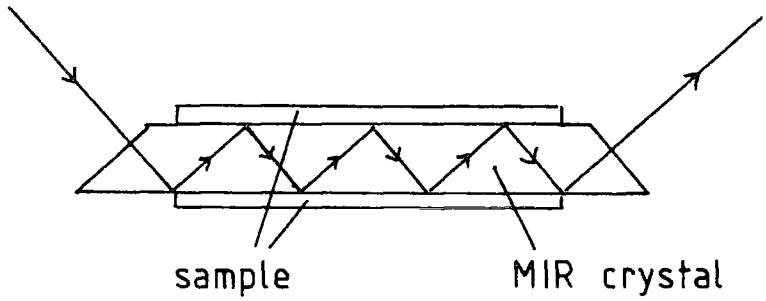

MIR Crystal and Sample

Figure 4.4.2

The MIR IR spectra reproduced in the following figures were obtained using a 25 reflection element with crystals of Thallium bromo-iodide, KRS-5, with refractive index ~ 2.4 and germanium, Ge, with refractive index ~ 4.0. The actual unit was a multiple internal reflection unit made by Specac and the spectra were recorded on a Perkin-Elmer 577 Infra Red Spectrometer. Consideration of equation 4.4.1 indicates that use of the germanium crystal will result in sampling a thinner layer than use of the KRS-5 crystal which will sample approximately twice the depth.

In the following spectra the peaks at 2910 and 2850 cm^{-1}, corresponding to CH_2 and CH_3 stretching vibrations, are omitted. Also omitted are the bands at 730 and 720 cm^{-1}, due to $-CH_2$ rocking. These latter bands were not observed using the Ge crystal as this

absorbs heavily in the same region. The spectra of both LDPE and HDPE show in general the same features, though not all bands have the same intensity. It was also found that the KRS-5 gave somewhat better spectra, with more intense absorption bands.

Before treatment both LDPE and HDPE gave absorbance bands at 2910 and 2850 cm^{-1}, 1470 and 1460 cm^{-1} (CH_2 and CH_3 bending) and at 730 and 720 cm^{-1}. Some transmission spectra were recorded and these showed the presence of isolated OH groups at 3610 cm^{-1} and possibly CH_3 bending overtones at 2650 cm^{-1}.

When MIR IR spectra for corona treatment were examined it was found that for discharge times of the order of 3 seconds it was only just possible to see any results. Longer treatment times gave more clearly recognised effects and these are listed below.

Wave Number of Observed Absorbance		Structural Features
3400 cm^{-1}	broad	Hydrogen bonded OH
1750, 1714	broad	Carbonyl stretch
1630	Broad	Enol β-diketone, C=C

Absorbance bands observed after Corona Treatment of Polyethylene

Table 4.4.1

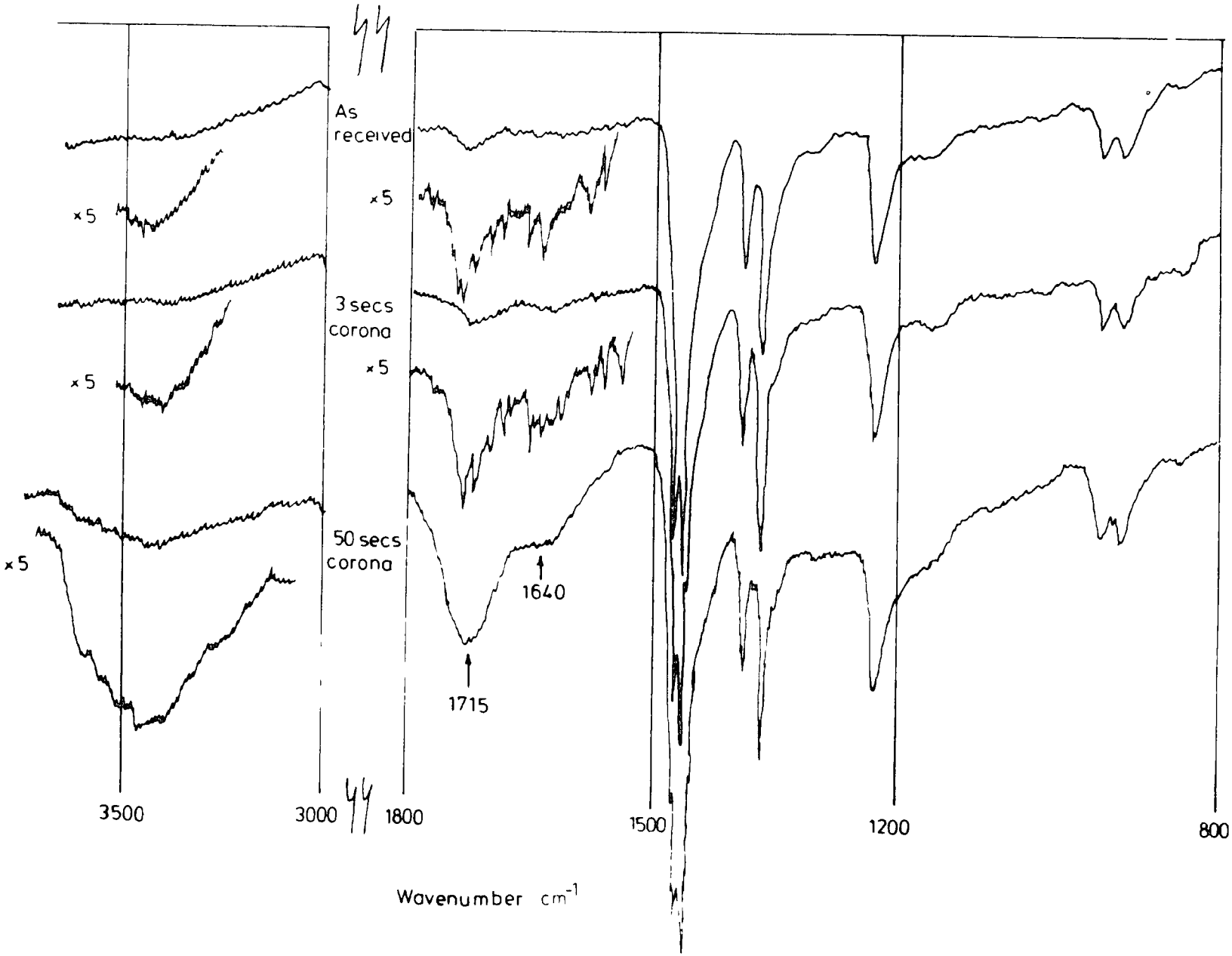
Low Density Polyethylene MIR IR KRS-5 45° N_2 flush
As received
×5
3 secs corona
×5
50 secs corona
×5
×5
1640
1715
3500
3000
1800
1500
1200
800
Wavenumber cm^{-1}

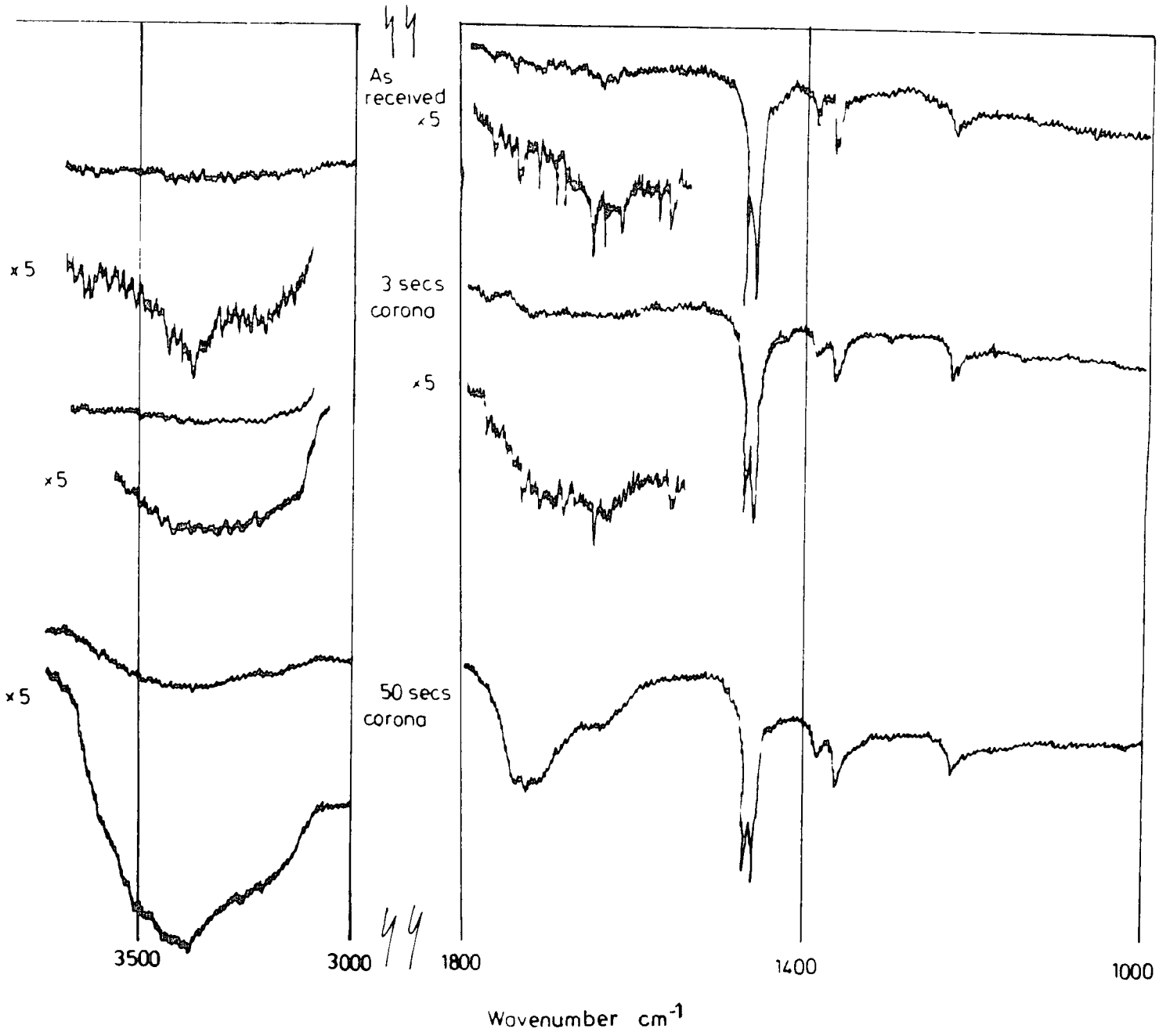
Low Density Polyethylene MIR IR Ge 45° N_2 flush
As received
×5
3 secs corona
×5
50 secs corona
×5
×5
×5
3500
3000
1800
1400
1000
Wavenumber cm^{-1}

High Density Polyethylene Corona Discharge in air 2mm gap

MIR IR KRS-5, 45° N_2 flush

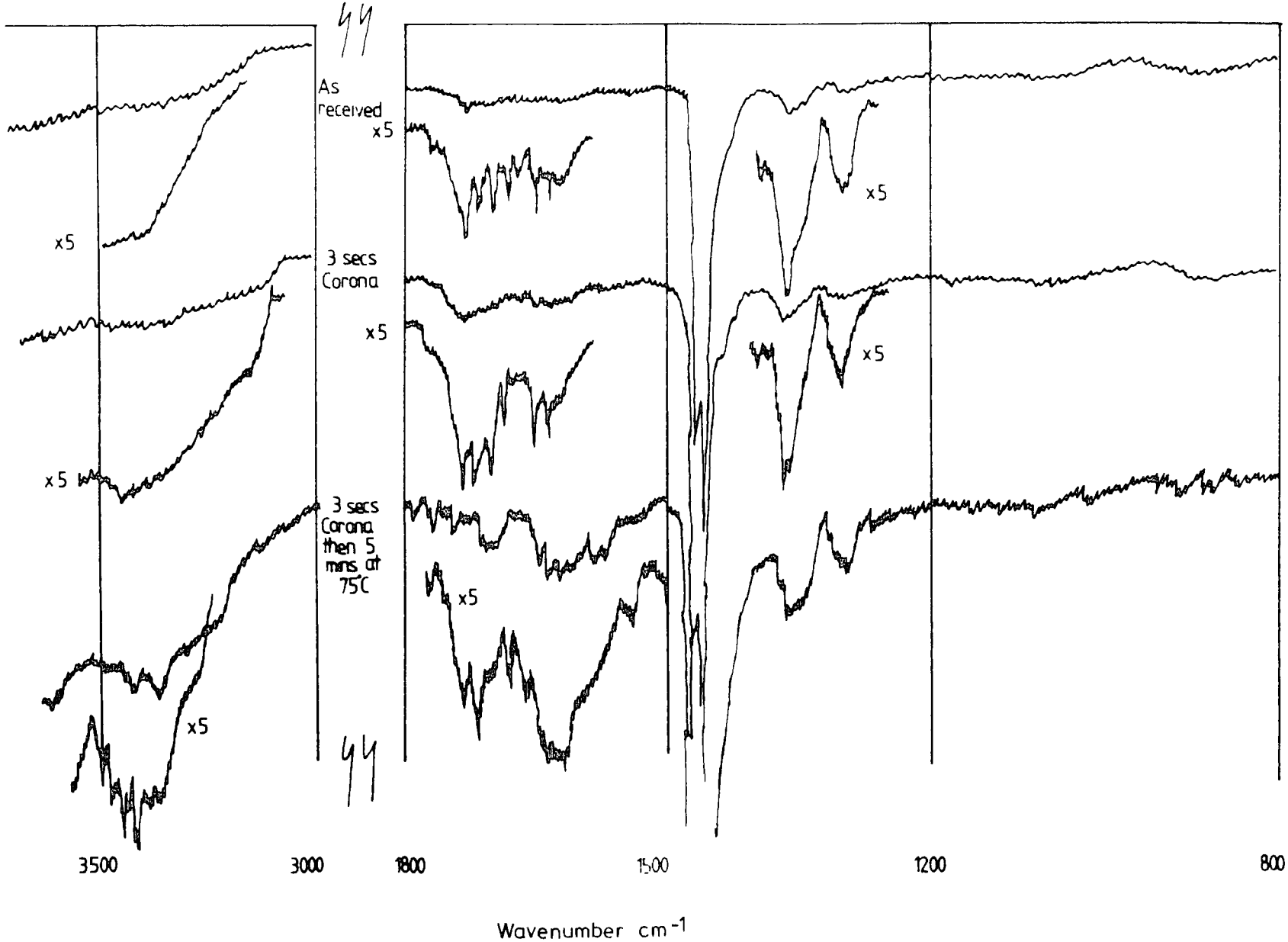

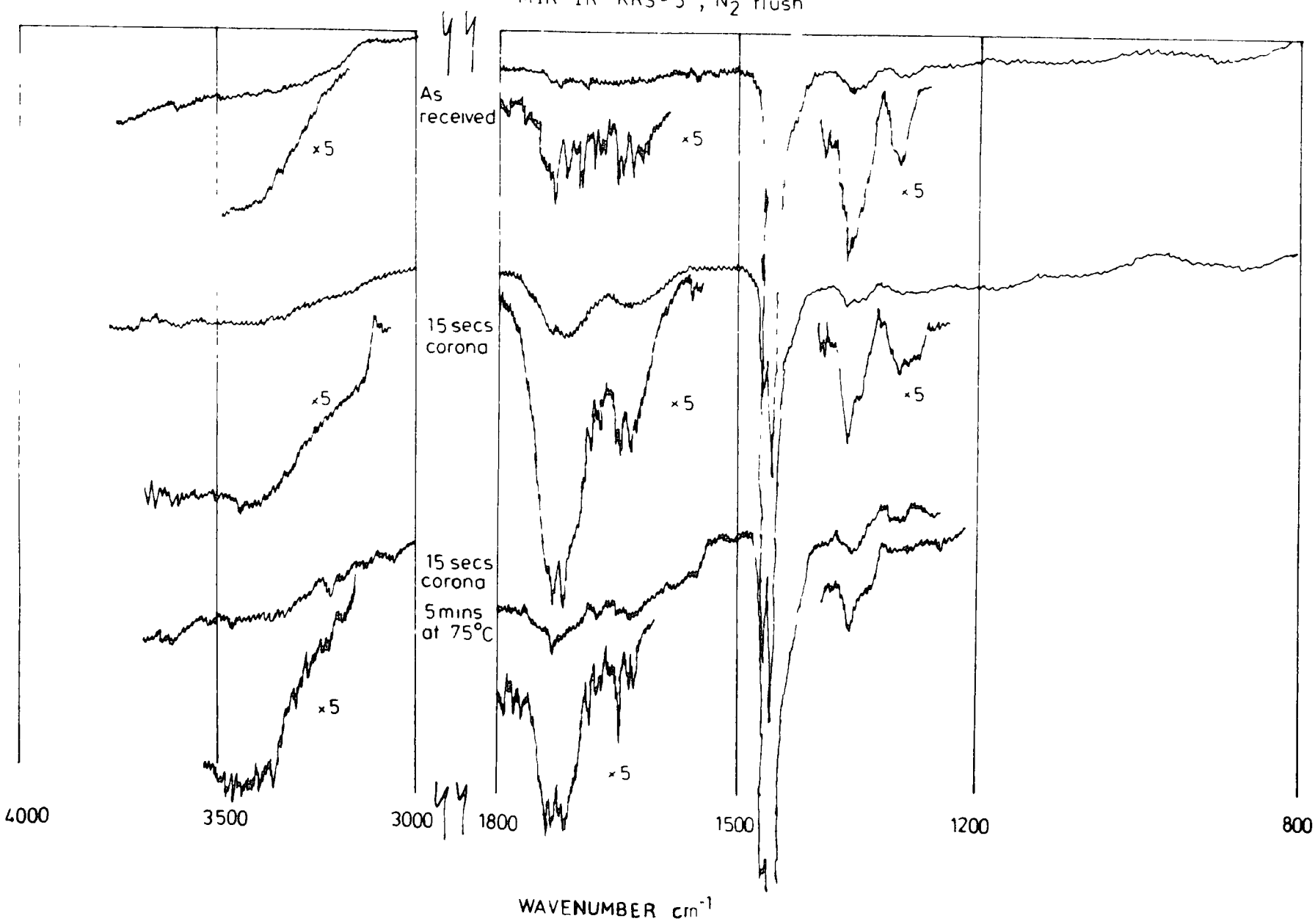
High Density Polyethylene, Corona Discharge in air, 2mm gap
MIR IR KRS-5, N_2 flush
As received
15 secs corona
15 secs corona
5 mins at 75°C
×5
4000
3500
3000
1800
1500
1200
800
WAVENUMBER cm^{-1}

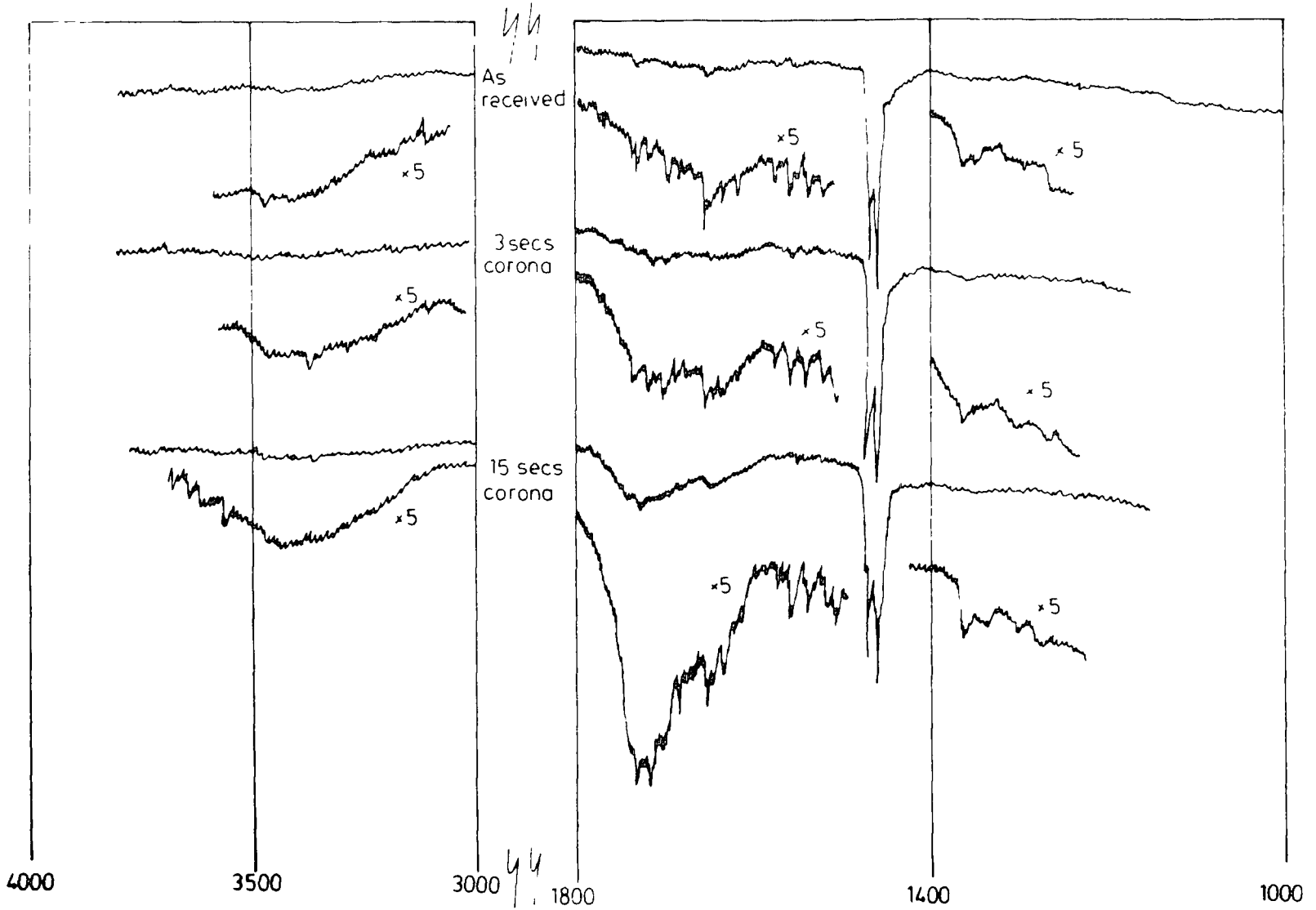
High Density Polyethylene, Corona Discharge in air, 2mm gap
MIR IR, Ge, N_2 flush
As received
3secs corona
15 secs corona
×5
4000
3500
3000
1800
1400
1000
Wavenumber cm^{-1}

High Density Polyethylene, Corona Discharge in air, 1mm gap
Transmission IR

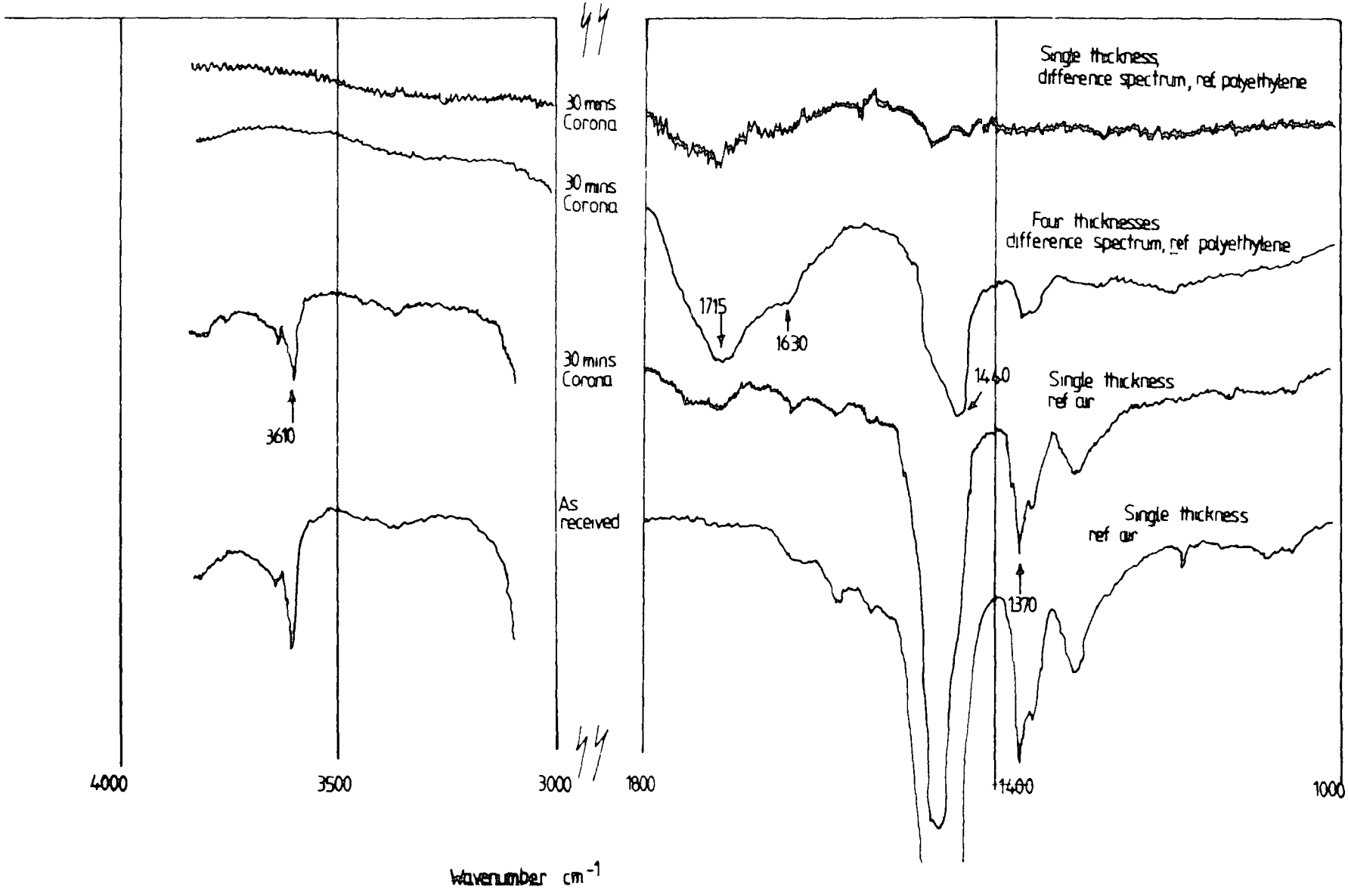

Crystals used for MIR IR at 45°, N_2 flush

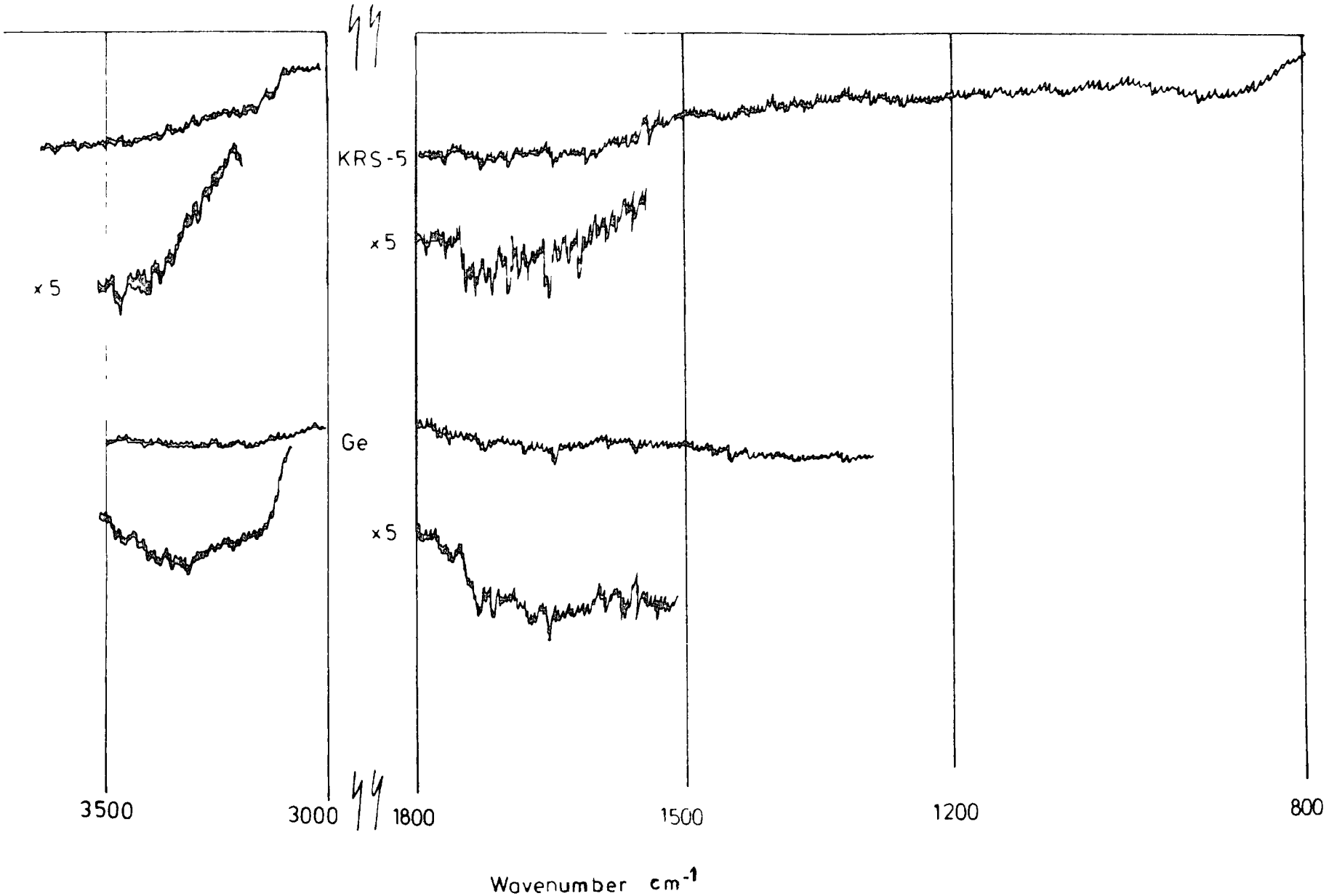

For transmission spectroscopy it was found necessary to use treatment times of the order of 30 minutes before it was possible to discern the features observed using MIR after treatment times of a few seconds.

The absorbance bands observed and given in Table 4.4.1 have been observed by many workers studying the surface oxidation and effects of "corona" discharges on polymers. Thus Benaissa and Mayoux[170], carrying out corona discharge treatment on wool, paper and polypropylene, report the production of carbonyl groups and hydroxyl groups. They refer to bands, arising from the formation of carboxyl groups at 1280 cm^{-1}. This was not observed in the spectra recorded for the work in this thesis. Zel'tzer, Britan, and Klyachko[171] carrying out corona treatment on polyethylene observed absorption bands at 1715-1730 cm^{-1} and at 1630-1640 cm^{-1}. Their spectra appear to be transmission spectra and their treatment times, to get measurable spectra, are rather long (minutes and hours). Carchano and Guastavino[172] studying the polymerisation of styrene by electrical discharge, discovered that bands due to hydrogen bonded hydroxyl groups 3600-3400 cm^{-1}, and carbonyl groups 1750-1650 cm^{-1}, were formed after oxidation by air. The formation of bands due to nitrate ion and nitrate ester, as reported by Zichy[163] from the surface scrapings of corona treated polypropylene, were not observed in the MIR IR spectra for corona treated polyethylene.

However, the treatment times she used are not mentioned and it is possible they would be observed by MIR IR after long corona treatment times.

It has been suggested by Lomonte[173] that the ester content of oxidised polyethylene might be determined from the infra red spectra. However, the low intensity of the band suggested for measurement, 1175 cm^{-1}, in the recorded spectra does not allow this.

Although as stated earlier the MIR IR spectra for LDPE and HDPE are similar there are important differences. Thus LDPE shows a larger absorbance at 1370 cm^{-1} due to CH_3 symmetrical bending movements. This is as would be expected since a branched alkane will have more terminal methyl groups than a more linear alkane. LDPE also shows two bands at 945 and 920 cm^{-1}, the latter possibly being due to vinyl end groups[174].

.5 Iodine Liberation

Following the work of Mair and Graupner[175] it was decided to investigate the possibility of iodine liberation from iodide ion as a means of examining peroxide formation on polyethylene surfaces during corona treatment. The technique suggested by Mair and Graupner[175] is well-established and involves treating the organic peroxide with a solution containing iodide ions. The peroxide bond is reduced by the iodide ion, which is oxidised to iodine. The free iodine will be complexed, in the presence of excess iodide ion to form the triiodide ion

$$I_2 + I^- \rightleftharpoons I_3^-$$

This triiodide ion may then be determined by any suitable analytical technique.

In view of the low concentration of the triiodide ion likely to be formed, after treatment of a surface containing peroxide groups it is desirable to carry out the reaction in an inert atmosphere. This is to prevent oxidation of the iodide ion by atmospheric oxygen. The following apparatus was therefore constructed to enable the iodide solution to be kept and used in an atmosphere of nitrogen. The iodide solution was a saturated solution of analar potassium iodide in analar acetone and the nitrogen was dried before use. The method of operation was to place the sample in the conical flask and by means of the three-way tap evacuate that section of the apparatus, including the graduated section. 5 cm^3 of the acetone/potassium iodide solution was then measured and added to the sample. After allowing 20 minutes for the reaction between the iodide ions and the possible peroxide groups a sample of the solution could then be removed from the conical flask, via the rubber septum, by a hypodermic syringe. The triodide solution was then examined by means of its ultra violet absorption spectrum, using the absorption at 360 nm. This was carried out by rapidly filling a quartz cell, path length 1 cm, with the solution and recording the

absorption spectrum. The reference cell was filled with a solution of acetone/potassium iodide that had been in contact with untreated polyethylene film for 20 minutes. The actual spectra

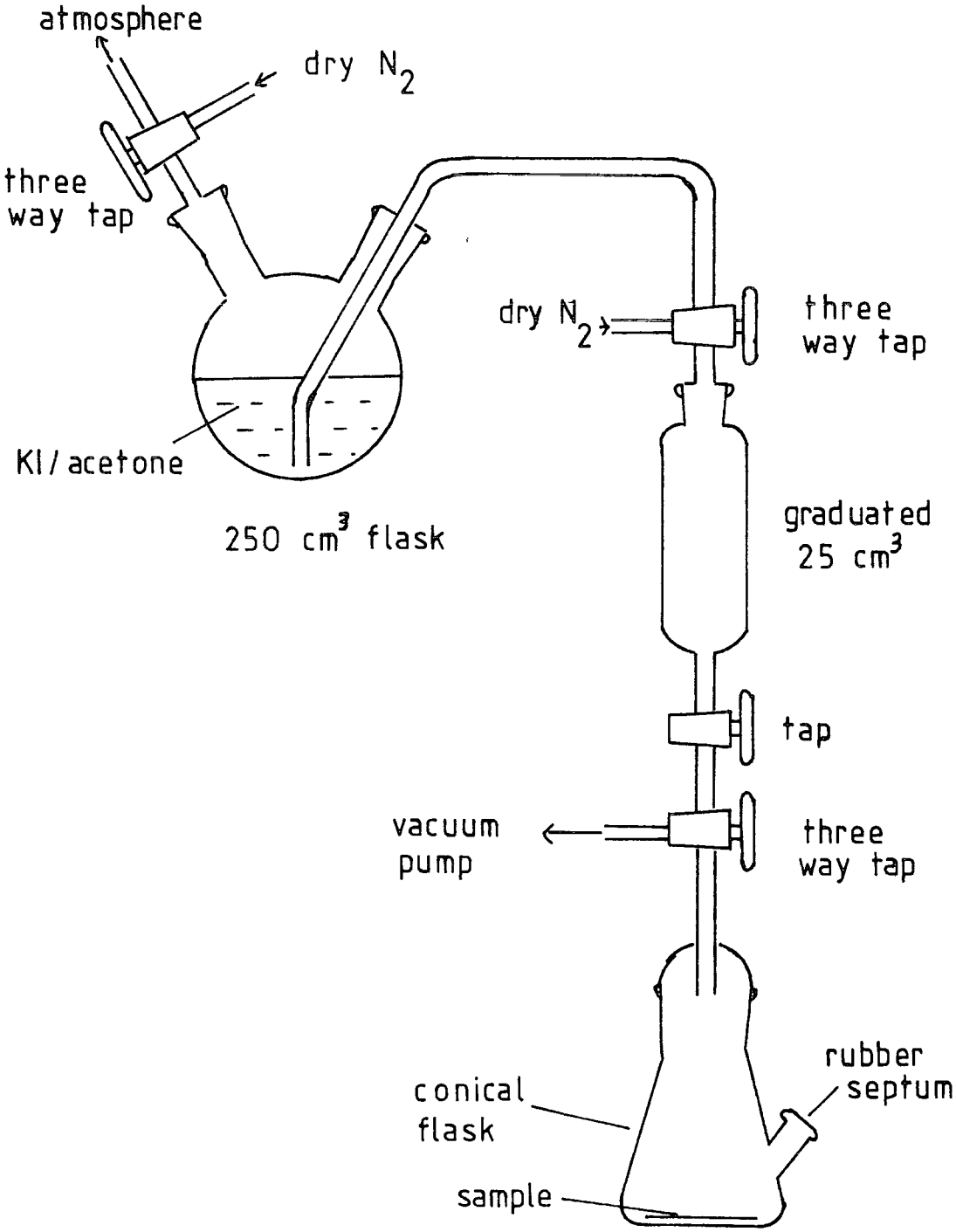

Figure 4 5 1

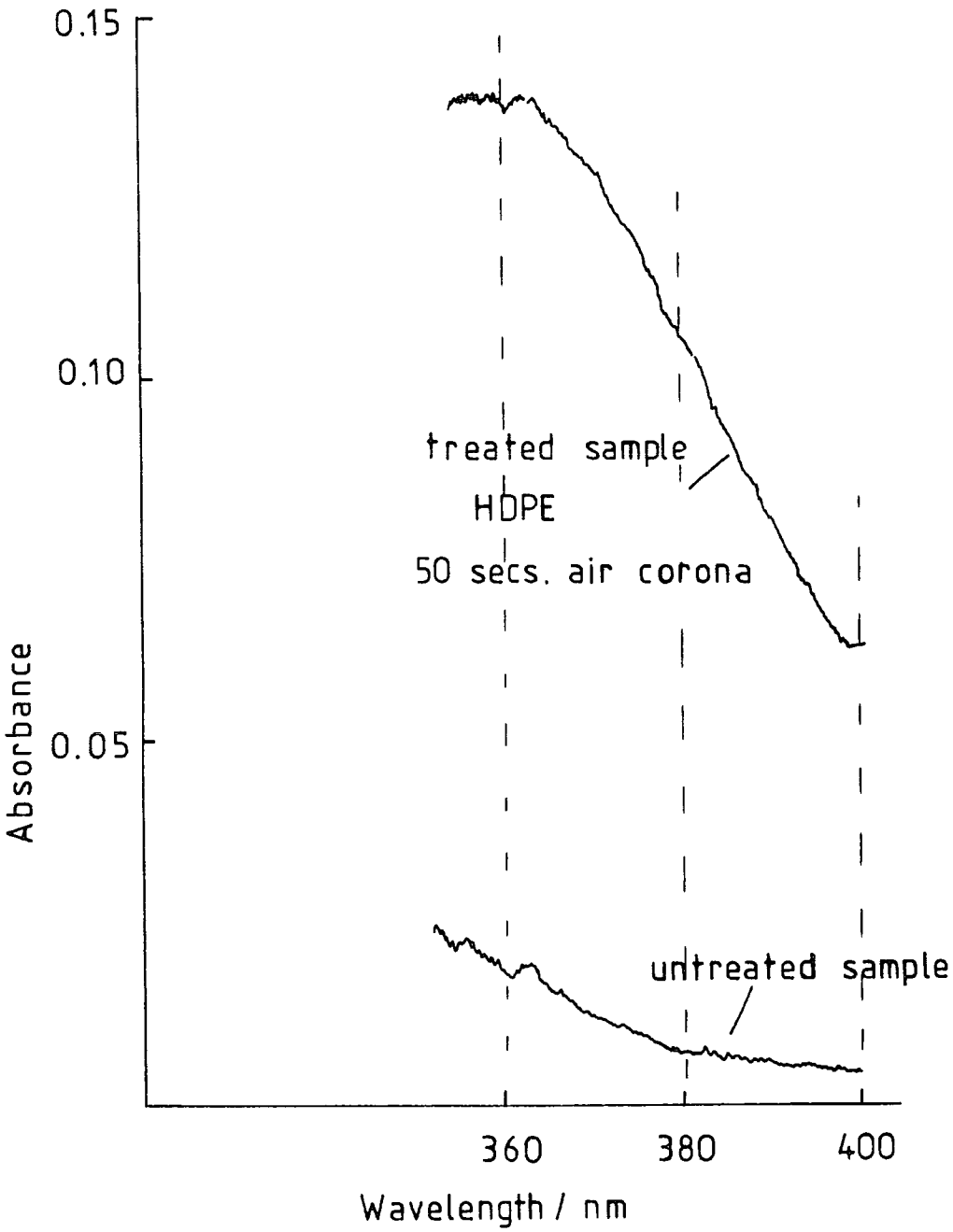

UV spectra for Triiodide solution obtained from HDPE

Figure 4.5 2

were recorded on a Beckman 25 Ultra Violet Spectrometer, and a typical result is shown in Figure 4.5.2.

Using the molar extinction coefficient for triiodide ion, 25000 at 360 nm, the concentration of triiodide for the sample in Figure 4.5.2 can be obtained as follows.

$$\text{Concentration of Triiodide} = \frac{\text{Absorbance}}{\text{Molar Extinction Coeff.}}$$

$$= \frac{0.12}{25000}$$

$$= 4.8 \times 10^{-6} \text{ moles dm}^{-3}$$

The total volume of acetone/potassium iodide solution used was 5 cm^3 and so the moles of iodine liberated is

$$\frac{5}{1000} \times 4.8 \times 10^{-6} = 2.4 \times 10^{-8} \text{ moles}$$

The piece of polyethylene had an area of approximately 4 cm^3, or 4×10^{-4} m^2 and so the moles of iodine liberated per square metre of polyethylene is approximately

$$\frac{2.4 \times 10^{-8}}{4 \times 10^{-4}} = 6 \times 10^{-5} \text{ moles } I_2 \text{ m}^{-2}$$

This corresponds to an equivalent number of moles of peroxide groups. The actual number of peroxide groups per square metre is obtained by multiplying by Avogadro's number and this gives the number of peroxide groups as

3.6×10^{19} m^{-2}. If this is compared to the approximate packing of atoms at the surface of the polymer of approximately 10^{19} atoms m^{-2} it would appear that the whole surface is covered with peroxide groups! This is of course a far too simplistic view since all the peroxide groups are not necessarily located on the surface. As was seen in the section above on the ESCA results there is considerable oxidation below the surface layer of the polyethylene and quite a high concentration of hydroperoxide. These subsurface peroxide groups may easily react with the iodide ions.

It would appear therefore that there is quite a high concentration of peroxide groups formed during corona discharge treatment and these peroxide groups may be detected by iodine liberation. The situation is however more complicated since other groups, e.g. nitrate, which have been reported as being formed[163], may also cause oxidation of the iodide ions. There is another problem in using iodine liberation techniques and that is the possibility that some of the iodine liberated may be absorbed by the polyethylene. In fact, Evans has shown[176], using radioactive iodine that this is so and also[177] that the absorption ratio increases rapidly as the concentration falls below 10^{-4} moles dm^{-3}. Further work is therefore needed in this area before the iodine liberation technique can be used to give a quantitative measure of the peroxide concentration on corona treated polyethylene.

Samples of polyethylene, after treatment with acetone and acetone/potassium iodide solution were examined by ESCA. The purpose of this was to see if low molecular mass material was removed and, also in the case of corona treated samples, if there were any changes observable in the oxygen functionalities. The samples were also examined to see if potassium or iodine were absorbed. The results of these experiments are shown in Tables 4.5.1 - 3. The spectrum of analar potassium iodide was also recorded (Table 4.5.3).

The deconvoluted oxygen spectra show that treatment with either acetone or acetone/potassium iodide results in a decrease in oxygen functionality at higher binding energies. This decrease can be explained as the effect of the acetone removing low molecular mass material which is highly oxidised. However, the oxygen functionality at lower binding energy is decreased for treatment with acetone but seems little changed when acetone/potassium iodide is used. This seeming contradiction can be explained by assuming that when hydroperoxide (high binding energy O_{1s}) reacts with iodide ions that the free radical momentarily formed can cross link to make a less soluble product

$$2\ ROOH + 2\ I^- \rightarrow 2RO^{\bullet} + 2OH^- + I_2$$

$$RO^{\bullet} \longrightarrow \text{Cross linked products}$$

low molecular mass (soluble)	High molecular Mass (insoluble)

When just acetone is used cross linking would be much reduced and so most of the highly oxidised material, containing hydroperoxides would be lost. With acetone/ potassium iodide the higher binding energy hydroperoxide would reappear as lower binding energy ether links and this could roughly balance the loss of soluble material with lower binding energy oxygen. The lack of change in the lower binding energy peaks for oxygen in this case is probably fortuitous rather than being connected.

The polyethylene control, sample A, Table 4.5.2, showed that neither potassium nor iodide ions were picked up by untreated HDPE. However, the oxygen spectra showed a very surprising result with a very large component at low binding energy. This was not matched by anything in the C_{1s} spectra so a wide scan ESCA sweep was made. This suggested the presence of silicon and a more detailed study gave an area ratio of Si_{2p}: O_{1s} of 7:10. This indicates that silicones are probably being picked up and the same effect was observed when the experiment was repeated some time later and on a different ESCA machine, Kratos ES 300. But this silicone contamination was not observed for corona treated samples or when just acetone was used. At the present time these differences in behaviour cannot be satisfactorily explained. Also although diffusion of silicones, from Scotch tape, is known to occur, it usually takes some time and the ESCA results were recorded within an hour

of the polyethylene being stuck on the probe tip. Contamination of the acetone/potassium iodide solution should have shown up when other samples were being run (C and D, Table 4.5.2).

It was interesting to see that both potassium and iodide ions were absorbed, from an acetone/potassium iodide solution, by corona treated polyethylene. The potassium ions though were absorbed to a far greater degree than were the iodide ions. Using the values for analar potassium iodide, and assuming this substance does not decompose when irradiated by X-Rays, the $K_{2p3/2}$ area should be approximately half the $I_{3d5/2}$ area for a one to one stoichiometry. For the polyethylene this area ratio is not seen and for a 70^{o} take off the area ratios (Table 4.5.3) suggest that the absorption of potassium ions is at least an order of magnitude greater than the absorption of iodide ions. For a 30^{o} take off no I_{3d} peaks were observable which suggests the iodide absorption is very much restricted to the surface. It is possible that the potassium ions are absorbed as counter ions for the carboxylate groups but as recorded the carboxylate peak, at 289.2 eV is not large enough to account for the observed potassium absorption. However, deconvolution was achieved assuming that the carboxylate function was present as the unionised carboxylate group. If the deconvolution is repeated using a peak shifted to lower binding energy for the carboxylate ion then a larger peak, approximate

	C_{1s}				N_{1s}		O_{1s}				
	286.6	287.8	289.2	290.3	402	400 5	530	532.7	533.5	534.3	535.5
A*	14 8	5 2	3 4	0 8	0.28	0 4			27.4		
	7	2.4	1	0					18.4		
B*	17.4	7.2	7.2	0 6	1.32	1			57		
	18	7.0	6 7	0.7	0.9	0.9			51.3		
C	4 2	1					0.3	0.8		0.1	
	4 6	1 4					1.5	2.7			
C´	5 6	0 9	0.3					2.1	0.1	0.5	0 2
	6.3	0.9	0.2					2.2	0	0.5	
D	14	10	8	0.2				24.6	6.7	22	3 3
	16	7	6.7	0.2				23.3	9.1	14	3.3
D´	8 2	3	2	0.2				10.4	1.5	5	1.4
	8.6	3.2	1.8	0.2				10.8	1.8	5	0.5

A LDPE 3 secs air corona, 19 days after Treatment. * O_{1s} peak not deconvoluted

B HDPE 15 secs air corona, 19 days after Treatment.

C and C´ HDPE untreated, before and after soaking in acetone for 20 minutes, air dried 2 hours.

D and D´ HDPE 15 secs air corona, before and after soaking in acetone for 20 minutes, and air dried for 2 hours

Table 4.5.1

	C_{1s}				N_{1s}	O_{1s}			
	286.6	287.8	289.2	290 3	408	532.7	533.5	534.3	535 5
A	3.4	O 7				56	18	5	
	3.2	O.6				76	4	7	
B	20	10	10	2	0.9	37	11	22	6
	12	10	6	O 2		28	9	18	2
C	10	4 4	1.8			24	3	6	1
	12.8	4 4	1.8			31	2	5	1
D	13	3.6	1.4			26	2	5	1
	14	4.4	1.9			30	2	4	1

A HDPE 20 minutes acetone/potassium iodide, air dried 2 hours

B HDPE 15 secs air corona

C & D HDPE 15 secs air corona, followed by 20 minutes acetone/potassium iodide, air dried 2 hours.

Area Ratios for HDPE Samples

Table 4.5.2

A HDPE 15 sec. Air Corona followed by 20 minutes acetone/potassium iodide and then air dried for 2 hours (see sample D in Table 4.5.2)					
	Area Ratios		Binding Energy	Area Ratios	Binding Energy
$K_{2p\frac{1}{2}}$	6		296.3 eV	$I_{3d\frac{3}{2}}$ 0	631.8 eV
		4.6		0.6	
$K_{2p\frac{3}{2}}$	10		293.5 eV	$I_{3d\frac{5}{2}}$ 0	620.6 eV
		9.2		1.0	
B Analar Potassium Iodide powder					
$K_{2p\frac{1}{2}}$	25		296 eV	$I_{3d\frac{3}{2}}$ 62	631.3 eV
		22.5		67	
$K_{2p\frac{3}{2}}$	50		293.3 eV	$I_{3d\frac{5}{2}}$ 100	619.8 eV
		45		100	

Relative Area Ratios for Potassium K^+ and Iodide I^- ions

(Analar Potassium Iodide values relative to $I_{3d\frac{5}{2}}$)

Table 4.5.3

area ratio 4% (relative to C_{1s} 285 eV) is needed. This peak is also much broader, FWHM 2.2 eV, which would be expected since the ionised carboxylate ion presents the potassium ion with alternative lattice sites and this leads to broadening of the peak. The relative areas of photo ionisation for potassium and carbon are in the approximate ratio of 4:1. This, taken with the C_{1s} area ratio given above of 4%, suggests that the total K_{2p} area should be about 16%. The actual values observed are 16% for the 30° take off and 13.8% for the 70° take off. This agreement is quite good and would tend to confirm the idea that the potassium ions are absorbed as counter ions to the carboxylate functions. The lack of iodine absorption is then simply explained since there are very few basic groups formed.

.6 Discussion and Consideration of Results

The results in this chapter show clearly the advantages of the ESCA technique over MIR IR when dealing with very thin surface layers. However, the MIR IR data is useful confirmation of the ESCA results and so is not to be despised. The iodine liberation technique described in section .5 above does give some information about the presence of hydroperoxides but more work is needed on this before quantitative results can be obtained. Perhaps a more interesting result arising from the iodine liberation experiments was the observation of potassium ion absorption in approximate quantitative amounts, as counter ion for carboxylate ion.

The presence of acidic groups, after corona treatment of polyethylene, has been shown by the work of Courval, Gray and Goring[178], who found that basic dyes could be absorbed by the polymer surface but that acidic dyes could not. They also found that after corona treatment in nitrogen only basic groups were formed since then acidic dyes were absorbed but basic dyes were not.

The ESCA results above, in section .3, show that after corona treatment in most gases a polyethylene surface acquires a high degree of oxygen functionality. Where gases other than air or oxygen are used the oxygen may come either from impurities in the gases or from gases absorbed on the surface of the polyethylene. The oxygen functions introduced are carboxyl groups, hydroperoxide, carbonates, carbonyls and various combinations of hydroxyl, ether and peroxide. Quite large, relatively speaking, quantities of hydroperoxide are usually formed. Also formed in small amounts are nitrate groups and amines (not when using nitrogen). For the spectra recorded for this thesis nitrate ions were not always observed while amine groups were commonly observed. Yet other workers in this field[163,201] report the formation of nitrate ion as a usual occurrence. This may well be due to the way the spectra were recorded and the time of exposure to X-Rays. In sections .3a and 3 above, the results of leaving a sample exposed to X-Ray radiation for 2 hours and then recording the spectra, are discussed. What was observed was that nitrate groups could suffer photo reduction with time and since the nitrogen spectra were always recorded last, that

is in fact after about an hour, this could explain the usual absence of nitrate groups. On the other hand after exposure to X-Rays hydroperoxides were observed to decrease as they are decomposed by the radiation. It would therefore not seem possible to measure, for one sample, the amounts of nitrate and hydroperoxide with great accuracy.

When using nitrogen as the corona gas the oxygen functionality as with other gases is increased but there are important differences. There was very little carbonate function and probably no hydroperoxide formed. On the other hand there were formed considerable amounts of amine and amide functions. This latter was seen both in the nitrogen and oxygen 1s spectra.

Degradation of polymer surfaces, after corona discharge, has been observed as have changes in surface morphology[6]. Thus Kim and Goring[6] found that corona treatment of low density polyethylene in oxygen or oxygen containing gases leads to surface roughening, but discharges in other gases did not. Electron micrographs revealed the formation of definite bumps on the surface that appeared to grow with time. They suggest that during the treatment degraded material may actually move to various points on the surface causing the bumps to grow. This could explain, in part, why there is not a decrease in mass during the treatment. They in fact report a slight increase in mass which they suggest is caused by the addition of oxygen

compensating for the loss of any polymer material.

The "corona" discharge used for treatment purposes is known to be composed of electrons, ions, excited neutral species and radiation, this latter being principally in the ultra violet region. It would be useful to know the way in which the total energy of the discharge is distributed among these but at the present time this is not known. It would also be useful to know the relative importance of the various components of the discharge in bringing about the observed effects on polymers. This information would be of value not only to people concerned with increasing the surface energy of polymers but also to electrical engineers whom it might be said would often rather the effects did not take place. Mayoux[13,164] has studied the effects, separately, of electron, ion and ultra violet radiation on polyethylene. He found that an electron beam, accelerating voltage 1500 V, produced a brown spot on polyethylene. Using MIR IR he was able to show the formation of hydroxyl and carbonyl groups and that this effect was confined to the surface of the film on which the electrons impinged. Other groups detected were ethylenic and carboxyl groups. When bombardment with ions or irradiation with ultra violet light was carried out he observed the same groups but that these were not necessarily formed to the same extent in each case. Furthermore he concluded that corona treatment in air could not be considered as the simple sum of the

effects of electrons, ions and ultra violet radiation. One other effect of electron radiation that is not usually looked for is the formation of free radicals. This has been observed, by Waterman and Dole[179], using 1 MeV electrons on polyethylene at liquid nitrogen temperatures. The free radicals were found to persist at room temperatures. Free radicals are also known to be formed as a result of ultra violet radiation. It is therefore possible that free radicals are formed during normal corona treatment. That they are not observed after the treatment[176,188] may simply be due to the fact that in the presence of oxygen and oxygen containing species free radicals readily react to form hydroperoxides and other oxygen containing groups.

The oxidation of polyethylene[180] and polypropylene[181] by ultra violet radiation has been shown to be dependent on the presence of hydroperoxides and free radicals. Thus Chew, Gan and Scott[180] suggest that the hydroperoxide formed by the reaction of oxygen with free radicals

$$R^{\bullet} + O_2 \rightarrow RO_2^{\bullet} \qquad (i)$$

$$RO_2^{\bullet} + RH \rightarrow ROOH + R^{\bullet} \qquad (ii)$$

is then photolysed to give an alkoxy radical and eventually a carbonyl compound

$$ROOH \xrightarrow{h\nu} RO^{\bullet} + {}^{\bullet}OH \qquad (iii)$$

$$RO^{\bullet} + RH \rightarrow ROH + R^{\bullet} \qquad (iv)$$

$$RO^{\bullet} \rightarrow R' - \underset{\underset{O}{\|}}{C} - R'' + H^{\bullet} \qquad (v)$$

The reaction is a chain one, new initiating radicals being formed in reactions (iii) and (iv). Termination is likely to be by disproportionation of the alkylperoxide radicals.

$$2\ R\ O_2^{\bullet} \longrightarrow \text{stable products}$$

Carlsson, Gorton and Wiles[181] in their work on polypropylene suggest that with this material hydroperoxides may be formed by the reaction of singlet oxygen with double bonds as well as by the reaction of ordinary oxygen with free radicals.

Reactions similar to the one discussed in section .3f above have been proposed for treating the surfaces of polymers, both natural and synthetic. Thus Sakata and Goring[182] found that ethyl acrylate could be grafted onto cellulose film by corona treatment. Unfortunately they do not report any spectroscopic examination of the polymer surface formed. Hay[137] has found that a corona discharge causes polymerisation of monomers, which he carried out using a moving film as a carrier for the deposited polymer. Pachonik[183] has suggested the use of electrical discharges to produce very thin layers of polymers as dielectrics in electrical capacitors. However, the pressures he uses are less than atmospheric, 3×10^3 Nm^{-2}, so his process may be the one usually called plasma polymerisation (see Chapter 6) rather than a "corona" induced polymerisation.

When using corona reactions for grafting onto surfaces or for producing thin polymer films it cannot be assumed that the polymer formed is exactly the same as that produced from the monomer by the more usual chemical reactions. Thus Carchano and Guastavino[172] found that the polystyrene produced by corona discharge was insoluble in the solvents which could normally be used to dissolve polystyrene. They also observed a difference in the infra red spectra.

Other examples of the use, present or suggested for corona induced grafting and modification of polymer surfaces will be found in the references given in Chapter one.

Chapter 5

Effects and Uses of Corona Treatment on Polyethylene

.1 Introduction

.2 Surface Energy and Critical Surface Tension for Wetting

a) Theory

b) Measurement of Critical Surface Tension for Wetting

c) Results and Discussion

.3 Adhesion

a) Theory

b) Lap Shear Test

c) Results and Discussion

Shear Strength, ESCA and MIR IR

.4 Surface Charging

a) Electrical Properties of Polymers

b) Measurement of Charge

c) Results and Discussion

.5 Conclusions and Uses of Corona Treatment

.1 Introduction

The low surface energy of many polymers leads to poor wetting by commercial printing inks and low adhesion when used with normal glues and adhesives. There is generally a need to ensure that the surface energy of the polymer is at least 40 mN m^{-2} before use with the ordinary commercial inks and adhesives[184]. A method that is cheap and clean and needs little or no pretreatment or cleaning up after the process is required. The commonest methods[2] are i) using flame and plasma torches[4], ii) corona treatment, dealt with in Chapter 4 and this chapter, and iii) plasma treatment at low pressures, dealt with in Chapter 6.

The method of corona treatment of polymer surfaces has been the subject of quite extensive patent literature by industrial users (see section .5 below).

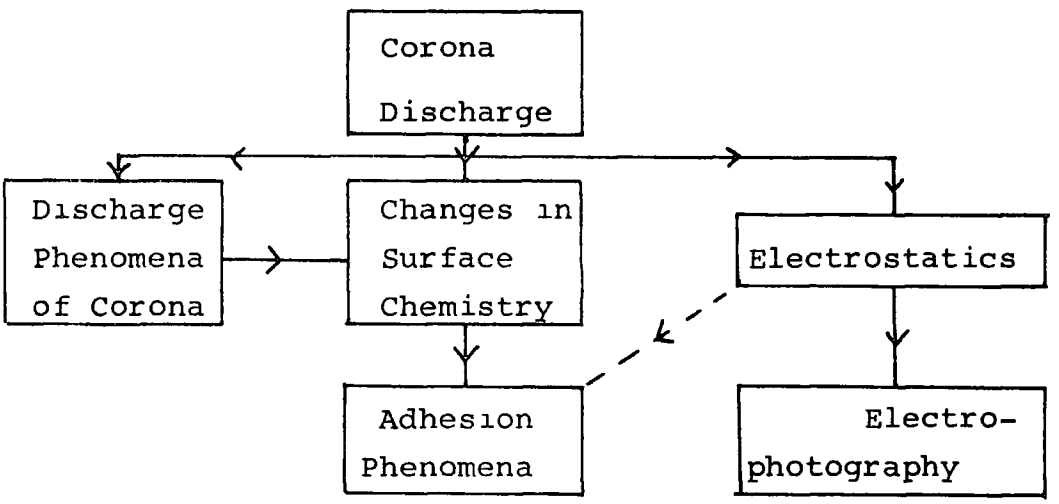

Although it is known that corona treatment increases the critical surface tension for wetting it has not always been very clear why it should do so. Clearly the treated surface is able to exert some increased attraction for the ink and adhesive molecules. Van der Waals forces, weak and induced dipoles can be used[185] to explain this increase provided that the surfaces are ideal, that is clean and atomically smooth and planar. However, surfaces are usually far from ideal and so somewhat larger forces than simple Van der Waals forces are needed to explain the observed increases in surface energy. The formation of large permanent dipoles, such as are present in hydroxyl groups could explain some of the increase. The formation of definite covalent bonds between the polymer and the ink (or adhesive) would of course produce large forces. These covalent links could be formed by the fission of peroxy bonds or by ester formation from hydroxyl and carboxyl groups (Chapter 4.3). Evidence that a polymer may form covalent bonds with another surface has been put forward by Buckley and Brainard[186] from their work with polytetrafluoroethylene and polyimide polymers and tungsten. Ionic bonds could be formed by the ionisation of carboxylic acid groups on the polymer surface or the presence of other ionic groups. Thus Courval, Gray and Goring[178] report the formation of basic groups on the surface of polyethylene subject to a corona discharge in nitrogen. The presence of trapped electrons[187], forming an electret

material, might also produce the effect of having negatively charged groups attached to the polymer material. In fact it has been suggested by Kim, Evans and Goring[188] that these comparatively deep seated electrons are largely responsible for the increased autoadhesion of corona treated polyethylene.

It is possible that all the forces mentioned above, Van der Waals, covalent, ionic and electret charge are involved to some degree in increasing the ability of corona treated polyethylene to accept inks and adhesives. Furthermore it is possible that the relative effect of each component force may change with time from the proportion of each, immediately following printing and glueing. Thus electret attraction and Van der Waals forces may be responsible initially and ionic and covalent forces may become more important with time. There is another effect not mentioned so far and that is diffusion of material at the interface[181]. This could lead to an increase in adhesive strength due to mutual entanglement of the different materials. It has been suggested by Schonhorn[181] that the increased adhesive strength is due more to removal of weak surface layers than due to increased critical surface tensions for wetting. This idea will be discussed further in the sections below.

.2 Surface Energy

a) Theory

The energy for a liquid to spread must arise

from the intermolecular forces between the liquid and the solid surface. These forces will, in general, consist of dispersion, orientation and induction forces, assuming no chemical bonding occurs. This latter is unlikely except for liquid adhesives being spread on the surface. The dispersion forces arise from the interaction of the fluctuating electron clouds of the molecules. Dispersion forces are common to all molecules and Kaelble[189] has shown that for many polymers the dispersion forces are the main component of the total surface energy of the polymer. The orientation forces arise from permanent dipoles, within the liquid and solid, which can rotate so they are attracted to each other. Induction forces arise when a dipole moment in one phase can induce a temporary dipole moment in the other phase, thus giving rise to attraction. Orientation and induction forces are often included under the general heading of polar forces and the polar component, γ_p, of surface energy may be written as[190]

$$\gamma_p = \gamma_{pp} + \gamma_{pi} + \gamma_h \qquad 5.2.1$$

where γ_{pp} is the dipole - dipole component,

γ_{pi} is the dipole - induced dipole component,

and γ_h is the hydrogen bonding component (a hydrogen bond is an "extreme" dipole-dipole attraction).

The effects of the forces, polar and dispersion, when a liquid is placed on a surface, can be considered[181] in

terms of the surface energy of the two phases. When a drop of liquid is placed on a surface the energy available for wetting is the difference between the energy γ_{SV} of the solid-vapour interface, which is lost when the surface is covered by the drop and the energy γ_{SL} of the solid-liquid interface that replaces it.

Thus $$T = \gamma_{SV} - \gamma_{SL} \qquad 5.2.2$$

where T is the energy available for wetting.

The separate values of γ_{SV} and γ_{SL} cannot be determined experimentally but the difference can be, by considering the contact angle, θ, at the edge of a drop of liquid on the solid surface.

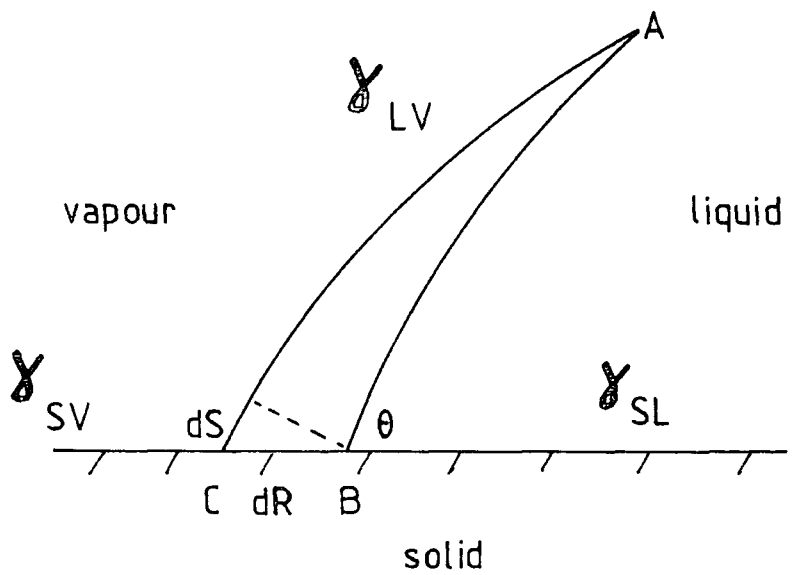

Liquid Drop on Surface

Figure 5 2 1

If the edge of the drop, radius R, advances from B to C the periphery of the drop is now AC instead of AB and the change in free energy dG, is given by

$$dG = 2\pi R dR \gamma_{SV} - 2\pi R dR \gamma_{SL} - 2\pi R dS \gamma_{LV} \qquad 5.2.3$$

but $dS = dR\cos\theta$

therefore $$dG = 2\pi R dR (\gamma_{SV} - \gamma_{SL} - \gamma_{LV}\cos\theta) \qquad 5.2.4$$

When the drop is in equilibrium dG = 0 and

therefore $$\gamma_{SV} - \gamma_{SL} = \gamma_{LV}\cos\theta \qquad 5.2.5$$

This is known as the Young-Dupré equation and substitution in equation 5.2.2 gives

$$T = \gamma_{LV} \cos\theta \qquad 5.2.6$$

The surface energy of a liquid can readily be measured and the contact angle, θ, of the liquid on the surface is also easily measured and hence T can readily be calculated. Since γ_{LV} is a property solely of the liquid, the property which characterises the effect of the interactions of the solid and the liquid to promote wetting is $\cos\theta$.

Since a surface on which a drop is spreading is in equilibrium with the vapour above the drop, absorption of the vapour must take place. This absorption must reduce

the surface energy of the solid from its vacuum value and this must reduce the contact angle. The reduction of the surface energy of the solid below its vacuum value, γ_S, is called the spreading pressure of the liquid, π_S, and is given by

$$\pi_S = \gamma_S - \gamma_{SV} \qquad 5.2.7$$

The Young-Dupré equation, 5.2.5, then becomes

$$\gamma_S - \pi_S - \gamma_{SL} = \gamma_{LV} \cos\theta \qquad 5.2.8$$

$$\text{and } \cos\theta = \frac{\gamma_S - \gamma_{SL}}{\gamma_{LV}} - \frac{\pi_S}{\gamma_{LV}} \qquad 5.2.9$$

The term $\frac{\gamma_S - \gamma_{SL}}{\gamma_{LV}}$ is solely concerned with pure clean surfaces and if assumptions concerning the value of π_S can be made, information can then be obtained as to how molecular structure determines contact angles. Various approaches to this problem have been made[189,191,192], both theoretical and empirical. Zisman's approach[192] to the problem of wetting is semi-empirical and is one of more immediate usefulness.

According to Zisman the ability of a liquid to spread on a solid is determined by the spreading coefficient S, where S is the decrease in the free energy of the system when the liquid drop spreads. Since during this process a solid-liquid interface and a liquid-vapour interface

are formed and a solid-vapour interface is lost

$$S = -\Delta G = \gamma_{SV} - \gamma_{SL} - \gamma_{LV} \qquad 5.2.10$$

Since S must be positive if the liquid is to spread and γ_{SV} for many organic polymers is small, < 40 mN m^{-2}, a liquid will only spread provided that γ_{SL} and γ_{SV} are also small. The investigations of Zisman have shown that there is a linear relationship between $\cos\theta$ and γ_{LV} of the form

$$\cos\theta = b - c\,\gamma_{LV} \qquad 5.2.11$$

where a and b are constants for a homologous series of liquids on a given polymer surface.

The value of γ_{LV} for which $\theta = 0$, and $\cos\theta = 1$, is the maximum value for the surface tension of the liquid if the surface forces are to assist the wetting process, that is if S is to be positive. This maximum value of γ_{LV} has been called by Zisman the "critical surface tension for wetting", γ_c. This does not mean that if $\gamma_{LV} > \gamma_c$ that no spreading will occur since gravitational and other forces will cause some spreading and at equilibrium establishment of a drop of liquid on the surface with contact angle θ. The critical surface tension for wetting is reproducible even when non-homologous liquids are used, though in this case there is more scatter in the values of $\cos\theta$ and γ_{LV}, which give rise to some uncertainty in the value of the critical surface tension for wetting. Because of this reproducibility Zisman was able to take γ_c as a fundamental surface

property of the surface and to relate it empirically to structural features. Using Zisman's results Kaelble[189] has been able to show that there is a fair correlation between γ_C and γ_S, the relationship being

$$\gamma_C = \phi^2_{LS} \cdot \gamma_S \qquad 5.2.12$$

where $0.3 \leqslant \phi^2_{LS} \leqslant 1$

and therefore $\gamma_C \leqslant \gamma_S$ 5.2 13

Where γ_C as found by Zisman is less than γ_S it is suggested by Kaelble that this is due to the fact that γ_C tends to underestimate the polar component γ_{ps} of the solid surface tension.

The above discussion has assumed that the liquid spreads on a smooth flat surface. If the surface is rough or has a composite nature then contact angles are different from those expected and furthermore a hysteresis effect is observed for the contact angle θ depending on whether the liquid drop is advancing or receding over the surface. For an advancing drop θ will be larger and the surface less easily wetted while for a receding drop θ will be smaller and the surface more easily wetted[8,191].

When the surface is rough then equation 5.2.2 becomes

$$T_R = r\,(\gamma_{SV} - \gamma_{SL}) \qquad 5.2.14$$

where r is the roughness factor and each surface is multiplied by r while T_R refers to unit area of the

apparent surface. Hence from equation 5.2.6 the contact angle on the rough surface ϕ, will be given by

$$\cos \phi = \frac{\gamma^{TR}}{\gamma_{LV}} \qquad 5.2.15$$

which with equation 5.2.14

becomes $$\cos \phi = r \frac{(\gamma_{SV} - \gamma_{SL})}{\gamma_{LV}} \qquad 5.2.16$$

and substituting, using equation 5.2.5 this becomes

$$\cos \phi = r \cos \theta \qquad 5.2.17$$

and $$\frac{\cos \phi}{\cos \theta} = r \qquad 5.2.18$$

This is known as Wenzel's equation and shows that if the intrinsic contact angle θ of a liquid on a solid is less than 90^{o} then the apparent contact angle ϕ will be reduced by roughening while if θ is greater than 90^{o} then ϕ will be increased. For a composite surface it can be shown in a similar manner that the apparent contact angle is given by

$$\cos \Phi = \Omega_1 \cos\theta_1 + \Omega_2 \cos\theta_2 \qquad 5.2\,19$$

where Ω_1 , Ω_2 and θ_1 , θ_2 are the relative areas and intrinsic contact angles respectively of the two components.

The observed hysteresis in contact angle measurements has been explained by Dettre and Johnson[193] as being due to measurements being made on drops in metastable

equilibrium. According to them the most stable position for the edge of a drop, on a rough surface, is close to the top of a trough and as the drop advances or recedes it must pass through higher energy states as it moves from crest to crest.

Using a simple model for the surface of the polymer, as shown in figure 5.2.1, the maximum and minimum values of ϕ can be found. The intrinsic contact angle is θ but the measured contact angle will be

$\phi_A = \theta + \alpha$ for an advancing edge, and

$\phi_R = \theta - \alpha$ for a receding edge.

So ϕ_A will be larger than ϕ_R and the critical surface tension for wetting for the solid will appear to be less if the liquid drop is advancing than if it is receding.

When a liquid is placed on a composite surface, the advancing contact angle will be greater than the receding contact angle. This is because (assuming the contact angle is not zero) that as the liquid edge is advancing it will be held back by the areas of lower surface energy which it cannot wet so easily. When the liquid edge is receding it will be held back at the areas of higher surface energy as these require more energy to expose them. This is illustrated in figure 5.2.2.

In practice it is likely that a surface will be both rough and composite in nature. The resulting contact angles, advancing and receding, together with the corresponding critical surface tensions for wetting will then be determined by a combination of both these factors.

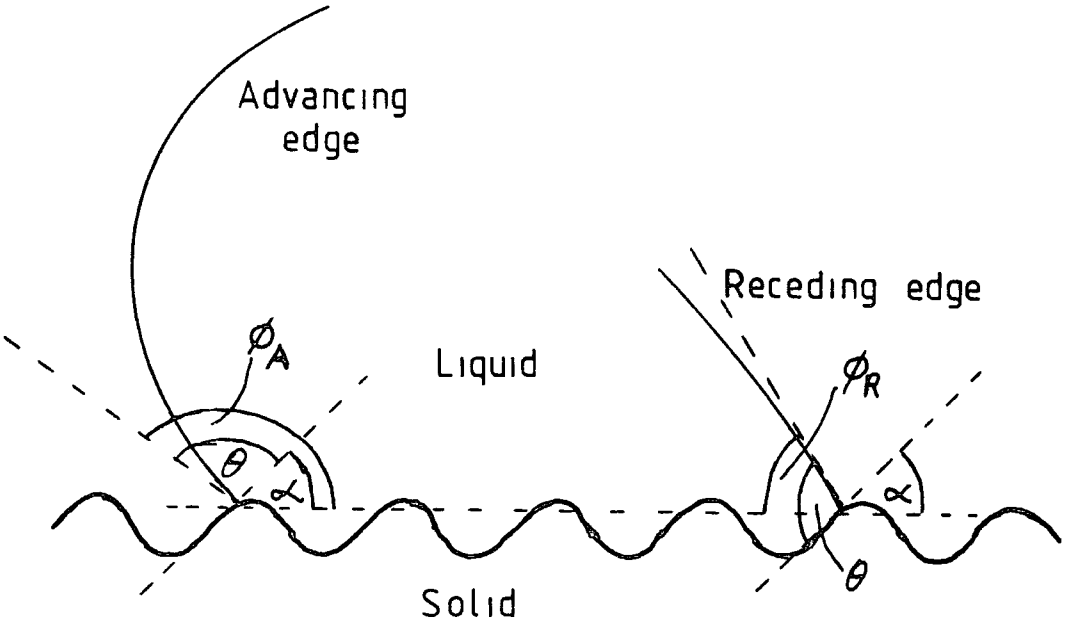

Advancing and Receding Liquid Edges on a Rough Surface

Figure 5 2 1

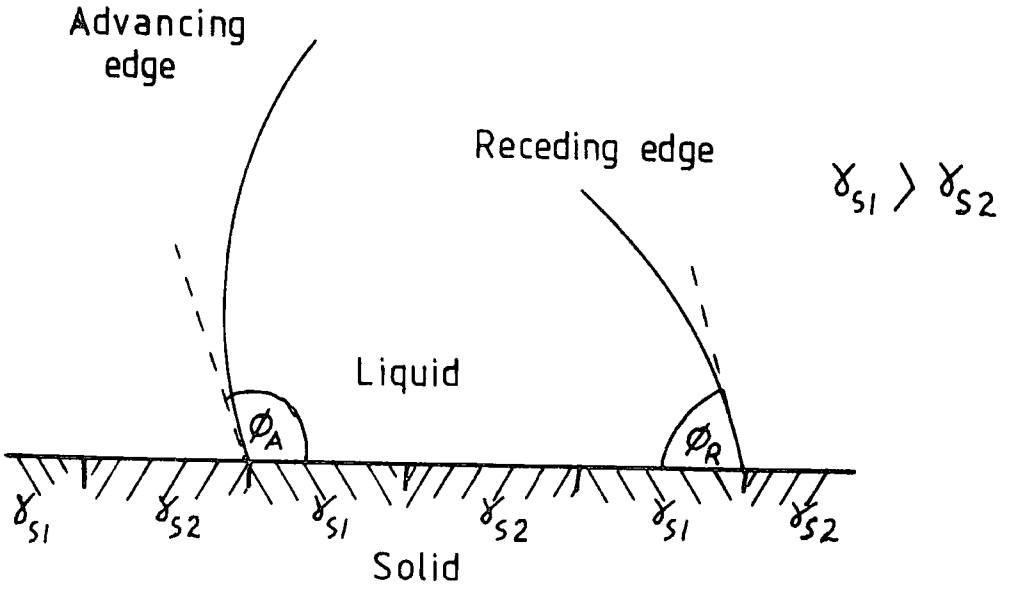

Advancing and Receding Liquid Edges on a Composite Surface

Figure 5 2.2

b) Measurement of Critical Surface Tension for Wetting.

The critical surface tension for wetting was obtained in two ways; by the ASTM wipe test and by calculation from the contact angle of a drop of water placed on the surface. The ASTM wipe test has been described previously in Chapter 3.4a, and involves observing different liquids "wiped" on the surface and noting the one which just does not "draw together" and from separate drops. It can be concluded, from the method of carrying out the test, that the value it gives, γ_w for the critical surface tension for wetting, is close to that for a receding liquid drop. Placing a liquid drop on a surface and measuring the contact angle gives a value for the critical surface tension for wetting that corresponds to that for an advancing drop of liquid. The method used for obtaining the contact angles for water drops on the polyethylene surfaces was as follows. A 1 microlitre drop of water was placed on the surface and allowed to equilibrate for about 30 seconds. A photograph was then taken from the side and the contact angle was then either measured directly, from a print, using a protractor or indirectly from the height of the drop and its radius of contact on the surface. From these two measurements the contact angle ϕ is given by

$$\tan \phi/2 = \frac{h}{R}$$

where h is the height of the drop and R is its radius on the surface (see appendix 4).

The critical surface tension for wetting can then be obtained from the contact angle $\emptyset$ by means of the empirical equation of Kim, Evans and Goring[184]

$$\gamma_{C\emptyset} = A + B \cos \emptyset$$

For water A has the value of 32 mN m^{-1} and B has the value 21 mN m^{-1}.

c) Results and Discussion

When the results of both LDPE and HDPE, Tables 5.2.1 and .3, are compared it is seen that for comparable corona treatment times, that both types of polyethylene reach similar values of critical surface tensions for wetting. The limiting value appears to be of the order of 50 mN m^{-1}. Also the difference between γ_{CW} and $\gamma_{C\emptyset}$ is only small with $\gamma_{C\emptyset}$ tending to be smaller than γ_{CW}. The value of the critical surface tension for wetting rises very rapidly with treatment time and after a very short time, of the order of 1 second there is very little change and after 3 seconds virtually no change. This initial rapid increase in wettability during corona treatment has also been observed by Leclercq and co-workers[194] using poly(ethylene terephthalate). They suggest that the increased wettability observed is due to the increase in polar groups formed at the surface of the polymer. The ESCA results given in the tables in Chapter 4 would support the idea of the formation of polar groups. It is important to remember here that spectra recorded at 70^{o} take off

	Corona Time / Sec				
Air \	0.5	1	2	3	50
ϕ	61^{o}	59^{o}	57^{o}	50^{o}	
$\gamma_{C\phi}$	42	43	44	45	
γ_{CW}	39	46	47	49	48
Nitrogen					
γ_{CW}	40	42	46	48	48
Oxygen					
γ_{CW}	48	48	48	48	
Argon					
γ_{CW}	41	42	44	46	50

Critical Surface Tensions for Wetting, γ_C/mN m^{-1}, for LDPE after Corona Treatment in various gases

Table 5.2.1

Corona Time/Sec	Heating Time / Sec					
	0	10	15	20	25	40
0.75	43	40	38	38	38	40
1.75	45	40	40	40	40	40
2.5	47	45	43	42	40	42
3	48	46	45	43	40	42

Critical Surface Tensions for Wetting, γ_{CW} /mN m^{-1}

Effect of Heating at 80°C on Critical Surface Tension for Wetting of LDPE after Corona Treatment in Air

Table 5.2.2

	Corona Time / Sec			
Air \	0	0.25	0.5	0.75
ø	91	66	61	56
$\gamma_{C\emptyset}$	32	41	42	44
γ_{CW}	32			

	Corona Time / Sec			
Air \	1	3	7	15
$\gamma_{C\emptyset}$	45	46	46	48
γ_{CW}	45	45	43	50
Nitrogen				
$\gamma_{C\emptyset}$	43	49	49	49
Oxygen				
$\gamma_{C\emptyset}$	47	48	49	50
Argon				
$\gamma_{C\emptyset}$	50	48	47	46

Critical Surface Tensions for Wetting, $\gamma_{C\emptyset}$,/mN m^{-1} for HDPE after Corona Treatment in different gases

Table 5.2.3

HDPE subject to DC discharge for 5 minutes, 2 mm gap

Upper Electrode Voltage + 12 kV γ_{CW} 33 mN m^{-1}

+ 25 kV γ_{CW} 38 mN m^{-1}

- 25 kV γ_{CW} 38 mN m^{-1}

Table 5.2.4

correspond to the actual surface of the polymer, but still contain some electrons sampled from subsurface layers. The Tables in Chapter 4.3 do show that especially for LDPE the outer layer, as revealed by the 70° take off spectra does rapidly acquire polar groups and that this takes place within about 1 second and is virtually complete within 3 seconds. The oxygen corona experiments are the simplest to explain since for both LDPE and HDPE γ_c reaches its final value very rapidly and this corresponds to the composition of the outer layer as revealed by ESCA. For HDPE and gases other than oxygen, the ESCA studies show that polar groups are produced and that after an initial rapid rise the formation then takes place more slowly. This corresponds quite well with the results of γ_c in Table 5.2.3 which show an initial rapid rise and then only a small increase to the final value observed. The results, for corona treatment in argon of HDPE, of $\gamma_{c\emptyset}$ are somewhat anomalous since they actually decrease with treatment time. The ESCA results, Table 4.3.17 do show some strange variations, though, which might explain this to some extent. Thus the O_{1s} 534.3 eV 70° take off peak does decrease and so do the 535.5 and 535.5 eV peaks. These peaks all correspond to possible polar groups, carboxy, hydroxyl and carboryl, and carbonate. There is possibly therefore a small reduction, after an initial oxidation has bound up absorbed oxygen and water vapour, in the oxygen functionality representing polar groups.

This could explain the slight reduction observed in the critical surface tension for wetting.

In the case of nitrogen the polyethylene takes longer to reach its critical surface tension for wetting and this is matched by a longer time for the oxygen functionality to reach its maximum value. The oxygen functionality arises from impurities in the nitrogen, due to the construction of the apparatus, leaks and unswept areas, from absorbed oxygen and water vapour on the polyethylene, and from the fact the nitrogen was not purified. It is difficult to estimate the effect on wettability of the nitrogen functionality, that is for amine groups, though it is known that these are polar and absorb anionic dye materials[175]. Since the peak area for the nitrogen at 400 eV is substantial, Table 4.3.14 and 15, it is reasonable to assume that the nitrogen functionality does have some effect.

It is not possible in the ESCA data obtained to pick out any particular peaks that would correlate exactly with the observed changes in the wettabilities. This is probably partly due to the deconvolution process which assumes particular binding energies for functional groups. This does not allow for secondary shifts nor for the fact that in the O_{1s} spectra a deconvolution peak may include more than one type of group. The O_{1s} 533.5 eV peak, for example, includes carbonyl, hydroxyl, ether and peroxide and it is not possible to decide the amount of each that is present.

The formation of carbonyl groups and hydroxyl groups on the surface of the polyethylene is also shown in the MIR IR spectra, which have been reproduced in Chapter 4.4. The carbonyl group shows as a broad peak at 1715 cm^{-1} and the hydroxyl group as a broad peak at approximately 3400 cm^{-1}. This broadening of the hydroxyl peak, as discussed previously (Chapter 4.4) may be due to hydrogen bonding with other groups which may be other hydroxyl groups but could also include peroxides, amines and carbonyl groups.

Leclercq and co-workers[150] were able to show the presence of polar groups by the absorption of radioactive calcium ions. It should be noted here that this assumes that all the polar groups are negative in character and also acidic. There is though a distinct possibility that some of the polar groups will be positive in character, possibly amines[174]. If the polar groups on the surface will absorb calcium ions then it may well be assumed that they will absorb other positive ions. This was shown in Chapter 4.5 where it was seen that potassium ions were absorbed by corona treated polyethylene in approximately quantitative amounts corresponding to carboxylate groups. It was noted in those experiments that very little negative ion (iodide) absorption took place which agreed with the ESCA data that showed there to be very little amine functionality to be present. ESCA absorption experiments were not carried out for nitrogen corona

treated polyethylene, which was shown in Chapter 4.3c to possess nitrogen functionality in the form of amine and amide groups. This matter of the formation of polar groups and their detection by ESCA absorption experiments is one that might merit further investigation. Due to the fact that the absorption takes place in a surface layer rather than at the surface it is not possible, from the absorption experiments, to calculate the number of polar sites per unit area of the surface. Calibration of the ESCA data would be a problem since the depth of corona treatment is greater than the ESCA sampling depth. Thus active sites below the ESCA sampling depth would not be recorded using ESCA but might well be recorded if radioactive tracers were used.

The presence of polar groups, on corona treated polyethylene, has been deduced by Carley and Kitze[196] who examined the contact angles of different liquids on the surface of treated polyethylene. They were then able to calculate the dispersion and polar components of the surface energy of the polyethylene. These results showed that the polar component increased in magnitude quite considerably while the dispersion component tended to decrease.

The fact that the ASTM wipe test, γ_{CW}, and the contact angle method, $\gamma_{C\emptyset}$, results, Tables 5.2.1 and .3, are very similar suggest that the surface composition is reasonably uniform and that the surface roughness produced is not

important. The surface morphology of polyethylene is known to change when it is subjected to corona treatment and the surface has been shown to be roughened[197]. It is possible that the changes in morphology, though clearly present, are too smooth to affect the wettability.

There is a possibility that there is some change in the crystallinity of the surface of the polyethylene sample. Schonhorn and Ryan[198] have shown that an increase in the crystallinity of polyethylene will produce an increase in the critical surface tension for wetting. They give the value of γ_c for polyethylene as $35.4 \leqslant \gamma_c \leqslant 66.1$ mN m^{-1} depending on the degree of crystallinity. Some calculations on γ_D and γ_P have also been carried out by Kaelble[185] on the results of Schonhorn and Ryan for polytetrafluoroethylene nucleated on a gold surface. He found that γ_S was 45.6 mN m^{-1} instead of 15.5 mN m^{-1} and that this was caused by γ_D = 36.3 and γ_P = 9.3 mN m^{-1} instead of γ_D = 14.5 and γ_P = 1.0 mN m^{-1} for normal PTFE. It has been suggested that during corona treatment material is removed from the surface of the polyethylene. Since the outer layer tends to be amorphous, while the subsurface is more crystalline this would result in an increase in the crystallinity of the surface and so cause an increase in the wettability. However, in that case LDPE would require longer treatment times since its surface amorphous region is thicker than that of HDPE and would take longer to remove. The results show that this is not

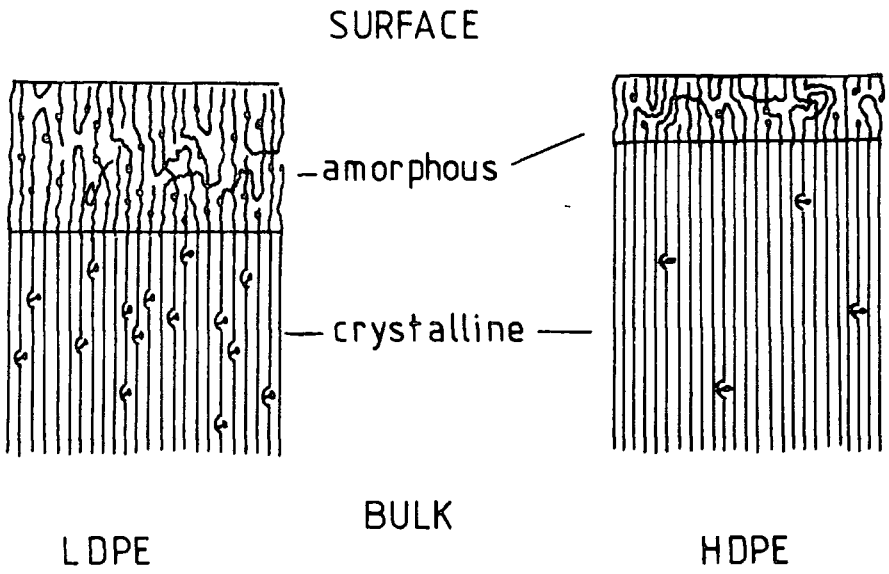

Surface and Sub-surface Features of LDPE and HDPE (ref 199)

Figure 5 2.3

the case and so it is concluded that changes in crystallinity and morphology are not responsible for the increased wettability.

The formation of electrets may be partly responsible for the increase in wettability. This idea has in fact been suggested by Kim and co-workers[184] to explain increases in autoadhesion of polyethylene after corona treatment. As will be seen in section .4 of this Chapter quite deep-seated negative charges are produced during corona treatment. These could give a similar effect to polar groups and here it is interesting to note that when subject to a DC discharge a slight increase in wettability, γ_{CW}, was observed. After the DC discharge the polyethylene was found to be electrically charged but the oxygen functionality was virtually unaltered (see Table 4.3.6).

This particular line of enquiry, though perhaps of interest to manufacturers of electret materials, was not pursued as it was regarded as diverging too far from the main body of the work.

When samples of polyethylene were heated, Table 5.2.2, it was found that the critical surface tension for wetting fell, but not to the original value for untreated polyethylene. This can be explained by assuming that some polar groups are lost by volatilisation of low molecular mass material and also by turning in of polar sections of the polyethylene chain. A corresponding reduction in carbon and oxygen functionality is also observed by the reductions in the C_{1s} and O_{1s} ESCA spectra when corona treated polyethylene is heated, Table 4.3.7. It is seen that after a short period of heating, of the order of a few minutes, the carbon and oxygen functional groups reach a lower limiting value. There are large reductions in the oxygen peaks which are associated with polar groups and with most of the carbon peaks. The carbon peak at 286.6 eV is however not greatly reduced and this may be as a result of the decomposition of hydroperoxides (O_{1s} 534.3 eV) which may then form ether links. This idea is suggested by the rather low value of the O_{1s} 533.5 eV peak which is not large enough to be caused by hydroxyl groups, C_{1s} 286.6 eV, but would correspond closer to ether groups.

Washing the polyethylene in organic solvents, such as chloroform, alcohol and acetone and washing with aqueous

detergent had no apparent effect on the wettability of the surface.

The results obtained above suggest that the increased wettability of polyethylene subjected to corona discharge is largely the result of oxidation of the surface forming polar groups with some smaller contribution from the surface charge. The importance of polar groups has been suggested by many other workers. Baszkin and Saraga[200] measured the thermodynamic free energy of adhesion W_A and the density of polar groups for chemically oxidised polyethylene. They were able to correlate the two and to show that it was the polar component of the free energy, γ_p, that had increased while the dispersion component γ_D was very little changed. They also found that W_A and γ_p increased rapidly at first and then rose more slowly to their maximum values. Briggs and co-workers[201], using corona treatment on polyethylene found similar correlations between the contact angle for water drops on the surface and the time of treatment. They found using ESCA and MIR IR that the surface oxidation of polyethylene increased with time and that much of this increase came from groups that had polar characteristics, that is hydroxyl, carbonyl and carboxylic acid functions. In addition they tried the effect of corona treatment in other gases and found that there was usually an increase in the oxygen functionality and an increase in the wettability. When using hydrogen, however, they found that

there was virtually no change in contact angle upon treatment compared to the untreated polyethylene and this was matched by virtually no increase in the oxygen functionality. Rather similar results were obtained by Kim, Evans and Goring[184] who carried out corona treatment in different gases including hydrogen. They suggest that the increased wettability may be linked with increased surface oxidation and compare the results with the effect of treating the surface of polyethylene with ozone.

.3 Adhesion

a) Theory [202-5]

When an adhesive bond is made between two materials, two surfaces are destroyed and an interface is made. If only polar and dispersive forces are involved then the decrease in free energy is the work of adhesion, W_A. For a liquid on a surface this latter quantity has been defined[202] by Dupre as

$$W_A = \gamma_S + \gamma_{SV} - \gamma_{SL} \qquad 5.3.1$$

where γ_S is the surface energy of the solid and γ_{SV} and γ_{SL} are the surface energies of the two interfaces. In the case of an adhesive joint involving two solids, the adhesive and the material being joined, this becomes

$$W_A = \gamma_a + \gamma_b - \gamma_{ab} \qquad 5.3.2$$

where γ_a, γ_b and γ_{ab} are the surface and interface energies of the two solids.

It can be shown[206] that

$$\gamma_{ab} = \gamma_a + \gamma_b - 2(\gamma_{Da}\,\gamma_{Db})^{\frac{1}{2}} - 2(\gamma_{Pa}\,\gamma_{Pb})^{\frac{1}{2}} \qquad 5.3.3$$

where D and P refer to the dispersion and polar components of the surface energies, and equation 5.3.2 then becomes

$$W_A = 2(\gamma_{Da}\,\gamma_{Db})^{\frac{1}{2}} + 2(\gamma_{Pa}\,\gamma_{Pb})^{\frac{1}{2}} \qquad 5.3.4$$

(Though this has been disputed by some workers[205]). Therefore the work of adhesion W_A is the result of the interactions of the polar and dispersive components of the surface energies. The intrinsic failure energy Θ_o may be defined as the energy to break unit area of atomic bonds across the fracture plane. If only polar and dispersive forces are involved then Θ_o should correspond very closely to W_A and this is in fact what has been observed by Andrews and King[202]. In cases where chemical bonding between the two surfaces can occur, or where entropy can increase by inter-diffusion at the interface, then the decrease in free energy and Θ_o will be much larger than W_A. This has in fact been observed[202] for a number of polymers subjected to surface treatment when the intrinsic failure energy may be more than an order of magnitude greater than W_A. Furthermore, in cases where $\Theta_o \approx W_A$ it was possible to show that failure was interfacial while where $\Theta_o \gg W_A$ the failure was found to be partly cohesive either in the substrate or in the adhesive.

When chemical bonding is involved it may be covalent, for example

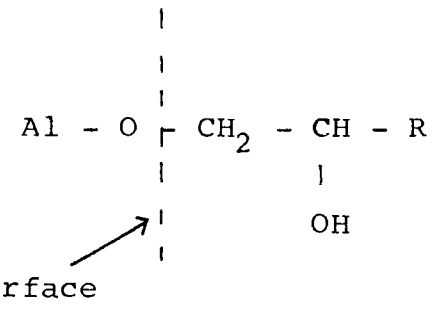

or it may arise as a result of ionic attractions. Included in this latter is the possibility of electric charge attraction which has been suggested on several occasions[176,188,205]. The injection of charge into the surface of polyethylene during corona discharge treatment, is well established and will be dealt with in greater detail in section .4 of this chapter below. Hydrogen bonds should probably be considered here as a form of chemical bonding though they are formally polar forces. Their much greater magnitude, than normal polar forces, makes it unrealistic to include them as a simple component of γ_p. The possible effects of mechanical "keying", due to surface roughness, should be taken into account when considering adhesion. To some extent this effect may be due to the increase in surface area, which roughening produces[205]. This means that the atomic interactions are operating over a greater area, and thus producing a greater force than that deduced from a smooth surface. Mechanical keying may have some direct effect though and in fact most metal and

other dental fillings stay in tooth cavities because of this keying rather than by adhesion.

b) Lap Shear Test

The adhesive properties of polymers, both before and after surface treatments are often investigated by either lap shear tests or peel tests[205]. Peel tests were not used for the work in this thesis and so will not be discussed further.

The double lap shear test avoids the distortion which is often seen when a simple lap joint is strained (see figure 5.3.2). Due to this distortion failure is not due to pure shear forces but is the result of tensile forces. It was thought that the double lap joint, which avoided this distortion, gave a true shear failure. However, it has been shown that when using this joint with a brittle epoxy adhesive failure occurs by crack propagation from the points of greatest stress[205,207]. These points are the ends of the joint or the fillet of adhesive exuding from the end of the joint. It is also thought that with the same type of adhesive a simple lap joint, even though it distorts, fails by crack propagation starting in the same manner. Therefore, for the lap shear tests described below, simple lap joints were used rather than double lap joints.

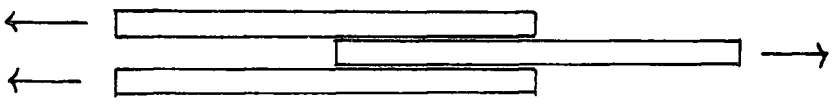

Double Lap Shear

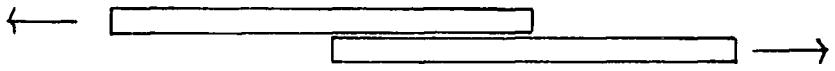

Lap Shear

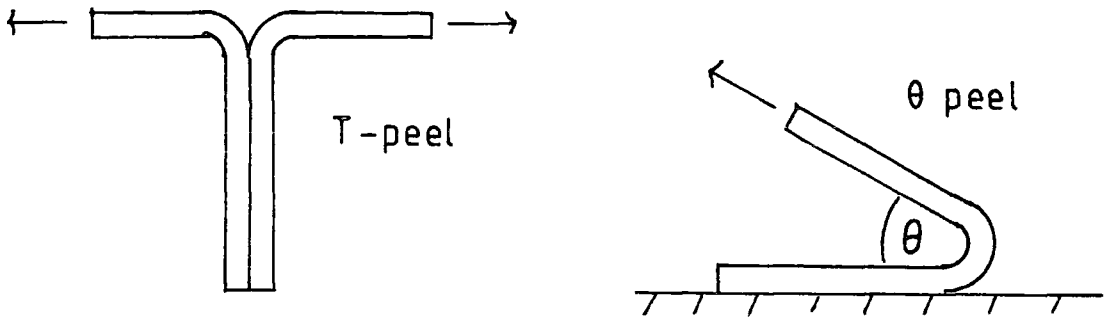

Lap Shear and Peel Tests

Figure 5.3.1

Distortion of Lap Shear Joint

Figure 5 3.2

c) Results

The lap joints were made up as shown in figure 5.3.3. High density polyethylene was used and was treated on both sides by corona discharge in air, using the disc electrodes. The aluminium used was 25 mm wide and 3mm thick,

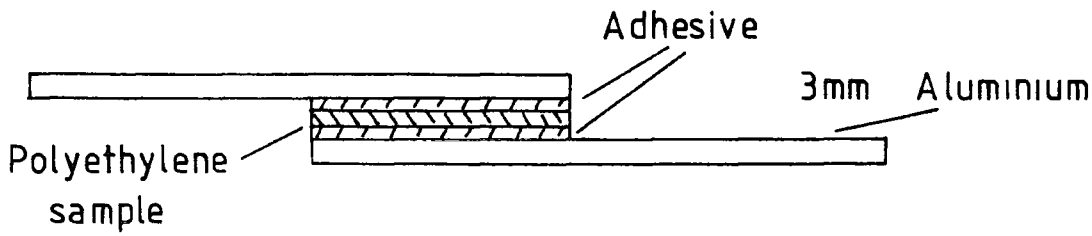

Lap Joint Construction

Figure 5.3 3

this thickness being determined by the need to drill a hole in the end for ease of attachment in the Hounsfield Type W Tensile Strength Testing Machine. When thinner aluminium was used, it was found that the aluminium strip tended to distort round the hole. The length of overlap was approximately 24 mm and this, with the strip width of 25 mm, gives the area of contact as being approximately 6 cm^2. The adhesive used was a standard Araldite adhesive. Details of this as given by the manufacturers CIBA being that it is a bisphenol AV100 which is mixed before use with a polyamide HN100. No other details were released by the manufacturers concerning the composition of the adhesive.

Before making up the lap joints, the aluminium surfaces, where the adhesive was to be spread, were subjected to a surface oxidation process. It has been found that such processes give more consistent results and stronger joints than using the metal without any such treatment[204]. The process used was first to degrease the aluminium strips using boiling 1, 1, 2 - trichloroethane and then, after air drying to immerse the aluminium strips for 30 minutes in a bath containing 350g of sulphuric acid. 50g of flake chromium VI trioxide and water to give a total volume of 1 dm^3. The bath temperature was held between 60° - 70° C and after 30 minutes the aluminium strips were removed, washed well with distilled water and then air dried. Although the British Standard procedure recommends use within a certain time this was not always done as the principal aim was to examine the joints after fracture rather than achieve maximum strength.

The joints were made up in the following fashion. The araldite was mixed according to the manufacturers' instructions and spread on the end of one aluminium strip. A 3cm square of treated polyethylene was placed on top of the adhesive and a second aluminium strip with adhesive placed on top of this. The whole assembly was held in a simple jig while the adhesive set, to produce a test piece as shown in figure 5.3.3. While the adhesive was setting a 2 kg weight was placed on the joint to apply pressure but shims or other devices were not used to control the thickness of the adhesive in the joint.

Nevertheless visual inspection of fracture revealed a reasonably consistent thickness. When the adhesive had set and preferably before it became too hard excess adhesive and polyethylene were trimmed from the joint leaving the area of contact, as already stated, as $6cm^2$.

When the adhesive had fully hardened, that is after a time interval of approximately 24 hours the test specimens were tested to destruction on a Hounsfield Tensile Strength tester. All samples were tested at the same strain rate, which was 0.16 cm $minute^{-1}$ and all the failures appeared to be by fracture cleavage.

The results of the experiments are given in Table 5.3.1 which includes the ESCA results for the cleaved surfaces. For each separate corona treatment time 5 test pieces were prepared and broken and the ultimate "shear" strength at fracture given as the average value. In view of the limited number of tests, which show considerable variation, of the order of $\pm$ 15%, a statistical treatment of the results was not attempted. Typical results of the tests are shown in figure 5.3.4. Normally only one test piece was subjected to ESCA. MIR IR spectra were attempted, using the method given in Chapter 4.4, but due to poor contact the spectra were very weak.

The results in Table 5.3.1 show that the shear strength, for the corona times and power inputs used, varies very little and also the shear strengths for the composites is not much less than that for an araldite/ aluminium lap shear joint. This more or less constant

Relative Area Ratios after Joint Failure

	C_{1s}				N_{1s}			O_{1s}					Shear strength
	286.6	287.8	289.2	290.3	402	400.5	399	531	531.8	532.7	533.5	534.3	MN m^{-2}
Araldite on	12	8	2			13.2	24	13.2	7.8	4.8			
Al foil	24	4.5	0			41	16.8	2.2	8	4.2	1.8	1.2	
I	42	8	0.8		1.1	2.6	2.9	0	2	16	9	12	
Araldite/Al Lap Shear	26	5	0		0	2.8	2.8	3.2	4.2	12	6.8	3.8	4.8
II	36	11	1.5	1.2	2	4.6	7	6	18	28	24	14	
	31	7	2	0	0	2.4	3.2	6	16	27	15	8	
HDPE	6.2	1.0	0.2							0.7	0.1	0.6	
(No Treatment)	7	1.8	0.2							1.2	0.2	1.4	0.5
Araldite	14	6	0.2			1	8.2	3	7.2	8.4	4.2	2.4	
	15.2	4.4	1.0			2.4	6.4	3.2	7.8	9.2	2	2	
	42	5.0	2.4	1.2	0.3	3.3	0.8		5.6	10.8	14.4	3.0	
HDPE	40	5.2	4.4	2.4	0.2	2	0		0.1	12	20	20.7	3.7
1 sec Araldite	12	2.4	0.5		0.5	1.0	1.8	0.6	6	7	4.4	3	
	12	2.4	0.5		0.2	2	1.2	0.6	6.8	7	2.4	1.6	

Araldite/Polyethylene Lap Shear Tests

Table 5.3.1

	C_{1s}				N_{1s}			O_{1s}					MN m^{-2}
	286.6	287.8	289.2	290.3	402	400.5	399	531	531.8	532.7	533.5	534.5	
HDPE	38	10.4	1.6		0	3.7	8.6		16	9	9	6	
(3 sec)	26	6.0	1.0		0.6	5	5		15	6.6	4.8	3.6	3.2
Araldite	38	6	1		0	5.2	3.6		30	38	8	6	
	18	7	2		0.8	3.6	4.8		20	24	7	5	
HDPE	3.0	1 0			0.2	0.2	1.6		2	4.32	1.2	0.66	
(7 sec)	10 2	1 8				0.6	1.4		9	4	3.4	0.8	3.7
Araldite	7.4	1 6	0.3			0.5	1.7		3.3	4.5	0 9	0 6	
	5	1 6	0.3			0.6	1.5		3.2	6.8	0.6	1.0	
HDPE	41	13	1.3		1.6	3	5		11	5	30	8.7	
(7 sec)	36	13	1.3		1.2	3	4		10	6	33	10	3.3
Araldite	36	10	1.1		1.2	1.8	3.6		9	7	28	12	
	31	8	1.2		1	0.9	3.6		13	13	19	7	
HDPE	8	1.8	0.1		0.2	0.2	0.6	0	3	3	4	1.8	
(15 sec)	9	2	0		0	0	0	4	4.4	2.6	1.5	1.2	4.0
Araldite	14	3	0.5		0.4	0.7	2.7		7	6	4	2	
	9	3.1	0.4		0.4	0.7	2.4		7	6	4	1.2	

Table 5.3.1 cont.

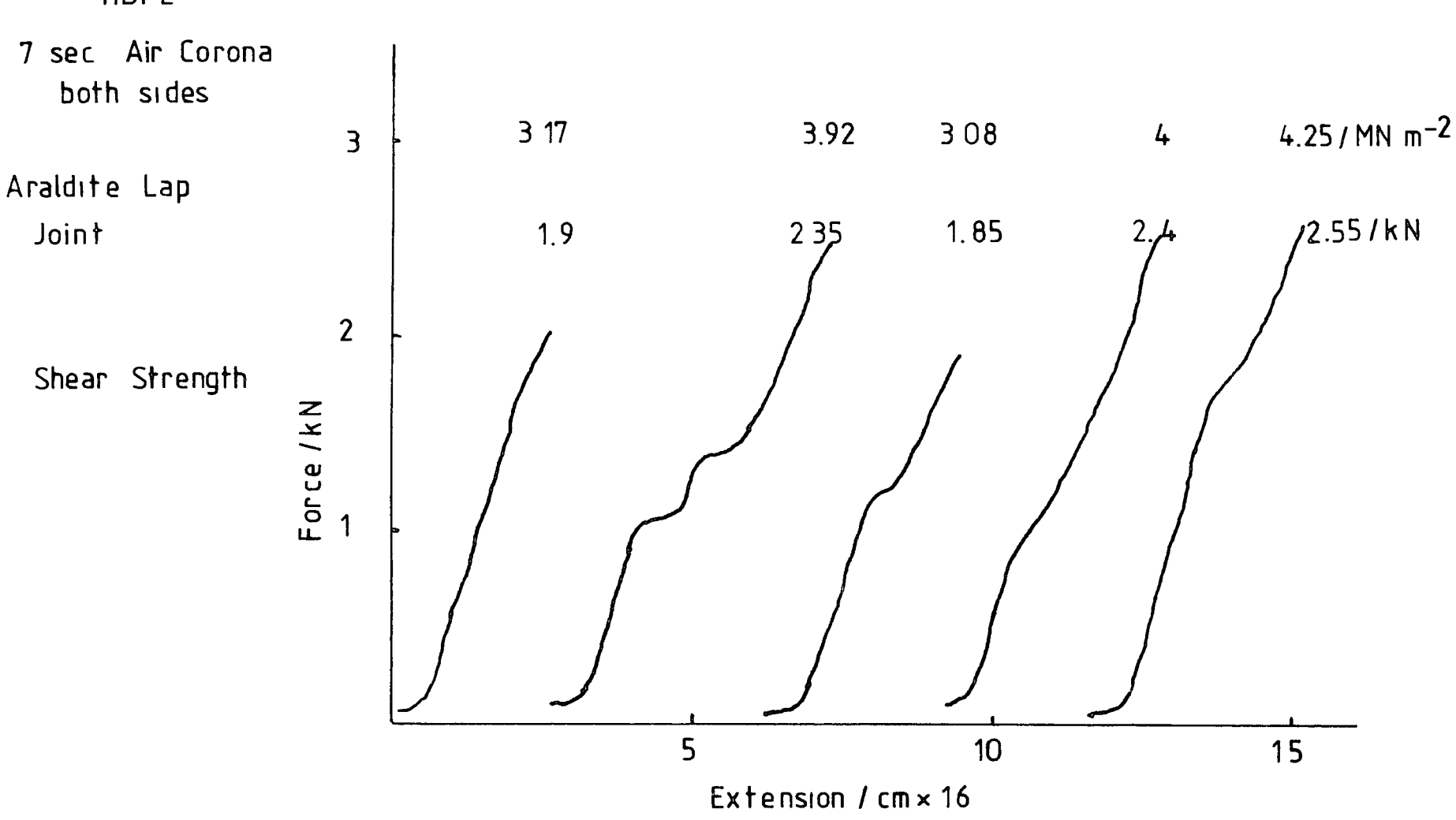
HDPE
7 sec Air Corona
both sides
Araldite Lap
Joint
Shear Strength
3 17
3.92
3 08
4
4.25 / MN m^{-2}
1.9
2 35
1.85
2.4
2.55 / kN
Force / kN
3
2
1
5
10
15
Extension / cm × 16

Figure 5.3.4

value for the shear strength does not fit the simple idea that it is surface oxidation that is responsible for the increase in shear strength compared to untreated polyethylene. On this basis increased oxidation should give increased adhesive strength and Table 4.3.5 shows that increased corona treatment time results in a higher level of oxidation. However, as was stated in Chapter 4, increased oxidation may be at the expense of increased chain scission and much of the increased oxidation may be contained in low molecular mass compounds. These would only be weakly attached to the surface and might diffuse into the adhesive (see Chapter 4.5 and the effects of soaking in acetone). The result then might be a more constant level of oxidation at the surface, which would not change with time and might be expected to give a more or less constant shear strength. This "levelling off" of the adhesive strength has been reported by Briggs and Brewis[208] who noted that after reaching a maximum adhesion of polyethylene did not increase even though oxidation levels might do so. Below this maximum adhesion level it does appear[196] that adhesion does increase with time of corona treatment and therefore with level of oxidation. This increase in adhesion with oxidation of polyethylene has also been observed by Briggs and co-workers[209] when examining the adhesion of polyethylene extruded as a melt onto aluminium. Their lap shear strengths are also comparable to those observed in the aluminium-araldite-polyethylene lap joints used in the work for this thesis.

The ESCA results in Table 5.3.1 enable conclusions to be drawn as to whether the failure is entirely interfacial or whether failure is partly cohesive in character. First a sample of araldite was prepared by spreading on aluminium foil. This foil was taken straight off a roll and would have a surface contamination of hydrocarbon from the rolling process of its manufacture. Then the various lap joints were made and the ESCA spectra measured after carrying out the strength test. It was found that the lap joint made using untreated polyethylene gave results that resembled very closely the spectra for untreated polyethylene, Table 4.3.5, and the araldite spread on aluminium foil. It can therefore be concluded that this failure was purely interfacial, the failure crack separating the two surfaces. The shear strengths of these test pieces were also very weak, an order of magnitude less than the others and they tended to break under zero load if twisted or knocked. The araldite lap shear test pieces were surprisingly different from the simple araldite surface and this may be caused by "turning-in" of polar groups which would give a lower surface energy for the spread araldite. This would cause the level of oxidation as recorded to be lower than that of the araldite lap shear test pieces and this is in fact what is observed. The oxygen 1s spectra were deconvoluted by using peaks set at 534.3, 533.5 and 532.7 eV[167] and in addition two peaks at 531.8 and 531 eV. The first of

these two latter peaks will probably correspond to amide features[210], or oxygen bound to carbon associated with nitrogen. The last, at 531 eV, cannot be readily assigned to a functional group but since it is not always present it may be an artificial effect arising from the method of deconvolution.

The ESCA results for corona treated polyethylene araldite lap joints all show that failure is not simply interfacial but is at least in part cohesive. Furthermore, the cohesive failure would seem to be largely in the araldite rather than in the polyethylene. Thus the C_{1s}, N_{1s} and O_{1s} spectra all resemble the araldite spectra, either for simple spreading or for lap shear rather than the polyethylene spectra. This is not inevitably true and for some samples, at 7 and 15 seconds corona treatment, the C_{1s} spectra are very similar to that for untreated polyethylene. However, even for these samples the N_{1s} and O_{1s} spectra are more like the araldite spectra. This might of course be due to diffusion of some low molecular mass material into the polyethylene. That the bond between the polyethylene and araldite was strong was also revealed by the fact that it was impossible to tear or peel the polyethylene from the aluminium. This is why the MIR IR spectra were so poor since a piece of aluminium had to be cut, with the adhesive-polyethylene adhering and this then used to record the absorption spectra. What can be said of the MIR IR spectra is that, like the ESCA spectra,

they showed that failure was at least partly cohesive and in the araldite rather than in the polyethylene. The failure in the araldite may be explained by the fact that a crack in the polyethylene would tend to become blunted, due to plastic deformation and the stress intensification at the crack tip would then become reduced. Within the araldite, essentially a three dimensional cross linked epoxy resin, the ability of a crack to be blunted would be substantially less. The stress intensification at the crack tip would not be reduced and so the crack could propagate within the adhesive. Near the interface plastic deformation could also occur and so the crack could not either propagate in or pass through the interface into the polyethylene.

The O_{1s} spectra show considerable difference to that for the original corona treated polyethylene. There is no oxygen functionality at 535.5 eV, corresponding to carbonate or peroxy acid groups though this is clearly evident before the polyethylene is used to make the joint (Table 4.3.5). The O_{1s} peak at 534.3 eV is usually quite evident and would normally be ascribed to either carboxylic or hydroperoxide groups. It would seem unreasonable to suggest that substantial quantities of hydroperoxide remain in the set adhesive but the carbon 1s peak at 289.2 eV is usually insufficient, in most spectra, to account for all the oxygen functionality at 534.3 eV. There is of course the possibility of differential

sample charging brought about by the fracture process[211]. This could result in displacement of some peaks relative to others and may be responsible for some results that do not seem consistent with the general conclusions. For example the O_{1s} spectrum for HDPE with one second of corona treatment shows, at 70^{o} take off, a much higher degree of oxygen functionality at 534.3 eV than the other spectra.

The carbon 1s peak at 286.6 eV is normally associated with carbon singly bound to one oxygen. However, carbon singly bound to nitrogen would also produce a peak near this value and this will account for the fact that the 286.6 eV peak in the C_{1s} spectra is too large just to correspond to the O_{1s} peak at 533.5 eV, even if all the groups are ether groups. There is though a fairly substantial nitrogen functionality, largely present it is assumed as amino groups and these, as stated, will produce a carbon functionality near 286.6 eV.

The nitrogen functionality, for most spectra normally deconvolutes as two peaks at 400.5 and 399 eV, with in some instances a third peak at 402 eV though this latter is usually very small. The N_{1s} peak at 400.5 eV is most likely to be nitrogen singly bound to one carbon while the peak at 399 eV is probably due to amide nitrogen. The effect of the carbonyl group in the amide would be expected to produce a lowering of the N_{1s} binding energy which is in fact what is observed. The amide oxygen 1s

spectra will also be expected to appear at low binding energy and would account for the peak observed at 531.8 eV binding energy.

It has been suggested by Schonhorn and Ryan[213] that the increase in adhesive joint strength on surface treatment of polyethylene arises more from the removal of the weak boundary layer than from other effects. Schonhorn[214] in fact suggests that cross linking on the surface, producing in effect a strong boundary layer by oxidation. For corona treatment of polyethylene it was found, during the work of this thesis, that though surface levels of oxidation increased the joint strength was remarkably constant. Also Briggs and co-workers[201] found that autoadhesion increased rapidly to a maximum before the maximum level of surface oxidation was reached. This would agree partly with the observations of Schornhorn and Ryan[213] if considered with the idea of Kim and Goring[6]. They suggest that during the corona treatment of polyethylene bumps of low molecular mass products accumulate on the surface. These low molecular mass products, it might be argued, are more highly oxidised than the rest of the surface and on spreading the adhesive they would dissolve, leaving the stronger subsurface layer in contact with the adhesive. That low molecular mass products containing high degrees of oxygen functionality are present and can dissolve in solvent was shown in Chapter 4.5. This would also explain the observation that

wettability does not necessarily correlate with adhesive strength. Wettabilities are often measured under conditions which do not permit ready solution of surface material, so highly oxidised and therefore polar products in polyethylene surfaces will not necessarily result in stronger adhesive joints.

However, simple removal of the weak surface layer is probably not the only cause of the increased adhesion observed in corona treated polyethylene. Stradal and Goring[215] have shown that the autoadhesion of LDPE is increased to a greater degree than that of HDPE on corona treatment. Yet presumably LDPE has a thicker weak boundary layer (see section .2a above). They[215], Owens[216] and Briggs and co-workers[201], suggest that ketones that can enolise to give rise to hydrogen bonds are responsible for much of the observed increase in autoadhesion. LDPE with its more highly branched chains would be oxidised to a greater degree and thus its autoadhesion would be increased. This is not the case though since it was shown in Chapter 4.3 that HDPE becomes more highly oxidised than LDPE. It is possible though that chain mobility is important in forming hydrogen bonds and LDPE with its more mobile branches would be able to produce stronger hydrogen bonds as groups could turn to give shorter separation distances. The suggestion of cross linking at the surface[214] was examined by Kim and Goring[6] for corona treated polyethylene. They examined the gel fractions for polyethylene both before and after corona treatment but were unable to find any significant difference.

From this they concluded that cross linking was not an important feature of corona treatment for polyethylene.

.4 Surface Charging

a) Electrical Properties of Polymers

The electrical properties of polymers are of considerable interest to commercial users. Many synthetic polymers are very poor conductors of electricity as far as the bulk is concerned and so it is the ability of the polymer to hold or disperse static charges that is of greatest importance. There are some instances where the ability of a material to hold static charge is desirable for example in xerography and electret manufacture, but in most cases static charge is a nuisance and may even be dangerous[211]. Thus static build up during corona treatment of polymer film may result in poor printing as the ink may spread in a spiky fashion due to electrostatic forces[2]. The build up of charge as a result of friction can give rise to hazards when sparking on discharge to a large metal object occurs. This can produce uncomfortable shocks to people and animals and may in some instances cause fires and explosions due to ignition of flammable materials[210]. Another important effect is the attraction of dust particles to the surface of the polymer which then affect the appearance and frictional properties of the polymer.

It has been suggested by Lewis[212] that the charge induced on a polymer, either by friction or by corona

treatment is initially deposited on the surface or in the surface layer. With time the charge decays either by conduction along the surface or by conduction into the bulk. Due to the very low conductivity of the bulk polymer charge induced in the bulk will have a very low mobility which may be as low as 10^{-10} cm^2 V^{-1} S^{-1}. This means that in effect the charge is trapped very strongly and may take times of the order of years to decay. This of course is the basis of electret materials. Since the surface layers of many materials and polymers are different to the bulk decay of surface charge by conduction along the surface is more feasible. This is made more likely when polar groups are present at the surface, which can attract water molecules and ions thus increasing the surface conductivity.

It is often assumed that the charge induced in the polymer is the result of trapped electrons[217] and that the traps are formed as a result of the absorption of oxygen[218]. This is probably true for negatively charged polymers but some other type of trap would be required for positively charged surfaces and where the charging is carried out in the absence of oxygen. The surface charge is often measured by the technique described by Davies[219] using an electrometer-probe. Using this method Lewis[212] and others [217,218] have examined the movement of electrical charge on polymer surfaces. Lewis[212] has found that at the surface normal breakdown of the surrounding atmosphere has the effect of limiting the surface charge to less

than 10^{-5} C m^{-2}, which corresponds to approximately 60×10^{12} ions m^{-2}. This is small compared to the average surface packing for atoms in a polymer which is approximately 10^{19} m^{-2}. A somewhat simpler technique for measuring surface charge is to use a Faraday cage and to measure the voltage produced when a piece of charged material is dropped in. This gives the average charge for the whole piece of polymer which is quite useful and is the method used to obtain the results in section b below. It does not however give as much detail as the electrometer-probe method and is not very useful for measuring movement and decay of charge.

b) Surface Charging of Polyethylene by Corona Discharge

The measurements were made using a Faraday cage connected to a vibrating reed voltmeter. The actual cage consisted of a stainless steel cylinder as shown in figure 5.4.1 and the voltages were measured by a Keithley 621 Electrometer.

The Faraday cage was supported by a rigid nylon tube so that it was approximately 20 cm away from any nearby objects. When charged by a 9V battery it was not found that there was any appreciable discharge over a period of about 5 minutes. The capacity of the cage and measuring system was found by charging a small condenser (150 pF) by the battery and then connecting this condenser to the Faraday cage. Knowing the voltage of the battery, the capacity of the small condenser and the final voltage

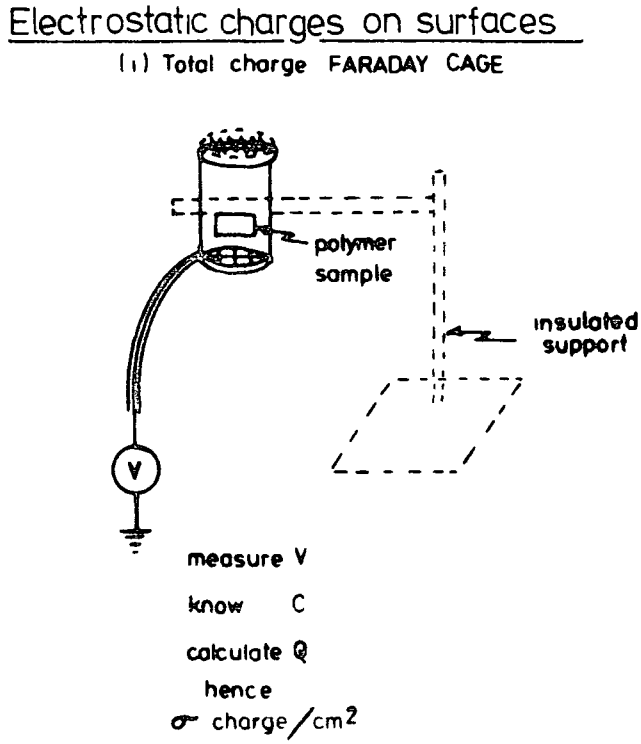

Figure 5 4.1

enables the capacity of the equipment to be obtained from

$$Q = \frac{C}{V}$$

where Q is the charge, C is the capacity and V is the voltage.

This gave the capacity of the equipment as 265 pF and hence by measuring the voltage when pieces of polyethylene were dropped in the charge could be calculated. The pieces of polyethylene were dropped in by cutting a large piece so that a small piece, approximately 1 cm^2

dropped in and thus handling was avoided. The size of the piece was such that it was not thought likely to alter the capacity of the system. It was found that the voltage was not affected by nearby movement unless objects were held closer than 5 cm. The area of the polyethylene sample was found by weighing a larger piece, 10 cm x 10 cm, and also weighing the sample after its charge had been measured. Hence the area could be found and then the charge per m^2 and the equivalent number of ions per m^2 of the surface.

c) Results and Discussion

The results are given in Table 5.4.1 and are for HDPE that has been corona treated in air, nitrogen and argon. The polyethylene was normally found to acquire an overall negative charge, though for short periods of time some samples acquired a positive charge. The results are averages for two values and considerable variations (not shown) were sometimes found; in fact for 1 second in argon and 3 seconds in nitrogen the samples had acquired opposite charges.

At first sight it would appear strange that an alternating discharge should charge the surface of the polyethylene since it might be thought that the charge produced on one half cycle would be neutralized on the other. However the discharge cycle is known to be assymetrical (see Chapter 4) and also there is no certainty that electron and ion avalanches will strike exactly the same area of surface. There will therefore be a

Max. surface effect 10×10^{-6} C m^{-2} and 60×10^{12} ions m^{-2},
surface packing 10^{19} atoms m^{-2}

	Air		Nitrogen		Argon	
	Charge/10^{-6}Cm^{-2}	Ions/10^{12}m^{-2}	Charge/10^{-6}C m^{-2}	Ions/10^{12}m^{-2}	Charge/10^{-6}Cm^{-2}	Ions/10^{12}m^{-2}
As received	- 1.5	9				
Slid in Corona Equipment	- 3	17				
1 sec M	+28	177	+ 22	138	+ 54	337
E	-76	477	0	0	+ 20	125
3 sec M	-41	257	+ 54	523	- 10	64
E	-90	559	+ 34	216	- 3	15
7 sec M	-55	345	- 22	136	- 23	147
E	-78	486	- 86	537	- 5	32
15 sec M	- 2	9	- 15	94	- 45	279
E	-57	357	- 47	294	- 39	241

Surface Charge Effects for Corona Treatment of High Density Polyethylene

M Middle of Discharge, E· Edge of Discharge

Table 5.4.1

resultant accumulation of charge in different areas, some of which may be positive and some negative. These ideas would also explain the observation that the charge, as measured in Table 5.4.1 does not change in a regular fashion with treatment time but sometimes increases and sometimes decreases. An attempt was made, using the Faraday cage, to see if the charge decreased with time. However, each time a measurement is made the charge may be modified or destroyed and the same piece of polyethylene cannot have its charge measured twice. The results were found to be inconclusive and it was decided that the method was too insensitive to give meaningful results in this area. The results in Table 5.4.1 are however in general agreement with the results of other workers[212,220,221,222] who often use DC corona for the charging process. It has been suggested by Lewis[212] and co-workers[222] that exposure to the corona light speeds up the decay of the charge produced and for this reason samples of the polyethylene were cut from the edge of the discharge treatment area as well as the middle. The results were not very conclusive though there does seem to be a tendency for the middle of the treatment area to end up with a slightly lower charge than the edge. Since the middle has the maximum exposure to the electromagnetic radiation of the corona this would agree with Lewis's observations.

From Table 5.4.1 it is possible to compare the level of charge produced with the maximum surface charge that

according to Lewis[212] can be formed before discharge to the atmosphere can occur. It is seen that the charges produced by corona treatment are well in excess of the maximum suggested and in fact may be nearly an order of magnitude greater. This is in good agreement with the suggestion that the charge is held partly on the surface, in shallow traps and also in deep traps[223] below the surface in the subsurface layers. These deep-seated charges, giving rise to electret behaviour, have been suggested[173,176] as being responsible for the autoadhesion of nitrogen corona treated polyethylene and also for the uptake of iodine by such polyethylene. However it should be noted here that the uptake of positive ions by air corona treated polyethylene may be explained in terms of counter ions for the carboxyl groups formed (see Chapter 4.5). It is possible therefore that the iodine is taken up in the form of counter ions for the amine groups that have been shown to be formed in nitrogen corona treated polyethylene (see Chapter 4.3).

It was found that the surface charge was removed by washing with organic solvents. This is not necessarily due to the removal of the trapped charges but could also be due to an effective neutralisation of the surface charge by absorbed ions etc. It was not possible to reach a decision on this from the experimental results but perhaps an examination of electret behaviour could resolve this problem.

.5 Conclusions and Uses of Corona Treatment

Corona treatment of polymer surfaces, in air using alternating supply voltages, has been found to bring about a marked improvement in surface energy and adhesive bond strength. These improvements have been found to be associated with an increase in the polar character of the surface. Using ESCA and to a lesser extent MIR IR it has been shown that the increase in polar character is largely due to an increase in the oxygen functionality of the surface. The polar groups found appear to be principally hydroxyl, carbonyl and carboxyl together with some carbonate and sometimes amine groups. When gases other than air are used the presence of small traces of air, oxygen and oxygen containing molecules, leads to the formation of the same groups but not necessarily in the same proportion. When nitrogen is used a considerable proportion of amine and amide groups are formed. However the surface energies are very similar regardless of the gas used, except for hydrogen where little change is observed[201].

There does not seem to be any simple direct correlation between the increases in surface energy, adhesive bond strength and changes in the oxygen functionality. Except that initially an increase in oxygen functionality is accompanied by increases in surface energy and adhesive bond strength. The oxygen functionality though continues to rise after the surface energy and adhesive character have reached their maximum values. Neither is there a

simple relationship between the surface energy and adhesive bond strength.

The autoadhesion of polymers and the strength of joints made using adhesives, after corona treatment, seem to be caused by different proportions of the same types of forces. Strada and Goring[215] found that autoadhesion in polyethylene fell as sample density increased while Schonhorn and Ryan[213] found that the strength of joints made using adhesives increased as the crystallinity increased. A possible explanation of this is that in autoadhesion hydrogen bonds are important and that in a low density polyethylene the presence of branched chains increased the probability of hydrogen bonds being made. When adhesives are used Schonhorn and Ryan[213] have shown that the presence of weak boundary layers reduces the bond strength. Increasing the crystallinity reduces the thickness of the weak boundary layer and therefore increases the strength of the bond. Increased crystallinity is often accompanied by increased density and so it may appear that increased adhesive bond strength goes with increased density which is the reverse of what is seen for autoadhesion.

When subjected to corona treatment surfaces often became charged and it is possible that this charge affects the surface energy. In fact it is known that excessive charge leads to poor printing[2] and experiments using a DC supply suggest that surface charge does cause an increase in surface energy (see section .2 above).

It would be interesting to know how the surface energy of electret materials changes, if at all, during the poling process.

There have been many patents taken out concerning the use of corona treatment of polymers. These uses are many and varied. For example, there is the British Patent by Dawes and Gupta[225] which deals with the use of corona treatment in making laminated plastics. Some of the uses are more straightforward as, for example, the U.S. Patent by Beatty and Vourlis[226] which simply deals with the corona treatment of polymers to improve their surface adhesive characteristics. During corona treatment manufacturers have often found that the surface charge introduced is a nuisance. This is overcome in the German Republic Patent by Gunther et al[154] by the use of a second corona treatment at a much higher frequency (1 megahertz).

The advantages for manufacturers of the corona treatment process is that it is quick, clean and comparatively cheap. The only chemical used is in fact air and other gases do not normally have any advantage over air. The only main disadvantage and hazard is the ozone produced though this is usually easily disposed of by means of a suitable ventilation system.

Chapter 6

Surface Oxidation by Plasma

.1 Introduction

.2 Experimental

a) Reactor and Sample Details

b) Results

i) ESCA Results using Air Plasma

ii) ESCA Results using Oxygen Plasma

iii) Surface Energy Studies

.3 Discussion

a) Comparison of Air and Oxygen Plasma Treatment

b) Comparison of Corona and Plasma Treatments

.1 Introduction

The use of plasmas, formed by radiofrequency electrical discharges in gases at low pressures, is an important industrial technique for treating polymer surfaces. The process is normally used for small articles[227] though some work has been done on fabrics[228] and also on the continuous treatment of monofilaments and fibres[227].

The process, like corona treatment, is essentially a "clean" one and involves little pretreatment or cleaning up after the operation. It is not as convenient as corona treatment for sheet and film material since it is, as normally operated, a batch process. This results from the normal operating gas pressure, of the order of 1 torr (1 torr is equivalent to a pressure of 1mm of mercury). This requires some form of pressure chamber, in which the objects to be treated can be placed, which can then be evacuated. Continuous treatment processes require either winding mechanisms inside the vacuum chamber[178], or narrow gaps through which a continuous fibre can pass and efficient pumping to maintain the low pressure[229].

Plasma treatment is very convenient for the treatment of small, awkwardly shaped articles especially as the treatment is not merely confined to the outer surface but also includes the inner surface. This can also produce an additional benefit since the treatment can be made to render articles sterile. Apart from plasma treatment the only alternative, albeit an effective one,

for the interior treatment of objects is to use a chemical etching process with the attendant disadvantages of cleaning up after the treatment. Flame treatment of bottle surfaces[2], although less complicated, is not suitable for small, irregular objects and does not treat the inside of containers in a satisfactory manner.

The plasma is excited by either resistive, capacitive or inductive coupling of the radiofrequency generator to the reaction chamber (see Chapter 3.5a). Typical frequencies are of the order of a few megahertz though Wrókel and co-workers[228] have used frequencies in the kilohertz range and lower. The use of low frequencies has the advantage that shielding of personnel is unnecessary and the problem of generator and load impedance matching are reduced. However, at low frequencies resistive coupling must be used, since capacitive and inductive coupling are inefficient at low frequencies. As a result electrodes must be replaced in the reaction chamber and these may become contaminated and cause contamination in turn of articles being treated. Also at low frequencies, down to 50 Hz, there is a possibility that the discharge may resemble the corona process and surface charging may occur. This could be a nuisance and in fact in corona treatment can be a problem (see Chapter 5.4). There is of course the possibility that plasma discharges at radiofrequencies could produce sample charging and this is a matter that could be investigated further. In

connection with this though it may be noted that a German patent by Agfa-Gevaert[154] specifies a discharge at approximately 1 MHz to remove the charge produced on polyethylene by corona treatment at 40 - 60 kHz.

Under the conditions normally used for plasma treatment, a few seconds at power loadings a few watts, pressure ~1 torr, it has been shown by Clark and co-workers[118,159] that the depth of plasma treatment is of the order of a few monolayers from the surface. That is a depth of the order of 10^{-9} metres. The concentration profile is believed to be like that shown in figure 6.1.1.

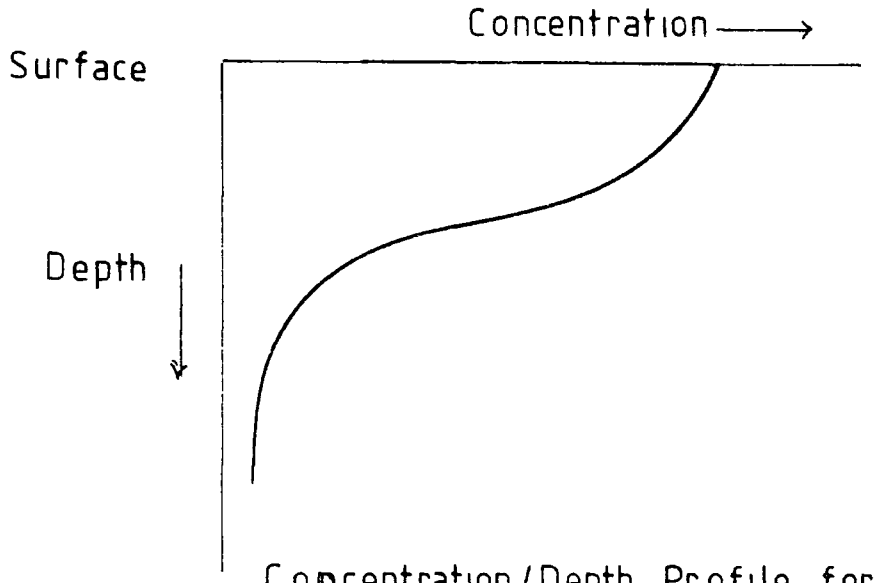

Concentration/Depth Profile for Plasma Treatment

Figure 6 1.1

As in the case of corona treatment the thinness of the treated layer prevents the use of conventional analytical techniques for determining the composition of the surface of the polymer after treatment. Electron microscopy has been used to examine the effect on the surface morphology[228,230] but this of course does not provide information regarding composition. Infra red spectroscopy may be employed and using a system of multiple internal reflection[168,228] it is possible to gain some information. However, in view of the thinness of the modified layer and the much greater depth of penetration of the MIR technique it is often difficult to identify all the changes that occur. They tend to be "swamped" and lost in the general noise compared to the spectral features of the bulk, untreated polymer. It is therefore necessary to use an analytical technique, such as ESCA, if detailed information concerning the changes in the surface layer following plasma treatment is required. The ESCA technique samples the surface to a depth of the order of 10^{-9} - 10^{-8}m (see Chapter 2.6f) and is therefore ideally suited to examining the surface of a polymer after plasma treatment. It also allows the subtle changes that occur when a plasma treated sample is subjected to further treatment processes to be followed[232,233].

.2 Experimental

a) Reactor and Sample Details

The reactor consisted of a pyrex tube, 5cm internal diameter, 30cm long and fitted with ground glass

flanges at each end. This was then "sandwiched" between two further ground glass flanges using 'O' rings as vacuum seals. Samples of polyethylene were introduced, two at a time, as described below, before assembling the apparatus. The whole assembly was pumped by an Edwards EDM 6 direct drive pump preceded by a cold trap. Air or oxygen were leaked in via a needle valve and the pressure in the reactor maintained at 0.2 torr. The air was not dried and the oxygen was not subjected to any purification but was used as supplied by British Oxygen.The temperature of the gases in the reaction vessel, before and after the plasma discharge, was ambient. When oxygen was used the flow of oxygen was maintained for approximately half an hour before initiating the discharge to purge the apparatus and flush out any air.

The discharges were excited by an approximately 4 micro henry copper coil wound coaxially on the pyrex reactor tube. The copper was 0.125 in copper tubing and the coil consisted of 10 turns wound over a distance of 7 cm. The coil was positioned with its centre approximately 7 cm from the gas inlet end of the reactor tube. While the discharge was running it was observed that the glow completely filled the section of the tube contained within the coil and also filled, but not completely the rest of the tube.

The plasma was excited by a Tegal Corporation RF generator, 13.5 M Hz and the power measured by a

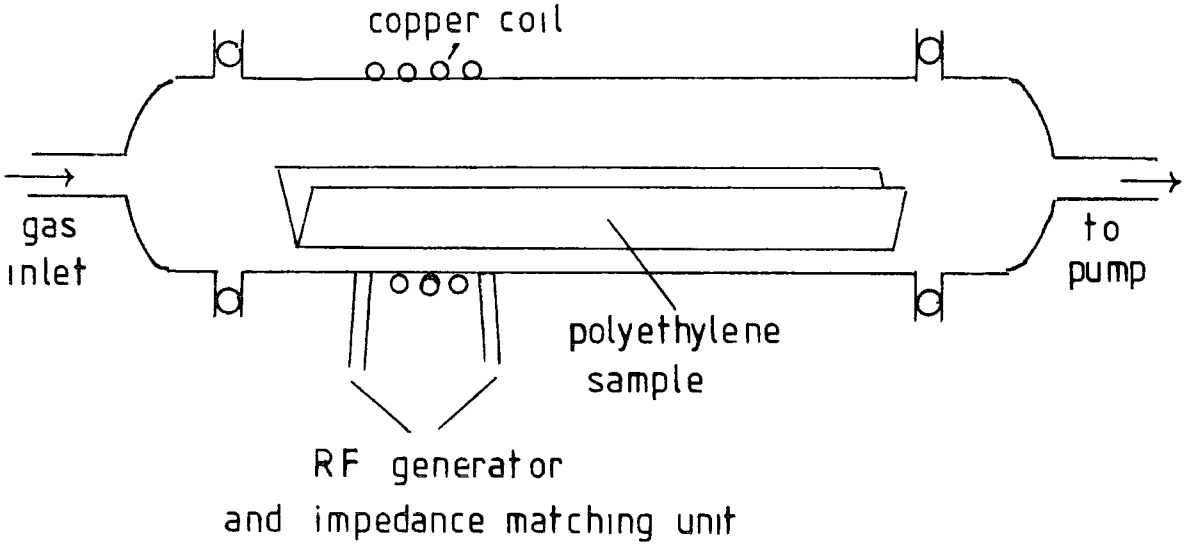

Plasma Discharge Reactor Tube

Figure 6.2 1

Heathkit HM 102 wattmeter. The reactor coil and generator impedances were matched using a Tegal Corporation matching network. This is necessary in order to maximise the transfer of power from the generator to the reactor coil. Failure to ensure at least a reasonable impedance match can also cause damage to the generator from reflected standing waves. The procedure for determining the best match is in fact to minimise the standing wave ratio and in this equipment was done using the impedance matching unit which

had variable controls. The other advantage of matching the impedances of the reactor coil and the RF generator is that the power input to the reactor coil is the same as the power output of the RF generator.

It has been found that the surface of polyethylene may be modified by using quite modest power loadings, of quite short time durations. Using the equipment described above, this was found to be of the order of a watt and the time of the order of a second. For the work described in this chapter, a power input of 0.5 watt for one second was used. At this power level it was sometimes found difficult to initiate and maintain a plasma discharge using a continuous mode for the RF supply. The problem is overcome by using a pulsed supply of higher power and in this instance 10 watt pulses were used and by adjusting the pulse width and frequency an average input of 0.5 W sec^{-1} to the coil round the reactor tube was obtained.

The polymer used in the following experiments was high density polyethylene TFE 554 supplied by the Metal Box Company. The material was relatively free from additives and the levels of antioxidants are as described in Chapter 4.2. The samples were cut from the roll and their sizes were approximately 3 cm by 30 cm and the thickness was 0.1 mm. No pretreatment was used and it was found that the film possessed sufficient rigidity to keep it from contact with the sides of the reactor tube. That is apart from the edges of the strips.

In view of the short treatment time, 1 second, it was necessary to carry out the impedance matching and arrange the power setting without the sample in the reactor tube. The experiment was then repeated with the samples in position, without altering the power settings and switching the power supply on for the one second duration. This method assumes that the presence of the sample has little effect on the impedance of the reactor assembly. In view of the dielectric properties of polyethylene and the volume of the samples this is probably a reasonable assumption.

While the discharge was running it was observed that most of the sample was completely within the glow discharge region except for the part furthest from the coil and nearest the pumping system. As a result of this it was found that both sides of the strip of polyethylene appeared to receive the same intensity of treatment.

After carrying out the plasma treatment, using either air or oxygen, a piece of the polyethylene, from the section within the region of the copper coil, was removed and examined by ESCA. The rest of the section was placed in the oven, held at 75^{o}C and pieces removed for analysis at regular intervals. In addition the samples were examined for wettability using the techniques described in Chapter 5.2. The results of the experiments are presented in the following section.

b) Results

As in Chapter 4.3 the spectra were recorded on

an AEI ES 200 AA/B spectrometer using $Mg_{K\alpha 1,2}$ radiation of energy 1253.7 eV. The same assumptions were made concerning the binding energies of the carbon and oxygen functionalities and spectra were deconvoluted as before[167]. That is using a Dupont 310 curve resolver peaks were set up at 285, 286.6, 287.8, 289.2 and 290.3 eV corresponding to C_{1s} signals from hydrocarbon, singly bonded C - O, doubly bonded C = O, carboxylic carbon and carbonate functions respectively. For the oxygen 1s peak the curve resolver was set up with peaks at 531.8, 532.7, 533.5, 534.3 and 535.5 eV corresponding to amide oxygen, oxygen doubly bonded in carboxyl, oxygen singly bonded in alcohols, ether and peroxide, oxygen singly bonded in acids, esters and hydroperoxides and singly bonded oxygen in carbonate, peroxy acid and peroxy esters respectively. The carbon : oxygen peak ratio for a stoichiometry of one to one was taken as before as

C : O :: 1 : 1.7

No allowance was made for carbon peaks corresponding to carbon in amines and amides. Since however as will be seen the nitrogen functionality introduced is only small this does not produce a serious error in the deconvolution of the carbon peaks.

i) ESCA Results using Air Plasma

As can be seen from figure 6.2.2 the effect of

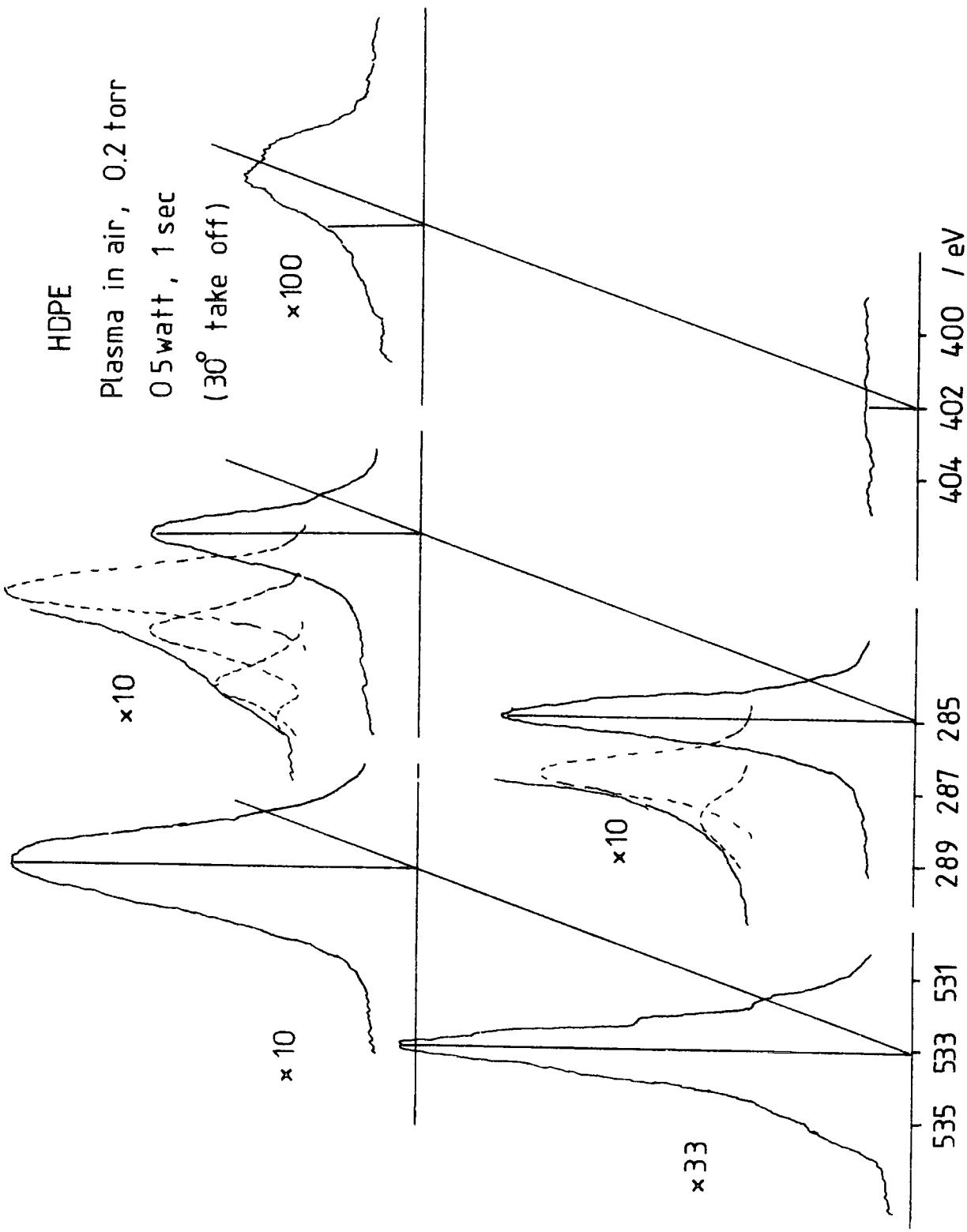
HDPE
Plasma in air, 0.2 torr
0.5watt, 1sec
(30° take off)
×100
×10
×10
×10
×33
535 533 531 289 287 285 404 402 400 / eV

Figure 6.2 2

	Binding Energies /eV												
	C_{1s}				N_{1s}			O_{1s}					
	286.6	287.8	289.2	290.3	402	400.5	399	531.8	532.7	533.5	534.3	535.5	
As received	5.2	1.2	0.02						1.16	0.3	0.16		
	5.2	1.3	0.15						1.14	0.6	0.48		
After Plasma	13.4	6.4	3.8	0.8	0.2	0.58	0.2	0	8	9.6	8	4.4	
Treatment	11.2	6.2	2.4	0.6	0.1	0.64	0.4	1	7.4	8.4	7	1.7	
2 min	13.4	7.2	1.7	0.7	0.36	0.24	0	0	6	7.6	6	1.4	
at 75°C	10	4.2	1.6	0.5	0.04	0.34	0.3	2.3	6	4.4	4	0.8	
5 mins	10.8	4.4	1.6	0.44	0.17	0.6	0.2	2.4	7.6	6.4	4.6	1.7	
	8.3	4.7	1.0	0.3	0	0.72	0.9	4.2	6	3	4.4	0.4	
10 mins	11.6	5	2.6	1.1		0.4	0	0.2	3.4	4.2	10.2	1.8	
	8.6	3.4	1.4	0.2		0.2	0.3	1.8	6	3.2	5	0.6	
15 mins	12	4.6	2.0	0.5	0.2	0.1	0	0.4	3.4	4.6	10.4	2.4	
	8	3.3	1.6	0.2	0	0.3	0.2	1.8	8	3.4	5.2	0.6	
20 mins	9.8	4.4	1.7	0.3		0.1	0	0	5.8	4.6	8.8	1.6	
	8	4	1.4	0.4		0.2	0.2	1.4	6.6	3	5	0.7	
24 hrs	12.6	4.2	2.4	0.3		0.1	0.1	0	10.2	6	10.8	1.6	
	13.2	4	1.4	0.4		0.3	0	1.6	9	6	7.2	0.7	

Area ratios. HDPE Plasma Treatment at 0.2 Torr and 0.5 W in Air for 1 sec

Heat Treatment at 75°C

Table 6.2.1

the plasma treatment is to increase both the nitrogen and oxygen functionalities and also the corresponding carbon ones. The more detailed results, after deconvolution, are given in Table 6.2.1 and from these results some idea concerning the functional groups can be obtained.

The deconvoluted nitrogen peaks suggest that amine, 402 and 400.5 eV, and amide, 399 eV, groups are formed and there is evidence for this latter group in the presence of an oxygen peak at 531.8 eV. The oxygen peaks at 535.5 and 534.3 eV provide some evidence for the existence of peroxy acid functionalities and hydroperoxide group. Taking the 289.2 and 290.3 eV C_{1s} peaks and using the relationship between carbon and oxygen peak areas and stoichiometry as above gives the following area ratios.

Binding Energies / eV					
289.2	290.3	534.3		535.5	
		calc.	obs.	calc.	obs.
3.8	0.8	6.5	8	2.7	4.4
2.4	0.6	4.1	7	2.0	1.7

Calculated and Observed O_{1s} Peak Areas (C_{1s} 285 eV = 100)

Table 6.2.2

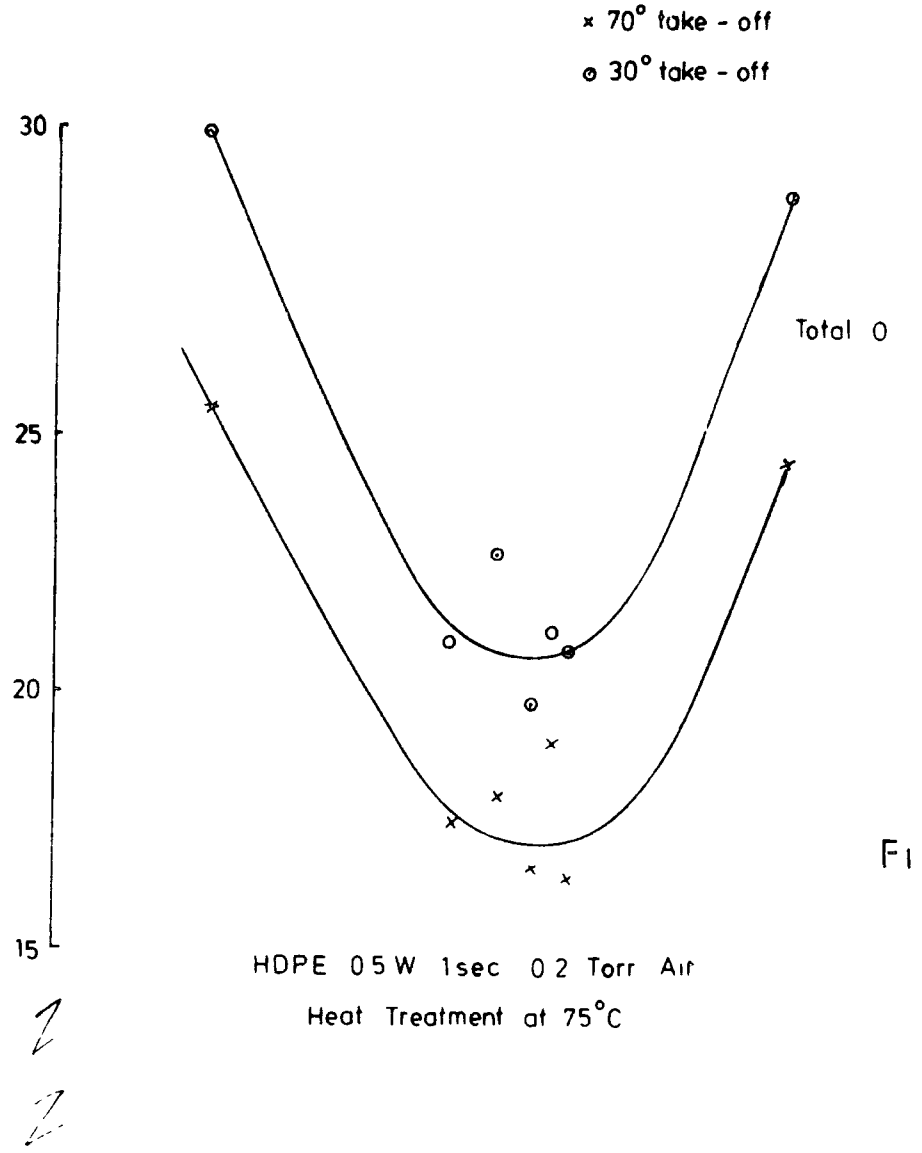
× 70° take - off
⊙ 30° take - off
30
25
20
15
Total O
HDPE 0 5 W 1sec 0 2 Torr Air
Heat Treatment at 75°C

Figure 6.2.3

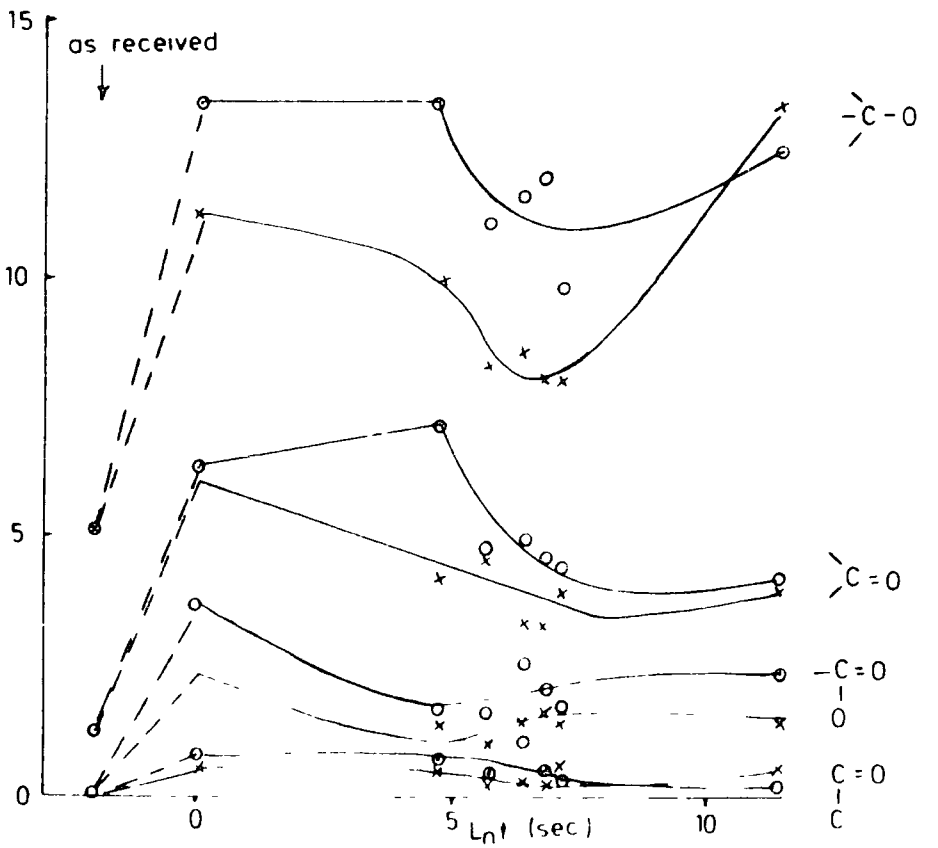
15
10
5
0
as received
-C-O
C=O
-C=O
O
C=O
C
0
5
10
Ln t (sec)

The 70^{o} take off values at 290.3 and 535. eV show that there does not seem to be much peroxy acid functionality in the surface layer. The values at 289.2 and 534.3 eV do suggest though the presence of hydroperoxide groups at the surface. The 30^{o} take off values at 290.3 and 535.5 eV do reveal though the presence of peroxy acid features in the subsurface to the extent that about a third of the 535.5 eV peak is due to peroxy acid features. In view of this the calculated O_{1s} peak at 534.3 eV should be reduced slightly since not all of the carboxyl group, C_{1s} = 289.2 eV, singly bonded oxygen will appear at 534.3 eV. The effect though will not be large but taking it into account it would seem that about a quarter of the O_{1s} peak at 534.3 eV arises from hydroperoxide groups.

It is probably unwise to rely too much on these calculations but the conclusion can be drawn that peroxy acid functional groups are formed in the subsurface layer and are either not formed at the surface or decompose, or rapidly turn inwards from the surface on being formed. Also hydroperoxides are formed both at the surface and in the subsurface layer.

It is not so easy to come to any firm conclusions from the peaks at 286.6, 287.8, 532.7 and 533.5 eV since not enough can be deduced concerning the relative amounts of free acid and hydroxyl groups. This is in fact one of the limitations of ESCA that hydrogen cannot be detected. It does seem though that, after allowing about 1 unit of

the 286.6 eV peak for hydroperoxide carbon, the O_{1s} peaks agree better with the idea of mainly ether links between carbon atoms rather than hydroxyl groups.

The effect of heat treatment is interesting and gives some quite surprising results. In figure 6.2.3 the variation in total oxygen functionality is shown and it is seen that at first the level of oxygen falls and then rises again. The detail in Table 6.2.1 shows that this increase is largely due to O_{1s} at 532.7 and 534.3 eV. These correspond to the O_{1s} signals from carboxylic acid functions yet it is seen that though the final values of these two peaks is eventually the same they do not initially increase at the same rate. Also the C_{1s} 289.2 eV peak is not sufficient to account for all this increase though the C_{1s} peak at 286.6 eV increases and could account for the increase in the O_{1s} 534.3 eV if it is due to hydroperoxide formation.

One possible explanation for the increase in oxygen functionality is that trapped free radicals are formed at the surface and in the subsurface layer. These free radicals could then react with oxygen in the air to produce carbonyl, carboxyl and hydroperoxide groups and the process of heat treatment would be expected to accelerate this process. Yasuda and co-workers[234] have in fact shown that free radicals are produced during plasma treatment. Yasuda[231] has also shown that the polymer produced by plasma discharge in acetylene has a high free

radical concentration, 2.8 x 10^{24} spins m^{-2}, and that these free radicals persist for times of the order of months under ambient conditions. Furthermore, the MIR IR spectrum at first showed no carbonyl stretching absorption but with the passage of time carbonyl features could be detected. The presence of water vapour in the acetylene led , he found, to no free radicals detectable by ESR and also a marked carbonyl absorption in MIR IR which did not change with time. He also found that for plasma polymerised ethylene the use of pulsed RF induced plasma gave a much higher concentration of free radicals than did the use of a continuous RF induced plasma. There would therefore seem to be some justification in assuming that free radicals are formed in the surface layers of the polyethylene during plasma treatment and that when subjected to heat treatment these free radicals react with oxygen in the air to bring about an increase in the oxygen functionality.

The C_{1s} peak at 290.3 eV and the O_{1s} peak at 535.5 eV would suggest that the effect of heating is to remove the peroxy acid features in the subsurface layer and also to reduce the overall carbonate functionality. There may be some turning in of these functional groups since at one point there is a slight increase in the C_{1s} 290.3 eV and the O_{1s} 535.5 eV peaks. The situation is however complex with loss of volatile material occurring at the same time. The amount of hydroperoxide does not initially seem to

change much when the plasma oxidised polyethylene is heated. This is complicated though by a possible increase in the amount of hydroperoxide, as explained above.

The deconvoluted C_{1s} spectra show fairly clearly that during the heat treatment process both loss of low molecular mass material occurs and also that the turning in of polar groups from the surface takes place. The loss of low molecular mass material is shown by the decrease, overall, of the peaks at 287.8, 289.2 and 290.3 eV. The turning in is revealed by the difference between the 70^{o} and 30^{o} take off peaks at 286.6 and 287.8 eV. For the former peak the 30^{o} take off value remains constant initially while the 70^{o} take off peak is falling. This might of course though be thought due to the surface layer losing material before the subsurface layer. In the case of the 289.2 eV peak though the 30^{o} take off peak does actually increase at first while the 70^{o} peak is decreasing which is indicative of a turning in process occurring.

ii) ESCA Results using Oxygen Plasma

As can be seen from figure 6.2.4 the effect of the plasma treatment is to increase the oxygen functionality and also that of the carbon. No nitrogen peaks were observed which indicates that nitrogen functionalities were not formed (from possibly occluded nitrogen), and also no amide oxygen at 531.8 eV was seen. One interesting aspect revealed in figure 6.2.3 is that the overall functionality of the surface layer, as revealed by the 70^{o} take off spectra, is greater than that of the

subsurface layer.

The oxygen peaks at 534.3 and 535.5 eV enable deductions to be made concerning the presence or otherwise of hydroperoxide groups and peroxy acid features. Taking the C_{1s} 290.3 eV peak calculations using

C : 20 :: 1 : 3.4

show that there is probably very little peroxy acid functionality either at the surface or in the subsurface layer. The C_{1s} 290.3 eV and O_{1s} 535.5 eV peaks are both small and in view of the inaccuracies of the deconvolution process it is likely that there is only a small amount of carbonate function and this is sufficient to account for the O_{1s} 535.5 eV peak. The C_{1s} 289.2 eV peak may be used to calculate the expected O_{1s} 534.3 eV peak corresponding to carboxylic acid functions. Comparing this to the observed oxygen peak then enables the presence of hydroperoxide to be decided. These calculations are presented in Table 6.2.4 together with the observed values.

The results of the calculations show that in the subsurface there is initially a high proportion of hydroperoxide since most of the 30^{o} take off signal appears to be due to hydroperoxide. At the surface however there does not seem to be initially such a high proportion of hydroperoxide.

	Binding Energies /eV							
	C_{1s}				O_{1s}			
	286.6	287 8	289.2	290.3	532.7	533.5	534 3	535.5
After Plasma	18	6.0	1.6	0.4	10	4 4	9.4	2 2
Treatment	18	6.6	2.2	0.4	16	6	5	1
Heating	15	5.5	1.4	0.3	5.4	4.8	7 4	1.6
Time 5 min	17	6.4	1.9	0.6	6.6	5	5 6	1
10	14	5	1	0 15	5	4.4	6.6	1.6
	16	6.4	1 8	0.4	7.6	4.2	7	1
15	13	4.4	1	0.15	5.6	4.3	4.4	1
	16	5 8	1.6	0.3	5.2	3	6 6	1
20	13	5	1	0.1	5	4.3	6.2	1
	16	5.6	1.5	0.2	3	3.2	8.2	1.2
25	13	4.6	0.9	0.12	4.8	4.2	6.2	1
	17	5 8	1.6	0.4	4.8	4	7	1.2
24 hrs	11	4.1	0.9	0.02	2.8	3.8	6.8	1.2
	15	5.2	1.5	0.3	3	3	7.8	1.6

Area ratios. HDPE Plasma Treatment at 0.2 Torr and 0.5 W in Oxygen for 1 sec.

Heat Treatment at 75°

Table 6.2.3

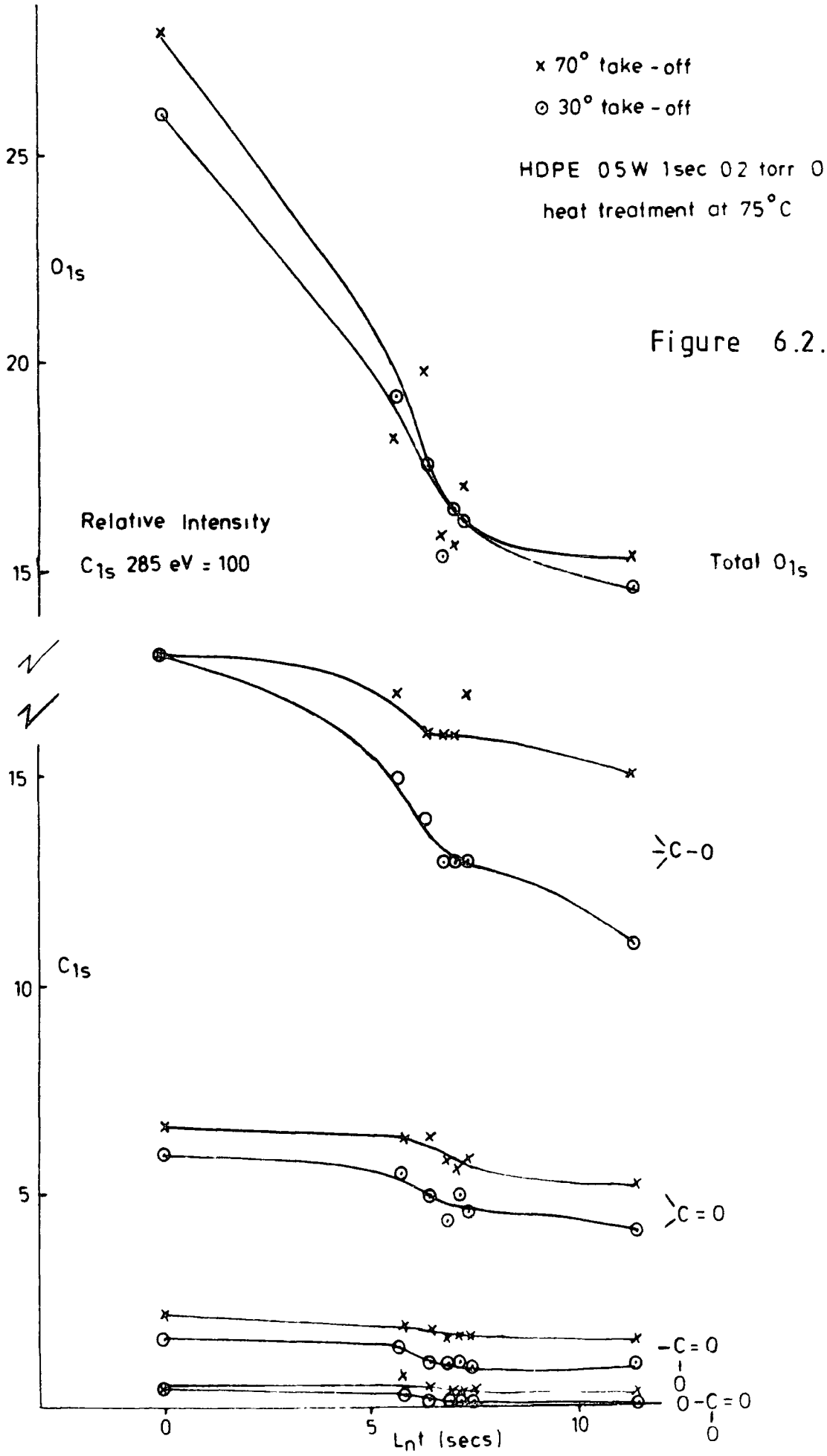
× 70° take - off
⊙ 30° take - off
HDPE 05W 1sec 02 torr O_2
heat treatment at 75°C
25
20
15
O_{1s}
Relative Intensity
C_{1s} 285 eV = 100
Total O_{1s}
15
10
5
C_{1s}
C-O
C=O
-C=O
O
O-C=O
O
0
5
10
Ln t (secs)

Figure 6.2.4

Binding Energies / eV

Treatment	289.2	534.3	
		calc.	obs
Plasma	1.6	2.7	9.4
	2.2	3.7	5
At 75°C for			
5 mins	1.4	2.4	7.4
	1.9	3.2	5.6
10 mins	1	1.7	6.6
	1.8	3.1	7
15 mins	1	1.7	4.4
	1.6	2.7	6.6
20 mins	0.9	1.5	6.2
	1.5	2.6	8.2
25 mins	0.9	1.5	6.2
	1.6	2.7	7
24 hrs	0.9	1.5	6.8
	1.5	2.6	7.8

Calculated and Observed O_{1s} Peak Areas (C_{1s} 285 eV = 100)

Table 6.2.4

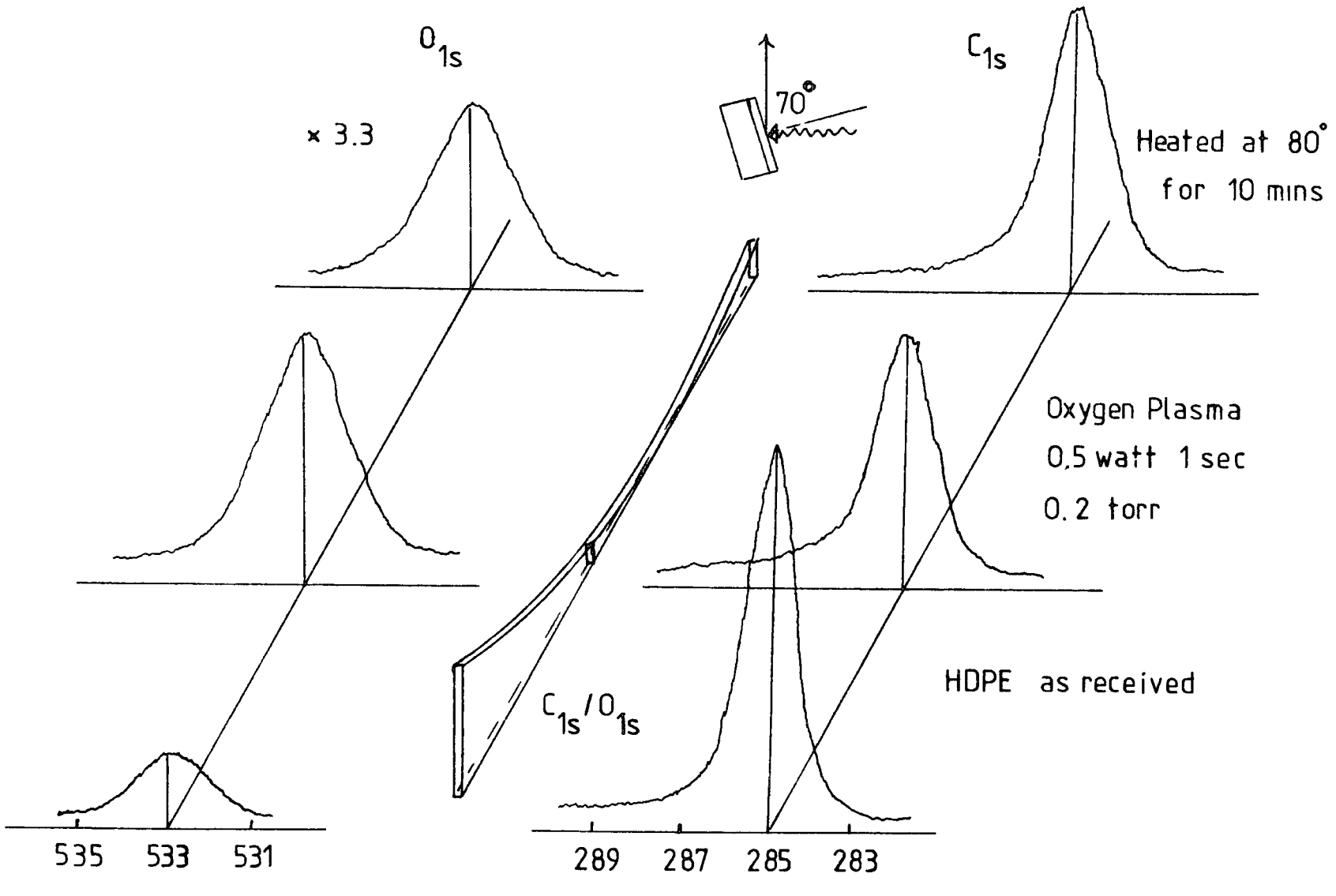
O1s
× 3.3
70°
C1s
Heated at 80°
for 10 mins
Oxygen Plasma
0.5 watt 1 sec
0.2 torr
HDPE as received
C1s/O1s
535
533
531
289
287
285
283

Figure 6.2.5

Again it is not easy to come to any firm conclusions from the peaks at 286.6, 287.8, 532.7 and 533.5 eV. The situation is complicated by the deconvolution procedure and it is possible that some of the recorded O_{1s} 532.7 eV peak is really due to singly bonded oxygen which was assumed to appear at 533.5 eV. This being so it would seem that, after making allowance in the 286.6 eV peak for hydroperoxide carbon, there is very little peroxide bonding between carbon atoms but that there is substantial ether linking.

The effect of heat treatment is much simpler than the case for air plasma treated polyethylene. Figure 6.2.4 and Table 6.2.3 show that there is an overall reduction in all the functional groups and little evidence of oxygen being taken up. Overall the total oxygen functionality falls and this is matched by corresponding decreases in the carbon functionality. The one group that appears not to alter is the hydroperoxide function which seems to remain remarkably constant, as shown by the values of the 534.3 eV peak in tables 6.2.3 and 6.2.4. This lack of oxidation on heating, compared to the case of air plasma treated polyethylene, is in good agreement with the results of Yasuda[231] mentioned above in section 1).

It would seem therefore that the effect of heat treatment is merely to bring about the loss of low molecular mass material and that there is no evidence for the turning in of functional groups or for any oxidation

processes taking place. One aspect not revealed in these studies is the possibility of cross linking taking place between polymer chains at the surface. It is known that this process can occur[214] and has been shown by Clark, Dilks and Shuttleworth[159] to take place for other, similar, polymers when subjected to plasma treatment.

iii) Surface Energy Studies

The critical surface tensions for wetting, γ_c, which may be equated with surface energies (see Chapter 5.2a) were measured by the advancing water drop method, $\gamma_{c\phi}$ and by the ASTM wipe test, γ_{CW}.

The results are presented in Tables 6.2.5 and 6.2.6 and in figure 6.2.7. The general arrangement is also shown schematically in figure 6.2.6. The majority of the results were obtained for the section of the polyethylene sample that lay within the region of the R.F. coil, which is also the section for which the ESCA data is available. Measurements were also made on some LDPE for comparison purposes. In the case of the oxygen plasma ASTM wipe tests were carried out along the whole length of the sample and it is these results that are shown in figure 6.2.6.

As can be seen from Table 6.2.5 the effect of plasma treatment is to raise the surface energy of both LDPE and HDPE to some value exceeding 57 mN m^{-2}, the maximum value of Viskin solution used. This however is using the ASTM wipe test which corresponds to a receding liquid drop

and the advancing drop method gives a much lower value. This difference could be due to an incomplete coverage of the surface or roughening caused by the removal of surface material[230]. Both of these are known to cause the values of $\gamma_{c\phi}$ and γ_{cw} to differ, see Chapter 5.2a. There is another possibility and that is that the difference arises partly from the way the tests were carried out. For the advancing drop test, $\gamma_{c\phi}$ water was used and for the receding drop test the liquid is the standard Viskin solution supplied, and this may have some effect.

The fact that the surface energy increases, after plasma treatment, from about 32 mN m^{-2} to over 57 mN m^{-2} does agree with the ESCA data in sections (i) and (ii) which show an increase in oxygen functionality and therefore presumably an increase in polar groups.

When subjected to heat treatment the plasma oxidised polyethylene reveals a difference between using air and using oxygen as the plasma gas. Using oxygen the value of γ_{cw} falls steadily reaching what appears to be a limiting value of 48 mN m^{-2}. This same value is also reached on keeping a sample for three weeks at ambient temperatures. This fall in surface energy is also revealed in the information shown in figure 6.2.7. The results agree quite well with the ESCA results, Table 6.2.3, and figure 6.2.4 which show a corresponding fall in functionality at the surface which also reaches a limiting value.

When air is used it would seem from Table 6.2.6 that there is very little change in surface energy when the

Plasma Wettability Studies

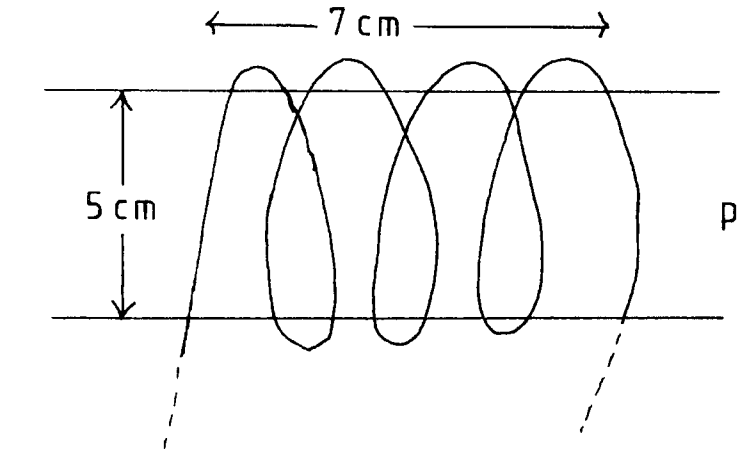

plasma 0.5 watt , 0.2 torr

wetting solutions

35, 40, 45, 50, 55, 57 mN m^{-2}

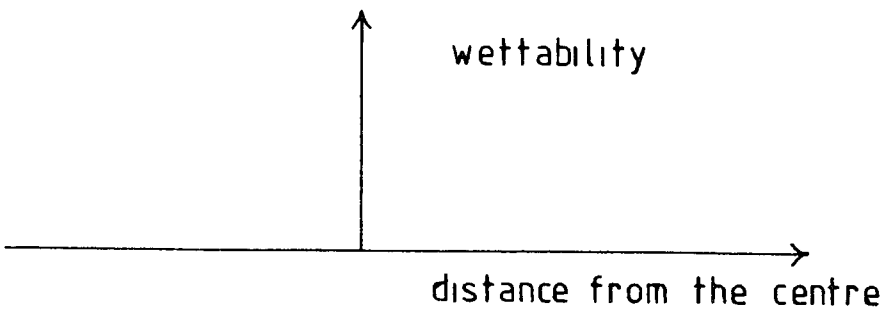

Figure 6.2.6

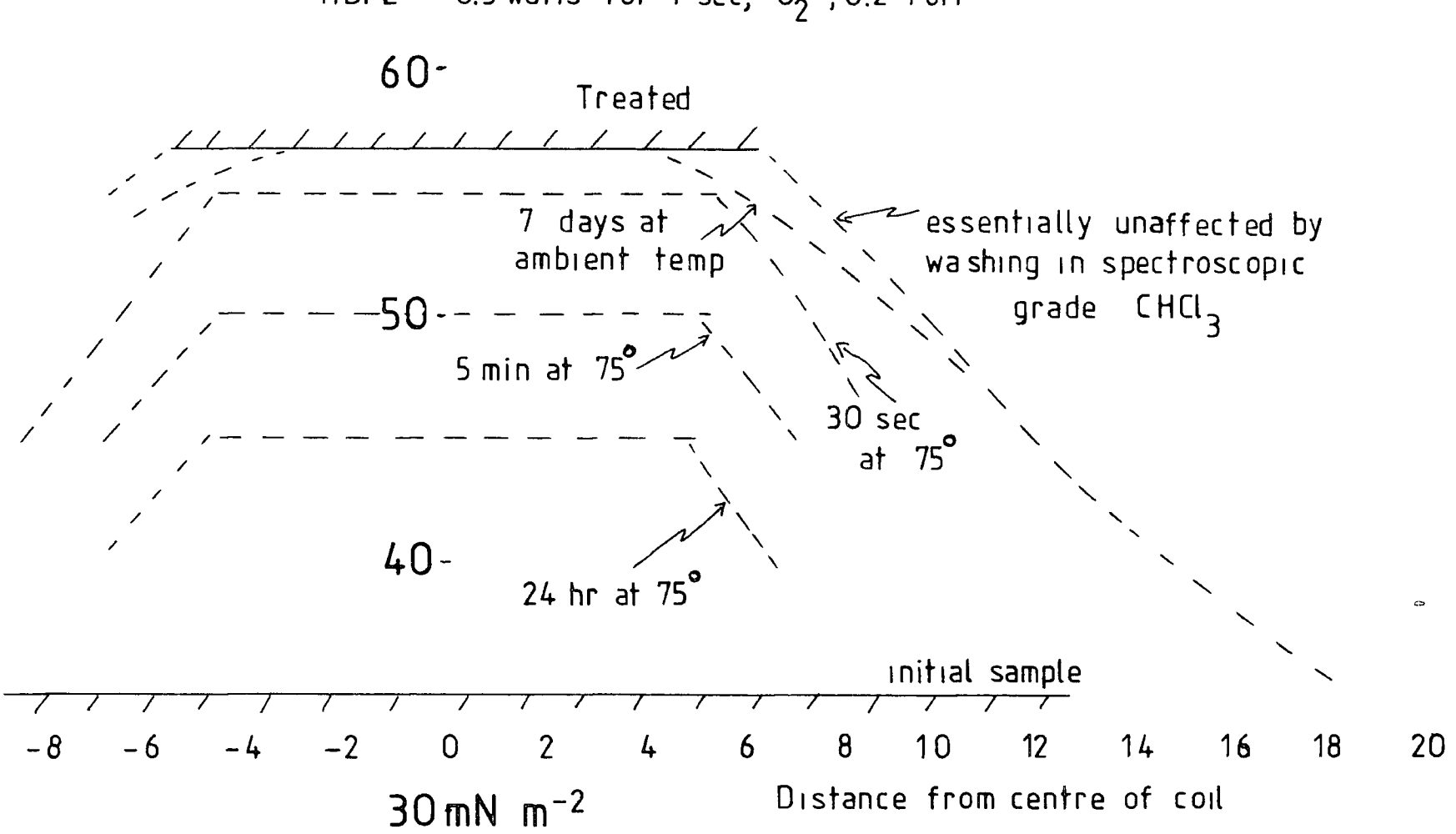
HDPE 0.5 watts for 1 sec, O_2 , 0.2 torr
60
Treated
7 days at ambient temp
essentially unaffected by washing in spectroscopic grade $CHCl_3$
50
5 min at 75°
30 sec at 75°
40
24 hr at 75°
initial sample
-8 -6 -4 -2 0 2 4 6 8 10 12 14 16 18 20
30 mN m^{-2}
Distance from centre of coil

Figure 6 2.7

Polymer and Treatment	Contact Angle ϕ^o	$\gamma_{c\phi}$	γ_{cw}
LDPE			
Air Plasma	81	35	57
O_2 Plasma	64	41	57
HDPE			
Air Plasma	74	38	57
O_2 Plasma	52	45	57

Table 6.2.5

Heat Treatment at 75°C Time	O_2 Plasma γ_{cw}	Air Plasma γ_{cw}
2 min	55	57
5	50	55
10	50	55
15	50	55
20	50	57
24 hours	48	
7 day ambient	57	
21 day ambient	48	

Critical Surface Tensions for Wetting, γ_c /mNm^{-2}

Table 6.2.6

plasma oxidised HDPE is subjected to heat treatment. There is however a slight dip in the value of γ_{CW} and it is possible that this correlates with the dip in oxygen functionality and carbon singly bonded to oxygen functionality observed in figure 6.2.3. Also the surface of the air plasma treated polyethylene has a higher maximum value of oxygen functionality than the minimum value reached by the surface of the oxygen plasma treated polyethylene. This agrees with the fact that the minimum value of γ_{CW} for air plasma, 55 mN m^{-2} is higher than the the final value of γ_{CW}, 48 mN m^{-2} reached when using oxygen plasma treatment.

.3 Discussion

a) Comparison of Air and Oxygen Plasma Treatment

After exposure to plasma for the same time and at the same power and pressure it is seen, figure 6.3.1, that the total oxygen functionality in the subsurface layer of HDPE is less than that at the surface when oxygen is used. In oxygen the surface layer, as shown by the 70^{o} take off spectra reaches a higher level of oxygen functionality than the subsurface layer though the difference is only small. In air it is the subsurface layer which becomes more highly oxidised and the difference between the surface and subsurface layers is larger. These differences in oxygen functionality are matched by corresponding values for the carbon 1s peaks. These show

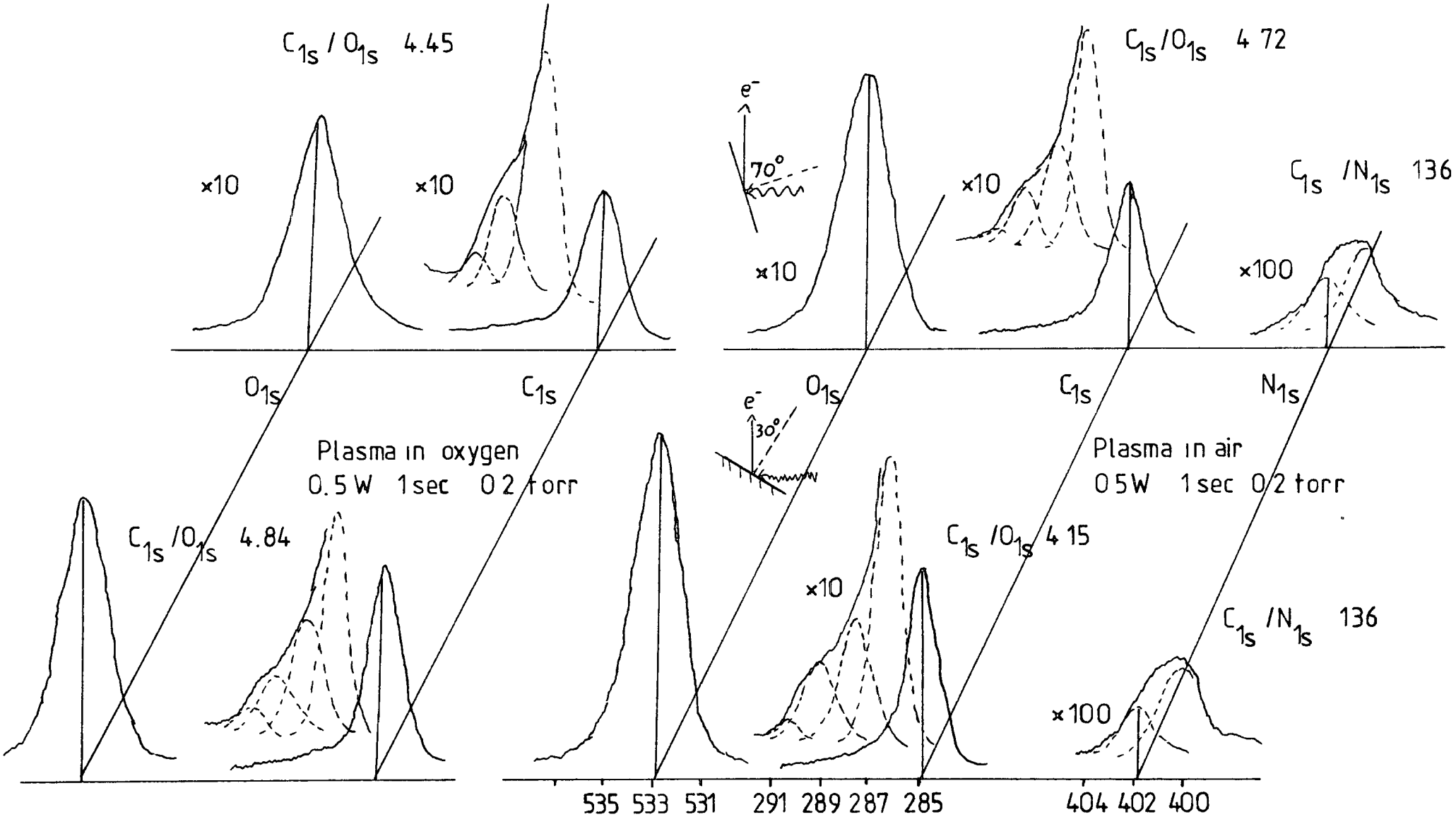
C1s / O1s 4.45
×10
×10
O1s
C1s
Plasma in oxygen
0.5 W 1 sec 0.2 torr
C1s /O1s 4.84
C1s /O1s 4 72
e⁻
70°
×10
×10
C1s /N1s 136
×100
O1s
C1s
N1s
e⁻
30°
Plasma in air
0 5W 1 sec 0.2 torr
C1s /O1s 4 15
×10
C1s /N1s 136
×100
535 533 531
291 289 287 285
404 402 400

Figure 6.3.1

bigger values for the subsurface layer compared to the surface layer for air plasma, Table 6.2.1, while the reverse is true for oxygen plasma, Table 6.2.3. The deconvoluted oxygen spectra show that there is more hydroperoxide produced in the subsurface layer when oxygen is used but at the surface the amount of hydroperoxide is much less and seems to be about the same for both air and oxygen plasmas. The effect of heating the plasma treated HDPE reveals some differences between air and oxygen plasma treatments. After air plasma treatment the oxygen functionality and the C_{1s} peaks fall at first during heat treatment and then rise. At the end of the heat treatment the oxygen functionality has reached very much the same value as at the beginning. Table 6.2.1 shows that some C_{1s} and O_{1s} peaks have become smaller while others have at first decreased and then increased. Calculations reveal that in fact there is more hydroperoxide at the end than at the start. The HDPE treated in oxygen plasma behaves in a much simpler way and the oxygen and carbon functionalities fall during the treatment, reaching a minimum value after which little change occurs. This behaviour can be explained by assuming free radicals are present in the HDPE after air plasma treatment but not after oxygen plasma treatment. On heating the samples volatile material is lost but the free radicals in the HDPE can react with atmospheric oxygen to form hydroperoxides which cause the oxygen functionality to rise. For the oxygen plasma treatment there are no free radicals left

at the end and so as low molecular mass material volatilises the oxygen functionality falls until no further change occurs. It is possible that free radicals are formed, by the ultra violet radiation from the plasma, during both treatments but in oxygen they may be destroyed by conversion into hydroperoxides etc., as soon as they are formed. In air there is not as much oxygen available and so at the end there may still be unreacted free radicals. These will be trapped below the surface and on heating they can react as oxygen diffuses in.

The surface energy of HDPE after plasma treatment seems to be much the same when either air or oxygen is used. When heated the surface energies follow very closely the trends observed in the oxygen functionalities. Thus for oxygen plasma the surface energy falls to a minimum value and then remains constant. After air plasma, followed by heating the surface energy falls slightly, as does the oxygen functionality, and then rises again to about the same value as at the start.

These results show that plasma treatment is a very effective way of increasing the wettability of the surface of polyethylene and that this is associated with an increase in the oxygen functionality. They also reveal that there is no advantage in using oxygen instead of air and in fact using air has some advantages. After using air the surface energy would seem to hold its value while after using oxygen the wettability will tend to fall slightly.

b) Comparison of Corona and Plasma Treatments

Corona treatment operates at atmospheric pressure and as a system is very suitable for the treatment of sheet and film material. Indeed it might be said that it is only really convenient for the treatment of flat surfaces and as a continuous treatment process it is not suitable for and in fact almost impossible to use on shaped objects of any kind. The process normally operates using air without any form of treatment other than possibly simply filtering to remove dust particles. The use of other gases is more difficult though in principle they could be used and might be added to the general air flow. The process though would tend to be wasteful, most materials cost money, and though recovery of unused material would be possible contamination by breakdown products would be a problem.

Plasma treatment operates at low pressures and is essentially a batch process working in a discontinuous manner, though some work has been done on the continuous treatment of yarn[229]. It can be used for any shaped object, flat or moulded and has the advantage over corona treatment that all of the surface of an object, exterior and interior, is treated. The process is very suitable for use with gases other than air and it is very easy to add other substances, which may be done after the plasma has been operated, for surface treatment and grafting[139]. In view of the low pressure at which the process operates the

amounts of gases and other substances used tend to be small and the enclosed nature of the plant (a vacuum chamber) chemical hazards are easily contained. The complete surface of the material, such as a spun yarn, will be treated when surface modification is being carried out. This is an advantage over corona treatment where only the immediate surface on which the corona discharge impinges is affected. The plasma process also has the advantage over corona treatment in that the formation of ozone, when using air, is much reduced.

Although other gases than air may be used for the plasma process, it would seem that if only an increase in surface energy is required then air is in fact better than oxygen (see section .2b above). With corona treatment the same applies and there does not seem to be any advantage in using oxygen instead of air when wishing to increase the surface energy though oxygen does seem to give a quicker increase in surface energy. Both the processes, plasma and corona, need only short treatment times and both give clean and largely sterile surfaces which need no additional treatment.

The values of surface energy as measured by the ASTM wipe test γ_{CW} and the water drop method $\gamma_{C\emptyset}$ reveal an interesting difference between corona and plasma treatment. Whereas for corona treatment the two values are very nearly the same, for plasma treatment the difference is quite large[187]. Both treatments are known to affect the

surface morphology[6,228] and there seems to be no reason to suppose that plasma treatment gives a less uniform coverage than corona treatment. The one factor that is different is the surface charge produced in corona treatment and it does appear that this can cause an increase in surface energy (see Chapter 5). It is possible therefore that this surface charge causes an increase in $\gamma_{C\emptyset}$ for corona treatment that is not seen in plasma treatment, this not normally producing a surface charge. The value of γ_{CW} produced by plasma treatment is much larger than the maximum produced by corona treatment so there must be some effect produced by plasma treatment that is much larger than that produced by corona treatment. At this stage it is not possible to put forward any suggestion as to what this is since the effects of the two processes do not seem markedly different (see below).

The adhesive bond strength of polyethylene surfaces increases when subject to corona and plasma treatment. It has been suggested by Schonhorn[214] that this is due mainly to the removal of weak surface layers and the formation of a strong boundary layer by increased crystallinity and cross linking. Cross linking of polymer surfaces has been detected as a result of plasma[233] and corona treatment[213].

The increase in surface energy caused by plasma and corona treatment seems to be associated with an increase in the oxygen functionality of the surface as well as any cross linking that takes place. It is difficult

to make accurate comparisons as to the levels of oxygen and carbon functionalities introduced by both processes since the power input to the corona is not accurately known. The calculations that have been made, see Chapter 4.2d, suggest a similar value for the power input in both processes, corona $\sim$0.6 J sec^{-1}, plasma 0.5 J sec^{-1}, but the corona volume is much less than the plasma volume. The two methods cannot therefore be run so that the total energy that impinges on unit area of the surface is the same but notwithstanding this some general conclusions can be drawn.

When using a corona discharge the levels of hydroperoxide that can be formed are much larger for air corona than for oxygen corona, Tables 4.3.5 and .12. An air plasma however produces a lower level of hydroperoxide, in the subsurface layer than an oxygen plasma, Tables 6.2.1, and .3. The air corona also seems to be capable of producing much higher levels of oxygen functionality than an air plasma. It was interesting to see that after heating the air plasma treated sample of HDPE for 24 hours its carbon and oxygen functionalities were very similar to the one second air corona treated HDPE, apart from the C_{1s} 286.6 eV peak. The surface energies however were very different, γ_{CW} for the air plasma treated HDPE being $\sim$57mN m^{-2} and for the air corona treated HDPE being $\sim$45mN m^{-2} . The main difference in the ESCA spectra for the same treatment time seems to be that plasma treatment

produces larger C_{1s} peaks at 286.6 and 287.8 eV, and for air plasma smaller O_{1s} peaks at 532.7 eV and larger O_{1s} peaks at 533.5 eV than corona treatment does. When oxygen is used the O_{1s} peaks at 532.7 eV are larger using plasma treatment and the O_{1s} peaks at 533.5 eV are smaller than those for corona treatment. The carbon 1s spectra suggest that plasma treatment produces a higher level of carbonyl function, C_{1s} binding energy 287.8 eV, than corona treatment and also, allowing for hydroperoxide, a higher level of ether linkages, C_{1s} binding energy 286.6 eV.

The effect of heating polyethylene samples after treatment reveals that following plasma treatment, using air, free radicals are probably present[231], trapped below the surface. The absence of any effect after oxygen plasma or corona treatment can be explained by assuming that any free radicals formed are removed immediately after formation by reaction with oxygen.

The two methods corona and plasma offer ways of increasing the surface energies for two different forms of product. The corona treatment is a convenient method for sheet and film while the plasma process is available for moulded objects and interiors. Both produce similar effects on wettabilities and adhesive bond strength and the effects produced seem largely due to an increase in oxygen functionality with cross linking being of some importance when forming adhesive joints. The surface

charging resulting from corona treatment, sometimes a nuisance, may have some effect on wettability but is not likely to be important when using adhesives.

Chapter 7

Some Aspects of the Structure and Bonding in the Perchlorodiphenylaminyl Radical

.1 Introduction

.2 Experimental

.3 Results and Discussion

.1 Introduction

There has been considerable interest on both an experimental and theoretical front in the investigation of multiplet effects accompanying core ionisation with the predominent emphasis to date being on paramagnetic metal complexes[31, 235-238]. With the present background of available information the investigation of multiplet effects in the core ionisation of transition metal complexes provides a useful tool for the investigation of spin state, stereochemistry, oxidation state and distribution of unpaired electrons which is becoming increasingly important[31, 235-238].

By contrast there have been relatively few investigations of paramagnetic organic systems; the published data being confined to the diphenyl picryl hydrazyl[239] radical and ditertiary butyl and ditrifluoromethyl nitroxide systems[240]. Although in principle ESCA studies of multiplet effects in such systems should (and in the case of the nitroxides does) provide a means of investigating unpaired spin distributions there are relatively few stable organic free radicals which may conveniently be studied with conventional instrumentation. From available theoretical calculations it is clear that even for systems in which an unpaired electron is essentially localised on an atom (e.g. C, N, or O) the multiplet splitting in the 1s core levels is predicted to be quite small (1-2 eV), comparable to the typical ESCA instrumental resolution[31,235,236,24(
Indeed for the two systems which have been studied in most

detail the multiplet splittings in each were manifest as broadenings of the core level signals since there is considerable delocalisation of the unpaired electron in both cases[240].

In recent years a new class of stable organic free radicals have been produced by synthetic routes pioneered by Ballester et al[241,242]. The basic rationale behind the work is to sterically shield the site of high spin density by appropriate chlorine substitution. In this way for example the perchlorodiphenylaminyl radical has been prepared[241,242], as a stable solid which may be kept in air on a time scale of months without appreciable oxidation. ESR studies at first sight suggest a high degree of spin localisation on nitrogen comparable with diphenyl picryl hydrazyl and somewhat less than for ditertiary butyl nitroxide. However the magnitude of the hyperfine splitting as a measure of spin localisation is ambiguous since distortion from planarity about the nitrogen can lead to substantial s character for the singly occupied molecular orbital, the net effect being that quite a small spin density could lead to an appreciable hyperfine coupling[243-246] The relative chemical inertness of the perchlorodiphenylaminyl radical could therefore possibly arise from extensive delocalisation of spin density over the phenyl substituents with a relatively small spin density on nitrogen which constitutes the reactive centre. Steric hindrance provided by the four ortho chlorines could then explain the relative inertness of the system. The substantial hyperfine splitting

on nitrogen in this case would be explicable in terms of significant 2s character on nitrogen for the singly occupied molecular orbital[243,246]. This is not unreasonable on the basis of molecular models which indicate considerable distortion about the CNC centre. The alternative rationalization of the available date would be that the unpaired electron is essentially localised on nitrogen, the chemical inertness again being attributable to the steric hindrance to approach provided by the four ortho chlorines. The magnitude of the hyperfine splitting however would suggest that if this were the case the singly occupied molecular orbital must have a large amount of nitrogen 2 p character so that the splitting arises from indirect polarization.

.2 Experimental

The sample of perchlorodiphenylaminyl radical was kindly supplied by Professor Ballester of the Department of Chemistry, Barcelona University. The sample ($\sim$ 1 mg) was sublimed onto a piece of gold foil which was then attached by double sided scotch tape to the spectrometer probe. The ESCA spectra were recorded at 30° take-off angle on an AEI ES 200 AA/B spectrometer employing $Mg_{K\alpha 1,2}$ radiation. Under the conditions employed the $Au_{4f7/2}$ level at 84.0 eV binding energy, used for calibration of the instrument, had a FWHM of 1.15 eV. The thickness of the film deposited was such that when samples were run the gold spectra were not observed. Energy referencing was therefore accomplished by studying hydrocarbon material (285 eV) selectively deposited onto the sample after the core level spectra had been recorded.

.3 Results and Discussion

The core level spectra (N_{1s}, C_{1s}, Cl_{2s} abd Cl_{2p}) for the perchlorodiphenylaminyl radical are shown in figure 7.3.1. Considering firstly the C_{1s} spectrum this consists of a single peak centred at 286.7 eV, somewhat lower in binding energy than the chlorine substituted carbons in pentachlorobenzene (287.5 eV)[247]. This is not entirely unexpected on the basis of the electronic effect associated with replacing hydrogen by a nitrogen functional group. The carbons directly attached to nitrogen are sufficiently perturbed by the chlorine substituents in the ring system to be considerably shifted to higher binding energy (CH in pentachlorobenzene 286.2 eV) such that fortuitously their binding energies are essentially the same as that appropriate to the C-Cl structural features[247]. The net effect therefore is that the overall line shape and line width for the direct photoionization peak for the C_{1s} levels is essentially that appropriate to a single component of FWHM 1.2 eV. Before discussing the satellites to the low kinetic energy side of the direct photoionization peaks, attributable to $\pi \rightarrow \pi^*$ shake up satellites, the measured binding energies and FWHM for the other core levels will be considered. The nitrogen core level spectrum shows a somewhat asymmetric line shape suggesting that it arises from the superposition of two components. Analysis of the line shape in terms of two components of intensity ratio 1:3 may be accomplished straightforwardly and the derived energy separation of 0.6 eV is comparable with that measured for the N_{1s} levels of the nitroxides but substantially smaller than for NO (1.4 eV) or NF_2 (1.9 eV) for which there is a

Table 7.3.1

Core level	FWHM (in eV)	Binding energies (eV)	Shake up satellites energy (eV)	% of direct photoionization peak
N_{1s}	1.1	401.4(1)	5.4	4.3
	1.1	400.8(3)		
C_{1s}	1.2	286.7	4.5	2
			5.6	6
			10.4	3
Cl_{2s}	2.1	271.8		
$Cl_{2p1/2}$	1.2	202.5	5.7	1.6*
$Cl_{2p3/2}$	1.2	201.0	5.7	1.6*

* Expressed as percentages of corresponding spin orbit split components

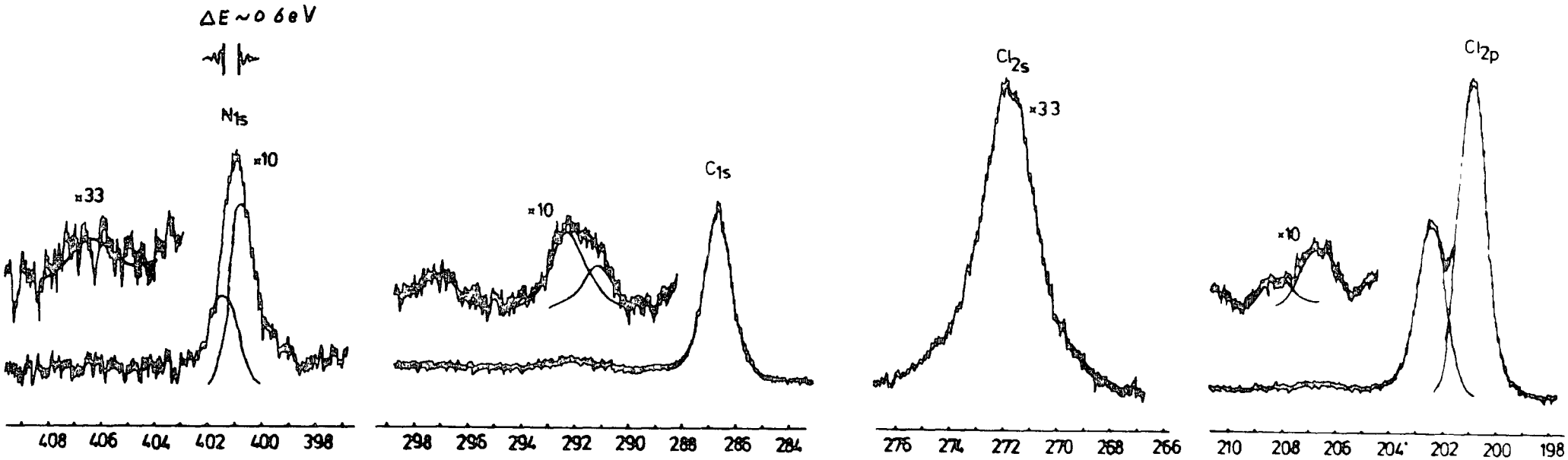

Core level spectra for the perchlorodiphenylaminyl radical

Fig. 7.3.1

large degree of spin localised on the nitrogen. The ESCA data show however that there must be a significant unpaired spin density on the nitrogen and the ESR data therefore imply a very small degree of nitrogen 2s character. The binding energy of the N_{1s} levels is closely similar to that for perchloroindolin which forms a suitable model for comparison purposes[248]. The Cl_{2s} and $Cl_{2p3/2}$ core levels having binding energies which again are consistent with pentachlorophenyl residues linked by nitrogen, being somewhat lower than for pentachlorobenzene.

The evidence from the direct photoionisation of the core levels therefore seems to support an interpretation of the ESR spectra in terms of considerable localisation of the unpaired electron although this does not necessarily preclude the possibility of there being a very small contribution from the nitrogen 2s orbital.

It is also of interest to note that for the dimethyl aminyl radical the hyperfine coupling constant is somewhat larger, 14.8 gauss[246], which is also indicative of more extensive delocalisation in the perchlorodiphenylaminyl system. The line width observed for the perchlorodiphenyl-aminyl radical is quite large, 4 gauss[241], which may be attributed to unresolved hyperfine splitting involving the chlorines.

For the N_{1s} hole state the multiplet splitting is given by $\Delta E = f \times K$ where f is the fraction of unpaired spin

density on nitrogen and K is the one centre exchange integral between a core and valence electron on nitrogen[236]. In the spirit of the transition formalism [249,250] it is clear that the unpaired spin density appropriate to this relationship is that for the half ionised species and as such the spin density is somewhat modified with respect to the ground state. Thus for a simple system such as NO the calculated, INDO, unpaired spin densities at the nitrogen and oxygen for the ground state are 15% and 28% larger respectively than those appropriate to the half ionised systems, computed from the equivalent cores species [249,250]. Unfortunately the perchlorodiphenyl aminyl radical is inconveniently large for calculations at the INDO level to be straightforwardly available. As a prototype system to investigate the likely relationship between spin density in the ground state therefore calculations have been carried out on conformers of the parent diphenylaminyl radical and the N_{1s} core hole state species simulated by the appropriate equivalent cores species. For an angle about nitrogen of 103.4^{o} and standard bond lengths [251] the unpaired spin density on nitrogen for the neutral system is somewhat dependent on the relative conformation of the two phenyl groups. Thus with the plane of the ring at an angle of 45^{o} with respect to the plane through the nitrogen and attached two carbon atoms the unpaired spin density on nitrogen is some 5% lower for the equivalent core species. With one of the phenyl groups in plane and the other rotated by 90^{o}

the change in unpaired spin density in going from the ground state to the half ionised species is even less, 2%. It is clear from this that the spin densities appropriate to the interpretation of multiplet effects in ESCA and in hyperfine splittings in ESR are subtly different. For the former the spin distribution is that appropriate for a half ionized system as is clear from the transition formalism, whilst for the latter the spin distribution is that appropriate to the neutral system. Model calculations would seem to provide strong evidence that the spin densities are not significantly different for the two situations. However, the tendency will undoubtedly be in a sense that the apparent spin density on nitrogen in the diphenylaminyl system will be slightly smaller as adjudged by data pertaining to the half ionized state. Since the exchange integral K does not depend strongly on the extent of s and p mixing, multiplet splitting should therefore reflect fairly directly the unpaired spin density at nitrogen. This contrasts strongly with the situation for the ESR spectra where the hyperfine coupling is a sensitive function of the s contribution to the singly occupied molecular orbital. In this respect therefore the unpaired spin density on nitrogen can more readily be investigated by ESCA and the multiplet splitting for the N_{1s} core levels would seem to indicate quite clearly that the unpaired spin density on nitrogen in the perchlorodiphenylaminyl radical is quite substantial.

The core level spectra displayed in figure 7.3.1 show evidence of satellites to the low kinetic energy side of the direct photoionisation peaks. Such satellites have been well documented for unsaturated systems and originate in $\pi \rightarrow \pi^*$ shake up transitions accompanying core ionisation[252,253]. For the C_{1s} levels shake up transitions centred approximately 4.5, 5.6 and 10.4 eV from the direct photoionisation peak are observed with relative intensity 3, 6 and 2% with respect to the direct photoionisation peak. For the Cl_{2p} and N_{1s} levels satellites are also observed at energy separations of $\sim$5.7 eV and $\sim$5.4 eV respectively, the satellites for the Cl_{2p} levels exhibiting the characteristic spin orbit coupling, 1.5 eV, of the direct photoionisation peak. The shake up intensities for the N_{1s} and C_{1s} levels are significantly higher than for the Cl_{2p} levels which is indicative of the fact that the transitions of the latter involve occupied and virtual orbitals with small contributions from Cl_{3p} valence orbitals. Although strictly speaking there is no sigma-pi separability it is nevertheless convenient to discuss the shake up transitions in terms of the local symmetry of the pi system of the component building blocks for the perchlorodiphenylaminyl system. Studies of the low energy shake up satellites of substituted aromatic ring systems by Clark et al[252,253] have shown that the low energy satellites in the region less than 8 eV from the direct photoionisation peaks originate in transitions involving the two highest occupied and lowestunoccupied molecular

orbitals of the pi systems. The situation with regard to systems with unpaired valence electrons is considerably more complex since transitions involving both the singly and doubly occupied orbitals are of some importance. The striking feature clearly evident in comparing the shake up structure for the C_{1s} levels of the perchlorodiphenyl-aminyl system with that for simple substituted phenyl derivatives however is the significantly higher intensity of the low energy shake up structure and the greatly reduced transition energies. The shake up intensity for both the N_{1s} and Cl_{2p} levels is considerably lower and the centroid of the peaks corresponds in energy to the higher energy of the two low energy satellites for the C_{1s} levels. By analogy with the substituted aromatic systems which have been studied[252-254], the low energy satellites almost certainly originate in transitions involving the two highest occupied and low unoccupied M.O.'s. In the particular case of the C_{1s} levels where the region to the low kinetic energy side of the direct photoionisation peak has been studied in somewhat more detail an additional higher energy, 10.4 eV, transition is also apparent. It is interesting to note that the lowest energy component of the shake up transitions for the C_{1s} levels corresponds quite closely in energy to the most intense of the UV-visible transitions for the radical, λ_{max} 296 x 10^{-9}m, 4.2 eV.

Rather similar low energy C_{1s} shake up peaks were also seen in the ESCA spectra of the perchloro-tri-biphenyl methyl and the p-methyl perchlorophenyl, diphenyl methyl radicals. However for these radicals it was not possible

to detect any unpaired spin density on the trivalent carbon atom. This was of course due to the presence of the other C_{1s} peaks. In view of this and the rather small splitting, 0.6 eV, of the nitrogen in the perchlorodiphenylaminyl radical it was concluded that this approach would not yield much information concerning the presence of free radicals in the surface layers of treated polyethylene. The results are interesting though and show that for smaller molecules, where the relative effect of multiplet splitting is larger (2.6 c ii) information concerning free radicals and the localisation of unpaired electrons can be obtained. It is also interesting to note that for the free radicals studied quite low energy C_{1s} shake up peaks are observed.

APPENDIX 1

References

1. A.J. East and G.R. Walker,
   Sixth Form Topics: Polymers 2, Synethetic Fibres,
   ICI Publications for Schools, 1972.

2. S.H. Pinner and W.G. Simpson,
   "Plastics: Surfaces and Finish", Butterworths, 1971.

3. L.F. Fieser and M. Fieser,
   Organic Chemistry, p.891 et seq. Heath, 1950.

4. K. Kiyozumi, T. Kitakoji, K. Uchiyaka and T.G. Fujitsu,
   J. Adhesion, Japan 6, 265, 1970.

5. W.T.M. Johnson,
   Official Digest of the Oil and Colour Chemists'
   Association 32, 1067, 1960.

6. C.Y. Kim and D.A.I. Goring,
   J. Appl. Poly. Sc. 15, 1357-1364, 1971.

7. D.T. Clark, "The Applications of ESCA to studies of
   Structure and Bonding in Polymers", in "Advances in
   Polymer Friction and Wear", Ed. L-H. Lee, Plenum, 1974.

8. H.N. Friedlander and V. Menikheim,
   "Chemical Reactions on Polymeric Fibre Surfaces" in
   "Molecular Behaviour and Development of Polymeric
   Materials", Eds., Ledwith and North, Chapman Hall, 1975.

9. D.T. Clark, W.J. Feast, W.K.R. Musgrave and I. Ritchie,
   "Structure, Bonding and Dynamics of Surface and Subsurface
   Polymer Films produced by Direct Fluorination as
   revealed by ESCA", in "Advances in Polymer Friction and
   Wear", Ed. L-H. Lee, Plenum, 1974.

10. W.M. Riggs and D.W. Dwight,
    J. Elect. Spec. and Rel. Phen. 5, 447, 1974.

11. A.L. Miller et al.
    J. Appl. Poly. Sc., 14, 257, 1970.

12. G. Smolinsky and M.J. Vasile,
    European Polymer Journal, 15, 87, 1979.

13. C. Mayoux,
    I.E.E.E. Int. Sym. on Electronics, Conf. Record, 276, 1976.

14. I. Sakata and D.A.I. Goring,
    J. Appl. Poly. Sc., 20, 573, 1976.

15. A. Ledwith and D.C. Sherrington,
"Catalytic applications of Synthetic Polymers"
in "Molecular Behaviour and Development of Polymeric
Materials", Eds., Ledwith and North, Chapman Hall, 1975.

16. T. Memetea and V. Stannett,
Polymer, 20 (4), 465, 1979.

17. H. Hertz,
Annalen der Physik, 31, 1887.

18. H. Hertz,
Ueber Strahlen elektrischer Kraft in Sitzungsberichte
der Berliner Akademie der Wissenschaften, Dec. 1888.

19. W. Hallwachs,
Wied Ann., 33, 301, 1888.

20. M. de Broglie,
Compt. Rend., 158, 1493, 1914.

21. M. de Broglie,
Compt. Rend., 163, 87,353, 1916.

22. H. Robinson and W.F. Rawlinson,
Phil. Mag., 28, 277, 1914.

23. H. Robinson,
Proc. Roy. Soc., A 104, 455, 1923.

24. H. Robinson,
Phil. Mag., 50, 241, 1925.

25. K. Siegbahn and K. Edvarson,
Nucl. Phys., 1, 137, 1956.

26. S. Hagstrom, C. Nordling and K. Siegbahn,
Z. Physik, 178, 439, 1964.

27. D.W. Turner, C. Baker, A.D. Baker and C.R. Brundle,
Molecular Photoelectron Spectroscopy, J. Wiley and
Sons Ltd., 1970.

28. K. Siegbahn, C. Nordling, A. Fahlman, R. Nordberg,
K. Hamrin, J. Hedman, G. Johansson, T. Berkmark,
S.E. Karlsson, I. Lidgren and B. Lindberg,
"ESCA, Atomic Molecular and Solid State Structure
Studied by means of Electron Spectroscopy, Almquist
and Wiksells, Uppsala, 1967.

29. L.S. Cederbaum and W. Domcke,
J. Elect. Spectro. and Rel. Phen. 13, 161, 1978.

30. H.B. Cullen,
Handbook of Physics, Section 8, Chap 2, Mcgraw Hill,1967.

31. K. Siegbahn, C. Nordling, G. Johansson, J. Hedman, P.F. Heden, K. Hamrin, U. Gelius, T. Bergmark, L.O. Werme, R. Manne and Y. Baer, 'ESCA applied to Free Molecules', North Holland, 1969.

32. D.T. Clark, 'Structure and Bonding in Polymers as revealed by ESCA' in Electronic Structure of Polymers and Molecular Crystals, Eds. J. Lodik, and J.M. Andre, Plenum Press, N.Y. 1975.

33. A. Rosen and I. Lindgen, Phys. Rev. 176, 114, 1968.

34. P.S. Bagus, Phys. Rev. A, 139, 619, 1965.

35. D.A. Shirley, Advances in Chem. Phys., 23, 85, Eds. I. Prigogine and S.A. Rice, Wiley, N.Y. 1973.

36. U. Gelius and K. Siegbahn, Fara. Disc. 54, 257, 1972.

37. L.C. Snyder, J. Chem. Phys., 55, 95, 1971.

38. P.B. Adams and D.T. Clark, Theoret. Chim. Act., 31, 171, 1973.

39. M.F. Guest, I.H. Hillier, V.R. Saunders and M.W. Wood, Proc. Roy. Soc. A 333, 201, 1973.

40. D.T. Clark, I. Scanlan and J. Muller, Theoret. Chim. Act., (Berl.), 35, 341, 1974.

41. T.A. Koopmans, Physica, 1, 104, 1933.

42. E. Clementi and H. Popkie, J. Amer. Chem. Soc., 94, 4057, 1972.

43. W. Meyer, J. Chem. Phys., 58, 1017, 1973.

44. B. Levy, P.H. Millier, J. Richard and J. Vink, J. Elect. Spec. and Rel. Phen. 4, 13, 1974.

45. D.T. Clark and I.W. Scanlan, J. Chem. Soc. Farad. Trans., II, 70, 1222, 1974.

46. R. Manne and T. Åberg,
Chem. Phys. Lett., 7, 282, 1970.

47. S. Pignatoro and G. Distofaro,
Z. Nuturforsch A, 30a, 815, 1975.

48. Ohta, Toshiaki, Fukitawa, Takashi, Furoda and Haruo,
Chem. Phys. Letts., 32, 369, 1975.

49. L. Yin, I. Adler, T. Tsang, L.J. Matienzo and S.O.Grim,
Chem. Phys. Letts., 24, 81, 1974.

50. T. Robert and G. Offergeld,
Chem. Phys. Letts., 29, 606, 1974.

51. M.A. Brisk and A.D. Baker,
J. Elect. Spec. and Rel. Phen. 7, 197, 1977.

52. D. Coster and R. de L. Kronig,
Physica, 2, 13, 1935.

53. E.H.S. Burhop, "The Auger Effect and Radiationless
Transitions", C.U.P. 1952.

54. A.E. Sandstrom,
"Handbook of Physics XXX. X-Rays", p.164, Ed.,
S.F. Flugge. Springer Verlag, Berlin, 1957.

55. C.C. Chang,
Surface Science, 25, 53, 1971.

56. J.P. Coad, M. Gettings and J.G. Riviere,
Farad. Disc. Chem. Soc., 60, 269, 1975.

57. Symp. on X-Ray and Electron Probe Analysis
ASTM 349, p.41-85. 1963.

58. B.L. Henke,
Adv. X-Ray Analysis, 13, 1, 1969.

59. K. Siegbahn, D. Hammond, H. Fellner-Feldegg and
E.F. Barnett,
Science, 176, 245, 1972.

60. R.M. Eisenberg,
"Fundamentals of Modern Physics", Chapter 14,
Wiley, N.Y. 1961.

61. K. Siegbahn,
T. Elect. Spec. and Rel. Phen. 5, 3, 1974.

62. D.T. Clark, H.R. Thomas, A. Dilks and D. Shuttleworth,
J. Elect. Spec. and Rel. Phen. 10, 455, 1977.

63. E.M. Purcell,
Phys. Rev. 54, 818, 1938.

64. J.C. Helmer and N.H. Weichert,
Appl. Phys. Letts. 13, 128, 1968.

65. D.T. Clark, A. Dilks and H.R. Thomas,
"ESCA applied to Polymers XXI", J. Polym. Sc.,
Polym. Chem. Ed. 1977.

66. P. Ascarelli and G. Missoni,
J. Elect. Spec. and Rel. Phen. 5, 417, 1974.

67. J.F. McGilp and I.G. Main,
J. Elect. Spec. and Rel. Phen. 6, 397, 1975.

68. G. Johansson, J. Hedman, A. Bendtsson, M. Klasson
and R. Nilsson,
J. Elect. Spec. and Rel. Phen. 2, 295, 1973.

69. D.A. Huchital and R.T. McKean,
Appl. Phys. Letts. 20, 158, 1972.

70. D.T. Clark,
"ESCA applied to Polymers" in "Advances in Polymer
Science", Springer Verlag, Berlin, 1977.

71. D.T. Clark, A. Dilks, D. Shuttleworth and H.R. Thomas,
J. Polym. Sc. 15, 1977.

72. D.T. Clark,
Physica Scripta (Sweden), 16, 307-328, 1977.

73. W.L. Jolly and D.N. Hendrickson,
J. Amer. Chem. Soc. 92, 1863, 1970.

74. C.S. Fadley, S.B.M. Hagstrom, M.P. Klein and D.A.Shirley,
J. Chem. Phys. 48, 3779, 1968.

75. D.T. Clark,
'Chemical Aspects of ESCA' in Electron Emission
Spectroscopy. Eds. W. Dekeyser and D. Reidel,
D. Reidel Pub. Co. Dordrecht, Holland, 373, 1973.

76. D.S. Urch and M. Webber,
J. Elect. Spec. and Rel. Phen. 5, 791, 1974.

77. D. Betteridge, J.C. Carver and D.M. Hercules,
J. Elect. Spec. and Rel. Phen., 2, 327, 1973.

78. G.R. Ginnard and W.M. Riggs,
Anal. Chem., 46 (9), 1306, 1974.

79. R.S. Swingle II and W.M. Riggs,
CRC Crit. Rev. Anal. Chem., 5, 267, CRC Press,Cleveland,1975.

80. C.W. Scherr, J.V. Silverman and F.A. Matsen, Phys. Rev. 127, 830, 1962.

81. L.C. Snyder and H. Basch, J. Amer. Chem. Soc. 91, 2189, 1969.

82. M.F. Chiu, M.F. Guest and V.R. Saunders, ATMOL 2 user notice 5, Atlas Computer Laboratory, March 1973.

83. C.R. Brundle, M. Robin and H. Basch, J. Chem. Phys., 53, 2196, 1970.

84. M.E. Schwartz, Chem. Phys. Letts. 6, 631, 1970.

85. P.E. Cade, K.D. Sales and A.C. Wahl, J. Chem. Phys. 44, 1973, 1966.

86. T.A. Carlson, M.O. Krause, and W.E. Moddeman, J. de Physique 32, C4-76, 1971.

87. U. Gelius, C.J. Allan, D.A. Allison, H. Siegbahn and K. Siegbahn, Chem. Phys. Letts., 11, 224, 1971.

88. L.J. Aarons, M.F. Guest and I.H. Hillier, J. Chem. Soc. Faraday Trans.II, 11, 1866, 1972.

89. J.M. Hollander and W.L. Jolly, Acc. Chem. Res. 3, 193, 1970.

90. D.T. Clark and D.B. Adams, J. Chem. Soc. Farad.Trans.II, 68, 1819, 1972.

91. D.B. Adams and D.T. Clark, J. Elect. Spec. and Rel. Phen. 2, 201, 1973.

92. W.J. Hehre, R.F. Stewart and J.A. Pople, J. Chem. Phys. 51, 2657, 1969.

93. R. Ditchfield, W.J. Hehre and J.A. Pople, J. Chem. Phys. 54, 724, 1971.

94. J.A. Pople and D.L. Beveridge, 'Approximate Molecular Orbital Theory', McGraw-Hill, New York, 1970.

95. D.T. Clark, D. Briggs and D.B. Adams, J. Chem. Soc., Dalton 19, 1973.

96. D.T. Clark and D. Kilcast, J. Chem. Soc. B. 2243, 1971.

97. D.T. Clark, R.D. Chambers, P. Kilcast and W.K.R. Musgrave, J. Chem. Soc,Farad.II, 2, 309, 1972.

98. M.E. Schwartz, Chem. Phys. Letts., 6, 631, 1970.

99. H. Basch, Chem. Phys. Letts. 6, 337, 1970.

100. D.W. Davis and D.A. Shirley, Chem. Phys. Letts., 15, 185, 1972.

101. H. Siegbahn, R. Medeiros and O. Goscinski, J. Elect. Spec. and Rel. Phen. 8, 149, 1976.

102. L.S. Cederbaum and W. Domcke, Adv. Chem. Phys. 36, 205, 1977.

103. W. von Neissen, G.F. Diercksen and L.S. Cederbaum, J. Chem. Phys. 67(a), 4124, 1977.

104. P.W. Alkins, 'Molecular Quantum Mechanics', Oxford U.P. London,1970.

105. R.E. Watson and A.J. Freeman, in "Hyperfine Interactions", Eds. A.J. Freeman and R.B. Frankel, Academic Press, New York, 1967.

106. C.S. Fadley, D.A. Shirley, A.J. Freeman, P.S. Bagus and J.V. Mallow, Phys. Rev. Lett., 23, 1397, 1969.

107. J.H. von Vleck, Phys. Rev. Lett., 45, 405, 1934.

108. D.W. Davis and D.A. Shirley, J. Chem. Phys. 56, 669, 1972.

109. J.C. Carver, C.A. Thomas, L.C. Cairn and G.K. Schweitar, in Electron Spectroscopy, Ed. D.A. Shirley, North Holland, 1972.

110. C.S.Fadley, in 'Electron Spectroscopy', Ed. D.A. Shirley, North Holland, 1972.

111. T. Novakov and J.M. Hollander, Bull Amer. Phys. Soc. 14, 524, 1969.

112. T. Novakov and J.M. Hollander, Phys. Rev. Lett. 21, 1133, 1968.

113. G.K. Wertheim,
'Mossbauer Effect: Principles and Applications',
Academic Press, New York, 1964.

114. J. Utriainer, M. Linkoaho, E. Rautavouri, T. Aberg
and G. Graeffe.
Z. Naturforsch, 23A, 1178, 1968.

115. L.G. Parrat,
Rev. Mod. Phys. 31, 616, 1959.

116. R.W. Shaw and T.D. Thomas,
Phys. Rev. Lett. 29, 689, 1972.

117. R.M. Friedman, J. Hudis and M.J. Perlman,
Phys. Rev. Lett. 29, 692, 1972.

118. D.T. Clark and A. Dilks,
J. Polym. Sc., Polym. Chem. Ed. 15, 2321, 1977.

119. B.L. Henke and R.L. Elgin,
Adv. X-Ray Anal. 13, 639, 1970.

120. C.J. Powell,
Surf. Sc. 44, 29, 1974.

121. D.R. Penn,
J. Elect. Spec. and Rel. Phen. 9, 29, 1976.

122. D.T. Clark and H.R. Thomas,
J. Polym.Sc., Polym. Chem Ed. 15, 2843, 1977.

123. D.T. Clark and D. Shuttleworth,
J. Polym. Sc., Polym. Chem.Ed. 16, 1977.

124. T.A. Carlson and G.E. McGuire,
J. Elect. Spec. and Rel. Phen. 1, 161, 1962.

125. C.S. Fadley, R.J. Baird, W. Siekhaus, T. Novakov
and S.A.L. Burgstrom,
J. Elect. Spec. and Rel. Phen. 4, 93, 1974.

126. B.L. Henke,
J. Phys. (Paris) C4, 115, 1971.

127. D.T. Clark and D. Shuttleworth,
J. Elect. Spec. and Rel. Phen. 17, 15-24, 1979.

128. A. Dilks,
Ph.D. Thesis, Durham, 1977.

129. J.H. Scofield,
Lawrence Livermore Laboratory Report UCRL 51326,Jan.1973.

130. J.H. Scofield,
J. Elect. Spec. and Rel. Phen. 8, 129, 1976.

131. J. Cooper and R.N. Zare,
J. Chem. Phys. 48, 942, 1968.

132. F.O. Ellison,
J. Chem. Phys. 61, 507, 1974.

133. J.J. Huang, J.W. Rabalais and F.O. Ellison,
J. Elect. Spec. and Rel. Phen. 6, 85, 1975.

134. A.F. Carley and R.W. Joyner,
J. Elect. Spec. and Rel. Phen. 16, 1, 1979.

135. C.D. Wagner,
Farad. Disc. Chem. Soc. 60, 306, 1975.

136. I.H. Munro,
Chem. in Brit. 15, 7, 330, 1979.

137. P.M.Hay
in "Chemical Reactions in Electrical Discharges",
Ed., R.F. Gould, Am. Chem. Soc. Pubs. 1969.

138. S.C. Brown,
in "Gaseous Electronics", Vol.1, Academic Press, 1978.

139. W.L. Fite,
in "Chemical Reactions in Electrical Discharges",
Ed., R.F. Gould, Am. Chem. Soc. Pubs. 1969.

140. "Electrical Breakdown of Gases",
Eds., Meek and Craggs, Wiley, New York, 1978.

141. Kondrat'ev,
"Chemical Kinetics of Gas Reactions", Chapter 8,
Pergamon, 1964.

142. E. Herbst, T.A. Patterson and W.C. Lindberger,
J. Chem. Phys. 61, 1300, 1974.

143. R.N. Franklin,
"Plasma Phenomena in Gas Discharges", Oxford, 1976.

144. A.T. Bell,
in "Techniques and Applications of Plasma Chemistry",
Eds., Hollahan and Bell, Wiley, New York, 1974.

145. W.L. Lama and C.F. Gallo,
I.E.E.E. Trans. on Ind. Appls. 1A-12 (3),288-293,1976.

146. Chapter 4 in
"Gaseous Electronics", vol.1, Academic Press, 1978.

147. R.M. Schaffert, "Electrophotography", Focal Press, London and New York, 1965.

148. M.M. Shahin in "Chemical Reactions in Electrical Discharges", Am. Chem. Soc. Pubs. 1969.

149. J.J. Rodaro, C. Mayoux and A. Loubière, R.G.E., 89 (9), 697-704, 1976.

150. H. McL. Ryan, Proc. IEEE, 114, 1815, 1967.

151. H. McL. Ryan and C.A. Walley, Proc. IEEE, 114, 1529, 1967.

152. T.C. Manley, Trans. Electro. Chem. Soc. 84, 83-96, 1943.

153. L.A. Rosenthal and D.A. Davies, IEEE Trans. Ind. Appl. IA-11 (3), 328-335, 1975.

154. G. Bayer, H.G. Fitzky, H. Hoyer, G. Lüttgens and W. Müller-Bardoff, Deutsches Patentamt. Offenlegungsschrift, DT 2519 233A1,1976

155. J.C. van der Heide and H.L. Wilson, Modern Plastics, 199, 1961.

156. J.C. Fraser, in "Chemical Reactions in Electrical Discharges", Am. Chem. Soc. Pubs. 1969.

157. J.H. Ingold, "Gaseous Electronics", vol.1, Chapter 2, Academic Press, 1978.

158. H. Suhr in "Techniques and Applications of Plasma Chemistry", Wiley, New York, 1974.

159. D.T. Clark, A. Dilks and D. Shuttleworth, Chapter 9 in "Polymer Surfaces", Eds. D.T. Clark and W.J. Feast, Wiley, N.Y. 1978.

160. D.T. Clark, A. Dilks and G.H.C. Freeman, J. Polym Sci. in press, 1980.

161. Physics and Temperatures of Low Temperature Plasmas, Ed., S.V. Dresvin, Iowa State U.P., 1977.

162. H.G. Tompkins,
Appl. Spec. 28 (4), 335-341, 1974.

163. H.A. Willis and V.J.I. Zichy,
Chapter 15 in "Polymer Surfaces", Eds., D.T. Clark and W.J. Feast, Wiley, N.Y. 1978.

164. C. Mayoux,
IEEE Trans. on Elec. Insul. vol El-11, No.4, 1976.

165. H.L. Spell and C.P. Christenson,
TAPPI 62, 77-81, 1979.

166. D.T. Clark and H.R. Thomas,
J. Polym.Sc., Polym.Chem.Ed., 14, 1671, 1976.

167. D.T. Clark, B.J. Cromarty and A. Dilks,
J. Polym. Sc., 16, 3173-3174, 1978.

168. A. Dilks,
in "Developments in Polymer Characterisation",
pub. Appl. Science, in press,1980.

169. J.M. Evans,
J. Adhesion 5, 9-16, 1973.

170. B. Benaissa and C. Mayoux,
Die Angewardte Makromolekulare Chemie,66, 155-167, 1978.

171. Zel'tser, Britan and Klyachko,
Plastcheskie Massy (Soviet Plastics),7, 67, 1976.

172. H. Carchano and J. Guastavino,
European Polymer Hournal,11, 575-580, 1975.

173. J.N. Lomonte,
Analytical Chemistry, 36, 192-194, 1964.

174. J.Runt and I.R. Harrison,
J.Polym.Sc., Polym.Phys., Ed., 16, 375-377, 1978.

175. R.D. Mair and A.J. Graupner,
Analytical Chemistry, 36, 194-204, 1964.

176. J.M. Evans,
J. Adhesion, 5, 1-7, 1973.

177. J.M. Evans,
J. Adhesion, 5, 29-37, 1973.

178. G.J. Courval, D.G. Gray, D.A.I. Goring,
J. Polym. Sc., Polym. Letts. Ed., 14, 231-235, 1976.

179. D.C. Waterman and M. Dole,
J. Phys. Chem, 74, 1913-1922, 1970.

180. C.H. Chew, L.M. Gan and G. Scott,
European Polymer Journal, 13, 361-364, 1977.

181. D.J. Carlsson, A. Garton and D.M. Wiles,
Macromolecules, 9, 695-701, 1976.

182. I. Sakata and D.A.I. Goring,
J. Appl. Polym. Sc., 20, 573-579, 1976.

183. H. Pachonik,
Thin Solid Films, 38, 171-182, 1976.

184. I. Rendall,
Converter, p.22, Sept. 1974.

185. H. Schonhorn,
"Surface Modification of Polymers for Adhesive Bonding" in "Polymer Surfaces", Eds., D.T. Clark and W.J. Feast, Wiley, N.Y. 1978.

186. D.H. Buckley and W.A. Brainard,
"The Atomic Nature of Polymer and Metal Interactions in Adhesion, Friction and Wear", in "Advances in Polymer Friction and Wear", Ed. Lieng-Huang Lee, Plenum, 1974.

187. P.K. Watson,
"The Transport of Electrons from the Surface into the Bulk of Polystyrene", in "Polymer Surfaces", Eds., D.T. Clark and W.J. Feast, Wiley, N.Y. 1978.

188. C.Y. Kim, J. Evans and D.A.I. Goring,
J. Appl. Polym. Sc., 15, 1365-1375, 1971.

189. D.H. Kaelble,
J. Adhesion, 2, 66-81, 1970.

190. S. Wu,
J. Adhesion, 5, 39-55, 1973.

191. B.W. Cherry,
"Aspects of Surface Chemistry and Morphology", in "Plastics: Surface and Finish", Eds., S.H. Pinner and W.G. Simpson, Butterworths, 1971.

192. W.A. Zisman,
in Advances in Chemistry Series 43, Am. Chem. Soc. Pubs. 1963.

193. R.H. Dettre and R.H. Johnson,
J. Phys. Chem. 69, 1507, 1965.

194. B. Leclercq, M. Sotton, A. Baszkın and
L. Ter-Minassıan-Saraga,
Polymer, 18, 675-680, 1977.

195. D.T. Clark,
Chapter 16 ın "Polymer Surfaces", Eds., D.T. Clark
and W.J. Feast, Wıley, N.Y. 1978.

196. J.F. Carley and P.T. Kıtze,
Polym. Eng. and Sc., 18, 32-39, 1978.

197. C. Mayoux and Buı Aı,
J. Appl. Phys. 44, 3423-3424, 1973.

198. H. Schonhorn and F.W. Ryan,
J. Phys. Chem, 70, 3811-3815, 1966.

199. F.J.B. Calleja, G. Ortega and J.M. de Salazar,
Polymer, 19, 1094-1099, 1978.

200. A. Buskın and L. Ter-Mınassıan-Saraga.
Polymer, 19, 1083-1088, 1978.

201. A.R. Blythe, D. Briggs, C.R. Kendall, D.G. Rance
and V.J.I. Zıchy,
Polymer, 19, 1273-1278, 1978.

202. E.H. Andrews and N.E. Kıng,
Chapter 4 ın "Polymer Surfaces", Eds., D.T. Clark
and W.J. Feast, Wiley, N.Y. 1978.

203. E.H. Andrews and N.E. King,
J. Mat. Sc., 11, 2004-2014, 1976.

204. E.W. Garnısh,
J. Oıl and Col. Chem. Assoc. 60, 69-74, 1977.

205. W.C. Wake,
Polymer, 19, 291-308, 1978.

206. D.H. Kaelble and K.C.Uy,
J. Adhesıon, 2, 50, 1970.

207. Y. Kaplevatsky and V. Raevsky,
J. Adkesıon, 6, 65-77, 1976.

208. D. Brıggs and D.M. Brewıs,
Polymer Surfaces Symposium, Durham, 1977.

209. D. Briggs, D.M. Brewıs and M.B. Konieczko,
European Polymer Journal, 14, 1-4, 1978.

210. D.T. Clark and H.R. Thomas,
J. Polym. Sc., Polym. Chem. Ed., 16, 791, 1978.

211. N. Wilson,
Chapter 7 in "Polymer Surfaces", Eds. D.T. Clark and W.J. Feast, Wiley, N.Y. 1978.

212. T.J. Lewis,
Chapter 4 in "Polymer Surfaces", Eds., D.T. Clark and W.J. Feast, Wiley, N.Y. 1978.

213. H. Schonhorn and F.W. Ryan,
J. Polymer Science A-2, 6, 231-240, 1968.

214. H. Schonhorn,
Chapter 10 in "Polymer Surfaces", Eds., D.T. Clark and W.J. Feast, Pub. Wiley, N.Y. 1978.

215. M. Stradal and D.A.I. Goring,
J. Adhesion, 8, 57-64, 1976.

216. D.K. Owens,
J. Appl. Poly. Sc. 19, 265-271, 1975.

217. E. Matsumoto, K. Kamisako and K. Shinohara,
Jap. J. Appl. Phys. 15, 37-41, 1976.

218. M.M. Perlman and J.J. Sonnonstine,
J. Electrostatics, 3, 187-193, 1977.

219. D.K. Davies,
J. Sci. Instrum. 44, 521-524, 1967.

220. R.A. Moreno and B. Gross,
J. Appl. Phys. 47, 3397-3402, 1976.

221. I.B. Jordan,
J. Electrochem. Soc. 122, 290-293, 1975.

222. E.A. Baum, T.J. Lewis and R. Toomer,
J. Phys. D. Appl. Phys. 10, 487-497, 1977.

223. P.K. Watson,
Chapter 5 in "Polymer Surfaces", Eds., D.T. Clark and W.J. Feast, Wiley, 1978.

224. P.B. Sherman,
Coating 2/77, 31, 1977.

225. D.H. Dawes and K.L. Gupta,
The Patent Office, London, Patent Specification 1472376, May 1977.

226. T.R. Beatty and H. Vourlis,
United States Patent 4029876, June 1977.

227. R.L. Bersin,
Polymer News, 2, 13-18, 1971.

228. A.M. Wróbel, M. Kryszewski, W. Rakowski,
M. Okoniewski, and Z. Kubacki,
Polymer, 19, 908, 1978.

229. K.S. Lee and A.E. Pavlath,
Textile Research Journal 45(8), 625-629, 1975.

230. D.H. Reneker and L.H. Bolz,
J. Macromol. Sc. Chem. A.10(3), 599-608, 1976.

231. H. Yasuda,
J. Macromol. Sc. Chem.A.10(3), 383-420, 1976.

232. H. Yasuda,
Radiat. Phys. Chem. 9, 805-817, 1977.

233. D.T. Clark and A. Dilks,
J. Polym. Sc., 16, 911-936, 1978.

234. N. Morosoff, B. Crist, M. Bumgarner, T. Hsu and
H. Yasuda,
J. Macromol. Sc. Chem. A. 10(3), 451-471, 1976.

235. C.S. Fadley, Electron Emission Spectroscopy, ed.
W. Dekeyser, Reidel, Dordrecht, Holland, 1973 .

236. D. Shirley, Advances in Chemical Physics, eds.
I. Prigogine and S.A. Rice, Vol.XXIII, Interscience,
Wiley, New York, 1973 .

237. T.A. Carlson, J.C. Carver, L.J. Saethre, F. G.
Santibanerz and G.A. Vernon, J. Electron Spectroscopy
and Related Phenomena, Conf. Procs., Namur
Meeting, 1974 .

238. B. Wallbank, I.G. Muir and C.E. Johnson, Ibid.
Conf. Procs., Namur Meeting, 1974.

239. I.W. Drummond and H. Harker, Nature, Phys. Sci. 232,
71, 1971.

240. D.W. Davis, R.L. Martin, M.S. Banna and D.A. Shirley,
J. Chem. Phys. 59 (8), 4235, 1973.

241. M. Ballester, J. Castaner and S. Olivella,
Tetrahedron Letters, 7, 615, 1974.

242. M. Ballester, Bull. Soc. Fr. 1, 7-15, 1966.

243. R. Bersohn, Determination of Organic Structures by Physical Methods (eds. F.C. Nachod and W.D. Phillips), pp. 563-616, Academic Press, New York, 1962.

244. A.R. Forrester, J.M. Hay and R.H. Thomson, Organic Chemistry of Stable Free Radicals, Academic Press, New York, 1968.

245. A. Carrington and A.D. McLachan, Introduction to Magnet Resonance, Harper International, New York, 1967.

246. W.C. Danen and T.T. Kensler, J. Am. Chem. Soc. 92, 5235, 1970.

247. D.T. Clark, D. Kilcast, D.B. Adams and W.K.R. Musgrave, J. Electron Spectros. Relat. Phenom. 6, 117, 1975.

248. R. King, Ph.D. Thesis, University of Durham, 1974.

249. O. Goscinski, B.T. Pickup and G. Purvis, Chem. Phys. Letters, 22 (1), 167, 1973.

250. W.L. Jolly, Faraday Discuss. Chem. Soc. 54, 13, 1972.

251. Interatomic Distances, Chem. Soc. Special Publication, 18, 1965.

252. D.T. Clark, Molecular Spectroscopy (ed. A.West), Heyden, London, 1977.

253. D.T. Clark, in Progress in Theoretical Organic Chemistry, (ed. I.G. Csizmadia), Vol.II. Elsevier, Amsterdam,1977.

254. D.T. Clark and A. Dilks, J. Polymer Sci., Polymer Chem. Ed. 14, 533, 1976.

Appendix 2

Circuit Diagrams Corona Apparatus

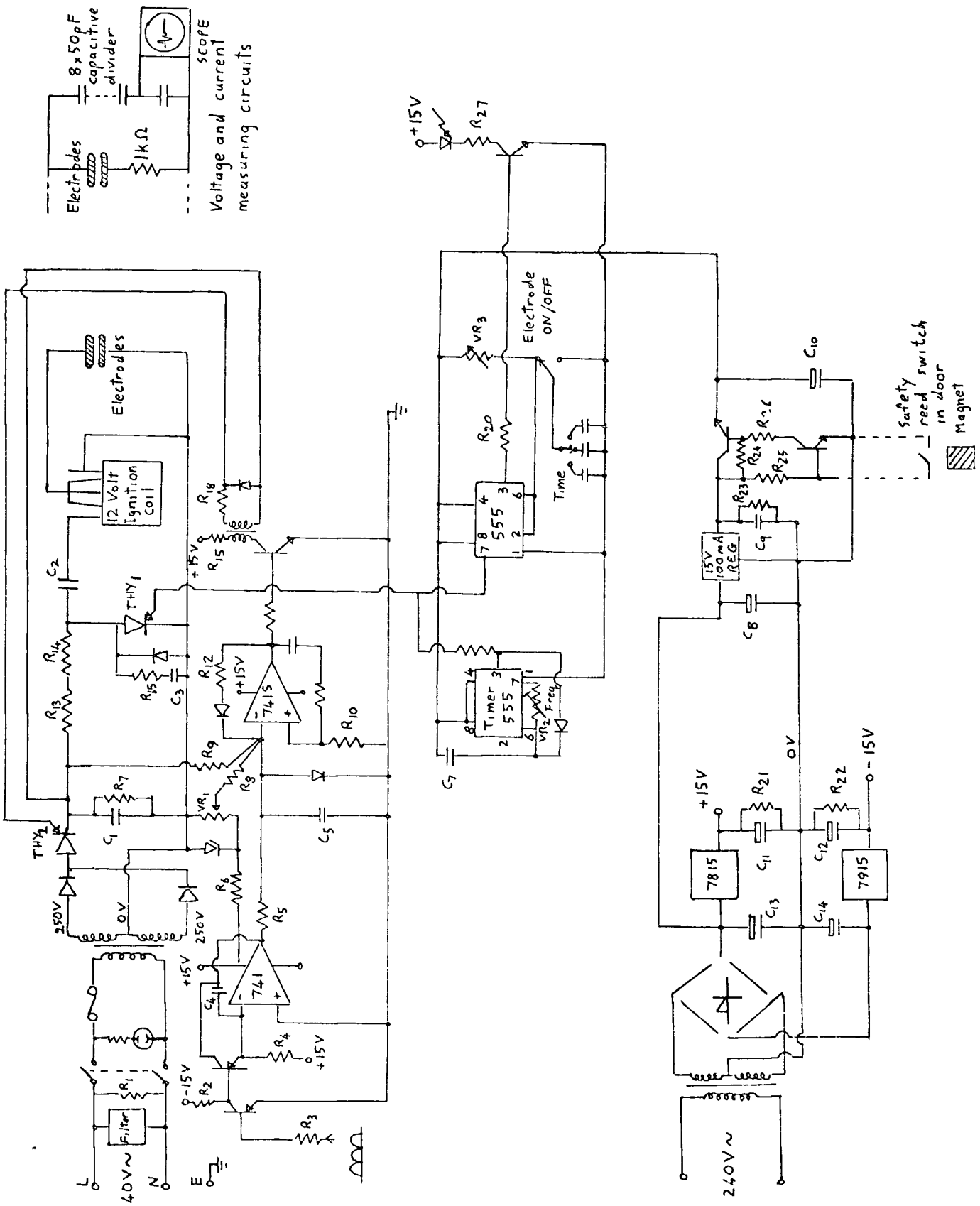

Appendix 3

Corona Discharge Apparatus

Scale 1/2

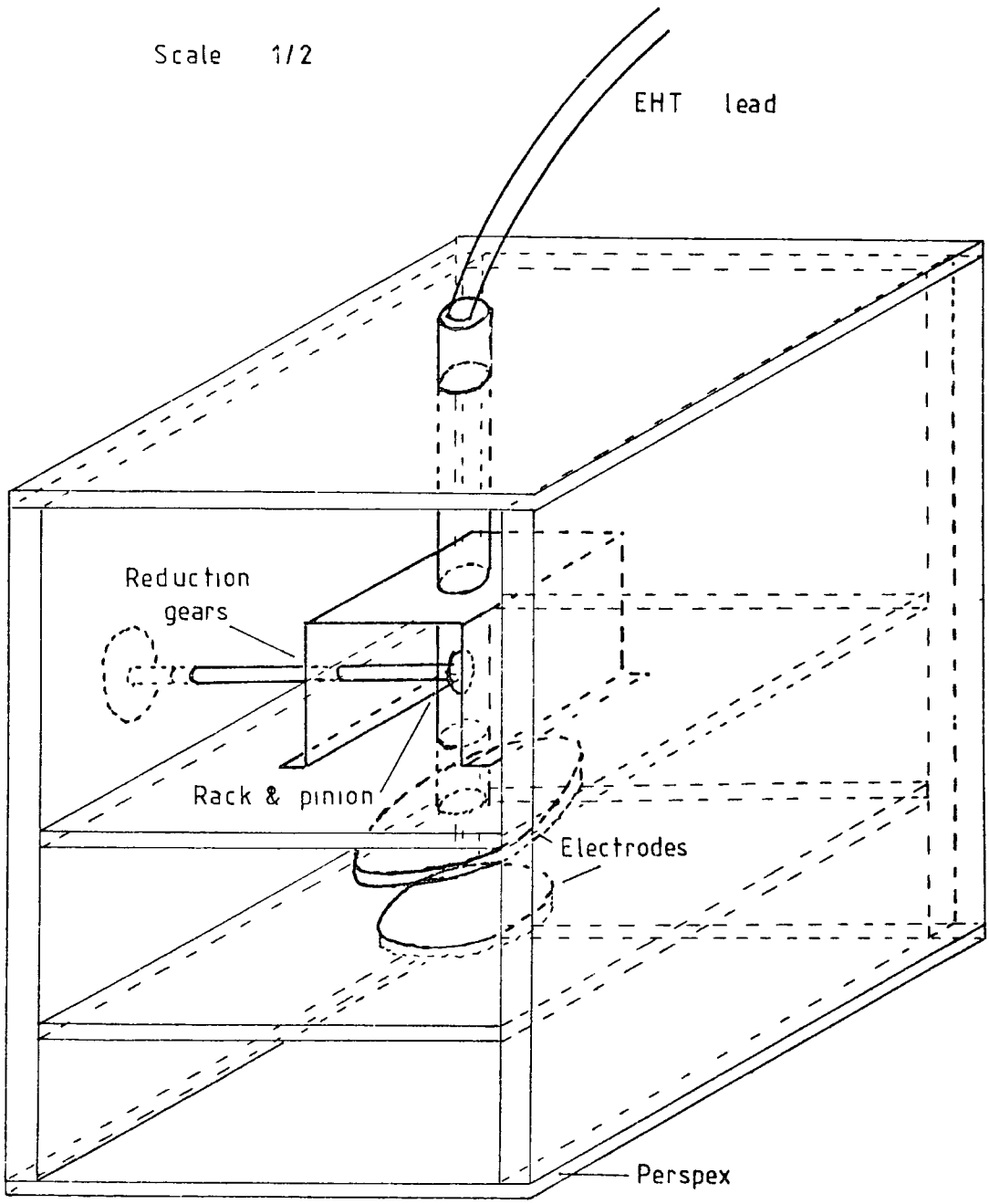

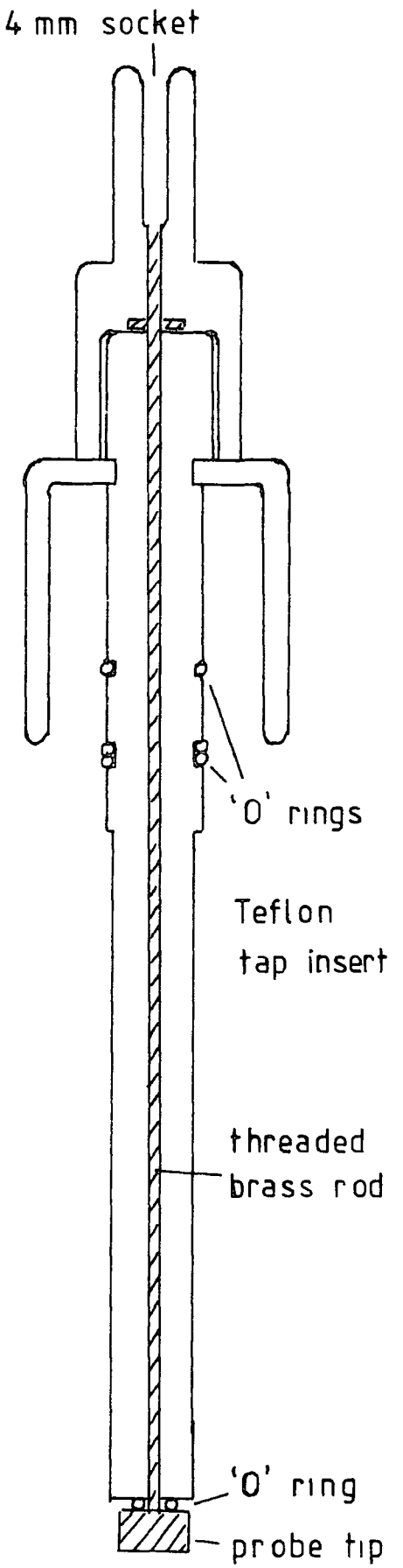
4 mm socket
'O' rings
Teflon
tap insert
threaded
brass rod
'O' ring
probe tip

Full scale

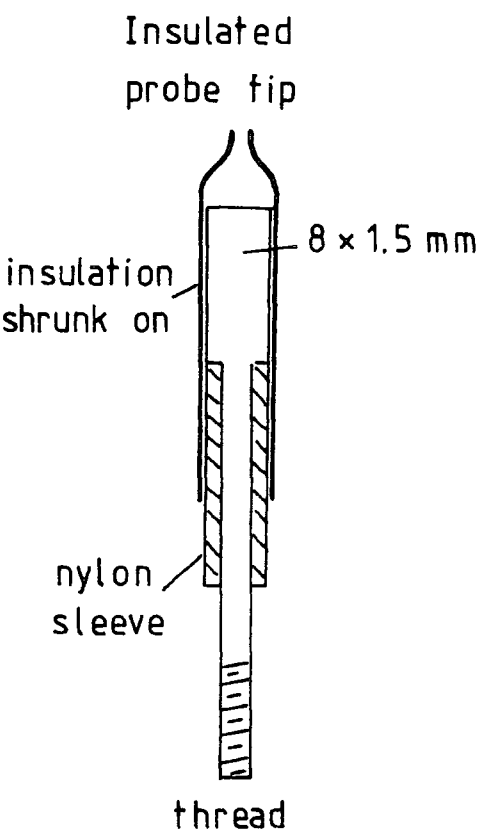
Insulated
probe tip
8 x 1.5 mm
insulation
shrunk on
nylon
sleeve
thread

Appendix 4

Calculation of Contact Angles from Dimensions of Water Drops

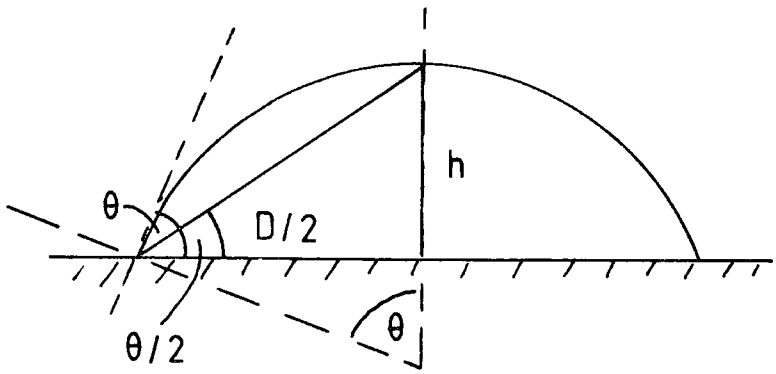

$$\tan \theta/2 = 2h/D$$

where h is the height and D is the diameter of the water drop

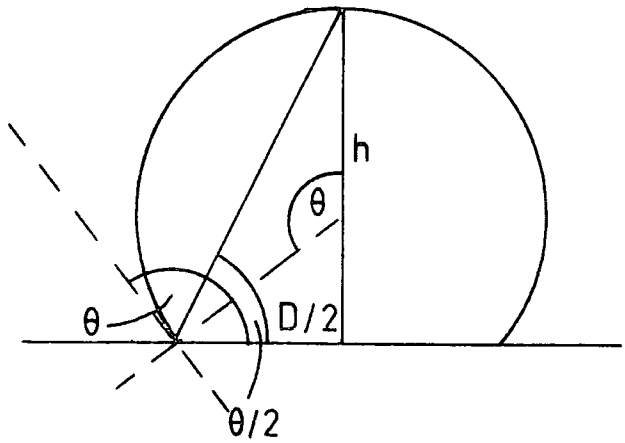

APPENDIX 5

The Board of Studies in Chemistry requires that each postgraduate research thesis should contain an appendix listing all research colloquia, seminars and lectures (by external speakers) arranged by the Department of Chemistry during the period when research for the thesis was carried out.

Research Colloquia, Seminars and Lectures Arranged by the Department of Chemistry between October 1976 and May 1980

20 October 1976

Professor J.B. Hyne (University of Calgary), "New Research on an Old Element - Sulphur"

10 November 1976

Dr. J.S. Ogden (University of Southampton). "The Characterisation of High Temperature Species by Matrix Isolation"

17 November 1976

Dr. B.E.F. Fender (University of Oxford), "Familiar but Remarkable Inorganic Solids"

24 November 1976

Dr. M.I. Page, (Huddersfield Polytechnic), "Large and Small Rate Enhancements of Intramolecular Catalysed Reactions"

8 December 1976

Professor A.J. Leadbetter (University of Exeter), "Liquid Crystals)

26 January 1977

Dr. A. Davis (E.R.D.E.), "The Weathering of Polymeric Materials"

2 February 1977

Dr. M. Falk (N.R.C. Canada), "Structural Deducations from the Vibrational Spectrum of Water in Condensed Phases"

9 February 1977

Professor R.O.C. Norman (University of York), "Radical Cations; Intermediates in Organic Reactions"

23 February 1977

Dr. G. Harris (University of St. Andrews), "Halogen Adducts of Phosphines and Arsines"

25 February 1977

Professor H.T. Dieck (Frankfurt University), "Diazadienes - New Powerful Low-Valent Metal Ligands"

2 March 1977

Dr. F. Hibbert (Birkbeck College, University of London), "Fast Reaction Studies of Slow Proton Transfers Involving Nitrogen and Oxygen Acids"

4 March 1977

Dr. G. Brink (Rhoes University, South Africa), "Di-electric Studies of Hydrogen Bonding in Alcohols"

9 March 1977

Dr. I.O. Sutherland (University of Sheffield), "The Stevans' Rearrangement: Orbital Symmetry and Radical Pairs"

18 March 1977

Professor H. Bock (Frankfurt University), "Photo-electron Spectra and Molecular Properties: A Vademecum for the Chemist"

30 March 1977

Dr. J.R. MacCallum (University of St. Andrews), "Photo-oxidation of Polymers"

20 April 1977

Dr. D.M.J. Lilley (Research Division, G.D. Searle), "Tails of Chromatin Structure - Progress Towards a Working Model"

27 April 1977

Dr. M.P. Stevens (University of Hartford), "Photo-cycloaddition Polymerisation"

4 May 1977

Dr. G.C. Tabisz (University of Manitoba), "Collison Induced Light Scattering by Compressed Molecular Gases"

11 May 1977

Dr. R.E. Banks (U.M.I.S.T.), "The Reactions of Hexafluoropropene with Heterocyclic N-Oxides"

18 May 1977

Dr. J. Atwood (University of Alabama), "Novel Solution Behaviour of Anionic Organoaluminium Compounds: The Formation of Liquid Clathrates"

25 May 1977

Professor M.M. Kreevoy (University of Minnesota), "The Dynamics of Proton Transfer in Solution"

1 June 1977

Dr. J. McCleverty (University of Sheffield), "Consequences of Deprivation and Overcrowding on the Chemistry of Molybdenum and Tungsten"

6 July 1977

Professor J. Passmore (University of New Brunswick, Canada), "Adducts Between Group $\underline{V}$ Pentahalides and a Post-script on S_7I^+"

27 September 1977

Dr. T.J. Broxton (La Trobe University, Australia), "Interaction of Aryldiazonium Salts and Arylazoalkyl Ethers in Basic Alcoholic Solvents"

19 October 1977

Dr. B. Heyn (University of Jena, D.D.R.), "σ-Organo-Molybdenum Complexes as Alkene Polymerisation Catalysts"

27 October 1977

Professor R.A. Filler (Illinois Institute of Technology), "Reactions of Organic Compounds with Xenon Fluorides"

2 November 1977

Dr. N. Boden (University of Leeds), "N.M.R. Spin-Echo Experiments for Studying Structure and Dunamical Properties of Materials Containing Iteracting Spin-$\frac{1}{2}$ Pairs"

9 November 1977

Dr. P.A. Madden (University of Cambridge), "Raman Studies of Molecular Motions in Liquids"

14 December 1977

Dr. R.O. Gould (University of Edinburgh), "Crystallography to the Rescue in Ruthenium Chemistry"

25 January 1978

Dr. G. Richards (University of Oxford), "Quantum Pharmacology"

1 February 1978

Professor K.J. Ivin (Queens University, Belfast), "The Olefin Metathesis Reaction: Mechanism of Ring-Opening Polymerisation of Cycloalkenes"

3 February 1978

Dr. A. Hartog (Free University, Amsterdam), "Some Surprising Recent Developments in Organo-Magnesium Chemistry"

22 February 1978

Professor J.D. Birchall (Mond Division, I.C.I. Ltd.), "Silicon in the Biosphere"

1 March 1978

Dr. A. Williams (University of Kent), "Acyl Group Transfer Reactions"

3 March 1978

Dr. G. van Koten (University of Amsterdam), "Structure and Reactivity of Arylcopper Cluster Compounds"

15 March 1978

Professor G. Scott (University of Aston), "Fashioning Plastics to Match the Environment"

22 March 1978

Professor H. Vahrenkamp (University of Freiburg), "Metal-Metal Bonds in Organometallic Complexes"

19 April 1978

Dr. M. Barber (U.M.I.S.T.), "Secondary Ion Mass Spectra of Surfaces Adsorbed Species"

15 May 1978

Dr. M.I. Bruce (University of Adelaide), "New Reactions of Ruthenium Compounds with Alkynes"

16 May 1978

Dr. P. Ferguson (C.N.R.S., Grenoble), "Surface Plasma Waves and Adsorbed Species on Metals"

18 May 1978

Professor M. Gordon (University of Essex), "Three Critical Points in Polymer Science"

22 May 1978

Professor D. Tuck (University of Windsor, Ontario), "Electrochemical Synthesis of Inorganic and Organometallic Compounds"

24/25 May 1978

Professor P. von R. Schleyer (University of Erlangen, Nurnberg),

(i) "Planar Tetra-Coordinate Methanes, Perpendicular Ethylenes and Planar Allenes"

(ii) "Aromaticity in Three Dimensions"

(iii) "Non-Classical Carbocations"

21 June 1978

Dr. S.K. Tyrlik (Academy of Sciences, Warsaw), "Dimethylglyoxime-Cobalt Complexes - Catalytic Black Boxes"

23 June 1978

Professor W.B. Person (University of Florida), "Diode Laser Spectroscopy at 16 m"

27 June 1978

Professor R.B. King (University of Georgia, Athens, Georgia, U.S.A.), "The Use of Carbonyl Anions in the Synthesis of Organometallic Compounds"

30 June 1978

Professor G. Mateescu (Cape Western Reserve University), "A Concerted Spectroscopy Approach to the Characterisation of Ions and Ion Pairs: Facts, Plans and Dreams"

15 September 1978

Professor W. Siebert (University of Marburg, West Germany), "Boron Heterocycles as Ligands in Transition Metal Chemistry"

22 September 1978

Professor T. Fehlner (University of Notre Dame, U.S.A.), "Ferraboranes: Syntheses and Photochemistry"

12 December 1978

Professor C.J.M. Stirling (University of Bangor), "Parting is Such Sweet Sorrow - the Leaving Group in Organic Reactions"

14 February 1979

Professor B. Dunnell (University of British Columbia), "The Application of N.M.R. to the Study of Motions in Molecules"

16 February 1979

Dr. J. Tomkinson (Institute of Laue-Langevin, Grenoble), "Studies of Adsorbed Species"

14 March 1979

Dr. J.C. Walton (University of St. Andrews), "Pentadienyl Radicals"

28 March 1979

Dr. A. Reiser (Kodak Ltd.), "Polymer Photography and the Mechanism of Cross-Link Formation in Solid Polymer Matrices"

5 April 1979

Dr. S. Larsson (University of Uppsala), "Some Aspects of Photoionisation Phenomena in Inorganic Systems"

25 April 1979

Dr. C.R. Patrick (University of Birmingham), "Chlorofluorocarbons and Stratospheric Ozone: An Appraisal of the Environmental Problem"

1 May 1979

Dr. G. Wyman (European Research Office, U.S. Army), "Excited State Chemistry in Indigoid Dyes"

2 May 1979

Dr. J.D. Hobson (University of Birmingham), "Nitrogen-centred Reactive Intermediates"

8 May 1979

Professor A. Schmidpeter (Institute of Inorganic Chemistry, University of Munich), "Five-membered Phosphorus Heterocycles Containing Dicoordinate Phosphorus"

9 May 1979

Dr. A.J. Kirby (University of Cambridge), "Structure and Reactivity in Intramolecular and Enzymic Catalysis"

9 May 1979

Professor G. Maier (Lahn-Giessen), "Tetra-tert-butyltetrahedrane"

10 May 1979

Professor G. Allen, F.R.S. (Science Research Council), "Neutron Scattering Studies of Polymers"

16 May 1979

Dr. J.F. Nixon (University of Sussex), "Spectroscopic Studies on Phosphines and their Coordination Complexes"

23 May 1979

Dr. B. Wakefield (University of Salford), "Electron Transfer in Reactions of Metals and Organometallic Compounds with Polychloropyridine Derivatives"

13 June 1979

Dr. G. Heath (University of Edinburgh), "Putting electrochemistry into Mothballs - (Redox Processes of metal Porphyrins and Phthalocynanines"

14 June 1979

Professor I. Ugi (University of Munich), "Synthetic Uses of Super Nucleophiles"

20 June 1979

Professor J.D. Corbett (Iowa State University, Ames, Iowa, U.S.A.), "Zintl Ions: Synthesis and Structure of Homopolyatomic Anions of the Post-Transition Elements"

27 June 1979

Dr. H. Fuess (University of Frankfurt), "Study of Electron Distribution in Crystalline Solids by X-ray and Neutron Diffraction"

21 November 1979

Dr. J. Muller (University of Bergen), "Photochemical Reactions of Ammonia"

28 November 1979

Dr. B. Cox (University of Stirling), "Macrobicylic Cryptate Complexes, Dynamics and Selectivity"

5 December 1979

Dr. G.C. Eastmond (University of Liverpool), "Synthesis and Properties of some Multicomponent Polymers"

12 December 1979

Dr. C.I. Ratcliffe (University of London), "Rotor Motions in Solids"

19 December 1979

Dr. K.E. Newman (University of Lausanne), "High Pressure Multinuclear NMR in the Elucidation of the Mechanisms of Fast, Simple Inorganic Reactions"

30 January 1980

Dr. M.J. Barrow (University of Edinburgh), "The Structures of some Simple Inorganic Compounds of Silicon and Germanium - Pointers to Structural Trends in Group IV"

6 February 1980

Dr. J.M.E. Quirke (University of Durham), Degradation of Chlorophyll-a in Sediments"

23 April 1980

B. Grierson, B.Sc., (University of Durham), "Halogen Radiopharmaceuticals"

14 May 1980

Dr. R. Hutton (Waters Associates, U.S.A.), "Recent Developments in Multi-milligram and Multi-gram Scale Preparative High Performance Liquid Chromatography"

21 May 1980

Dr. T.W. Bentley (University of Swansea), "Medium and Structural Effects in Solvolytic Reactions"